National Library
of Canada

Acquisitions and
Bibliographic Services Branch

395 Wellington Street
Ottawa, Ontario
K1A 0N4

Bibliothèque nationale
du Canada

Direction des acquisitions et
des services bibliographiques

395, rue Wellington
Ottawa (Ontario)
K1A 0N4

Your file Votre référence

Our file Notre référence

NOTICE

The quality of this microform is heavily dependent upon the quality of the original thesis submitted for microfilming. Every effort has been made to ensure the highest quality of reproduction possible.

If pages are missing, contact the university which granted the degree.

Some pages may have indistinct print especially if the original pages were typed with a poor typewriter ribbon or if the university sent us an inferior photocopy.

Reproduction in full or in part of this microform is governed by the Canadian Copyright Act, R.S.C. 1970, c. C-30, and subsequent amendments.

AVIS

La qualité de cette microforme dépend grandement de la qualité de la thèse soumise au microfilmage. Nous avons tout fait pour assurer une qualité supérieure de reproduction.

S'il manque des pages, veuillez communiquer avec l'université qui a conféré le grade.

La qualité d'impression de certaines pages peut laisser à désirer, surtout si les pages originales ont été dactylographiées à l'aide d'un ruban usé ou si l'université nous a fait parvenir une photocopie de qualité inférieure.

La reproduction, même partielle, de cette microforme est soumise à la Loi canadienne sur le droit d'auteur, SRC 1970, c. C-30, et ses amendements subséquents.

Canada

UNIVERSITY OF ALBERTA

THE GEOLOGY AND GEOCHEMISTRY OF GOLD MINERALIZATION, ULU CLAIMS, NORTHWEST TERRITORIES, CANADA

by

Peter Anthony Kleespies ©

A THESIS
SUBMITTED TO THE FACULTY OF GRADUATE STUDIES AND RESEARCH IN PARTIAL FULFILLMENT OF THE REQUIREMENTS FOR THE DEGREE OF MASTER OF SCIENCE.

DEPARTMENT OF GEOLOGY

EDMONTON, ALBERTA

Fall, 1994

National Library
of Canada

Acquisitions and
Bibliographic Services Branch

395 Wellington Street
Ottawa, Ontario
K1A 0N4

Bibliothèque nationale
du Canada

Direction des acquisitions et
des services bibliographiques

395, rue Wellington
Ottawa (Ontario)
K1A 0N4

Your file Votre référence

Our file Notre référence

The author has granted an irrevocable non-exclusive licence allowing the National Library of Canada to reproduce, loan, distribute or sell copies of his/her thesis by any means and in any form or format, making this thesis available to interested persons.

L'auteur a accordé une licence irrévocable et non exclusive permettant à la Bibliothèque nationale du Canada de reproduire, prêter, distribuer ou vendre des copies de sa thèse de quelque manière et sous quelque forme que ce soit pour mettre des exemplaires de cette thèse à la disposition des personnes intéressées.

The author retains ownership of the copyright in his/her thesis. Neither the thesis nor substantial extracts from it may be printed or otherwise reproduced without his/her permission.

L'auteur conserve la propriété du droit d'auteur qui protège sa thèse. Ni la thèse ni des extraits substantiels de celle-ci ne doivent être imprimés ou autrement reproduits sans son autorisation.

ISBN 0-315-95057-9

Canada

UNIVERSITY OF ALBERTA

RELEASE FORM

NAME OF AUTHOR: Peter Anthony Kleespies

NAME OF THESIS: GEOLOGY AND GEOCHEMISTRY OF GOLD MINERALIZATION, ULU CLAIMS, NORTHWEST TERRITORIES, CANADA

DEGREE: MASTER OF SCIENCE

YEAR THIS DEGREE WAS GRANTED: Fall, 1994

Permission is hereby granted to THE UNIVERSITY OF ALBERTA LIBRARY to reproduce single copies of this thesis and to lend or sell such copies for private, scholary or scientific research purposes only.

The author reserves other publication rights, and neither the thesis nor extensive extracts from it may be printed or otherwise reproduced without the authors written permission.

P.A. Kleespies
(Students signature)

92 Woodlands Road
(Permanent address)
St. ALBERT, ALBERTA

T8N 3G9

Date: July 20, 1994

UNIVERSITY OF ALBERTA
FACULTY OF GRADUATE STUDIES AND RESEARCH

The undersigned certify that they have read, and recommend to the faculty of Graduate Studies and Research for acceptance, a thesis entitled THE GEOLOGY AND GEOCHEMISTRY OF GOLD MINERALIZATION, ULU CLAIMS, NORTHWEST TERRITORIES, CANADA submitted by PETER ANTHONY KLEESPIES in partial fulfilment of the requirements for the degree of MASTER OF SCIENCE.

Dr. R. Morton
Supervisor

H. Baadsgaard
Dr. H. Baadsgaard

RE Folinsbee
Dr. R.E. Folinsbee

Dr. J. Gray

Date: July 20, 1994

Dedicated to the memory of my Father

Adolf Joseph Kleespies
October 3, 1929 - March 16, 1984

who inspired within me a wonderment of the natural world

ABSTRACT

Archean, greenstone-hosted, auriferous quartz veins occur within the Ulu Claims, situated in the north-central Slave Structural Province. The veins are hosted by a succession of deformed Archean mafic volcanics, gabbros and sediments, which have been metamorphosed to lower amphibolite facies, and intruded by several granitoid suites. Deformation is polyphase, with the main structural features in the area being large D_2 isoclinal folds, overprinted by a pervasive D_3 cleavage.

Two distinct suites of felsic intrusives are present in the area. An early episode, which occurs post D_2 but pre-D_3 is termed the internal suite and consists of trondhjemitic dykes and plugs, which are characterized by high K/Rb (252-346) and low Rb/Sr (0.14-0.35) ratios and HREE depletion ($(La/Yb)_N$ = 11.28-37.32). A later episode, termed the external suite, truncates both D_3 and D_2 structural elements, and forms extensive granite batholiths surrounding the supracrustal succession. These rocks are characterized by high Rb/Sr (30-37) and low K/Rb (100-125) ratios and relatively flat REE profiles ((La/Yb_N) = 0.50-0.56) with pronounced negative Eu anomalies. U-Pb zircon data indicates that all of the intrusives are late Archean in age.

Three types of mineralization are recognized within the Ulu Claims. Type I is limited in areal extent, and consists of deformed, metamorphosed syngenetic base-metal mineralization. Type II is the primary exploration target, and consists of Au-As bearing ribbon, breccia and replacement veins hosted primarily by mafic volcanics. These veins occur within dilatent structures associated with D_2 deformation and are crosscut by trondhjemitic dykes. Alteration assemblages associated with the veins indicate that mineralization postdates peak metamorphism. Temperature of mineralization, from arsenopyrite geothermometry is estimated to be 360 to 515 °C. Type III mineralization consists of shear and tension veins, hosted by supracrustal rocks and internal granitoids. Type III veins bear a Au-Bi association, and have negligible associated alteration. The presence of bismuth within these veins constrains the temperature of mineralization to less than 300°C.

Light stable isotope studies indicate Type II mineralizing fluids are consistent with a deep crustal source (δO^{18}_{fluid}= 8.2-12.3‰, δD_{fluid} = -67, $\delta^{13}C$ = 3.5‰). A fluid derived by metamorphic devolatization/dehydration is implied. Type III mineralizing fluids display isotopic ($\delta^{18}O$ = 0.6-4.7‰, δD = -59‰) and geochemical characteristics which suggest mixing of a magmatic and low $\delta^{18}O$ surface waters

A model, in which the Ulu Claims supracrustals, intrusives and auriferous mineralization were generated in a ensialic rift setting characterized by high temperature - low pressure regional metamorphism is proposed, and implications for exploration are examined.

ACKNOWLEDGEMENTS

Foremost, I would like to thank my advisor Dr. Roger Morton for discussions, advice and encouragement to advance my knowledge of geology. I am also indebted to Dr. Morton for those aspects of my education which have allowed me to apply my knowledge beyond the academic realm.

I would like to thank Neil leNobel, Harry Muntanion, Paul Cowley and Eugene Flood of BHP Minerals Canada for suggesting the Ulu project, and providing ideas and encouragement. Access to, and use of proprietary information during the course of this study is gratefully acknowledged. Thanks is also extended to Marshall Himes of BHP Utah International, Salt Lake City for providing the microprobe analyses.

I would like to thank Dr. Baadsgaard for guiding me through the fascinating and sometimes frustrating world of U-Pb zircon dating. Other members of his research group, Dr. Pat Cavell and Wayne Day are thanked for their assistance during many long hours of mineral separation and zircon picking.

Acknowledgements are extended to Dr. J. Gray for the use of his stable isotope laboratory, and to Dragan Krstic and Nick Mys who performed the carbon and oxygen isotopic analyses.

Dr. K. Muehlenbachs and his technical staff are thanked for lab access and performing the deuterium analyses used in this study, and Dr. B.E. Nesbitt is gratefully acknowledged for the generous use of his computing facilities.

Conversations and discussions with my fellow students both past and present have contributed immeasurably to my education, and thanks are due to Bob S., Andrew, Eugene, Rob H., Ralph, Jackie, Agnes, Gerald, Arndt, James, Bjarni and Stuart.

Services rendered by departmental technicians Frank Dimitrov and Alex Stelmach are acknowledged.

A thank you Andrew Locock, Barbara Kleespies and Jody Dahrouge for the expert editing of this thesis, which greatly improved upon early manuscripts.

Last and certainly not least, the time spent in the field during production of this thesis provided the opportunity to work with many fine geologists, geophysicists and assistants. The friendship, moral support, and conversation provided by the following people during the drudgery and insanity associated with long periods of isolation is greatly appreciated; Ross, Dave, Jeremy, Mark, Greg M., Lauren, Calvin, Michelle and Mark K., Nick, John, Dierdre, Sally, Val, Karen,

Marnie, Freeman, Rob G., Rhonda, Jeff, Ray, Martin, Greg H., Will, Tom B., Darren, Tom K., Gina, Bruce, Bob C., Rick, Neil, Shelly, Anita, Tracy, and Lynn.

TABLE OF CONTENTS

Chapter Page

1. INTRODUCTION 1
    - GENERAL STATEMENT 1
        - The Study Focus 2
        - The Objectives of the Study 2
    - LOCATION, ACCESS, PHYSIOGRAPHY, CLIMATE 2
        - Location 2
        - Access 2
        - Physiography 4
        - Climate 4
    - EXPLORATION HISTORY 5
    - THE ULU PROPERTY HISTORY 6
    - PREVIOUS GEOLOGICAL STUDIES 7
    - PURPOSE OF THE PRESENT STUDY 9

2. REGIONAL GEOLOGY 11
    - THE SLAVE PROVINCE 11
        - Introduction 11
        - Pre-Yellowknife Supergroup Rocks 11
        - Yellowknife Supergroup Rocks 13
        - Archean Granitoid Rocks 14
        - Structure and Metamorphism 15
        - Post Archean Intrusives 16
        - Tectonic Evolution of the Slave Province 16
    - THE HIGH LAKE BELT 17
    - THE ULU CLAIMS AREA 18
        - Introduction 18
        - Supracrustal Rocks 20
        - Plutonic Rocks 21
        - Deformation, Structure and Metamorphism 21

3. GEOLOGY OF THE ULU CLAIMS 23
    - INTRODUCTION 23

TABLE OF CONTENTS (continued)

HOST ROCK GEOLOGY - PETROGRAPHY 23
Supracrustal Rocks 23
Volcanics 23
Sediments 26
Gabbro 27
Intrusive Rocks 28
Internal Granitoid Suite 29
Quartz-Feldspar Porphyry Dykes 29
Grey Aplite Dykes 33
Granodiorite 33
External Granitoid Suite 34
Eastern Granite 37
Western Granite/Granodiorite 38
Proterozoic Diabase Dykes 41
STRUCTURAL GEOLOGY AND METAMORPHISM 42

4. WHOLE ROCK CHEMICAL RELATIONS 44
INTRODUCTION 44
SUPRACRUSTAL LITHOLOGICAL UNITS 44
Mafic Volcanics/Gabbros/Diabase 44
Major Element Chemical Variations 44
Trace Element Chemical Variations 47
Petrogenesis 50
Sedimentary Rocks 50
FELSIC INTRUSIVE PHASES 53
Major Element Chemistry 53
Trace and Rare Earth Element Chemical Relations 60
Petrogenesis 71

5. U-Pb ZIRCON GEOCHRONOMETRY 73
INTRODUCTION 73
METHODS 73
SAMPLE DESCRIPTIONS 74
93 HVRT-0 74

TABLE OF CONTENTS (continued)

93 HVRT-1 74
93 HVRT-2 75
93 HVRT-3 75
ANALYTICAL RESULTS 75
DISCUSSION 77

6. GEOLOGY AND PETROGRAPHY OF MINERALIZATION 78
INTRODUCTION 78
TYPE I MINERALIZATION 78
TYPE II MINERALIZATION 80
Introduction 80
Flood Zone Morphology and Structure 80
Vein Characteristics and Textures 82
Vein Mineralogy 86
Quartz 86
Wall-rock Fragments / Vein Selvages 87
Calcite 88
Potassium Feldspar 88
Amphibole 88
Apatite 91
Titanite 91
Tourmaline 91
Ore Petrology 91
Arsenopyrite 92
Pyrrhotite 93
Pyrite 93
Chalcopyrite 96
Sphalerite 96
Gold 96
Alteration 96
Vein Paragenesis 99
P-T Conditions of Mineralization Determined From Alteration Assemblages 105

TABLE OF CONTENTS (continued)

Timing of Mineralization and Alteration Relative to Regional Metamorphism 106

TYPE III MINERALIZATION 107

Introduction 107

Occurrence and Vein Morphology 107

Vein Mineralogy 108

Quartz 109

Ore Petrology 109

Sulphides 109

Native elements 110

Other minerals 110

Alteration 110

Paragenesis 110

7. GEOCHEMISTRY OF MINERALIZATION 117

ARSENOPYRITE GEOTHERMOMETRY 117

Analytical Methods 117

Introduction to the Arsenopyrite Thermometer 117

Flood Zone Sulphides 120

Pyrite 120

Pyrrhotite 120

Arsenopyrite 123

GEOTHERMOMETRY OF TYPE III VEINS 125

TRACE ELEMENT GEOCHEMISTRY OF MINERALIZATION 126

Chemical Analysis 126

Element Variations in Type II and Type III Mineralization 127

GEOCHEMISTRY OF TYPE II MINERALIZATION 129

Evaluation of Immobile Elements 130

Immobile Elements in Basaltic Andesites 131

Immobile Elements in Sediments 131

Elemental Gains/Losses in Altered/Mineralized Basaltic Andesites 135

TABLE OF CONTENTS (continued)

Elemental Gains/Losses in Altered/Mineralized Sediments 138
Mass Balance Considerations for Ulu Type II Mineralization 141

8. LIGHT STABLE ISOTOPE STUDY 143
INTRODUCTION 143
ANALYTICAL PROCEDURES 143
SILICATE OXYGEN ISOTOPE STUDY 144
Results 144
Whole Rocks 144
Vein Quartz 144
Type II Veins 144
Type III Veins 144
Discussion of Results 149
Whole Rock Oxygen Isotope Data 149
Type II Veins 150
Type III Veins 152
Other Veins 152
HYDROGEN ISOTOPE STUDY 152
Results 153
Interpretation of Hydrogen Isotopes 153
CARBON ISOTOPE STUDY 155
Results 155
Discussion of Carbonate Isotope Results 155
STABLE ISOTOPE COMPOSITIONS OF MINERALIZING FLUIDS 157
9. DISCUSSION AND SUMMARY 160
SUMMARY 160
RELATIONSHIP OF MINERALIZATION TO TECTONIC SETTING 166
IMPLICATIONS AND RECOMMENDATIONS FOR EXPLORATION 169

TABLE OF CONTENTS (continued)

FURTHER STUDIES 171

REFERENCES CITED 173

APPENDIX 1. Sample List 189

APPENDIX 2. Whole Rock Chemical Data 201

APPENDIX 3. CIPW Normative Mineralogy for Felsic Intrusive Rocks 208

APPENDIX 4. Sulphide Mineral Analyses 211

APPENDIX 5. Formulae Used for Stable Isotope Calculations 217

LIST OF TABLES

Table		Page
4-1	Average trace element contents (ppm) for internal and external suite granitoid rocks, Ulu Claims, N.W.T. GD refers to granodiorites, QFP to quartz-feldspar porphyry dykes. Trace element contents of standard granite G-1 (Mason and Moore, 1982) shown for comparison.	64
4-2	Rb/Sr and K/Rb ratios for internal and external suite granitoids, Ulu Claims, N.W.T.	65
5-1	Analytical data from Ulu Claims zircon samples	75
7-1	Major and trace element chemistry of average basaltic andesite and mineralized basaltic andesite. Major oxides in weight %, Au in ppb, all other elements in ppm. Average gains/losses given in percentages for mineralized samples relative to average unaltered basaltic andesites, based upon immobile behavior of Ti and Zr. Isocon slope and mass change are also given. Mass change indicated for mineralized samples by assumption of constant Ti and Zr. Fe_2O_3 t=total iron	137
7-2	Major and trace element chemistry of greywackes and mineralized equivalents. Major oxides in weight percent, Au in ppb, all other elements in ppm. Average gains/losses given in percentages for mineralized samples relative to unaltered equivalents (91VLT 3049 relative to 91VLT 3048 and 91VLT 3051 relative to 91VLT 3050), based upon immobile behavior of Ti. Isocon slope (IS) and mass change (MC) are also given. Mass change (MC) indicated for mineralized samples by assumption of constant Ti. Fe_2O_3 t=total iron	140
8-1	Ulu Claims stable isotope data	145
9-1	Characteristics of the Ulu Claims auriferous veins	163

LIST OF FIGURES

Figure Page

1-1. Location of the Ulu Claims 3

2-1. General geology of the Slave Structural Province, modified after Henderson et al.(1992); Padgham (1992) 12

2-2. General geology of the Ulu Claims area, modified after Jackson et al. (1986); Henderson et al. (1993) 19

3-1. General geology of the Ulu Claims, modified after Flood et al. (1991) Henderson et al. (1993) 24

4-1. AFM (A=Na_2O+K_2O, F=FeO_{total}, M=MgO) plot for Ulu mafic volcanics and gabbros (solid dots), internal granitoids (open squares) and external granitoids (shaded squares) 45

4-2. Major element Harker plots for Ulu Claims mafic volcanics (solid circles), gabbros (shaded squares) and Proterozoic diabase (crosses). All oxides in weight percent 46

4-3. Chemical classification of Ulu Claims mafic volcanics (solid ellipses), gabbros (open rectangles) and Proterozoic diabase (triangles), based on total versus silica (modified after Le Bas and Streckeisen, 1991)...... 48

4-4. Trace element Harker plots for Ulu Claims volcanics (solid circles), gabbros (shaded squares) and Proterozoic diabase (crosses). Oxides of Si and Cr in weight percent, Sr, Zr, Ba, Co, Nb, La, Y and Ni in ppm by weight 49

4-5. K_20/Na_2O ratios in Ulu Claims greywackes (open squares) and cordierite bearing pelites (shaded squares). Also shown are K_2O / Na_2O) ratios for average Archean greywacke (1) and slate (2) (Ojaknagas, 1985), Yellowknife Supergroup Burwash Formation greywackes (3) and slates (4) (Henderson,1975b) 52

4-6. AFM diagram for Ulu Claims greywackes and pelites (solid dots). Also plotted are pre-Yellowknife Supergroup basement granodiorite (1) (Easton, 1985), average Yellowknife felsic volcanic (2) (Barager and Goodwin, 1969) and average Ulu Claims mafic volcanic (3)........ 52

4-7. Major element (TiO_2, Al_2O_3, and Fe_2O_3) Harker plots for felsic intrusives, N.W.T. All oxides given in weight percent 54

4-8. Major element (CaO, Na_2O, and K_2O) Harker plots for felsic intrusives, N.W.T. All oxides given in weight percent 55

LIST OF FIGURES (continued)

4-9. Major element (MgO, MnO, P_2O_5) Harker plots for felsic intrusives, N.W.T. All oxides given in weight percent 56

4-10. Triangular plot of the relative percentages on normative quartz (Q), orthoclase (Or) and albite (Ab) for internal (solid diamonds) and external (open circles) granitoids. Ulu Claims, N.W.T. Aplites, pegmatites and suspected contaminated rocks removed. Eutectic position for Ab/An=3.8 (1), and Ab/An =7.8 (2), at P_{H2O}=2Kbar, projected from the Q-Ab-Or-An-H_20 system (Winkler, 1976). Calc-alkaline (C-A) and trondhjemitic trends after Barker and Arth (1976) 59

4-11 Triangular plot of the relative percentages of normative orthoclase (Or), albite (Ab) and anorthite (An) for internal (solid diamonds) and external (open circles) granitoids, Ulu Claims, N.W.T. Aplites, pegmatites and suspected contaminated rocks removed. Plot after O'Connor (1976), field boundaries after Barker (1979) 59

4-12 Trace element (Sr, Ba, and Zr) Harker plots for felsic intrusives, Ulu Claims, N.W.T. Trace elements in ppm by weight, SiO_2 in weight percent 61

4-13 Trace element (Hf, Ta, and Pb) Harker plots for felsic intrusives, Ulu Claims, N.W.T. Trace elements in ppm by weight, SiO_2 in weight percent 62

4-14 Trace element (U, Y, and Rb) Harker plots for felsic intrusives, Ulu Claims, N.W.T. Trace elements in ppm by weight, SiO_2 in weight percent 63

4-15 K/Rb (A) and Rb/Sr (B) variation diagrams for internal (open squares) and extenal granitoids (solid diamonds), Ulu Claims, N.W.T. Aplites, pegmatites and suspected contaminated dykes not plotted 66

4-16 Chondrite normalized (Boynton, 1983) REE plots for internal (A) and external (B) granitoid suites, Ulu Claims, N.W.T 68

5-1 Concordia plot of U/Pb results for Ulu Claims zircons. 2 sigma error ellipses are shown 76

6-1 Location of Type I, Type II and Type III mineralized zones, Ulu Claims, N.W.T. Numbers refer to showings included in this study. Type I (1-Rhonda Lake). Type II (2-Flood Zone, 3-Gnu Zone, 4-NFN). Type III (5-Ulu West, 6-Emerald Lake, 7-GBZ, 8-Gnu, 9-Ravine, 10-East Limb, 11-NFN) 79

LIST OF FIGURES (continued)

6-2. Mineralogy and paragenetic sequence for Type II mineralized veins, Ulu Claims, N.W.T. Early and advanced refer to stages of vein development. Alteration minerals are in terms of both intensity of alteration and time, with advanced alteration assemblages overprinting early alteration assemblages 104

6-3 Mineralogy and paragenetic sequence for Type III veins, Ulu Claims, N.W.T. 115

7-1 Pseudobinary T-X section along the pyrite löllingite join showing arsenopyrite composition as a function of temperature, at% As, and coexisting equilibrium phases. All assemblages include vapour. Ulu Type II mineralization arsenopyrite analyses are shown plotted as an equilibrium assemblage of asp+po+py. Shaded data points correspond to those analyses which plot outside the stability field for this assemblage (refer to text for further explaination). Asp-arsenopyrite, po-pyrrhotite, py-pyrite and lö-löllingite. Modified after Kretschmar and Scott (1976) 119

7-2 S-Fe-As ternary diagram showing the composition of arsenopyrites, pyrrhotites and pyrites from Type II Flood Zone mineralization 121

7-3 As/S variations in arsenopyrite from Type II Flood Zone mineralization. Cross in upper left shows error bars corresponding to analytical error for individual analyses. (0.60 at%) 121

7-4 Atomic percent Fe in Type II Flood Zone pyrrhotite 122

7-5 Distribution of temperatures determined by arsenopyrite geothermometry for Flood Zone Type II mineralization 122

7-6 Log-Log plots for Au vs. As, Ag, Cu and Bi, and Bi vs. As, Ag, and Cu. All elements in ppm. Type II veins as solid squares, Type III veins as open squares 128

7-7 Immobile element X-Y plots for mineralized and non-mineralized basaltic andesites. Mineralized samples shown as solid squares, unmineralized samples as open squares. Al_2O_3 and TiO_2 in wt%, Zr and Y in ppm. Regression coefficients for each element pair is given in upper right of graph 132

7-8 Immobile element X-Y plots from mineralized and nonmineralized sediments. Mineralized samples shown as solid squares, nonmineralized greywackes as grey squares and pelites as open squares. Tielines are between mineralized and nonmineralized pairs. Al_2O_3 and TiO_2 in wt%, Zr and Y in ppm 133

LIST OF FIGURES (continued)

7-9 Percentage gains and losses for altered/mineralized basaltic andesites, Type II mineralization, Ulu Claims. Slope given in the right hand corner of diagram is the slope of the Ti-Zr isocon. Slopes less than one indicate mass increase. Error of 20% is shown by horizontal line.......... 136

7-10 Percentage gains and losses for mineralized/altered sediments, Type II mineralization, Ulu Claims. Slope given in upper right of diagrams is the slope of the Ti isocon. Slopes less than one indicate a mass increase. Error of 50% is shown by horizontal line.......... 139

8-1 Oxygen isotope composition of whole rock and quartz vein samples from the Ulu Claims N.W.T. Whole rock samples are shown as shaded ellipses, Type II vein quartz as solid diamonds and Type III vein quartz as shaded rectangles.......... 148

8-2 Oxygen isotopic composition of vein quartz and hydrogen isotopic composition from fluid inclusions from vein quartz: **a**. Oxygen, Type II mineralization, **b**. Hydrogen Type II mineralization, **c.** Oxygen Type III mineralization, **d**. Hydrogen, Type III mineralization.......... 151

8-3. Carbon and oxygen isotope compositions of vein calcites from the Ulu Claims N.W.T.......... 156

8-4 Plot of δD vs. $\delta^{18}O$ of hydrothermal fluids which generated Type II and Type III auriferous veins within the Ulu Claims, N.W.T. Also shown are fields of metamorphic (9) and magmatic (8) waters (Taylor 1974; 1979), the meteoric water line (Craig, 1961) and calculated isotopic compositions on mineralizing fluids for other Canadian and Australian Archean auriferous veins; 1) Macassa (Kerrich and Watson, 1984; Kerrich, 1983), 2) Timmins (Fyon et al., 1982, 1983), 3) Hollinger (Wood et al.,1986), 4) Eldrich (Kennedy, 1985 from Kerrich, 1987), 5) Princess Royal, 6) Victory-Kambalda, and 7) Mount Charlotte (Golding and Wilson, 1987; Golding 1990).......... 158

9-1 Order of Archean geological events for the Ulu Claims, N.W.T. The temporal relationships between the geological events depicted in this diagram are based upon observations of field relationships and textural considerations.......... 161

LIST OF PLATES

Plate		Page
3-1a	90VD-44 (292.7m) Quartz-feldspar porphyry from drill-core. Note large zoned plagioclase phenocryst	32
3-1b	90PAK-QFP Foliated quartz-feldspar porphyry from a surface exposure proximal to Flood Zone mineralization	32
3-1c	Photomicrograph, (xpl), 90VD-44 (292.7m) Zoned/twinned plagioclase phenocryst with weak sericite-carbonate alteration, in a fine-grained quartz+plagioclase+biotite matrix	32
3-1d	Photomicrograph, (xpl), 90VD-44 (292.7m) 'Quartz eye' consisting of an aggregate of recrystallized, equant quartz grains	32
3-2a	92VKT-4204 Handspecimen of internal suite granodiorite from surface occurrence, showing strong iron staining and late microfractures. Note weak foliation defined by elongation of biotite grains	36
3-2b	Photomicrograph, (xpl), 92VKT-4204 Typical altered textures displayed by internal suite granodiorite. Note extreme turbidity within sericite-carbonate altered feldspars	36
3-2c	90VD-44 (565.5m) Specimen of grey aplite from drillcore	36
3-2d	Photomicrograph, (xpl), 90VD-44 (565.5m) Microtextures displayed by grey aplites. These rocks are texturally similar to the quartz-feldspar porphyries, however they lack significant plagioclase or biotite phenocrysts. Note small 'quartz eyes'	36
3-3a	90PAK-GRAN Handspecimen of eastern granite, collected proximal to the Flood Zone mineralization	40
3-3b	Photomicrograph (xpl), 90PAK-GRAN Typical granoblastic texture displayed by external granites. Note lack of alteration of feldspars relative to internal suite granitoids	40
3-3c	92VKT-4208 Handspecimen of pink aplite dyke with green muscovite glomerocrysts	40

LIST OF PLATES (continued)

3-3d Photomicrograph, (xpl), 92VKT-4208
Trachytic texture defined by subparallel alignment of plagioclase laths, typical of the pink aplites 40

6-1a 90PAK-US-14
Ribboned quartz vein. The ribbons are the altered/sulphidated remnants of mafic volcanic wallrock septa incorporated into the vein during successive episodes of fracturing and silica flooding 85

6-1b 90PAK-US-27
Crack and seal vein, with incorporation of planar mafic volcanic wallrock septa. Wallrock shows variable degree of alteration and up to 30% acicular arsenopyrite. Continued alteration of wallrock septa results in ribbons as seen in 90PAK-US-14 (Plate **6-1a**) 85

6-1c. 90PAK-US-25
Brecciated crack-seal vein containing fragments of mineralized mafic volcanics. Dark mass at left of photograph is massive tourmaline. Dark bands within wallrock are also due to the presence of tourmaline 85

6-1d 90PAK-US-35
Breccia vein containing altered/mineralized mafic volcanic wallrock fragments 85

6-2a Photomicrograph, (xpl), 90PAK-US-14
Recrystallized vein quartz. Note equant morphology of individual crystals, predominance of triple 120° grain boundaries and lack of straining 90

6-2b Photomicrograph, (xpl), 90PAK-US-25
Recrystallized vein quartz with carbonate. Note triple 120° and sutured grain boundaries between quartz grains, and the occurrence of carbonate (calcite) interstitial to and along quartz grain boundaries 90

6-2c Photomicrograph, (ppl), 90PAK-US-14
Wallrock ribbon with mineral assemblage of arsenopyrite (opaque)+tourmaline+microcline+quartz. Tourmaline (brown mineral with pseudo-hexagonal cross-sections) makes up the majority of the photograph. In handspecimen (Plate **6-1a**) tourmaline bearing wallrock ribbons are black in color 90

LIST OF PLATES (continued)

6-2d Photomicrograph, (ppl), 90PAK-US-8
Strongly altered/mineralized wallrock clast from breccia vein. Mineral assemblage consists of microcline+titanite (ti)+arsenopyrite (asp)+minor quartz and biotite.......... 90

6-3a Photomicrograph, (ppl), 90PAK-US-25
Acicular arsenopyrite within altered wallrock fragments incorporated into quartz vein. Note diamond shaped cross-sections and atoll textures within large grains in center of photograph.......... 95

6-3b Photomicrograph, (ppl), 90PAK-US-25
Coexisting arsenopyrite (asp), pyrite (py) and pyrrhotite (po) within altered small wallrock fragment within a quartz vein. Pyrrhotite shows strong retrograde alteration to marcasite displaying 'birds eye' textures. Retrograde alteration of pyrrhotite is ubiquitous in Type II mineralization within surface and shallow drillcore samples.......... 95

6-3c Photomicrograph, (xpl), 90PAK-US-25
Close-up of coexisting arsenopyrite (asp), pyrite (py) and pyrrhotite (po), using a Normarski phase interference lense.......... 95

6-3d Photomicrograph, (ppl), 90PAK-US-16
Late pyrite (py) with brecciated textures occuring within vein quartz adjacent to arsenopyrite (asp) rich, altered mafic volcanic wallrock..... 95

6-4a Photomicrograph, (ppl) 90PAK-US-25
Native gold intergrown with acicular arsenopyrite within altered mafic volcanic wallrock fragment. Note titanite (ti) overgrowth on ilmenite (il) grains on left side of photograph.......... 98

6-4b Photomicrograph, (ppl), 90PAK-US-14
Native gold occuring with arsenopyrite, and within silicate gangue adjacent to the arsenopyrite grain.......... 98

6-4c Photomicrograph, (ppl), 90PAK-US-25
Native gold grain in contact with an arsenopyrite (asp) crystal, overgrown by pyrite (py), occuring within altered mafic wallrock fragment.......... 98

6-4d Photomicrograph, (ppl), 90PAK-US-10
Native gold grain in association with late pyrite, occuring within quartz adjacent to arsenopyrite rich altered mafic volcanic wallrock.... 98

6-5a 90VD-25 (187.75m)
Drillcore sample of weak biotite alteration from mafic volcanics between several mineralized lenses. Biotite occurs as thin stringers

LIST OF PLATES (continued)

and as a weak pervasive alteration mineral. Darker green domains occurring adjacent to biotite stringers are massive recrystallized (hydrothermal) hornblende.......... 101

6-5b Photomicrograph, (ppl), 90VD-25 (187.75m)
Relatively unaltered mafic volcanics with typical mineral assemblage of hornblende+plagioclase+ilmenite displaying an palimpsest texture of quickly chilled basalts (radiating aggregates of hornblende). Minor biotite alteration is visible in lower right of photograph.......... 101

6-5c Photomicrograph, (ppl), 90VD-25 (187.75m)
Details of biotite stringer. Note the biotite alteration is centered about a tiny tourmaline (tm) veinlet.......... 101

6-5d Photomicrograph, (ppl), 90VD-25 (187.75m)
Close-up of biotite replacing metamorphic hornblende. Note titanite (ti) grains after ilmenite within biotite alteration.......... 101

6-6a 90VD-47 (347.00m)
Drillcore sample of advanced alteration associated with Type II mineralized veins. Dark domains represent weakly or unaltered hornblende rich mafic volcanics. Degree of alteration appears to diminish away from sub-centimetre scale, irregular quartz veinlets. Sample contains 1/2% acicular arsenopyrite, occurring primarily at the boundary between weakly/unaltered mafic volcanics and clinozoisite rich alteration.......... 103

6-6b Photomicrograph, (ppl), 90VD-47 (349.90m)
Tourmaline (tm)+quartz+clinozoisite (cz) veinlet in unaltered hornblende rich mafic volcanics. Minor biotite is also present, associated with the veinlet.......... 103

6-6c Photomicrograph, (xpl), 90VD-47 (347.00m)
Alteration of mafic volcanics consisting of clinozoisite (displaying anomolous blue interference colors)+biotite+titanite with an overprint of late euhedral actinolite crystals (pale green) and minor euhedral acicular arsenopyrite (opaques). In handspecimen (Plate **6-6a**) the clinozoisite-rich alteration apppears as creamy white domains.......... 103

6-6d Photomicrograph, (xpl), 90VD-47 (347.00m)
Strong, advanced alteration of mafic volcanics consisting of actinolite+microcline+quartz adjavcent to quartz veinlet. 103

LIST OF PLATES (continued)

6-7a 90PAK-US-47
Handspecimen of Type III mineralization from the Ulu West area. Coarsely crystalline grey quartz vein. Note massive pyrite occurring within vugs and between quartz grains.......... 112

6-7b Photomicrograph, (xpl), 90PAK-US-47
Quartz in thin section from 90PAK-US-47 (Plate **6-7a**). Note the sutured, embayed grain boundaries and strained nature of quartz grains.......... 112

6-7c Photomicrograph, (ppl), 90PAK-US-47
Grains of native bismuth occurring interstitial to quartz grains. Note small grain of native gold and native bismuth occuring within the quartz crystal to right of the large bismuth grain.......... 112

6-7d Photomicrograph, (ppl), 89VD-12 (24.9m)
Type III mineralized vein hosted within quartz-feldspar porphyry from the Flood Zone. Photograph shows native gold intergrown with native bismuth as inclusions within quartz crystals.......... 112

6-8a 91VFT-3803
Handspecimen of Type III mineralized vein from the Emerald Lake area. Sample consists of coarsely crystalline white to clear quartz with chalcopyrite and pyrrhotite occurring as late fracture fill.......... 114

6-8b Photomicrograph, (ppl), 91VFT-3803
Pyrrhotite (displaying retrograde alteration to marcasite) occurring within late fractures.......... 114

6-8c Photomicrograph, (xpl), 91VFT-3803
Quartz in thin section from 91VFT-3803, displaying weakly embayed grain boundaries and weak straining. Note the abundant secondary solid and fluid inclusion trails transecting the quartz grain boundaries. 114

6-8d Photomicrograph, (ppl), 91VFT-3803
Close up of secondary inclusion trails from Plate **6-8c**, showing abundant native bismuth inclusions.......... 114

1. INTRODUCTION

GENERAL STATEMENT

Lode gold deposits within Archean greenstone terrains are significant producers of gold, being second in worldwide production to the paleoplacers of the Witwatersrand Basin. Archean lode gold deposits have historically accounted for 16% of cumulative world gold production (Colvine, 1984), and within Canada the Archean Slave and Superior structural provinces have produced over 3950 tonnes of gold from lode sources (Colvine, 1988b; Padgham and Brophy, 1985).

The economic significance of Archean lode deposits is evident from the volume of literature produced concerning the genesis of these gold occurrences. Despite the amount of research that has been conducted, many enigmae remain, mainly concerning the source of the mineralizing fluids which implicates the crustal processes responsible for the formation of these deposits.

Current theories regarding the formation of Archean lode gold deposits abound, including metamorphic dehydration/replacement (e.g., Grove and Phillips, 1987; Kerrich, 1989), granulitization (e.g., Fyon et al., 1984; Colvine et al., 1984, 1988a; Cameron, 1988) , magmatic sources (e.g., Burrows et al., 1986; Cameron and Hattori, 1987; Hattori, 1987), syngenetic/exhalative (e.g., Hutchinson, 1976; Ridler, 1976), lateral diffusion (e.g., Boyle 1961, 1979), and lamprophyre related (e.g., Rock and Groves, 1988). There appears to be a current trend for researchers to categorize all Archean gold deposits into one genetic model based upon evidence from a specific deposit or metallogenic region. Others consider the overall variations in Archean gold deposits as a function of depth within the mineralizing system, and variations within individual deposits due to present erosional levels (Colvine, 1988; Groves, 1993). Based on the diverse mineralogical, lithological and geochemical variations displayed by these deposits, it seems more probable that Archean gold mineralization is a result of several mechanisms operating independently, but representing points along a continuum during greenstone belt tectonic/petrogenetic evolution.

Within the Archean Slave structural province of Canada, greenstone-hosted lode gold deposits have yielded 350 tonnes of gold since 1935, with 85% of this production coming from mafic volcanic-hosted shear systems in the Yellowknife greenstone belt. (Padgham, 1985). The remoteness of the remainder of the boreal Slave Province has limited the amount of exploration and hence the discovery of economically viable deposits.

The Study Focus

The Ulu gold deposit discovered in 1989, by BHP-Utah Mines Ltd, occurs within the High Lake greenstone belt of the Archean Slave province, approximately 600 kilometres north of Yellowknife, N.W.T. Mineralization consists primarily of structurally controlled, gold-arsenic- (Type II mineralization), and gold-copper-bismuth- (Type III mineralization) bearing quartz veins hosted by dominantly mafic metavolcanics. The Ulu property also hosts small amounts of deformed, gold bearing, stratiform base-metal occurrences (Type I mineralization) which are considered to be of syngenetic/pre-metamorphic origin.

The Objectives of the Study

The primary aim of this present study is to document the geology, geochronology and the geochemistry of gold mineralization and the associated host rocks, in order to elucidate the mechanisms of gold concentration and deposition during the evolution of the High Lake greenstone belt. The paucity of studies concerning gold mineralization within this remote area, as well as the apparent multistage nature of the mineralization, offered the major incentives to undertake this investigation.

LOCATION, ACCESS, PHYSIOGRAPHY, CLIMATE

Location

The Ulu claims lie above the Arctic Circle, approximately 600 kilometres due north of Yellowknife, N.W.T., and 120 kilometres southwest of Bathurst Inlet (Figure 1-1). The property straddles N.T.S. map sheets 76 L/15 and &76 L/14 and is centered at 66° 54' 31" N latitude and 109° 59' 20" W longitude.

The claims occupy 6125.6 hectares within the central portion of the High Lake greenstone belt, and cover both supracrustal and granitoid terranes. Gold occurrences investigated in this study occur within supracrustal domains located within the central portion of the property.

Access

Access to the Ulu claims is primarily by fixed wing aircraft or by helicopter originating from Yellowknife about 600 kilometres to the south. Lakes are the preferred landing sites for the fixed wing aircraft, equipped with skis, from October to June, and with floats during the ice-free months generally from July to

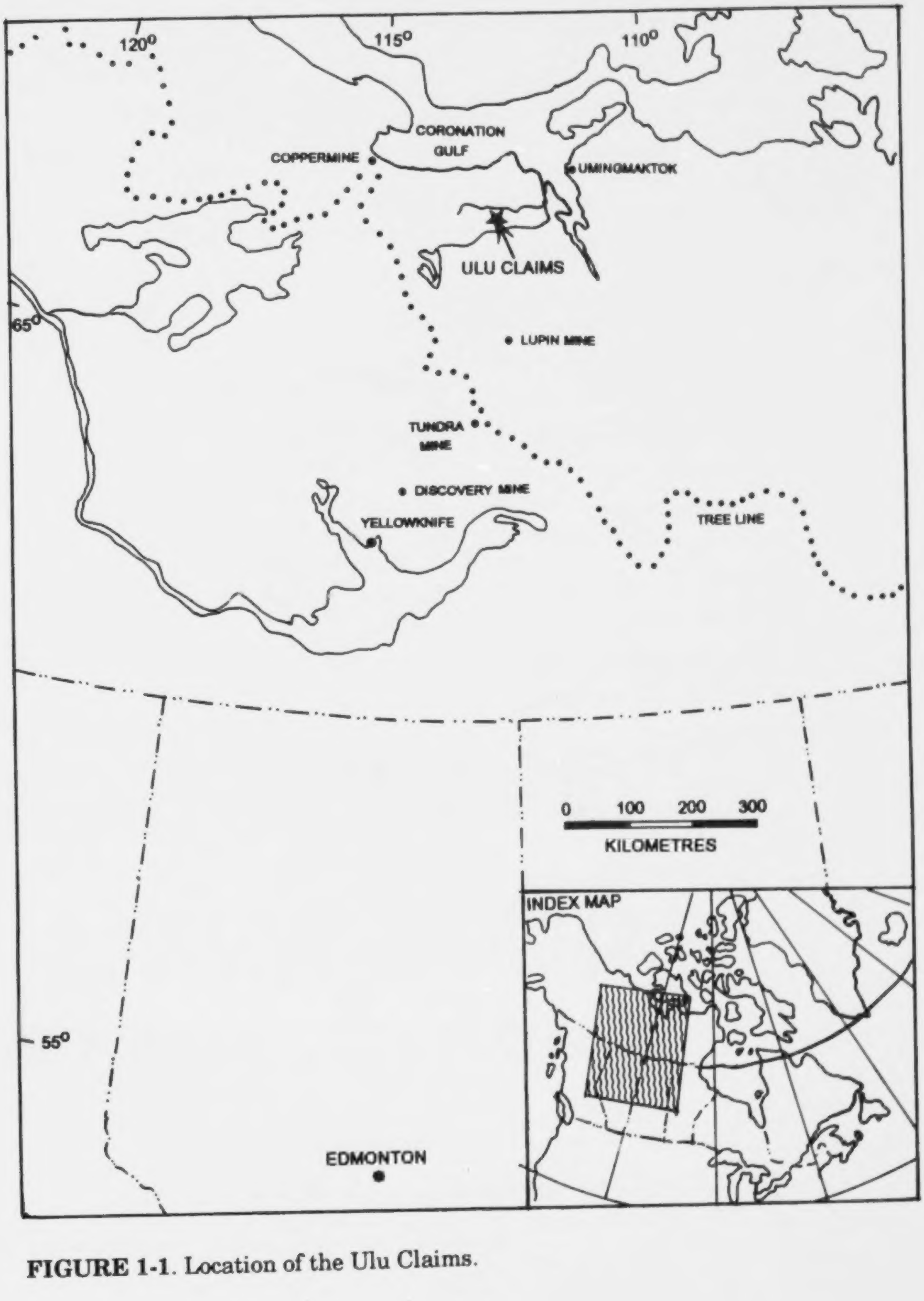
120°
115°
110°
CORONATION GULF
COPPERMINE
UMINGMAKTOK
ULU CLAIMS
65°
LUPIN MINE
TUNDRA MINE
DISCOVERY MINE
YELLOWKNIFE
TREE LINE
0 100 200 300
KILOMETRES
INDEX MAP
55°
EDMONTON

FIGURE 1-1. Location of the Ulu Claims.

September. During the brief break-up and freeze-up periods, (late June to early July and mid to late September) lakes are inaccessible to aircraft and local sand eskers provide suitable landing sites for aircraft equipped with wheels.

During the winter months of early 1991 the property was accessed by all terrain vehicles via ice roads, originating from the Lupin mine site approximately 100 kilometres to the south. This overland route provides economical transportation of fuel and equipment which has been airlifted to the Lupin minesite by Hercules aircraft from Edmonton or Yellowknife. Access to various parts of the property during the exploration season is by helicopter or by foot.

Physiography

The Ulu claims lie above the arctic circle, and are within the area classified as tundra, and colloquially referred to as the barrenlands. The area is totally devoid of trees, and is characterized by rolling grasslands with rocky knolls and abundant lakes. Locally the Ulu property consists of a broad upland with a maximum elevation of 477 metres above sea level.

The topography within the property boundaries is dominated by steep sided, north-south trending ridges and plateaux of resistant mafic metavolcanics, which generally have a relief of 10 to 30 metres. These positive features are separated by recessive meta-sedimentary units which form extensive grasslands and boulder fields. Granitoid dominated terrains are generally of moderate relief, and display extensive exfoliation. Frequent narrow, steep sided recessive linear features, interpreted both as dykes and faults, cross-cut the property at various orientations. Several northeast trending sand eskers transect the property forming sinuous ridges.

Rock exposure on the Ulu claims is generally quite good especially in the mafic metavolcanic domains, where it may reach 70%. Extensive felsenmeer development has occurred in many areas forming broad boulder fields dotted with occasional outcrops. Whilst the presence of felsenmeer limits the usefulness of surface structural measurements, the mapping of lithologies including small scale veins and dykes by the occurrence of frost heaved boulders is surprisingly accurate.

Climate

The weather in the region is typical of the continental barren lands with extremes in temperature ranging from below -50° celsius in winter and above 30°

celsius during the short summer season. The area is generally snow covered from mid-to late-September to mid-June, and the lakes remain ice free from early July until September.

Annual precipitation for the region, recorded at the permanent weather station located at Contwoyto Lake (Lupin minesite) 100 kilometres to the south, averages 129 millimetres of rainfall and 122 millimetres of snow. Weather information collected from a portable weather station during the 1990 field season indicated that prevailing winds are from the northwest, averaging 10-15 kilometres per hour and gusting up to 98 kilometres per hour.

EXPLORATION HISTORY

Intense exploration of the High Lake belt began with the discovery of the High Lake massive sulphide deposit in 1955 by Kennarctic. This volcanogenic massive sulphide deposit (hosted within felsic volcanics) is approximately 75 kilometres north of Ulu and contains a resource of 5,207,000 tons grading 3.53% Cu, 2.46% Zn, and 0.023 oz/ton Au. The area now containing the Ulu claims was most explored from the late sixties to early eighties when companies such as Borealis, Cominco, Long Lac, Tom Ursel and Associates and Noranda concentrated on exploring areas of felsic volcanics considered to be favorable for VMS deposits.

In 1968 PreCambrian Mining Services Ltd under contract to Norman H. Ursel and Associates investigated the High Lake belt north of the Hood River (N.T.S. 76L/15). Surface prospecting identified a number of pyrite/pyhrrotite gossans which contained low amounts of chalcopyrite (Blunt and McConnell, 1968).

During the 1969 and 1970, exploration seasons Borealis Exploration Ltd. conducted extensive airborne E.M. magnetometer and gamma-ray spectrometer surveys within 76L/15. Follow up surface prospecting located the Penthouse base-metal sulphide showing several kilometres east of the Ulu claims, and the Chuck base metal showing south of Ulu. Several grids ("B", "J", and "A") apparently covering airborne anomalies were established on the present day Ulu claims, however no significant mineralization was discovered (Byrne, 1970).

In 1975 Long Lac Mineral Exploration conducted surface geological mapping and ground E.M. surveys over several gossan zones south of Ulu, at the boundary between map sheets 76L/15 and 76L/10. Claims groups, (Dean and Spot) were staked over pyhrrotite/pyrite gossans containing low base-metal values (Johnson and Robinson, 1977).

In 1976 Cominco explored the High Lake belt south east of the current Ulu claims, south of the Hood River. Ground E.M., magnetometer, and gravity surveys resulted in the detection of parallel conductors, several of which had coincident magnetic anomalies (Klein, 1976).

In 1980 Noranda explored their Ralph claims staked over the old "Chuck" showing, just south of the current Ulu claims. Work consisted of geological mapping and prospecting, as well as ground magnetometer, horizontal loop E.M., and vertical loop E.M. surveys. This surface work was followed by the drilling of two diamond drill holes totalling 157.01 metres, which intersected low zinc, copper, lead, gold and silver values (Anderson and Bryan, 1982).

During the late eighties the area once again saw renewed activity likely spurred by strengthening gold prices. During this period Aber Resources, Cominco, Expeditor and BHP-Utah Mines Ltd were exploring in the area. As of late 1991 the ground in the area of 76L/15 is largely held by BHP-Utah and Aber Resources. (the Den, Fido and Jeb, and Blackridge claims). Noranda maintains the Ralph claims to the south.

Details of this latest exploration activity are not available, due to the several year confidentiality limit given to assessment work in the Northwest Territories, however the activities of several companies within N.T.S. 76L/15, proximal to the Ulu claims are summarized from a BHP- Utah internal company report.

In 1985, Aber Resources mapped, and drilled several holes on the Blackridge property located southeast of the Ulu claims. In 1988 Aber conducted a $150,000 prospecting, mapping and geophysical program on their Den, Fido, and Jeb claim blocks.

In 1987 Cominco conducted diamond drilling on their SGJV, JER claims and the surrounding prospecting permit 1031.

In 1988 Expeditor conducted geological mapping, rock, soil and stream sampling, as well as magnetometer surveys on their HY and TEC claim groups.

THE ULU PROPERTY HISTORY

Arsenopyrite-gold mineralization was discovered on what are now the Ulu claims in 1989 by BHP-Utah Mines Ltd. The mineralization was found by Eugene Flood using conventional surface prospecting techniques, and to his credit the main mineralized body has been dubbed the 'Flood Zone". Exploration drilling commenced late in the field season of 1989, and approximately 10,000 feet of NQ core outlined significant mineralization.

During the 1990 and 1991 field season approximately 100,000 feet of diamond drilling was conducted, primarily on the "Flood Zone". Peripheral drill targets throughout the property were also tested by approximately 15,000 feet of shallow drilling. Geological mapping at 1:5000 was conducted over the entire property, with favorable areas being mapped in detail at scales of 1:1000 or 1:2000. Surface prospecting, combined with rock and soil sampling, continued to outline areas of auriferous mineralization.

The Flood zone was characterized geophysically using magnetometer, VLF, E.M. radiometric, and induced polarization surveys, and these techniques have subsequently been used as exploration tools throughout the property.

PREVIOUS GEOLOGICAL STUDIES

The High Lake Belt in the vicinity of the Ulu Claims has been the subject of few geological studies. The area was originally included in a 1:250,000 bedrock map of the MacKenzie area (Fraser, 1964). More detailed, 1:50,000 mapping of bedrock and glacio-fluvial deposits of the Hood River area, which included a portion of the Ulu claims, was conducted in 1984 (Jackson, et al., 1986).

No published detailed studies of gold occurrences in the High Lake Belt exist, although some work has been done on the other gold deposits within the Slave province. Padgham and Brophy (1985) classified gold deposits in the Slave Province according to their lithological associations: stratabound felsic-mafic hosted (e.g., Con, Giant), close to, or at contacts between sedimentary and volcanic lithologies (e.g., Salmita, Discovery, Tundra), turbidite hosted (e.g., Bullmoose Lake, Ptarmigan) and iron formation hosted (e.g., Lupin, B-Zone). Hypotheses regarding the genesis of these deposits are quite varied, and work done to date demonstrates the enigmatic nature of Archean deposits within the Slave Province.

The stratabound gold deposits within felsic to mafic volcanics occur as zones of silicification or of quartz veining within zones of shearing or alteration. Those deposits associated with intense chlorite/sericite shear zones (e.g., Con, Giant) have been the most prolific gold producers. The shear related deposits near Yellowknife are believed to have been formed by low salinity, CO2 rich, methane bearing metamorphic fluids (Allison and Kerrich, 1979; Myers, 1979; Kerrich and Fyfe, 1988) at the transition between greenschist and amphibolite grade rocks, with the physical control on mineralization being the boundary between brittle and ductile deformation associated with this transition (Helmstaedt et al., 1981).

The Lupin and B-Zone deposits occur within silicate-and sulphide-facies amphibolitic iron formation. Gold mineralization is associated with the sulphide facies and is localized by strong structural controls. Lhotka (1987) postulated that the Lupin deposit was epigenetic, with mineralization being formed by hydrothermal fluids after deformation and synchronous with peak metamorphic conditions. Alternatively these iron formation hosted deposits are considered by some authors to be syngenetic-exhalative derived from hydrothermal fluids during deposition or early diagenesis of the iron formation (Padgham and Brophy, 1985).

Gold deposits related to contacts between sedimentary and volcanic rocks generally occur within zones of structural deformation (Padgham, 1985). The origin of these deposits is not entirely clear, and several hypotheses have been proposed. At the Discovery Mine, the contacts formed loci for the development of dilatent structures during regional deformation, which suggests epigenetic mineralization by hydrothermal fluids (Wiwchar, 1957). Pagdham and Brophy (1985) disputed the age relations of Wichar and propose that the veins were syngenetic-exhalative entities which have undergone regional greenschist metamorphism. Studies at the Salmita Mine (Ransom and Robb, 1986) suggested that this deposit was also syngenetic-exhalative in origin.This was based upon the general stratabound character of the mineralization, enhanced footwall alteration, and the presence of a possible footwall stringer zone.

The turbidite hosted deposits are clearly epigenetic, occurring as concordant to discordant, structurally-controlled quartz veins (Padgham and Brophy, 1985). These deposits are widely considered to have been derived from metamorphic fluids. This hypothesis is supported by the lack of spatial association of these deposits with plutons, and by fluid inclusion work from turbidite hosted veins within the Yellowknife basin (English, 1981). The inclusions were shown to contain CO_2 rich brines with minor methane which are generally consistent with fluids of metamorphic derivation (Pagdham and Brophy, 1985). Swatton (1987) studied the turbidite hosted deposit at Bullmoose Lake, and using oxygen and deuterium isotopes, postulated that the mineralizing fluids were most probably of metamorphic origin.

PURPOSE OF THE PRESENT STUDY

The genesis of Archean gold deposits, whilst the focus of many studies in the past, is not particularily well understood. The diversity of these deposits has lead to a plethora of hypotheses regarding the sources of the mineralizing fluids, with metamorphic and magmatic models dominating.

Mineralization on the Ulu claims appears to exhibit a multistage history, with individual mineralizing events showing discrete temporal relationships to deformational and intrusive events. The primary focus of this study, aside from the documentation of mineralization in this remote area, was to investigate the timing, mineralogy, and fluid geochemistry of the various vein types which occur on the property, and to attempt to constrain the relationship between crustal processes and gold mineralization. The findings of this study might then be used to form the basis of a model which could be applied to further exploration in the High Lake Belt, or in analagous domains.

The enigmatic and at times ambiguous nature of Archean mineralization requires an integrated approach, as the use of one technique does frequently not allow the constraint of a model which convincingly explains gold mineralization. The following aspects of the deposits were proposed for study in order to accomplish the goal of establishing an integrated exploration model for mineralization on the Ulu claims:

1. Descriptions of major host lithologies, mineralization and alteration;

2. Temporal relationships of major intrusive and deformation events with respect to episodes of mineralization;

3. Characterization of mineralizing fluids and conditions of vein formation;

4. Relationship between mineralization types and tectonic evolution of the southern-central High Lake Belt.

Nine months were spent on the property during the 1990, 1991 and 1992 field seasons, during which time detailed and cursory examination of over 30,000 metres of drill-core, and examination/mapping of the auriferous showings was conducted. Samples representing host lithologies, characteristic mineralization and alteration suites were collected from both drill core and from surface showings throughout the property.

The techniques that were be used to study the Ulu mineralization are summarized as follows:

1. Examination of thin and polished thin-sections of host rocks, mineralization, and alteration, supplemented by whole rock, trace element and R.E.E. data;

2. U-Pb zircon dating of granitic plutons and feldspar porphyry dykes. The absolute dates determined were intended to allow relative dating of the various mineralization events through geologic relations observed in the field;

3. Stable isotope studies (O, H, C) of vein material to determine possible sources of these fluid components in order to assess the role of metamorphic and magmatic processes in the formation of the various veins.

2. REGIONAL GEOLOGY

THE SLAVE PROVINCE

Introduction

The Slave Structural Province (Figure 2-1) is an Archean craton covering an area of approximately 180,000 square kilometres of northern Canada. The Slave encompasses an elliptical area 600 kilometers wide by 710 kilometers long, and is bordered to the west by the Bear Province, to the south and east by the Churchill Province, and to the north by Proterozoic sediments overlying sialic crust. The Slave province was tectonically active from 3.4 Ga to 2.6-2.5 Ga, and aside from minor Proterozoic faulting and intrusive activity, it has remained a stable cratonic area since the end of the Archean. This overview is based largely on the work of Padgham (1985, 1992) who has published several comprehensive reviews of the lithological and tectonic evolution of the Slave province.

The Slave Province forms a granite-greenstone terrane consisting of 50% granite batholiths, and 50% supracrustals (Padgham, 1985) which occur as 26 linear, north-northwest trending belts. Supracrustal strata, which in part overlie gneissic basement complexes, have been grouped together as the Yellowknife Supergroup (Henderson, 1970). The Slave Province displays systematic differences with other Archean cratons of similar age (i.e., Superior Province). Most significant is the distribution of lithologies within the supracrustal belts, with greywacke-mudstone comprising up to 80%, as compared to 20% in other provinces. Furthermore, ultramafic rocks are volumetrically insignificant or absent within the Slave Province. Structurally, the Slave province lacks strong linear zonations compatible with plate tectonics processes (Padgham, 1992) observed within other Archean cratons (e.g., Superior Province, Thurston and Chivers, 1990; and Yilgarn Block, Barley and Groves, 1990).

Pre-Yellowknife Supergroup Rocks

Several areas of pre-Yellowknife Supergroup sialic basement rocks, consisting dominantly of tonalitic-trondjhemitic to granitic-granodioritic gniesses and migmatites, occur within the Slave Province (Padgham, 1985, 1992). The presence of these ancient rocks was suspected as early as 1968 when 4000 Ma lead was identified during isotopic studies of sulphide minerals in the Yellowknife area (Robertson and Cumming, 1968). The best documented pre-supracrustal basement

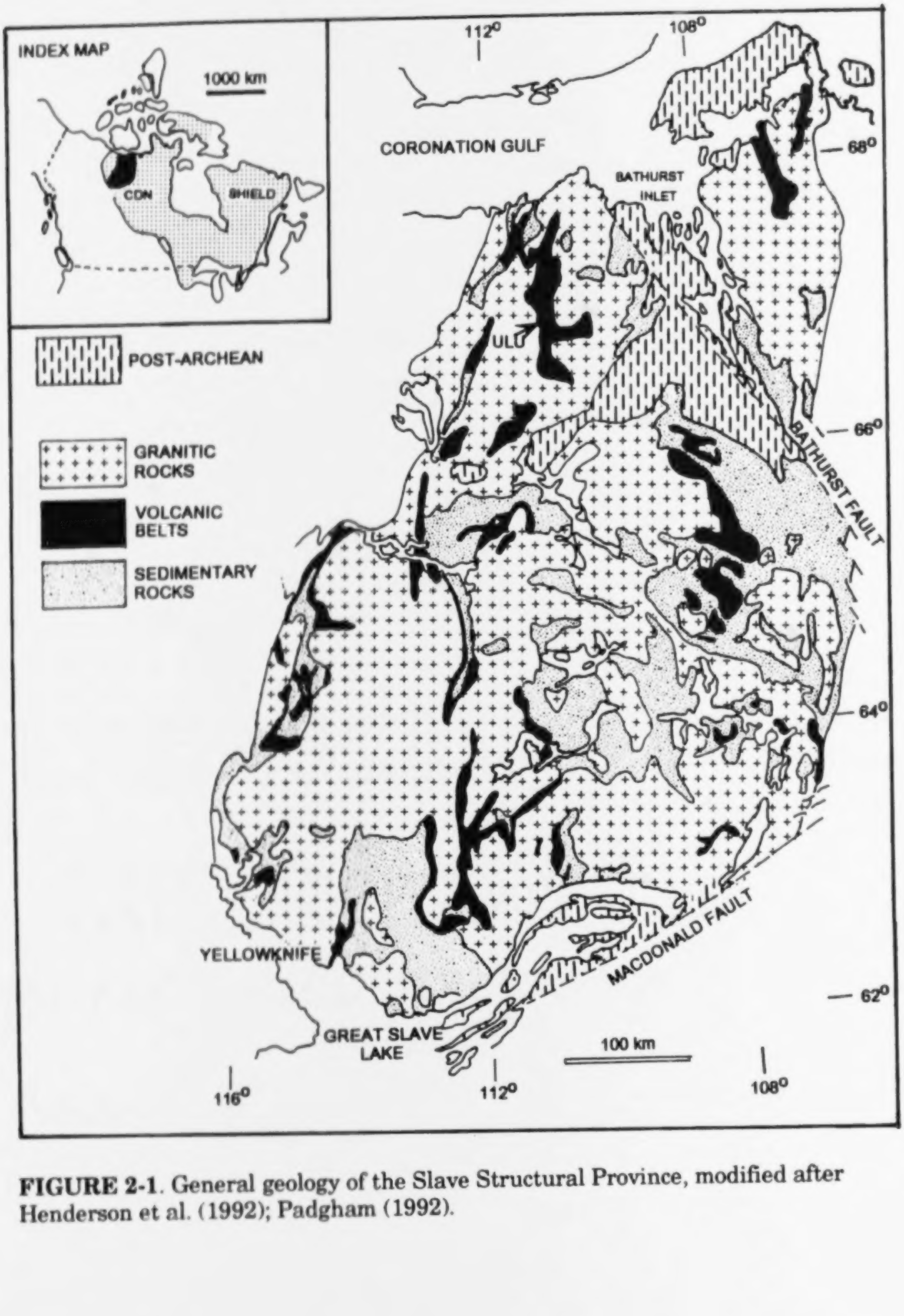
INDEX MAP
1000 km
CDN
SHIELD
POST-ARCHEAN
GRANITIC ROCKS
VOLCANIC BELTS
SEDIMENTARY ROCKS
112°
108°
CORONATION GULF
BATHURST INLET
68°
ULU
66°
BATHURST FAULT
64°
MACDONALD FAULT
YELLOWKNIFE
62°
GREAT SLAVE LAKE
100 km
116°
112°
108°

FIGURE 2-1. General geology of the Slave Structural Province, modified after Henderson et al. (1992); Padgham (1992).

occurs in the Point Lake area where Yellowknife supracrustals unconformably overlie 3700 Ma granodiorites and gneissies (Easton, 1985). While exposures of multiply deformed and metamorphosed rocks, thought to represent basement complexes, occur throughout the Slave Province (Padgham, 1985, 1992), their original extent is unknown. To date, occurrences of basement rock confirmed by isotopic dating (i.e., > 2900 Ma. Henderson et al., 1982; Easton, 1985; Frith et al., 1986; Bowring et al., 1989) are restricted to the western part of the Slave province. Pre-Yellowknife Supergroup basement may have originally been more widespread, however contacts with overlying supracrustals are commonly faulted and intruded by Kenoran syeno-granite batholiths which may have eradicated other basement complexes (Easton, 1985). The morphology of supracrustal successions within the Slave lends further support to the widespread occurrence of sialic basement. The sharp right angle bends that characterize the supracrustal belts are thought to reflect the edges of basement blocks that controlled the deposition of volcanics and sediments (Fyson, 1990).

Mature clastic sediments thought to pre-date the Yellowknife Supergroup, known as the Old Shelf Assemblage, overlie or are adjacent to basement gneisses in the west central Slave Province (Easton, 1985; Rice et al., 1990). Within the Beniah Lake area, Old Shelf Assemblage sediments consist of well rounded quartz pebble conglomerates to quartz arenites, and are interpreted as a shelf sequence derived from an older granitoid terrane (Rice et al., 1990). Quartz arenites of the Dwyer Formation, located beneath the north end of the Yellowknife greenstone belt, and in depositional contact with basement gneisses, contain detrital zircons yielding ages of 2.9 Ga to greater than 3.7 Ga (Isachsen et al., 1991).

Yellowknife Supergroup Rocks

The supracrustal rocks within the Slave province (Figure 2-1) are characterized by large turbidite domains including, and or partially bordered by, volcanic belts which are locally contemporaneous with sediment deposition (Padgham, 1992). The bulk of the metasedimentary rocks in the Slave are greywacke-mudstone turbidites, that interfinger with, but mainly overlie the volcanic belts (Fyson and Helmstaedt, 1988), Geochemical studies (Jenner et al. 1981; Easton, 1985; Lambert et al., 1990) indicate Yellowknife Supergroup volcanics have been the major source of sediments within the turbidites, however contributions from basement rocks are recognized in the Point Lake and Yellowknife areas.

Two types of volcanic belts are recognized within the Slave Province, the Yellowknife type, and the Hackett River type. The Yellowknife type occur within the west-central and southern portions of the province, and are characterized by a thick lower unit of mafic volcanics capped by felsic volcanic units (Padgham, 1985). The lower mafic units are predominantly massive and pillowed submarine flows with tholietic differentiation trends, which are locally characterized by an upward increasing calc-alkaline component, possibly due to contamination of tholietic magmas by sialic basement crust (Cunningham and Lambert, 1989; Barager, 1966). Compilation of U-Pb zircon dates (Mortenson et al., 1988) for felsic volcanics within the Slave Province indicate that the Yellowknife type belt volcanism occurred between 2675 and 2663 Ma.

Hackett River type volcanic belts, including the High Lake supracrustal belt, occur in the northern and eastern portions of the Slave province, and are characterized by a predomininance of felsic volcanic and pyroclastic rocks (Padgham, 1992, 1985; Easton, 1985; Kusky, 1989). These belts display calc-alkaline differentiation trends, and volcanism is dominated by felsic volcanic centers with remnant caldera collapse structures and synvolcanic intrusions (Lambert 1976, 1978). Whilst felsic volcanic rocks are dominant, a spectrum of compositions from basalt through rhyolite is present (Kusky, 1989) and mafic volcanic rocks are reported to occur at the top of the volcanic succession (Kusky, 1989; Padgham, 1992). U-Pb zircon dates for felsic volcanics in the Hackett River type belts indicates that volcanism occurred between 2698 and 2687 Ma (Mortenson et al., 1988). As an alternative to the occurrence of two distinct types of volcanic belts within the Slave Province, Tirrul and Bell (1980) suggested that the basal, mafic portion of the Hackett River type belts may have been selectively removed or assimilated by later granitoid rocks.

Archean Granitoid Rocks

Granitoid rocks which are coeval with, or postdate supracrustal assemblages underlie a large part of the Slave Province. Synvolcanic granitoid rocks are typically tonalites, trondhjemites, diorites and granodiorites, while later syn/post tectonic granitoids, are granitic to granodioritic in composition and often form large plutonic complexes with multiple intrusive phases (Padgham, 1992). Compilations of U-Pb zircon and monazite dates indicate two main intrusive episodes within the Slave Province, beginning with a syn-volcanic intrusive event at 2695 Ma to 2650 Ma, followed by syn-post tectonic plutonism at 2625 to 2580 Ma (van Breemen et al., 1991). The youngest post tectonic Archean granitoid rocks, abundant throughout the Slave Province, are strongly peraluminous and relatively rich in potassium. Late intrusives have been observed to truncate folding and cleavage, indicating that these plutons were diapirically emplaced, and reached present levels late in tectonic history (Drury, 1977; Fyson, 1982).

Structure and Metamorphism

Structural trends within Slave supracrustal rocks are generally curvilinear, with north-northeast trending fabrics in the western part of the province, and east to southeast trending fabrics in the east (McGlynn and Henderson, 1972). The rectilinear trends of the volcanic belts and the abrupt changes in these trends suggest that the volcanic rocks of the Slave were extruded along a system of old crustal fractures. As well, granitic intrusions bounding volcanic belts display similar rectilinear outlines, indicating granite emplacement may have been controlled by the same fracture system (Fyson and Helmstaedt, 1988).

Within the supracrustal belts, thick volcanic sequences form homoclinal panels that face away from bounding granitic rocks, while thin volcanic units occur in broad open folds paralleling those within metasediments (Fyson and Helmstaedt, 1988; McGlynn and Henderson, 1972). Slave Province greywacke-mudstone sequences record a complex history of late Archean deformation with 3 to 5 or more individual deformational phases being recognized (Padgham, 1992), generally with early, broad, isoclinal folds being overprinted by later small scale folds and foliations.

Shear zones occur within the volcanic sequences as chlorite-carbonate-sericite schists paralleling regional fabric, and along limbs, or within axial planes of tightly folded metasedimentary sequences (McGlynn and Henderson, 1972). Archean faults with several different ages and orientations occur throughout the Slave, and post Archean faults with northeast, northwest and northerly trends are common, and are likely coeval with Proterozoic diabase dyke emplacement. (McGlynn and Henderson, 1972).

All supracrustal rocks within the Slave Province have been metamorphosed to at least the greenschist facies, and cordierite bearing metasedimentary rocks indicate areas of higher metamorphic grade. Sillimanite has been identified within high grade migmatitic rocks in the Lac de Gras area (Folinbee, 1955). The high grade metamorphic supracrustals generally occur as broad halos surrounding late plutons and intrusive complexes (Padgham, 1992). Isograds defining these zones of higher grade metamorphism in the Contywoto Lake area, have been observed to cross large scale folds, while paralleling granitoid boundaries. This relationship indicates peak metamorphism was coeval with pluton emplacement and post-dates deformation in some regions of the Slave Province (Padgham, 1992, Davis et al., 1990).

Post Archean Intrusives

Evidence of Proterozoic activity in the Slave Province is restricted to volumetrically minor intrusive phases and associated faulting. Hoffman (1987) attributes the Proterozoic intrusive activity in the Slave to deep extensional faulting which tapped mantle sources during Proterozoic movement of the Slave craton. While Proterozoic intrusive complexes occur in the southern (peralkaline Blatchford Lake Complex and the Big Spruce Lake carbonatite) and northern (Booth River layered mafic-ultramafic complex) parts of the Slave Province, diabase dyke swarms are far more abundant.

Five episodes of Proterozoic diabase dykes and sheets intrude the supracrustals and granitoids of the Slave Province and these are summarized from McGlynn and Henderson (1972). The two oldest periods of dyke intrusion, at 2300-2400 Ma and 2000-2100 Ma, occur only within the Slave and are restricted to the southern part of the Province. The Mackenzie dyke swarm, dated at 1200 Ma, occurs throughout the western shield, and these dykes are the most abundant Proterozoic intrusives in the Slave Province. The dykes have a north-northwest strike and individual dykes may reach 30 metres in width. Two episodes of diabase sheet emplacement occur in the Bathurst Inlet region at 1400-1500 Ma and 600 to 700 Ma, and are restricted to northern portions of the Slave and Bear Structural Provinces.

Tectonic Evolution of the Slave Province

Models proposed for the tectonic evolution of the Slave Structural Province, can be divided into two general categories, ensialic rift models and accretionary models. Rift models in which Yellowknife Supergroup sediments were deposited in intracontinental rift basins with volcanism localized along marginal bounding faults have been suggested by McGlynn and Henderson (1972), Henderson (1981, 1985), and by Cunningham and Lambert (1989). Plate tectonic models have been proposed by Folinsbee et al. (1968), Helmstaedt et al. (1986), Hoffman (1986), Fyson and Helmstaedt (1988), and Kusky (1989). Evidence for formation of the

Slave Province by plate tectonic processes is not convincing (Padgham, 1992), mainly due to the lack of suture zones and strong linear zonations which would be typical of an accretionary model.

A growing body of evidence suggests that a model which incorporates more than one orogenic scheme is required to explain the tectonic evolution of the Slave Province (Padgham, 1992). In this model, early (3.0 Ga) subduction of oceanic crust from the east underplated the Slave, which at this time consisted of thin primitive crust in the east and thicker, more evolved sialic crust to the west. Uplift of the sialic crust resulted in erosion, and deposition of Old Shelf Assemblage arenites occurred along the boundary between the primitive and more evolved sialic crust. Later relaxation and thinning of both sialic and the primitive crust to the east, culminated in rifting and in the production of volcanics along northerly trending basement fracture zones.

THE HIGH LAKE BELT

The High Lake volcanic or supracrustal belt (HLVB) is located 445 kilometers north-northeast of Yellowknife (Figure 2-1) and is centered on longitude 118° 45' between latitudes 66° 30' and 67° 40' N. The belt extends north-south for 135 kilometers, and varies in width from 7 to 15 kilometers. Regional geological mapping in the High Lake belt was conducted in the mid-1980's by DIAND, and the G.S.C. began more detailed mapping in portions of the belt in 1992. The regional geology of the HLVB and the Ulu Claims area, located in the southern portion of the belt, are based on 1:250,000 regional (Jackson, 1991) and 1:30,000 local bedrock maps (Jackson et al.,1986), and updates on G.S.C. activities in the area (Henderson et al., 1993).

The supracrustals in the HLVB are surrounded by later, predominantly granitic intrusives, with minor deformed-metamorphosed rocks occurring peripheral to the supracrustals in the west-central part of the belt. The high grade rocks consist of banded orthogneisses, amphibolitic to tonalite-granodiorite in composition, and banded paragneisses of mixed sedimentary-volcanic origin. Jackson et al. (1986), state the gneissic rocks appear to be derived from the Yellowknife Supergroup.

The HLVB is considered to be of The Hackett River type (e.g., Padgham, 1985) and is thus characterized by a predominance of felsic volcanic rocks, although the ratio of felsic to mafic volcanics shows a systematic variation along the length of the belt. The volcanic sequence in the southern portion of the belt is dominated by mafic to intermediate pillows and pyroclastics, while the northern reaches are characterized by felsic tuffs and agglomerates. A similar variation is observed across the width of the HLVB with western portions containing the bulk of mafic volcanics present, while intermediate to felsic fragmentals and greywackes predominate in the east (Henderson, 1975). U-Pb zircon geochronology has established felsic volcanism in the HLVB at 2695±3 Ma north of the James River (Henderson et al., 1993) and at 2.96 Ga south of the James River in the Canoe Lake area (Mortensen et al., 1988).

Clastic metasediments ranging from greywacke to black argillites overlie and are interbedded with volcanics thoughout the belt, and carbonate rich sediments are found with metasedimentary and felsic volcanic rocks. A distinctive lithological association of mafic volcanics with greywackes, and intermediate-felsic volcanics with black argillites has been observed in the HLVB (Henderson et al., 1993). Stromatolites of Archean age overlying volcanic rocks are found at the contact between felsic volcanics and greywackes in the eastern portion of the HLVB, near Snofield Lake (Henderson, 1975).

Structurally the HLVB has been deformed into a major syncline with a subsidiary antiform in the central portion. Large scale folding is also present along the western, southwest, and northeast boundaries of the belt. Jackson (1991), attributed the N-NE trending isoclinal folds, including the regional syncline to a D_2 event. The prominent regional fabric is a NE trending schistosity that parallels major F_2 axial planes. Complex fault and fracture patterns with north-south and northeast-southwest trends occur in the HLVB, and major, discordant carbonate rich shear zones transect volcanic rocks in the Hood River and High Lake areas. Metamorphism of the supracrustals has generally reached greenschist facies increasing to amphibolite grade in the James River area, and is proximal to major intrusives in the remainder of the belt (Jackson et al.,1986).

THE ULU CLAIMS AREA

Introduction

The area containing the Ulu Claims (Figure 2-2) is located in the southern portion of the HLVB. Supracrustal rocks are surrounded and intruded by granitic intrusions, and an E-W trending apophysis of supracrustals extends eastwards along the Hood River. The supracrustal succession generally trends north-south and consists of dominantly mafic volcanics and greywackes in the west, overlain by

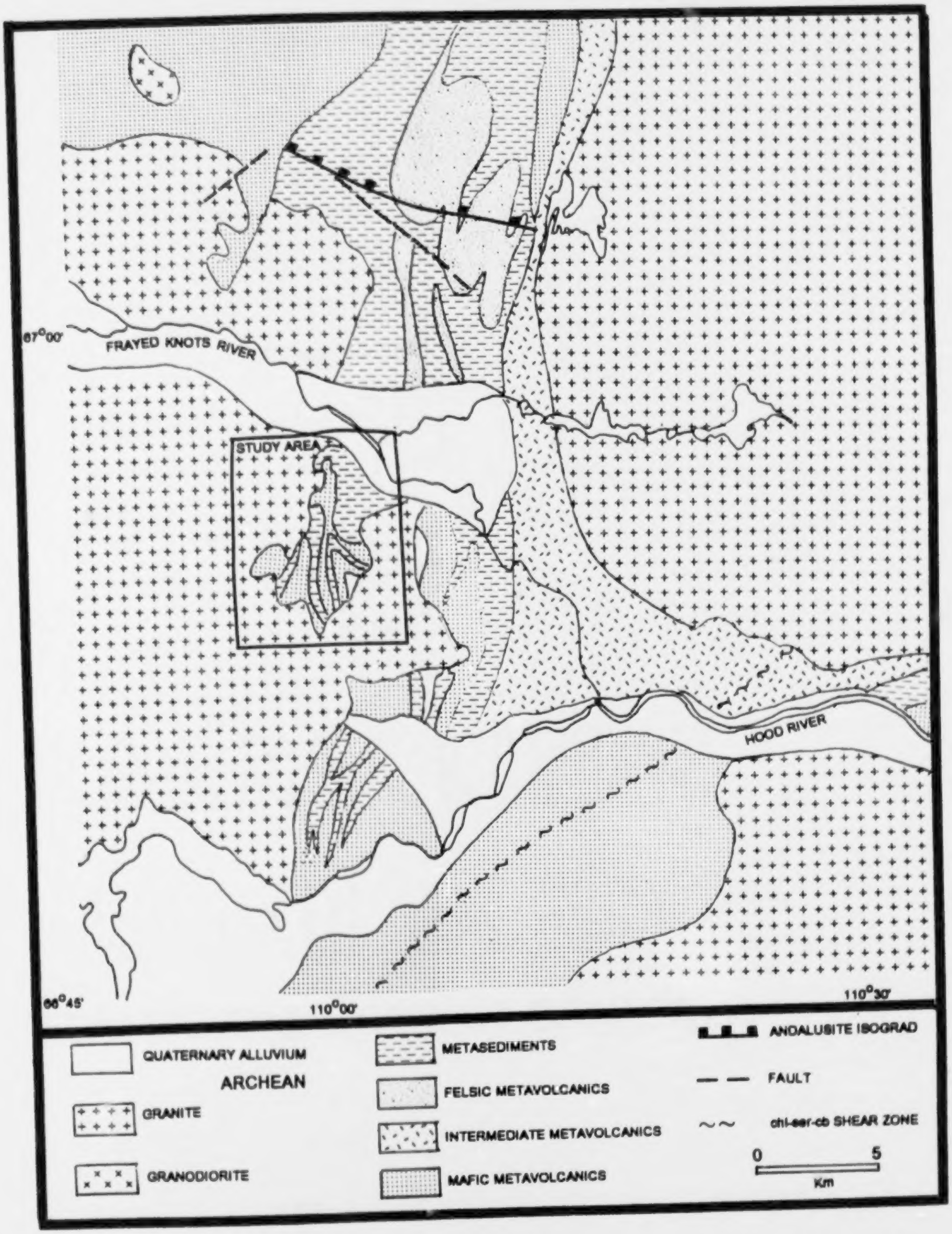
67°00'
FRAYED KNOTS RIVER
STUDY AREA
HOOD RIVER
66°45'
110°00'
110°30'
QUATERNARY ALLUVIUM
ARCHEAN
GRANITE
GRANODIORITE
METASEDIMENTS
FELSIC METAVOLCANICS
INTERMEDIATE METAVOLCANICS
MAFIC METAVOLCANICS
ANDALUSITE ISOGRAD
FAULT
chl-ser-cb SHEAR ZONE
0
5
Km

FIGURE 2-2. General geology of the Ulu Claims area, modified after Jackson et al. (1986); Henderson et al. (1993).

intermediate-felsic volcanics and black argillites to the east. Significant accumulations of mafic volcanics also occur at the extremity of the east trending apophysis of supracrustals, and are the dominant lithology south of the Hood River. A one kilometer wide arcuate zone of sheared, carbonate-sericite-chlorite bearing volcanics trends NE-SW occurs five kilometres south of the current study area. To date, no pre-Yellowknife Supergroup basement rocks have been recognized in the area (Henderson et al.,1993).

Supracrustal Rocks

The volcanic succession in the Ulu Claims area trends north-south, and individual units generally have steep, near vertical dips. Mafic volcanics and greywackes occur along the western margin of the supracrustals and are overlain to the east by intermediate-felsic volcanics and black argillites. Mafic and intermediate volcanics occur as massive and pillowed flows, commonly containing amygdules and plagioclase phenocrysts. Gabbroic intrusives, possibly representing local feeder dykes and subvolcanic sills, occur within and are folded along with mafic volcanic flows. Intermediate pyroclastics (lapilli tuffs) are found predominantly in the central portion of the belt and make up the bulk of volcanics in the area. Felsic volcanics are predominantly lapilli to ash tuffs, with minor porphyritic dacites and quartz eye rhyolites, and are most abundant to the east, although a relatively thin felsic unit occurs between sediments and intermediate volcanics to the west.

Exposed sedimentary rocks are abundant along the western margin of the area and consist of a graded greywacke-mudstone succession. Graded beds 1.0 to 0.10 metres thick are primarily greywackes and impure sandstones, capped by pelitic tops. Finer grained argillites associated with intermediate-felsic volcanics, are mainly thinly bedded black, graphitic-sulphidic slates and light grey siltstones, commonly with preserved primary sedimentary structures (Henderson et al., 1993). Sedimentary rocks proximal to mafic volcanics may contain lenses of amphibolite, derived from interbedded mafic lavas and gabbroic dykes. Near the contacts with intermediate-felsic volcanics, sediments are interbedded on a centimeter scale with felsic tuffs. The intercalated nature of sediments and volcanics suggest that the bulk of sedimentation in the area was coeval with volcanism.

Plutonic Rocks

At least two episodes of intrusive activity are indicated by cross-cutting relationships observed within plutonic rocks. Early intrusive rocks include 1) gabbro, quartz-diorite and hornblendite found within supracrustals but more commonly forming rafts in younger granitoids, and 2) mixed terranes of granite-tonalite and strongly foliated, melanocratic granite (Jackson, et al., 1986). A similar progression of Late Archean plutonism is observed in the Lac de Gras area (Folinsbee, 1955). Later intrusive rocks, comprised of granite to granodiorite, are more leucocratic than the earlier suite and form distinct plutons with well defined boundaries. A multi-episodic history of progressively evolving granites are suggested by the emplacement of the late intrusive suite. Two mica granites cross cut biotite-hornblende bearing megacrystic granite, and all later granitoids are cut by pegmatitic dykes (Jackson et al., 1986). The granite plutons bounding the HLVB are commonly discordant with the strike of layering in the adjacent supracrustal rocks, and generally are not foliated. However, minor foliation may occur in these granites for up to 100 metres from the supracrustal contact, where their boundaries are concordant with the layering in the country rocks (Henderson, et al., 1993). Several small, biotite bearing granodiorite plutons, containing discrete zones of foliation, occur within mafic volcanic dominated portions of the supracrustal succession, however the relationship between these plutons and other intrusives in the area is not known (Henderson et al., 1993).

Two episodes of post-Archean volcanic activity are indicated by presence of diabase dykes which crosscut all Archean lithologies. East trending dykes, possibly correlative with the 2.45 Ga Hearst-Matachewan swarm (Henderson et al., 1993), contain relict pyroxenes and plagioclase phenocrysts in a fine grained, green chloritic matrix, and are commonly altered and recrystallized. North-northwest trending dykes probably correlative with the 1.27 Ga Mackenzie swarm (Henderson et al., 1993), do not display significant alteration or recrystallization, and post-date east trending diabase dykes, and some post Archean faulting (Jackson et al., 1986).

Deformation, Structure and Metamorphism

Deformation within the Ulu Claims area is polyphase, with the earliest structural fabric recorded in the area being a weak cleavage D_1/S_1, which parallels, and is folded along with bedding and flow layering (S_0) in later D_2 folds (F_2). The F_2 folds form large scale features within the south central HLVB and are steeply plunging, tight to isoclinal, and lack associated axial planar cleavages (Henderson et al., 1993) In the Ulu Claims area, F_2 folds are dominantly north trending, and show stronger development in the western, mafic-sediment dominated portion of the HLVB, than in eastern intermediate to felsic volcanic rich domains. F_2 axial surfaces are strongly overprinted by a final D_3/S_3 event, which is manifested as small scale crenulations and a northeast-southwest trending schistosity.The D_3/S_3 is the main structural fabric observed within the area, and is particularly well developed within the metasediments. Emplacement of the granite batholiths bounding the HLVB postdates D_3 fabrics (Henderson et al., 1993).

Northeast-southwest and east-west trending lineaments, some with demonstrable fault offset occur within the area. Some lineaments are occupied by Archean quartz feldspar porphyry dykes, while others contain Proterozoic diabase dykes which continue from the supracrustals into late granitoids, this being suggestive of a Proterozoic movement history.

Metamorphic grade increases from north to south in the Ulu Claims area, and varies from lower greenschist to upper amphibolite, as determined from assemblages in metasediments (Jackson et al., 1986). Greenschist grade rocks contain biotite and muscovite, and cordierite marks the beginning of the lower amphibolite facies. Andalusite and garnet may also occur within the lower amphibolite rocks. Middle amphibolite facies sediments are characterized by the presence of sillimanite and are found proximal to late granite plutons (Jackson et al., 1986). Upper amphibolite facies rocks occur as paragneisses and orthogneisses possibly derived from the supracrustals and coeval granitoids, and are present as enclaves within late granitoid terranes (Jackson et al., 1986).

An andalusite isograd trending east-west occurs north of the Ulu Claims area, and metamorphic grade increases from north to south (Henderson et al., 1993). The trace of this isograd is not symmetrical with the north-south outline of the granites bounding the belt. Peak metamorphic minerals (cordierite and andalusite) within the amphibolite grade rocks developed during a period of static regional porphyroblastesis, and preserve trails of S_0 and S_1 cleavage that are overprinted by D_3 cleavages, indicating that peak metamorphism predated both D_3 deformation and late granite emplacement (Henderson et al., 1993).

3. GEOLOGY OF THE ULU CLAIMS

INTRODUCTION

The Ulu Claims cover a lobe of supracrustal rocks on the western boundary of the southern HLVB. The supracrustal sequence consists of mafic to intermediate volcanics, cogenetic gabbro sills, and greywacke-mudstone turbidites which have been folded into a north-south trending antiformal structure (Figure 3-1). All the supracrustal rocks have been metamorphosed to at least lower amphibolite facies, however precursor lithologies are readily identifiable. The prefix meta therefore, has been dropped in subsequent discussions. The western edge of the supracrustal lobe is bordered by an extensive granitic pluton. To the east, the supracrustals on the Ulu claims are partially bounded by a granitic embayment which separates it from the rest of the HLVB, and greywackes surround volcanic rocks to the north. The supracrustals on the claims have been intruded by a syn-tectonic suite of granitoid dykes and plugs which range in composition from trondhjemite to granodiorite. Pegmatite and aplite dykes associated with late post-tectonic bounding granites also transect the supracrustal succession.

A geological and petrographic study of the host rocks was undertaken to examine the relationship between the mineralization types and the petrogenetic evolution of the supracrustal and intrusive rocks within the Ulu claims. Surface outcrops, drill core, hand specimens, and thin and polished thin sections were examined in order to investigate the mineralogy and petrology of host rocks, alteration, and mineralization contained within the Ulu Claims. The geologic and petrographic studies provide a necessary framework for the interpretation of geochemical data, and the development of a spatial and temporal genetic model for the mineralization on the Ulu Claims.

HOST ROCK GEOLOGY-PETROGRAPHY

Supracrustal Rocks

Volcanics

Volcanic rocks compose approximately 35% of the supracrustals within Ulu Claims. The volcanic units are dominantly mafic (basaltic) in composition although slightly more intermediate (basaltic-andesite to andesite) varieties occur. Volcanic rocks of intermediate to felsic compositions are not found within the Ulu Claims.

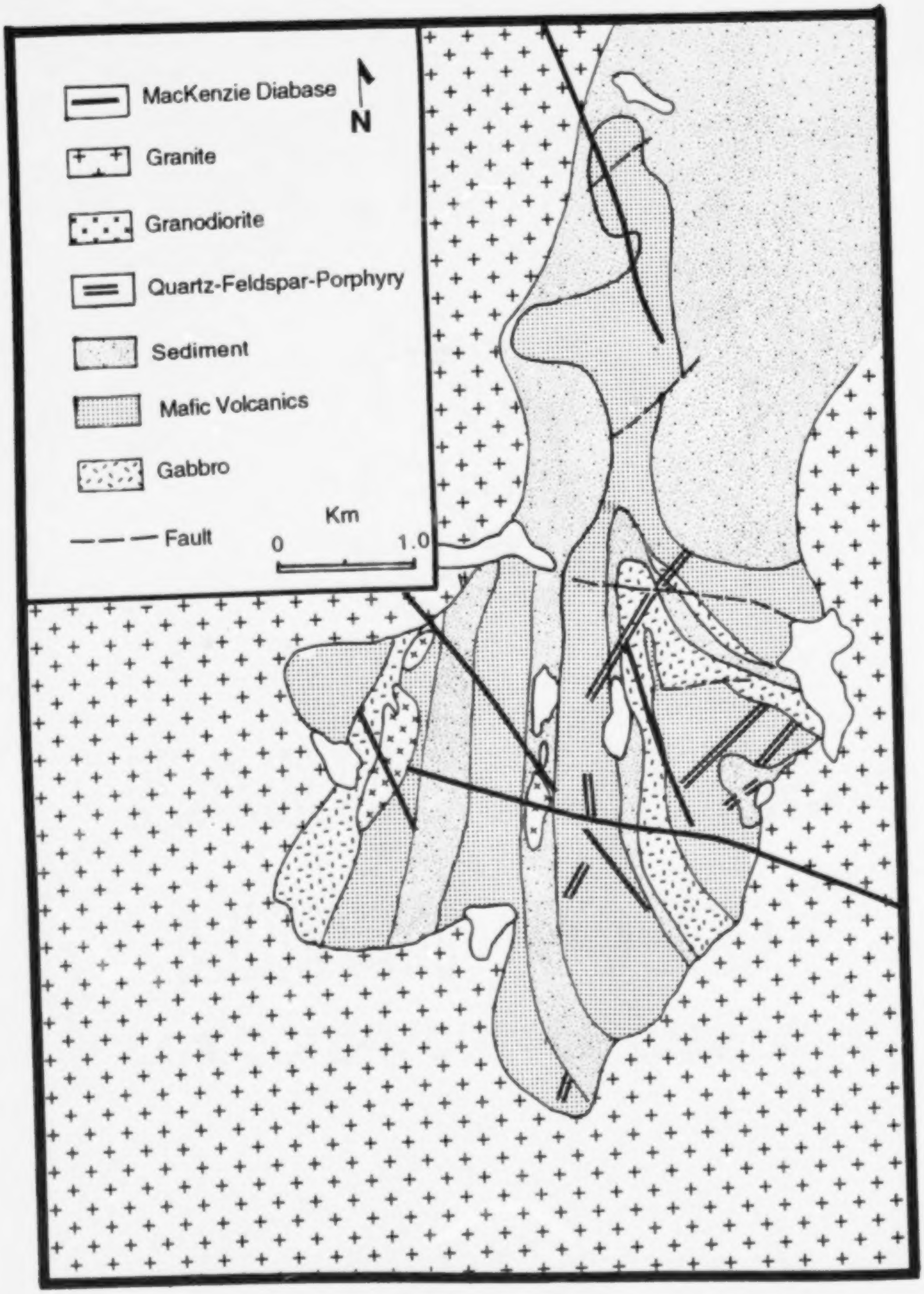
MacKenzie Diabase
N
Granite
Granodiorite
Quartz-Feldspar-Porphyry
Sediment
Mafic Volcanics
Gabbro
Fault
Km
0
1.0

FIGURE 3-1. General geology of the Ulu Claims, modified after Flood et al. (1991); Henderson et al. (1993).

The mafic volcanics are dense, dark green to black on weathered and fresh surfaces respectively, and are comprised of massive and pillowed flows, and minor pyroclastic or detrital units. The intermediate volcanics are distinguished from mafic compositions by their grey color and lower density, and occur as pillowed flows primarily within the western portion of the claims.

Pillow selvages are generally poorly preserved in surface outcrops, and occurrences on the western limb of the antiform indicate that volcanic stratigraphy youngs to the northwest (Flood et al., 1991). In drill core, pillow selvages are common in the mafic sequences, and occur as silicified breccias or biotite-almandine garnet segregations, and quartz/amethyst-calcite-epidote-tourmaline assemblages. Carbonate rich flow top exhalites and silicified flow top breccias are also present within the volcanic successions.

In drill core, mafic volcanics are interbedded with thin greywacke horizons, and the pyroclastic/detrital units are found near the contacts, though these units are not distinguishable on the surface. Pyroclastic/detrital units are distinguished by their higher biotite content, and the presence of almandine garnet, or less commonly cordierite porphyroblasts. Thin biotite units equivalent to those at contacts also occur throughout the volcanic stratigraphy and appear to represent local sediment accumulations during brief hiati in volcanism. The almandine garnet serves to distinguish tuffaceous and pelitic lithologies from biotite rich alteration assemblages.

Petrographic examination of dark green to black unaltered mafic volcanic rocks collected from drill-core reveals fine grained amphibolites composed primarily of hornblende and plagioclase with minor quartz and opaques (ilmenite). Grain size varies from 0.1 to 1.0 millimetres. Grain size within massive flows is gradational into gabbroic rocks, and are thought to be more slowly chilled flow cores or feeder dykes. The volcanic rocks have palimpsest textures indicative of quickly chilled basalts and include intersertal groundmass textures between larger grains and radiating spherical arrangements of hornblende crystal aggregates. Amygdules are common within the mafic flows and vary in size from several millimeters to 2 centimeters. The amygdules are composed of plagioclase and quartz, and commonly poikioblastically enclose small, green to blue green euhedral hornblende crystals and minute, crystals of anatase.

Euhedral to subhedral, lath to diamond shaped hornblende typically composes 65% of the mafic volcanic rocks, and exhibits pale yellow to dark green, or blue-green pleochroism. Plagioclase composes 25% of the rock, and albite twins are common in this mineral. Examination of the albite twinning indicates oligoclase (An_{15-25}) is the most dominant plagioclase composition. Quartz consists of small, anhedral, strain-free grains and constitutes less than 5% of the mafic volcanics examined. Opaques comprise up to 10% in these rocks and consist primarily of ilmenite, but pyrrhotite and pyrite are locally abundant as fine disseminations, especially as broad halos surrounding Type II mineralization.

Veining and alteration are extensive within the volcanic sequence, and aside from the widespread pervasive alteration associated with Type II mineralization (Chapter 6), several distinct types of alteration are present and can be classified on the basis of mineralogy and apparent temporal relationships. The earliest veins bear a calc-silicate assemblage (vesuvianite + grossular + quartz + calcite). These veins likely represent early alteration of the volcanic pile and have been metamorphosed along with their host rocks. Another set of veins with mineral assemblages observed in pillow selvages, quartz-amethyst-calcite-epidote (clinozoisite)-tourmaline (schorl) are also common and are thought to represent early metamorphic veins. Thin veinlets, generally less than 1 centimeter wide, of coarsely crystalline black tourmaline with pyrite-pyrrhotite occur within the volcanics and the density of these veinlets increases in abundance proximal to quartz-feldspar porphyries. The relationship between these veins and the dykes however is not clear. The youngest alteration observed within the volcanics is a retrograde assemblage consisting of relatively thin 0.1-0.75 metre bands of green-brown sericite and chlorite. These alteration bands are centered on small veinlets of white calcite, and are possibly associated with emplacement of Proterozoic diabase dykes.

Sediments

Sedimentary rocks underly approximately 40% of the Ulu Claims. In the southern portion of the claims, sediments are intercalated with mafic volcanics and gabbros, and occupy the core of the major F_2 antiformal structure. In the northern part of the claims, sediments form extensive terranes surrounding mafic volcanics. Sedimentary packages are characterized by recessive weathering and form extensive terranes of grassland and felsenmeer with limited outcrop exposures. Sedimentary lithologies found on the Ulu Claims are ubiquitously brown to grey, rusty weathering greywacke-mudstone turbidites, with localized areas of knotted schists containing cordierite and/or andalusite porphyroblasts. Contacts between sediments and volcanics are generally sharp, although some gradational contacts as mentioned above are present.

Within drill core, sediments occur as thick sequences of 1-2 metre greywacke bands capped by thin mudstone horizons up to about 50 centimetres thick. Drilling encountered these turbidite sequences in a top-up position in the west limb of the antiformal structure. Biotite and muscovite crystals within the greywacke show a strong preferential orientation (S_1) and define a moderate to strong fabric within these sediments that is overprinted by a D_3 crenulation cleavage, especially within the finer-grained pelitic bands. The mudstone bands commonly contain cordierite and less commonly almandine porphyroblasts. The abundance of the aluminosilicate porphyroblasts appears to be a function of the pelitic component within the sediments. Cordierite often displays preferential elongation that parallels the bedding (S_0) and early cleavage (S_1) directions (Henderson et al., 1993). Alteration within the sediments encountered in drill core, aside from that associated with mineralization, is manifested by pinitization of cordierite and bleached (chlorite-sericite) halos surrounding generally millimetre scale quartz veins.

Petrographic examination was carried out on sediments interbedded with mafic volcanics collected from drill core, and on those collected on surface from the core of the anticline proximal to the contact with the mafic volcanics. Lower greywacke sequences consist of poorly sorted 0.1 to 0.5 millimetre grains of quartz, feldspar, biotite, muscovite, and minor felsic rock fragments. The mudstone tops show an overall decrease in grain size to an average of 0.10 millimetre, and a increase in modal abundance of biotite and muscovite. The mudstone tops in the sections observed consist of repeating centimetre scale, fining-upward sequences, with cordierite porphyroblasts within the uppermost portion of each sequence. Cordierite porphyroblasts generally show incipient development and poikioblastically enclose small euhedral muscovite and biotite crystals. Pressure shadow overgrowths consisting of relatively coarse grained biotite often surround the cordierite crystals.

Gabbro

Gabbroic rocks underlie approximately 10% of the Ulu Claims and occur in two forms: as thick horizons intercalated with sediments and mafic volcanics, and as irregular bodies within mafic flows. Thick gabbro horizons are concordant with sedimentary and volcanic layers, and appear to have been folded along with the other lithologies. The thick horizons likely represent subvolcanic sills which were comagmatic with mafic volcanics (see Chapter 4), and are thus considered to be part of the supracrustal succession. Chilled margins are present within the gabbro flows adjacent to sharp contacts with the sediments. Due to the compositional similarity between the volcanics and their coarser grained equivalents, contacts between gabbros and mafic volcanics are generally less distinct than those with sediments. Gabbro sills form regions of prominent outcrop and weather with a characteristic 'leopard skin' pattern. Small irregular bodies of microgabbros occur within mafic sequences, and are interpreted as coarser grained cores of massive flows and as feeder dykes associated with pillowed flows. These microgabbros are geochemically (Chapter 4) indistinguishable from their hosts. Alteration other than that associated with the Type II mineralization is sparse within gabbroic rocks. Millimetre scale quartz±calcite veinlets surrounded by broad halos of patchy leucoxene after ilmenite are the most prevalent epigenetic alteration observed within these rocks.

Petrographically the microgabbros are mineralogically and texturally identical to the mafic volcanics, but are coarse-grained enough to warrant distinction from their finer grained equivalents. Petrography of the gabbro sills indicate these rocks are composed of 60% pale green to blue-green hornblende, 20% plagioclase (oligoclase An_{25}), 5-10% quartz, 5-10% opaques, and 5-10% biotite. Grain size is variable, and within the coarsest units individual hornblende laths may reach 1.0 centimetre. Opaque minerals (ilmenite-magnetite?) occur as skeletal grains within hornblende crystals and ubiquitously have biotite overgrowths, which in some cases are visible in hand specimens forming biotite porphyroblasts. The biotite is a red-brown titanium rich variety, which suggests that the bulk of the opaques are a titanium-bearing phase such as ilmenite. Symplectic intergrowths of plagioclase and quartz are present within coarse grained gabbro thin sections. Glomeroporphyritic varieties of gabbro are also present, with individual glomerocrysts consisting of plagioclase and quartz, often reaching several centimeters in size within coarser grained varieties. Zircon is a common accessory phase within gabbroic rocks, forming pleochroic halos within the biotite overgrowths.

Intrusive Rocks

Two major intrusive suites occur on the Ulu Claims, and members of each suite are distinguished primarily on the basis of geochemical criteria (Chapter 4).

An early suite (termed the 'internal suite'), which occurs totally within the supracrustals, can be further subdivided based on composition and occurrence, and consists of quartz-feldspar porphyry dykes with associated grey aplites, and granodiorite plugs and associated dykes. A later suite (the 'external suite') of granite to granodiorite plutons bound the supracrustals, and associated pegmatite and aplite dykes originating from these plutons intrude the supracrustals. Two types of Proterozoic diabase dykes are found on the Ulu Claims; both a single Hearst Matachewan swarm dyke, and multiple MacKenzie dykes cross-cut all supracrustals and Archean intrusive rocks.

Internal Granitoid Suite

Quartz Feldspar Porphyry Dykes

Intermediate felsic dykes mapped in the field as quartz-feldspar porphyries, are concentrated mainly within the southern, open end of the large D_2 antiform (Figure 3-1). These dykes are rusty weathering, and consist of white plagioclase phenocrysts and bluish quartz eyes in a fine-grained medium-grey matrix (Plate 3-1a). Individual dykes may be up to 30 metres in width and occur as a conjugate set trending 055° to 060° and 160° to 170°, which crosscut the D_2 antiformal structure. The quartz-feldspar porphyry dykes occupy linear features which may represent Archean faults, and also often occur at volcanic-sediment contacts. A large, continuous dyke oriented 060° 55° was encountered during drilling of the Flood Zone, and smaller dykes were frequently encountered in peripheral drillholes, particularly at volcanic-sediment contacts. The dykes in drill core exhibit chilled margins and are texturally variable, a characteristic which appears to be largely a function of dyke width and cooling history. Contacts between the quartz-feldspar porphyry dykes and wallrock of all lithologies are sharp and well defined, and small offshoots are common peripheral to larger dykes. Biotitization frequently occurs adjacent to the dykes within mafic volcanics, and small angular fragments of biotite-altered mafics occur within the dykes proximal to the contacts. It is not clear whether this alteration is associated with dyke emplacement or is a result of the dykes intruding previously altered volcanics.

The quartz-feldspar porphyry dykes largely appear to crosscut Type II mineralization. Weak shearing and minor arsenopyrite may occur within the dykes proximal to contacts with mineralized zones. Commonly the dykes are observed to occur as swarms of smaller dykes within the mineralized zones. This is indicative of limited dilatancy within these zones during dyke emplacement. The relationships between the quartz-feldspar porphyry dykes and Type II mineralization suggest that dyke emplacement occurred very near to the end of the mineralizing event. Furthermore, the emplacement of these dykes at sedimentary volcanic contacts, also a site of Type II mineralization, suggests similar dilatencies controlled the emplacement of both mineralization and the dykes, and supports a close temporal relationship between these two geological events.

Small mineralized Type III veins occur within the quartz-feldspar porphyry dykes as breccias and stockworks, and as thin veins at dyke-wallrock contacts. The dykes also commonly contain millimetre to centimetre scale quartz±hornblende veinlets with pale green to white bleached halos, although the affinity of these veinlets is not clear. Foliation manifested by alignment of biotite, plagioclase and quartz phenocrysts (Plate 3-1b) is locally present within the feldspar porphyry dykes and may be attributable to regional D_3 deformation.

Twelve thin sections representing the various textural varieties of the quartz-feldspar porphyry dykes were examined. Compositionally the dykes consistently contained quartz, sodic plagioclase, biotite, muscovite, microcline, and opaques. Retrograde alteration was observed in 11 of the sections. The grain size of matrix varied from 0.10 to 0.50 millimetres and plagioclase phenocrysts and quartz eyes occur up to 5 millimetres, although the abundance and size of the phenocryst phases is highly variable and causes the textural diversity observed within these rocks.

Modally the quartz-feldspar dykes contain 45% quartz, 40% plagioclase (oligoclase An_{15-20}), 10-15% biotite, 1% opaques (pyrrhotite), and trace amounts of muscovite and microcline. Zircon and apatite are relatively common accessory phases. Plagioclase occurs both within the matrix and as phenocrysts. It is commonly albite twinned and large phenocrysts may display oscillatory zoning (Plate 3-1c). Plagioclase within these rocks is commonly altered to a fine-grained assemblage of sericite and calcite, which gives the phenocrysts a white appearance in hand specimen. Minor symplectic intergrowth of quartz and plagioclase occurs within the groundmass. Quartz also occurs within the groundmass and as a phenocryst phase. Quartz eyes are invariably strained, although the degree of deformation is variable, ranging from completely recrystallized aggregates (Plate 3-1d) to moderately strained single crystals. Contacts between grains in the aggregates are embayed to sutured, and incipient subgrain development and mortar structures may be present. Biotite occurs as single crystals up to 1

Plate 3-1

3-1a 90VD-44 (292.7m)
Quartz-feldspar porphyry from drill-core. Note large zoned plagioclase phenocryst.

3-1b 90PAK-QFP
Foliated quartz-feldspar porphyry from a surface exposure proximal to Flood Zone mineralization.

3-1c Photomicrograph, (xpl), 90VD-44 (292.7m)
Zoned/twinned plagioclase phenocryst with weak sericite-carbonate alteration, in a fine-grained quartz+plagioclase+biotite matrix.

3-1d Photomicrograph, (xpl), 90VD-44 (292.7m)
'Quartz eye' consisting of an aggregate of recrystallized, equant quartz grains.

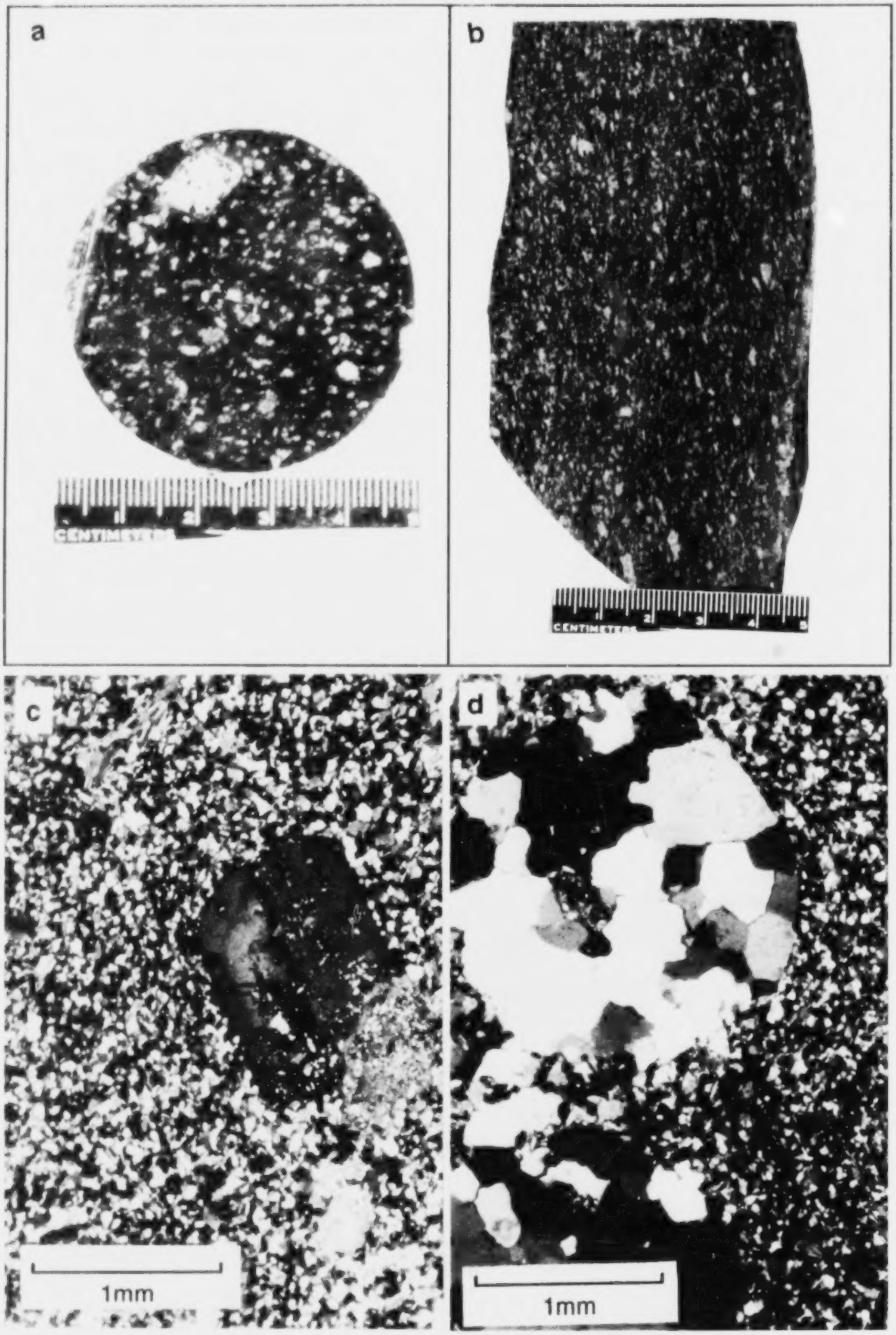
a
b
c
d
CENTIMETERS
1
2
3
4
5
1mm
1mm

millimetre in length, or as masses of fine crystals often reaching several millimetres. The biotite is partially to completely altered to chlorite.

Grey Aplite Dykes

Grey aplitic dykes, geochemically consanguineous with the quartz-feldspar porphyry suite (Chapter 4) occur within the drill core. Especially prevalent within fault structures, they are common proximal to Type II mineralization and associated dilational zones at the volcanic-sediment contact within the core of the antiformal structure. Though buff varieties have been noted, these dykes are medium grey, and are composed of an aphanitic groundmass with 10% phenocrysts (dominantly quartz) which are up to 2 millimetres in size (Plate 3-2c).

Petrographically, the grey aplite dykes are texturally similar to the quartz-feldspar porphyries (Plate 3-2d), though the mean grain size of the matrix is much smaller, being 0.01 to 0.10 millimetres, and there is an increase from the quartz-feldspar porphyries in the modal abundance of quartz. These rocks are composed of quartz, plagioclase (oligoclase An_{15-20}), biotite, muscovite, and pyrite occurs as an opaque phase. Plagioclase is altered and turbid, which is attributed to a very fine grained assemblage of sericite and calcite. Biotite is commonly altered to chlorite. A single sample of a grey aplitic dyke contained 10% muscovite as single grains which were orientated, and imparted a foliation to the rock. The phenocrysts occur as quartz eyes and as quartz-plagioclase-muscovite glomerocrysts, and show a weak alignment. Quartz within the phenocrysts is strained and partially recrystallized, and sutured boundaries between adjacent grains are common. Late, millimetre scale, irregular calcite veinlets occur, and are discordant with respect to other fabrics within the grey aplites.

Granodiorite

Several small plutons and associated dykes, mapped as granodiorite, occur within the supracrustal succession, and are spatially restricted to the western part of the Ulu Claims (Figure 3-1). This intrusive suite includes the granodiorites noted by Henderson et al. (1993). These plutons have been intruded into a sequence of gabbros and sediments, and unless they represent sills, these intrusives postdate D_2 deformation. The granodiorite plutons appear to be relatively concordant with layering of the supracrustals, and display a foliation which is concordant with D_3 fabrics in surrounding supracrustal rocks.

A series of dykes occur within the sheared sedimentary and gabbroic rocks and appear to be associated with the granodiorite plutons. Orientation of the dykes are generally in a north-south direction paralleling regional D_3 cleavage, and the contacts with the wallrock are sharp. These dykes are generally trondhjemitic in composition, and show a geochemical affinity (Chapter 4) to both the granodiorite and the quartz feldspar porphyries. Type III mineralization occurs within the sheared rocks hosting these dykes, and some veining occurs at the margins of the dykes.

The granodiorites are pervasively altered, and orange in color on both weathered and fresh surfaces due to iron staining (Plate 3-2a). Petrographically these intrusives are composed of 40-50% quartz, 30-35% plagioclase (composition unknown), 10-5% microcline, and 10% biotite, with zircon and pyrite as accessory phases. Texturally the granodiorites are holocrystalline and phaneritic with a grain size of 1-2 millimetres, and contain quartz eye phenocrysts to 7.5 millimetres. Biotite occurs as masses of fine grained crystals. These rocks are pervasively altered (Plate 3-2b), and a distinct fabric is apparent in hand specimen, showing elongation of the quartz eyes. Quartz within these rocks is variably strained, and in part recrystallized, with sutured grain boundaries and mortar structures. The feldspars, particularly the plagioclase, are heavily altered and turbid, and contain fine-grained sericite, muscovite and clinozoisite. Late millimetre scale fractures cross-cut and are discordant to the fabric in these rocks.

Dykes associated with the granodiorite are generally narrow (> 1.0 metres) and contacts with wallrock are sharp. These dykes are grey in color, and are composed of 45% quartz, 30% microcline, 15% plagioclase (composition undetermined), and up to 10% biotite, with zircon and apatite as accessory phases. Texturally these dykes are medium to coarse grained, holocrystalline and granoblastic. The coarser grained dykes, contain more biotite and are weakly porphyritic. The phenocryst phase consists of euhedral plagioclase crystals to 5-6 millimetres, which display convolute zoning. The feldspars in all varieties are weakly to moderately altered, and contain sericite and muscovite.

External Granitoid Suite

The late granitoid rocks are those which bound the supracrustal succession and associated aplitic and pegmatitic dykes. These plutonic phases occur to the west and north of the Ulu Claims, and include the lobe of granitoid rock which separates the portion of the HLVB containing the Ulu Claims from the main part

Plate 3-2

3-2a 92VKT-4204
Handspecimen of internal suite granodiorite from surface occurrence, showing strong iron staining and late microfractures. Note weak foliation defined by elongation of biotite grains.

3-2b Photomicrograph, (xpl), 92VKT-4204
Typical altered textures displayed by internal suite granodiorite. Note extreme turbidity within sericite-carbonate altered feldspars.

3-2c 90VD-44 (565.5m)
Specimen of grey aplite from drillcore.

3-2d Photomicrograph, (xpl), 90VD-44 (565.5)
Microtextures displayed by grey aplites. These rocks are texturally similar to the quartz-feldspar porphyries, however they lack significant plagioclase or biotite phenocrysts. Note small 'quartz eyes'.

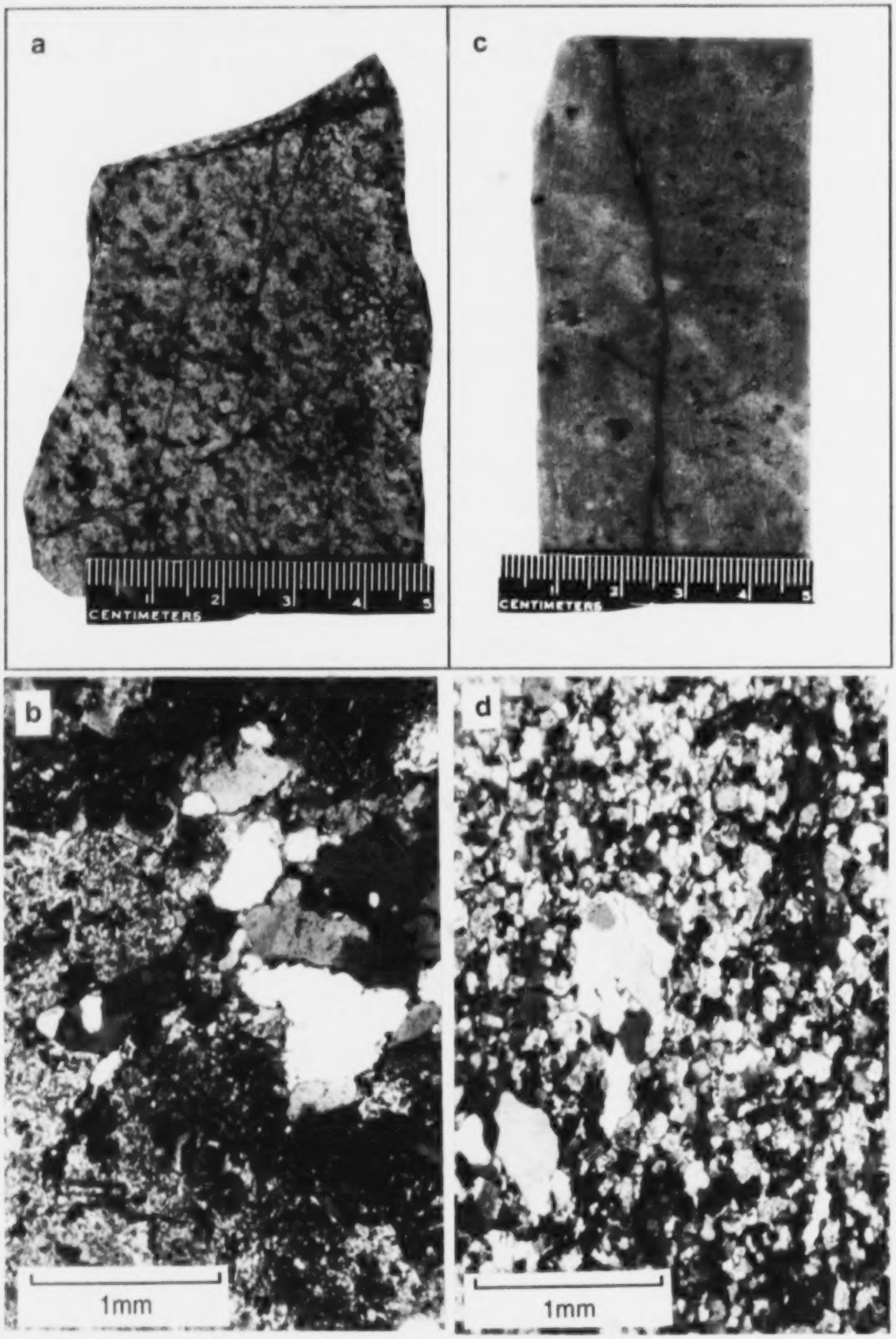
a
CENTIMETERS
1
2
3
4
5
c
CENTIMETERS
1
2
3
4
5
b
1mm
d
1mm

of the HLVB to the east. Contacts between the late granitoid plutons and the supracrustals are generally sharp and distinct, with minimal alteration confined to thin, often centimetre scale, halos of hematitic alteration. Barren, white quartz veins occur sporadically at the contacts between the granitoids and the supracrustals. These veins are oriented perpendicular to the contact and and occur primarily within the supracrustals, though these veins penetrate short distances into the granitoid rocks.

The eastern lobe of the late granitoid suite cuts layering and foliation within the supracrustals (Figure 3-1), and an aplitic dyke originating from and associated with this intrusive body discordantly cuts supracrustal rocks, foliation and a quartz-feldspar porphyry in the east limb of the antiformal structure. A pink pegmatitic dyke oriented northeast and likely originating from the eastern granite was encountered during drilling of the Flood Zone. Contacts of both the pegmatite and aplitic dykes are sharp and accompanied by negligible alteration.

In the northern portion of the Ulu Claims, north of the prominent north-east trending linear break (Figure 3-1), the western contact between the mafic volcanics and granitoid is less distinct, and rafts of volcanic material are found several hundred metres into the granitoids. As well, granitoid dykes, somewhat pegmatitic and up to 10 metres wide, cut the volcanics and are oriented north-south with a moderate easterly dip. These dykes are most abundant next to the contact and diminish in abundance to the east. Dykes also occur at the contact between mafic volcanics and underlying sediments in this area, where the contact also apparently has an easterly dip.

Distinct petrographical differences occur between the granitoids occupying the eastern lobe, and those bounding the supracrustals to the west, and therefore each of these plutons will be treated separately.

Eastern Granite

This intrusive is granitic in composition and is pink on weathered and fresh surfaces (Plate 3-3a). I is composed of 50% quartz, 25% microcline, 15% plagioclase (oligoclase/andesine An_{25-35}), 8% biotite, and 2% muscovite. Trace quantities of fluorite, tourmaline, zircon, titanite, apatite and molybenite occur as accessory phases. These granites show negligible alteration, though the quartz within these rocks is slightly strained. Texturally these rocks are holocrystalline and equigranular, and medium-to coarse-grained with a mean grain size of 1-2 millimetres (Plate 3-3a).

Whereas the zircon, titanite, and apatite are primary magmatic minerals, the presence of fluorite, tourmaline and molybdenite are suggestive of the presence of a late pneumatolytic fluid, possibly derived from the granite itself. Both purple and blue varieties of fluorite occur, and locally comprises 2% of the granite. Fluorite is associated primarily with biotite, and occurs as overgrowths on this mineral. Tourmaline occurs as subhedral to euhedral crystals intergrown with quartz and feldspar. The tourmaline (schorl) exhibits a brown-green pleochroism and in part has resorbed? surfaces.

The pink aplitic dyke in the eastern limb of the antiformal structure associated with the eastern granite, is composed of 60% plagioclase (albite, An_5), 40% quartz, locally up to 5% green, glomerocrystic muscovite (Plate 3-3c) and trace amounts of very fine grained biotite. These rocks are aphanitic with a mean grain size of 0.10 to 0.25 millimetres and contain minor megacrystic feldspars to 1.0 millimetre in diameter. The feldspar and quartz crystals are elongated parallel to the walls of the dyke to a maximum aspect ratio of 1:4, imparting a microcrystalline trachytic texture to these rocks in thin section (Plate 3-3d). These dykes also show negligible post emplacement alteration with the exception of slightly strained quartz, and chloritized biotite. Late fractures containing calcite and purple fluorite are oriented parallel to the fabric, whereas fractures with minor chlorite are oriented perpendicular to the fabric. The presence of fluorite in these dykes, which are geochemically consanguineous with the eastern granites (Chapter 4), supports the presence of late pneumatolytic fluids within this granitoid suite.

The pegmatite dyke encountered proximal to the eastern bounding granite is mineralogically composed of quartz, plagioclase, muscovite, and almandine with trace quantities of biotite and apatite. No potassium feldspar was noted in this dyke. Quartz within these rocks is strained, and embayed grain boundaries are common. Plagioclase crystals show bent, kinked twin lamellea interpreted as deformation twins. Muscovite crystals are also kinked and display undulatory extinction under crossed polars. Almandine as euhedral crystals to 0.5 millimetres may locally comprise up to 5% of these dykes, and is associated with muscovite.

Western Granite/Granodiorite

The granitoid rocks bounding the supracrustals to the west and north are dominantly granodioritic in composition. These rocks are pale weathering, and white and black on fresh surface. Mineralogically these rocks are composed of 40%

Plate 3-3

3-3a 90PAK-GRAN
Handspecimen of eastern granite, collected proximal to Flood Zone mineralization.

3-3b Photomicrograph (xpl), 90PAK-GRAN
Typical granoblastic texture displayed by external granites. Note lack of alteration of feldspars relative to internal suite granitoids.

3-3c 92VKT-4208
Handspecimen of pink aplite dyke with green muscovite glomerocrysts.

3-3d Photomicrograph, (xpl), 92VKT-4208
Trachytic texture defined by subparallel alignment of plagioclase laths, typical of the pink aplites.

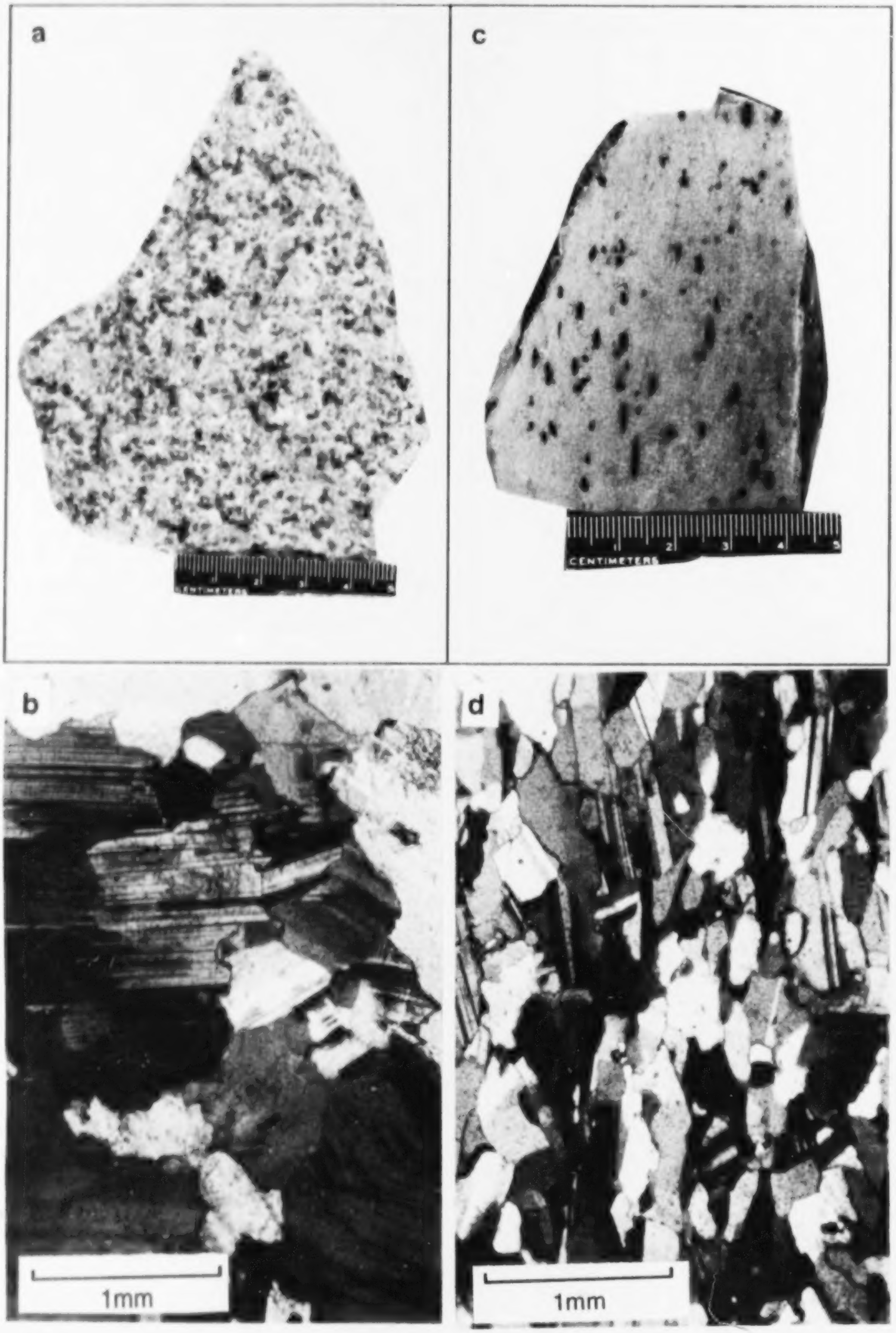
a
c
CENTIMETERS
1
2
3
4
5
b
1mm
d
1mm

quartz, 30% plagioclase (oligoclase/andesine), 15% microcline, and 15% biotite. Zircon, apatite, titanite, and almandine garnets occur in trace quantities as accessory phases. Texturally these rocks are holocrystalline and equigranular, and grain size varies from 0.50 to 2.0 millimetres. Some plagioclase is present as euhedral megacrysts to 4 millimetres which display oscillatory and convoluted zoning. Plagioclase within the groundmass is characterized by albite twinning. K-feldspar occurs only within the ground-mass, and its crystals are generally less than 1 millimetre in size. Biotite is sagenitic, containing epitaxial overgrowths of rutile likely due to exsolution of titanium from biotite upon cooling. Relatively rare garnets (almandine?) occur as small euhedral crystals to 0.15 millimetres, and are associated with biotite.

The samples representing the western granitoids were collected proximal to the northern contact with sediments, and abundant barren white quartz veining occurs both within granitoids and sediments at this locality. Thus the alteration displayed by these granodiorite samples examined petrographically is not necessarily representative of the western bounding pluton as a whole. This alteration occurs as clouding of feldspars, particularly the plagioclase megacrysts, which contain fine-grained sericite, and coarser muscovite crystals. Minor chloritization of biotite is also present.

Granite dykes, locally pegmatitic and aplitic are associated with the western bounding pluton. Mineralogically these rocks are composed of quartz, plagioclase, K-feldspar muscovite and almandine. The K-feldspar within the pegmatitic portions of the dykes are dark grey in color. Almandine is also very abundant within these dykes and locally may comprise in excess of 5% of these rocks.

Proterozoic Diabase Dykes

A single dyke of the 2.45 Ga Hearst Matachewan swarm occurs within the prominent east-west linear known as the 'ravine'. The dyke is relatively poorly exposed within the base of the linear, and consists of large (up to 3 centimetre) euhedral plagioclase phenocrysts set in a medium green matrix. This dyke was not examined petrographically or geochemically.

The Mackenzie dykes are abundant, and laterally continuous in both the supracrustal succession and Archean granitoids, and generally trend 160°. A second dyke set trending 070° to 080°, occurs on surface and within drill core in the Flood Zone area. These dykes may be correlative with 070° trending dykes in the Lac de Gras area which have been dated at 2310 Ma (Burwash et al., 1968). Both the 160° and 070° trending dykes are brown weathering and green-grey on fresh surface, and are highly magnetic. Individual dykes may be up to 20 metres thick and chilled margins adjacent to sharp wallrock contacts are ubiquitous. Within drill core fine-grained offshoots generally less than 1 metre thick occur proximal to larger dykes. The dykes are composed of a medium-to coarse-grained, equigranular assemblage of clinopyroxene, plagioclase (andesine/labradorite, An_{45-55}), amphibole and magnetite. Alteration, manifested as a brick red hematization, is commonly observed at the margins of these dykes and may extend into surrounding wallrock. In thin section, alteration of plagioclase to sericite, and breakdown of ferromagnesian minerals to hematite is common, though rocks may appear fresh in hand specimen.

STUCTURAL GEOLOGY AND METAMORPHISM

The dominant structural element within the Ulu Claims is the northward closing D_2 antiformal structure (Figure 3-1). This structure is non-cylindrical (Henderson et al., 1993) and varies in character along its strike. In the southern part of the claims, the plunge of the fold is to the northwest, and the limbs of the fold asymmetrically diverge, with the strata within the west limb having a steeper dip (Flood et al., 1991). In the central portion of the claims the limbs of the fold are isoclinal, and dip steeply to the east (Flood et al., 1991). Within the northern portion of the claims the plunge of the fold is to the south (Henderson et al., 1993; Flood et al., 1991), and beds within greywacke units dip inward. This geometry cannot be explained by simple fold models, however it is interesting to note that the region with the inward dipping beds corresponds to that portion of the fold which has been heavily intruded by granitoid dykes. A possible explanation of the observed geometry may be that the mafic volcanics in the northern portion of the fold have been detached and thrusted along their contact with the underlying greywacke during granite emplacement.

Axial planar cleavage related to the D_2 antiform is not present (Helmstaedt, 1992) and the S_3 cleavage with a mean orientation of 015° 80° is the dominant penetrative structural element (Henderson et al., 1993). Within the north Ulu area S_0 and S_3 have moderate to low dips, and are crenulated by a vertical S_4 cleavage which strikes north-northeast (Henderson et al., 1993).

Several linear features interpreted as faults occur within the Ulu area. A main east-west linear known as the 'ravine' occurs within the central area of the claims. This structure hosts the Hearst-Matachewan diabase dyke, and transects the entire HLVB as well as the bounding granites. Sinistral offsets of up to 300 metres occur within supracrustals along this structure in the Ulu area (Flood et al., 1991). Several small scale faults parallel to the ravine occur for one kilometre south, and sinistral displacements of 25-50 metres have been noted (Flood et al., 1991). North of the ravine, faults are oriented in a northeast-southwest direction and both sinistral and dextral offsets of 20 to 220 metres have been observed within supracrustals adjacent to these structures (Flood et al., 1991). Granite dykes in part occur within these structure in the northernmost portion of the Ulu Claims.

Metamorphic grade of the supracrustal rocks contained within the Ulu Claims is everywhere at lower amphibolite facies. Peak metamorphic mineral assemblages for basic and pelitic rocks have been plotted on P-T/mineral assemblage diagrams of Barker, (1990). The mineral transitions portrayed by these diagrams require that $P_{total} = P_{fluid} = P_{H2O}$, therefore these conditions have been assumed for Ulu supracrustal rocks. Metamorphic mineral assemblages within the basic volcanic rocks (hornblende+oligoclase) define a broad P-T space for peak metamorphic conditions between 480-700°C and 2-9 kilobars. Peak metamorphic mineral assemblages within pelitic rocks (biotite + cordierite ± andalusite ± almandine) allow tighter constraints on P-T conditions to be determined. The metamorphic conditions defined by the pelitic mineral assemblage are temperatures between 515° and 625°C and pressures of 0-4 kilobar. Combination of P-T conditions determined from mineral assemblages of pelitic and basic volcanic rocks constrain peak metamorphic conditions at 525-625° C and 2-4 kilobars pressure. Barker, (1990-) reports that almandine does not occur until temperatures of 480-500°C, and that pure almandine garnets do not form until temperatures of 550°C within the pressure range determined for the Ulu rocks. Microprobe analysis of the almandine garnets might allow more precise temperature determination of peak metamorphism to be made.

The pressure/temperature ranges of metamorphism exhibited by the Ulu supracrustals is typical of Slave Province rocks (Henderson et al., 1993; Thompson, 1989a,b), and may be classified as low pressure, high temperature regional metamorphism. The significance of this type of metamorphism with respect to petrogenetic evolution of the Ulu Claims rocks, and the relationship between timing of metamorphism and mineralization will be discussed in more detail in subsequent chapters.

4. WHOLE-ROCK CHEMICAL RELATIONS

INTRODUCTION

In order to investigate the petrogenetic history of the Archean succession hosting the mineralization at the Ulu claims, a whole rock geochemical study was undertaken. The presence of well preserved geologic relationships between the hosting supracrustals and various intrusive lithological units offers an opportunity to place Type II and Type III mineralization both in a temporal and petrogenetic framework with respect to the evolution of the High Lake Greenstone belt.

A sample suite consisting of 15 mafic volcanics, 8 gabbros, 3 diabases, 19 internal granitoids and associated aplites/felsites, and 6 external granitoids and associated aplites and pegmatites were collected from core and surface exposures. Petrological descriptions of these lithologic suites are given in Chapter 3. Samples sent for analysis were carefully selected in order to avoid samples containing the effects of hydrothermal alteration and weathering. Samples were analyzed for major and trace elements at two separate laboratories, a commercial laboratory Acme Analytical Laboratories (Vancouver, B.C), and a research facility, Washington State University (Pullman, Washington). Details of analytical procedures and results are given in Appendix 2.

SUPRACRUSTAL LITHOLOGAL UNITS

Mafic Volcanics/Gabbros/Diabase

Major Element Chemical Variations

The Ulu mafic volcanics and gabbros are plotted on an AFM ($A=Na_20+K_20$, $F=FeO$ as total Fe, $M=MgO$) diagram, Figure 4-1. The mafic supracrustal rocks are subalkaline and display a tholeiitic trend. Major element oxide versus SiO_2 Harker plots for the mafic volcanics, gabbros and MacKenzie diabase dykes are given in Figure 4-2. With the exception of the Proterozoic diabases, the data indicate that the suite of mafic volcanics and gabbros are cogenetic. Ti, Fe, Na, and P display positive correlations with increasing silica, while Al, Mg and Ca display negative correlations with increasing silica. K and Mn are not abundant and show minimal variation with increasing silica content. The silica content of the suite ranges from 50% to 58%, however rocks with silica contents of 50-53% are most common.

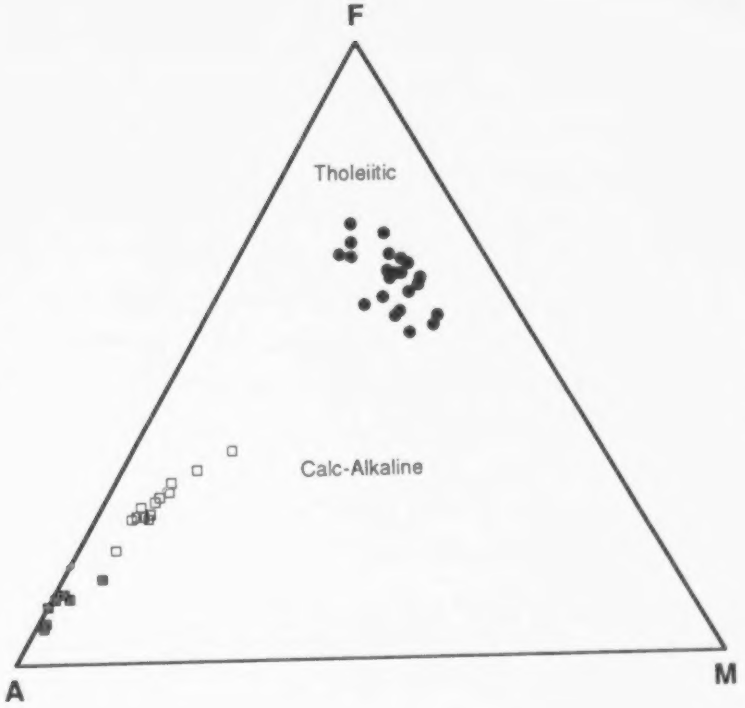

FIGURE 4-1. AFM (A=Na_2O+K_2O, F=FeO_{total}, M=MgO) plot for Ulu mafic volcanics and gabbros (solid dots), internal granitoids (open squares) and external granitoids (shaded squares).

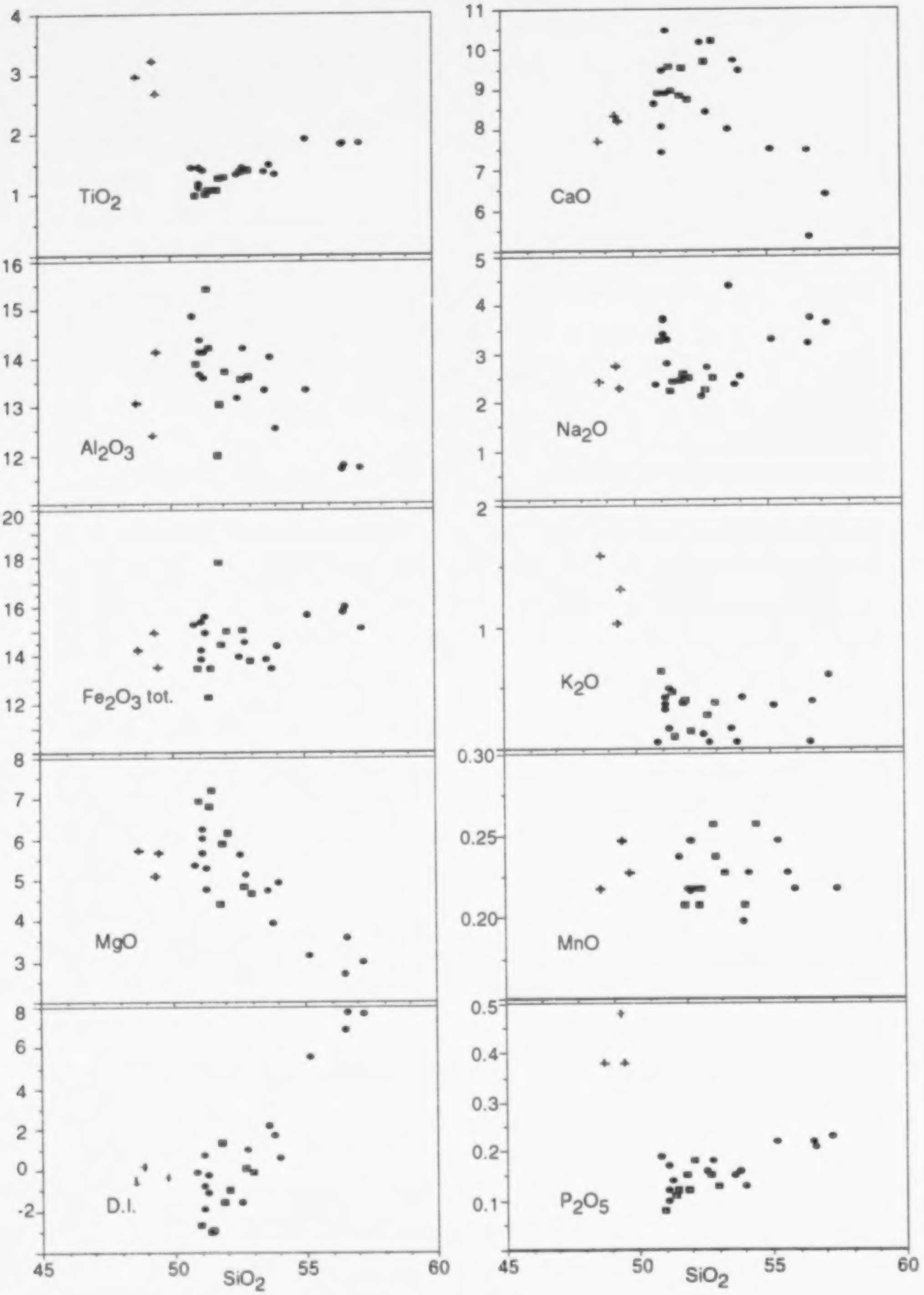

FIGURE 4-2. Major element Harker plots for Ulu Claims mafic volcanics (solid circles), gabbros (shaded squares) and Proterozoic diabase (crosses). All oxides in weight percent.

Classification using major element chemistry of the Ulu mafic volcanics and gabbros (Le Bas and Streckeisen, 1991) is shown on a total alkalis versus silica plot in Figure 4-3. The mafic volcanic rocks fall into either the basalt or the basaltic andesite field. Two weak trends in the mafic volcanic data are apparent, with one array of points displaying increasing alkali content with a constant silica content (50%), and a second trend of increasing alkalis with increasing silica content. This is thought to represent a constant magma source, whose pulses occasionally weakly differentiate during crystallization. The gabbros plot in a tight cluster straddling the basalt and basaltic andesite fields, central between the two arrays of mafic volcanics. The Proterozoic Mackenzie diabase samples plot within the basalt field.

It is apparent from the data that the majority of the rocks have relatively consistent chemistry, with a small proportion representing evolved or fractionated compositions. The rocks richer in silica (i.e. >55%) were collected in close proximity to the sediment-volcanic contact in the center of the D_2 antiformal structure. If these rocks are the most evolved members of the volcanic pile then they should represent the youngest members of the pile. However, structurally they occupy a position within the fold that suggests that they are the oldest. This discrepancy might be reconciled by considering the D_2 structure to be an overturned syncline rather than an anticlinal structure. Additionally, the sediments which form the center of the antiform, appear to have had a largely felsic volcanic source (see below) rather than being derived from a unknown origin (pre-supracrustal basement) and underlying the mafic pile.

Trace Element Variations

Trace element versus silica Harker plots for Ulu mafic volcanics, gabbros and diabase are shown in Figure 4-4. Cr, and Ni display negative correlations with increasing silica, while Zr and Y display positive correlation with increasing silica. Co likely displays a similar relationship as Ni, however possible contamination during sample preparation (crushing) has resulted in considerable scatter. Nb and La are at their detection limits and do not show variation with silica. Sr displays considerable scatter and therefore does not display any correlations with silica content. Ba is generally elevated within the higher silica members of the suite, however several of the lower silica mafic volcanics and gabbros also display high barium contents. The relationships displayed by these plots again suggest that the higher silica rocks represent evolved members, and are last to crystallize, having

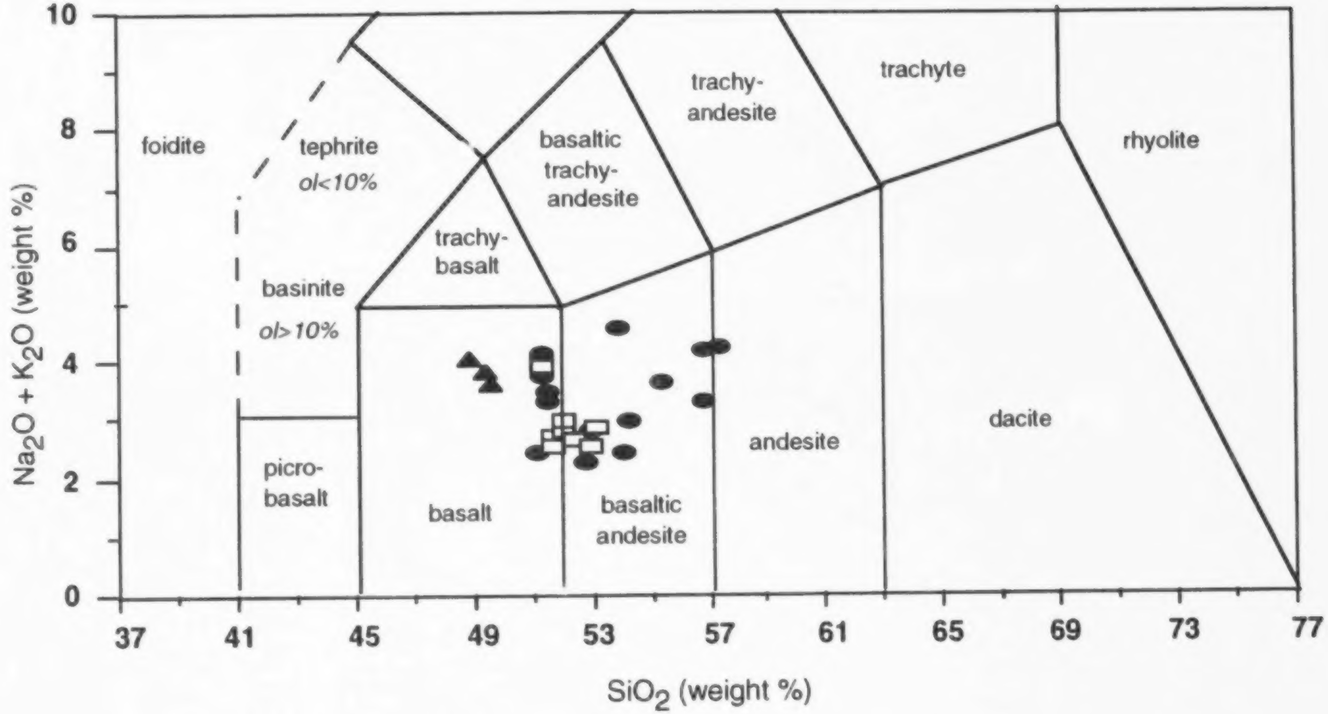

FIGURE 4-3. Chemical classification of Ulu Claims mafic volcanics (solid ellipses), gabbros (open rectangles) and Proterozoic diabase (triangles), based on total alkalis versus silica (modified after Le Bas and Streckeisen, 1991).

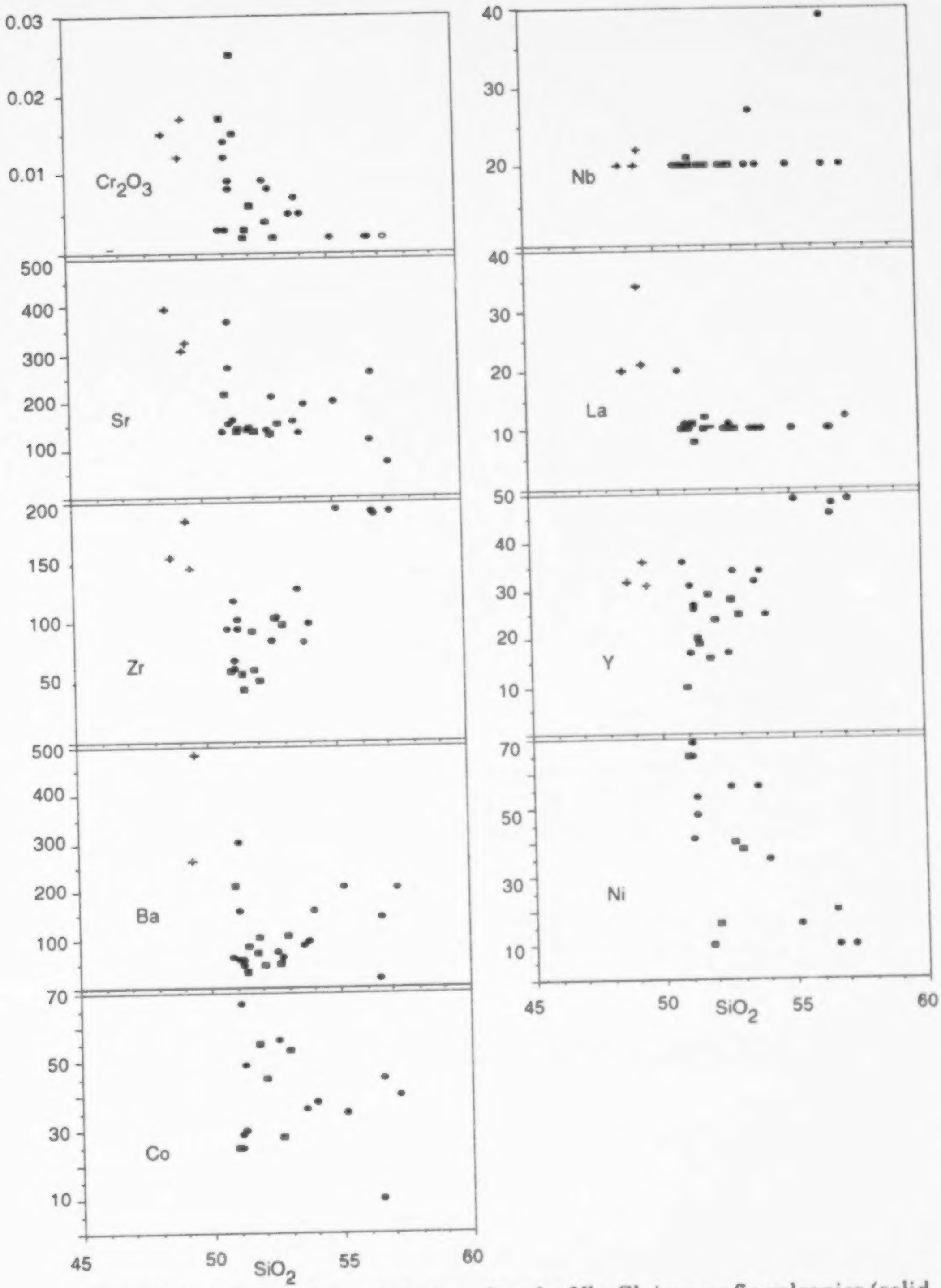

FIGURE 4-4. Trace element Harker plots for Ulu Claims mafic volcanics (solid circles), gabbros (shaded squares) and Proterozoic diabase (crosses). Oxides of Si and Cr in weight percent, Sr, Zr, Ba, Co, Nb, La, Y, and Ni in ppm by weight.

lower transition metal (Ni and Co) contents, while containing higher concentrations of the incompatible elements (Ba, Zr, Y).

Petrogenesis

Petrogenetic classification of Archean volcanics (Condie, 1976, 1981) is based largely upon rare earth elements (REE) and trace element data, due to the general disturbance of major element chemistry within these rocks (Condie, 1976; Cunningham and Lambert, 1987). Unfortunately REE and extended trace element data are not presently available for the Ulu mafic volcanics, therefore the petrogenesis of these rocks with respect to other Archean mafic volcanics cannot be investigated in great detail.

Tectonic discrimination diagrams for basaltic rocks using major and trace elements based upon modern tectonic environments are extensive (Pearce and Cann, 1973; Pearce, 1975; Pearce et al., 1977; Pearce and Norry, 1979; Meschede, 1986; Mullen, 1983). Use of these diagrams in the investigation of Archean basalts is tenuous due to uncertainty regarding Archean tectonic regimes, as well as disturbance of the chemical composition of these rock during their long crustal residence time (Cunningham and Lambert, 1987). Discrimination plots utilizing major elements, and trace elements which are at or near their detection limits (Nb, La) or exhibit mobile behavior are not considered here. However, plots derived from elements demonstrated to be largely immobile within Ulu volcanics (Chapter 7) may be useful in deciphering the tectonic setting of the Ulu mafic volcanics.

Ulu mafic volcanic trace element data were plotted on a series of discrimination plots using Ti, Zr, Y and Sr (Pearce and Cann, 1973). On all three plots (Ti/Zr, (Ti/100)/Zr/(Y/3), and (Ti/100)/ Zr/(Sr/2)) the Ulu mafic volcanics plotted dominantly within the ocean floor basalt field. While the tectonic setting of the Ulu mafic volcanics may not be accurately represented by the discrimination plots, the source and processes forming the melts may be considered to be analogous to modern ocean floor or mid ocean ridge basalts. This suggests that the Ulu mafic volcanics were derived primarily from a mantle source, and that their petrogenesis did not involve significant quantities of recycled crustal rocks.

Sedimentary Rocks

Major and trace element chemical compositions for five greywackes and pelites are given in Appendix 3. A significant degree of heterogeneity is apparent within the data, both between the greywackes and cordierite-bearing pelites, and amongst the greywackes. The geochemical data for the Ulu sedimentary rocks are limited, (no Rb or REE data), therefore precise determination of precursor rock types is not possible, however some conclusions regarding sediment provenance may be drawn from the available data.

The Ulu sediments are plotted on a K_2O versus Na_2O diagram (Figure 4-5) along with average chemical compositions of Archean greywackes and slates (Ojakangas, 1985), as well as greywackes and slates from the Yellowknife Supergroup Burwash Formation (Henderson, 1975b). With the exception of a single analysis the Ulu Claims greywackes and pelites are significantly richer in potassium than the other Archean sediments. This feature may be attributable to either a distinctive high potassium source for these rocks, or to the post-depositional addition of potassium (Okjakangas, 1985).The latter explanation is not consistent with chemical changes observed in the sediments during Type II mineralization/alteration where a net loss of potassium is observed within altered/mineralized sediments relative to unaltered sediments. Precluding addition of potassium during sediment diagenesis it is likely that provenance exerted the major influence on the sediment chemistry.

The Ulu sediments are also plotted on a AFM ($A=Na_2O+K_2O$, $F=FeO$ as total Fe, $M=MgO$) diagram (Figure 4-6) along with the average Ulu mafic volcanic, an average of Yellowknife felsic volcanic (Barager and Goodwin, 1969), and pre-Yellowknife Supergroup basement from the Point Lake area (Easton, 1985). Since no felsic/intermediate volcanic analyses are available, and no pre-supracrustal basement has yet been found in the Ulu Claims area, possible compositions of these lithologies have been used from other regions of the Slave Province. From Figure 4-6, it appears that a felsic volcanic/pyroclastic source with a possible minor intermediate/mafic volcanic contribution best describes the chemical composition of the Ulu Claims sediments. A felsic/intermediate plutonic source may also account for the origin of sedimentary rocks of this composition (Jenner et al., 1981), however all the known intrusives in the area are at least post-D_2 deformation. The implication of a predominantly felsic volcanic/pyroclastic source for the Ulu sediments would require the presence of high potassium volcanic rocks within the belt. A whole rock major and trace element and rare earth element study of the felsic lithologies east of the Ulu Claims, as well as a rare earth element study of the Ulu sediments would be useful in further investigating the relationship between these lithologies, and the potassium rich nature of these sediments.

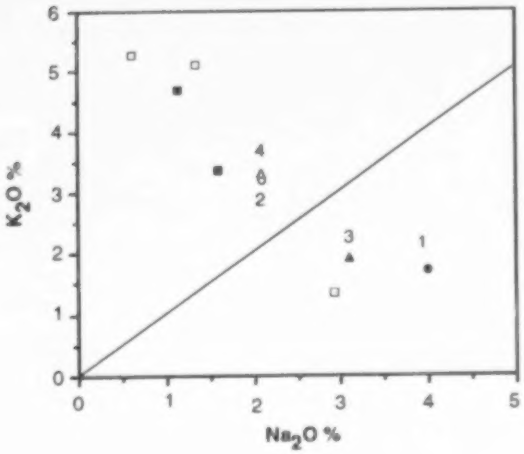

FIGURE 4-5. K_2O/Na_2O ratios in Ulu Claims greywackes (open squares) and cordierite bearing pelites (shaded squares). Also shown are K_2O/Na_2O ratios for average Archean greywacke (1) and slate (2) (Ojaknagas, 1985), Yellowknife Supergroup Burwash Formation greywackes (3) and slates (4) (Henderson, 1975b).

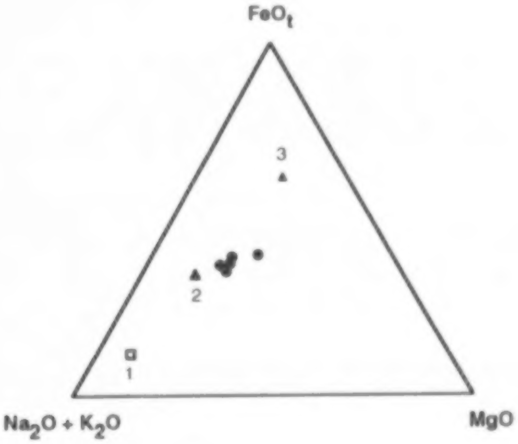

FIGURE 4-6. AFM diagram for Ulu Claims greywackes and pelites (solid dots). Also plotted are pre-Yellowknife Supergroup basement granodiorite Point Lake (1) (Easton, 1985), average Yellowknife felsic volcanic (2) (Barager and Goodwin, 1969) and average Ulu Claims mafic volcanic (3).

FELSIC INTRUSIVE PHASES

From geologic relationships observed in the field, as well as petrographic considerations (Chapter 3), it is apparent that there are at least two distinct felsic intrusive episodes present in the Ulu Claims area. An earlier episode, termed the internal suite, consists of small granodiorite plugs, quartz-feldspar-porphyry dykes, and associated grey aplites, that are intruded into the supracrustal package. The quartz-feldspar porphyry dykes associated with these intrusives cut the regional D_2 fold structure, as well as Type II mineralized horizons. All of the internal granitoids are affected somewhat by regional D_3 cleavages and also commonly host Type III veins.

The later episode of granitoid intrusives, termed the external suite, are the extensive batholiths which bound the supracrustal rocks. The external granitoids are granitic to granodioritic in composition, with associated pink aplites and pegmatites. The aplite and pegmatite phases of this intrusive episode occur as dykes which invade the supracrustal succession. A pink aplite dyke cross-cuts a quartz feldspar porphyry in the East-Limb area (see Figure 6-1) and the bounding granites truncate all structure and cleavage along the eastern edge of the supracrustals adjacent to the Flood Zone. From the geologic relationships, it is apparent that emplacement of the internal granitoid suite pre-dated that of the external suite. The geochemical data presented in this section is consistent with the interpretation based on field relations that the two suites of intrusive rocks are unrelated and likely represent two separate episodes of melting from two distinct source regions.

Major Element Chemistry

Major element versus SiO_2 Harker diagrams are given in Figures 4-7, 4-8 and 4-9 for both internal and external granitoid suites. From the plots it can be seen that the granodiorite from the internal suite represent the least evolved melts and may approximate the parental composition of this suite. The quartz-feldspar porphyry dykes and grey aplites form an array for most oxides which represents fractional crystallization from the parental magma composition. TiO_2, Al_2O_3, Fe_2O_3, CaO, MgO, MnO and P_2O_5 all decrease in abundance with increasing silica in the quartz-feldspar-porphyry dykes and aplites. Na_2O, K_2O do not display significant variations with increasing silica content within the quartz-feldspar porphyries. Two of the grey aplites, however display a nominal increase in Na_2O, accompanied by a corresponding decrease in K_2O. The third aplite displays an

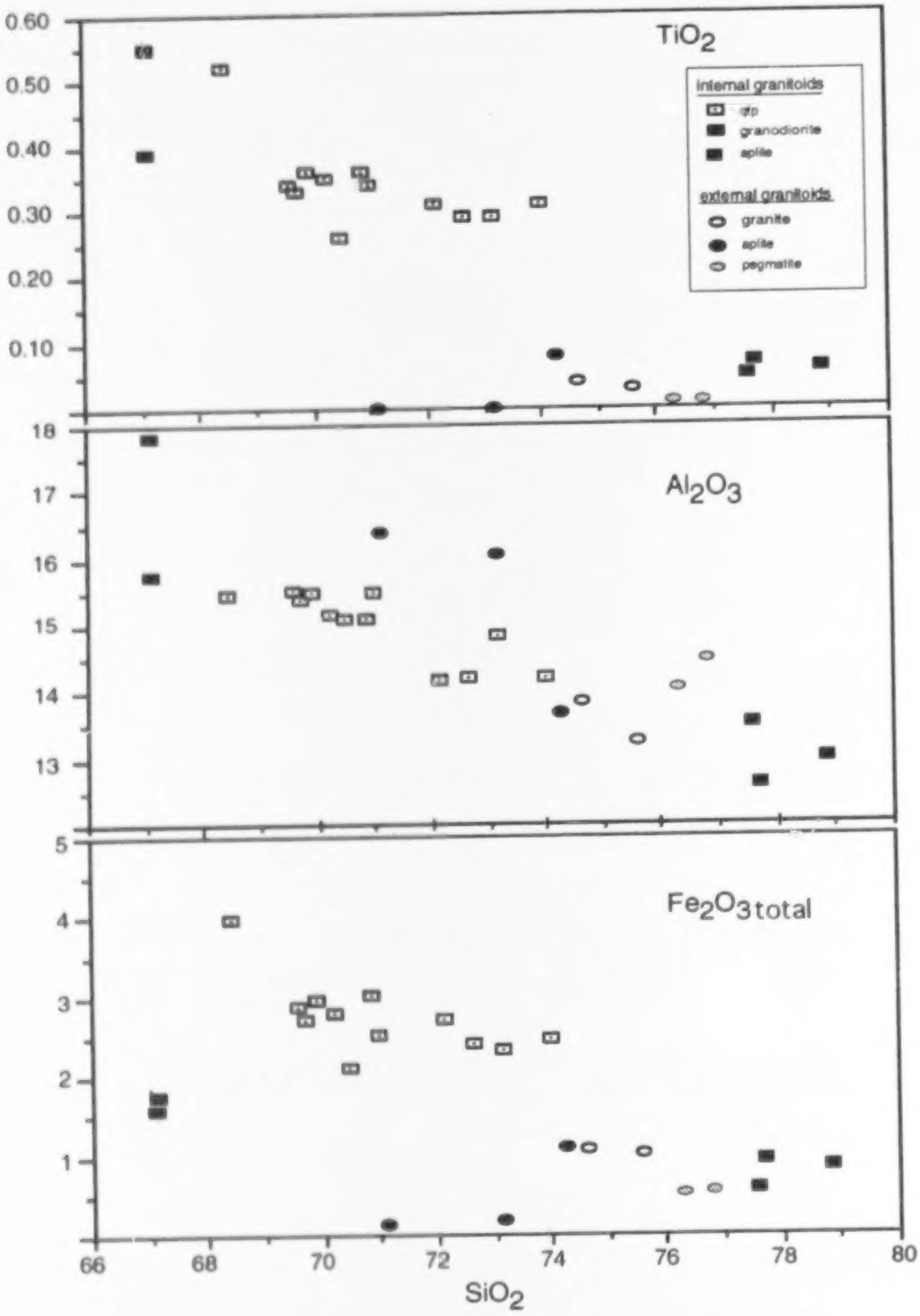

FIGURE 4-7. Major element (TiO_2, Al_2O_3, and Fe_2O_3) Harker plots for felsic intrusives, Ulu Claims, N.W.T. All oxides given in weight percent.

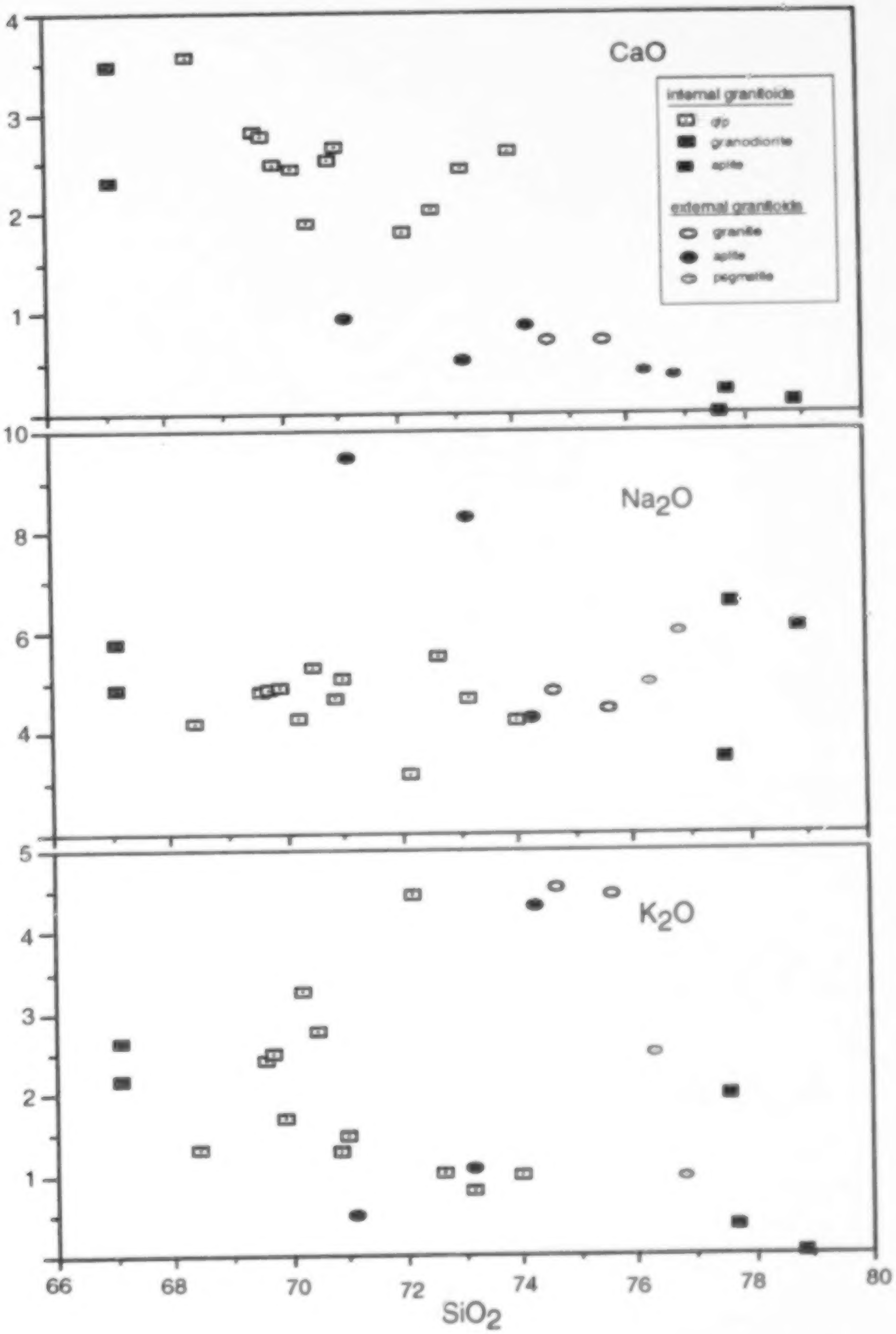

FIGURE 4-8. Major element (CaO, Na_2O and K_2O) Harker plots for felsic intrusives, Ulu Claims, N.W.T. All oxides given in weight percent.

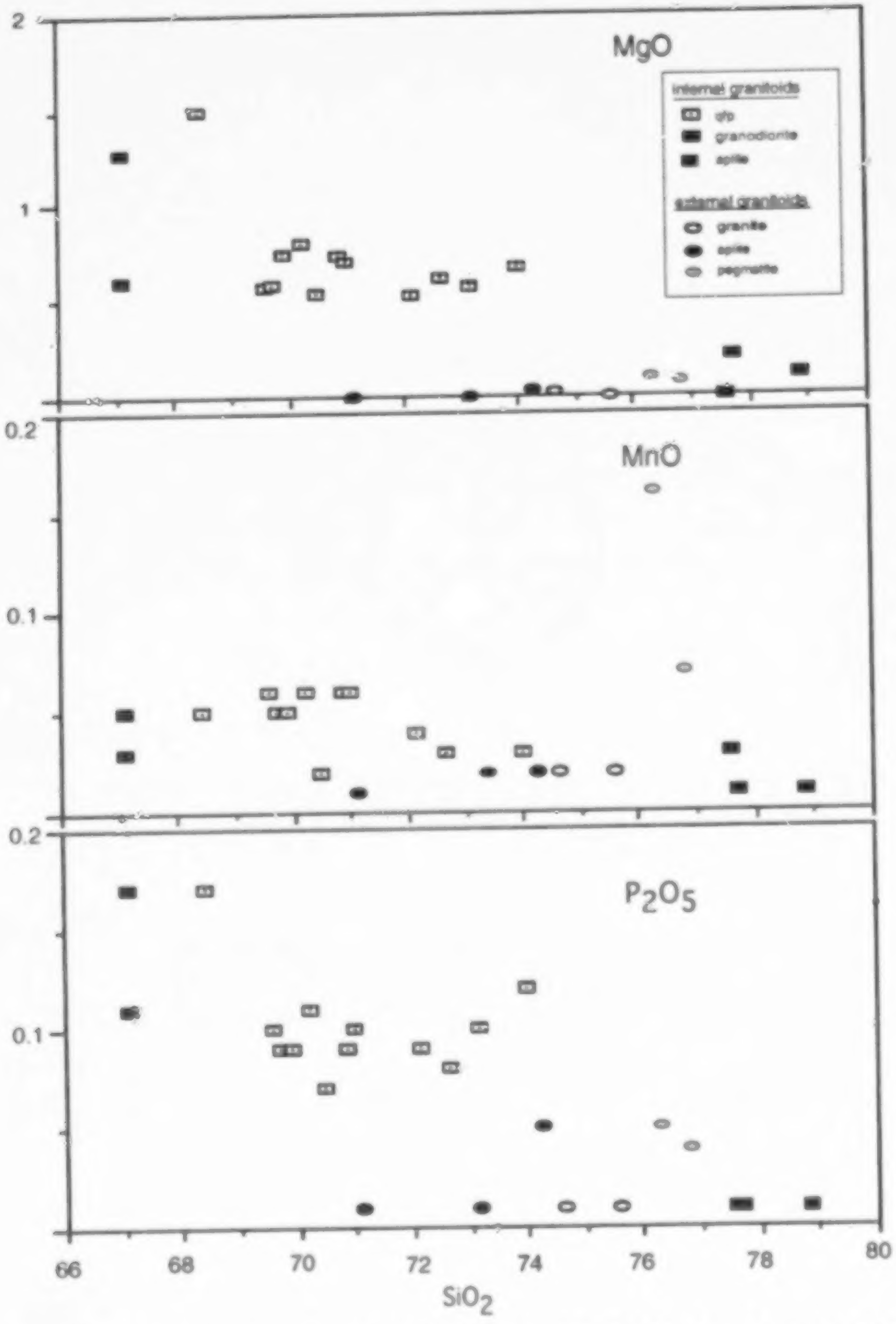

FIGURE 4-9. Major element (MgO, MnO, and P_2O_5) Harker plots for felsic intrusives, Ulu Claims, N.W.T. All oxides given in weight percent.

inverse relationship with an increase in K_2O and a decrease in Na_2O. These relationships indicate that two of the aplites represent late stage anhydrous distillates, while the third may have contained some aqueous fluids due to the common partitioning of K into the hydrous phases, and Na into anhydrous phases within late-stage granitic distillates (Hall, 1987).

Considerable differences are seen in the major element contents of the two granodiorites. This may be largely accounted for by the pervasive alteration (especially of the feldpars) and veining observed within this lithological unit. Alternately, these differences may represent primary heterogeneities within the plug. Similarly, the scatter seen in the K_2O, Na_2O and CaO contents of the quartz-feldspar-porphyry dykes may be attributable to the pervasive alteration of feldspars (Chapter 3) and accompanying alkali mobility, as well as analytical errors.

Two dykes, plotted as quartz-feldspar porphyries, collected in the Ulu West area, display higher K_2O and lower Na_2O contents than other rocks of the internal granitoid suite. The reason for this is not clear, though contamination may be a possibility. However, based upon major element, trace element, and rare earth element data, the dykes are similar to the internal granitoid suite.

The external granitoid suite (represented by analysis of two granites, two aplites, a granitic dyke, and two pegmatites) displays trends which vary considerably from those of the internal suite. Examination of the major element Harker plots (Figures 4-7, 4-8, 4-9) indicate that for TiO_2, Fe_2O_3, K_2O, MgO, and P_2O_5 the granites do not lie on the liquid descent line describing the fractional crystallization of the internal granitoid suite. With the exception of elevated K_2O, all the oxides in the above list are markedly less abundant within the external granites than they are within the internal granodiorites and quartz-feldspar porphyries.

The differentiation trends of the granite and its aplites and pegmatites differ significantly from the trends of the granodiorites, quartz-feldspar porphyries and the grey aplites. The pegmatites show increases in SiO_2, Al_2O_3, Na_2O, MgO, and MnO, and decreases in CaO, K_2O, Fe_2O_3 and TiO_2 relative to the granites. The pink aplites show increases in Al_2O_3, and Na_2O, decreases in SiO_2, TiO_2, Fe_2O_3, and K_2O, and little change in MgO, MnO, P_2O_5, and CaO, relative to the parental granites. The enrichment of Na and the depletion of K in both the pink aplites and pegmatites indicate that the late stage distillates were relatively anhydrous, though a lesser degree of K depletion in the pegmatites implies the presence of some aqueous fluids during the formation of these rocks.

The granitic dyke collected in the Ulu west area is chemically similar to the external granites, however, it displays elevated TiO_2 and P_2O_5 contents, possibly inherited from assimilated host rocks.

The most significant differences in the major element contents of the external and internal suites, is the low abundances of Fe, Mg and Ti oxides within the the external suite, and the variation in K and Na contents between the two suites. The primary constituents (aplites removed) of the internal suite contain an average of 1.87% K_2O, and have an average K/Na of 0.39, with a range of 0.17 to 0.76. The external granite and the granite dyke contain an average of 4.62 % K_2O, and have a K/Na of 1.0 with an range of 0.94 to 1.0.

The CIPW normative mineralogy for felsic intrusive phases is given in Appendix 3. The rocks representing the primary melt composition of the internal suite (quartz feldspar porphyries and granodiorites) are generally peraluminous, and contain normative corundum. Granite samples from the external suite do not contain normative corundum and are therefore metaluminous. The Q-Ab-An normative composition of the quartz-feldspar porphyries and granodiorites, as well as the granites are shown in Figure 4-10. The rocks from the two suites plot in distinctly different regions and by comparison to experimental data in the Or-Ab-An-Qtz-H_2O system, the conditions of melting and crystallization of these two rocks suites can be qualitatively modelled. For the purposes of this modelling, it is assumed that the composition of these rocks is similar to the magma from which they crystallized.

The internal suite rocks display a systematic shift away from the eutectic melting composition of for P_{H2O} = 2 kbar and Ab/An = 3.8 (Winkler, 1974) which is close to the average Ab/An for these rocks. This suggests that the internal suite rocks do not represent minimum melt compositions, and that their parental magmas formed and crystallized at 750-800°C, much above the eutectic of 695°C (Winkler, 1974). Partial melting may have also occurred under much higher P_{H20} conditions, which would also shift the melt composition towards the Ab apex (Winkler, 1974). The trend displayed by the internal suite with increasing An content away from the eutectic minimum is likely due to the fractional crystallization of this rock series demonstrated by the Harker plots.

In comparison, the external suite granites plot much closer to the eutectic, for Ab/An = 3.8, P_{H2O} = 2kbar. Additionally the Ab/An ratios of these rocks are

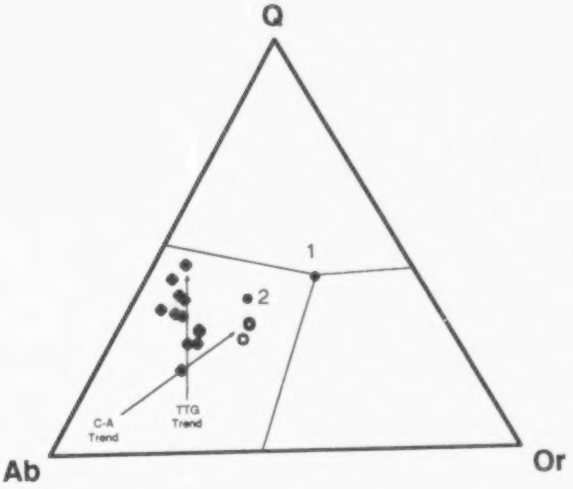

FIGURE 4-10. Triangular plot of the relative percentages of normative quartz (Q) orthoclase (Or)and Albite (Ab) for internal (solid diamonds) and external (open circles) granitoids Ulu Claims, N.W.T. Aplites, pegmatites and suspected contaminated rocks removed. Eutectic position for Ab/An = 3.8 (1) ,and Ab/An = 7.8 (2), at P_{H_2O}= 2Kbar, projected from the Q-Ab-Or-An-H_2O system (Winkler (1974). Calc-alkaline (C-A) and trondhjemitic (TTG) trends after Barker and Arth (1976).

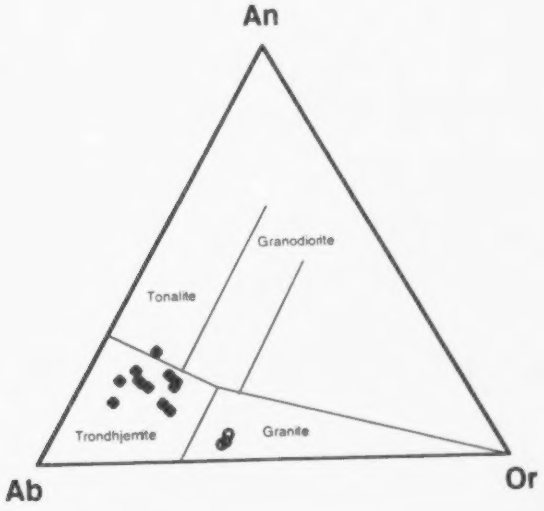

FIGURE 4-11. Triangular plot of the relative percentages of normative orthoclase (Or), albite (Ab) and anorthite (An) for internal (solid diamonds) and external (open circles) granitoids, Ulu Claims N.W.T. Aplites, pegmatites and suspected contaminated rocks removed. Plot after O'Connor (1965), field boundaries after Barker (1979).

closer to 12, which results in the eutectic minimum shifting closer to the composition of these rocks (Winkler, 1974). The composition of the external granites suggest that the magmas forming these rocks represent a minimum melt composition, assuming P_{H2O} = 2kbar that would crystallize at a temperature of approximately 650-675 °C.

Consideration of the volumes of internal and external granitoids present within the Ulu Claims area, and the degree of melting displayed by these rock suites on the Q-Ab-Or plot, implicate distinctive partial melting sources for these two rock suites. Assuming similar P_{H20} conditions, differing degrees of melting of the same source cannot explain the trends observed on the normative feldspar diagram (Figure 4-10) for these rocks. The external granites form extensive batholiths in the area, therefore a minimal melt composition from a low K source necessitates a unreasonably large volume of this source rock due to the low degree of partial melting required to form rocks of this composition. A reasonable volume of a high K source rock undergoing partial melting at or near the eutectic minimum is inferred. The high SiO_2, low K_2O internal suite appears to be formed from a low K source, by a reasonable degree of partial melting at temperatures much above eutectic minimum, resulting in a K poor melt. The possibility that the internal suite may represent a higher degree of partial melting from the same source which generated the external suite can be ruled out due to geological constraints which indicates emplacement of the internal suite pre-dates that of the external suite.

In order to chemically classify the intrusive rocks on the Ulu Claims, the data have been plotted on a normative feldspar variation diagram (O'Connor, 1965) for rocks containing more than 10% normative quartz, on which the fields of Barker (1979) have been superimposed. Samples determined to be late differentiates of both suites were not plotted, due to the chemical deviation of these rocks away from the bulk magma composition. The internal suite rocks plot almost entirely within the trondhjemite field, with a single sample in the tonalite field. The bulk composition of the external suite (granites) plots within the granite field.

Trace and Rare Earth Element Chemical Relations

Select trace elements versus SiO_2 Harker diagrams for the internal and external granitoid suites are given in Figures 4-12, 4-13 and 4-14. Trace elements plotted were selected for their effectiveness in defining differences in trends between these two intrusive suites. Average trace element contents of the

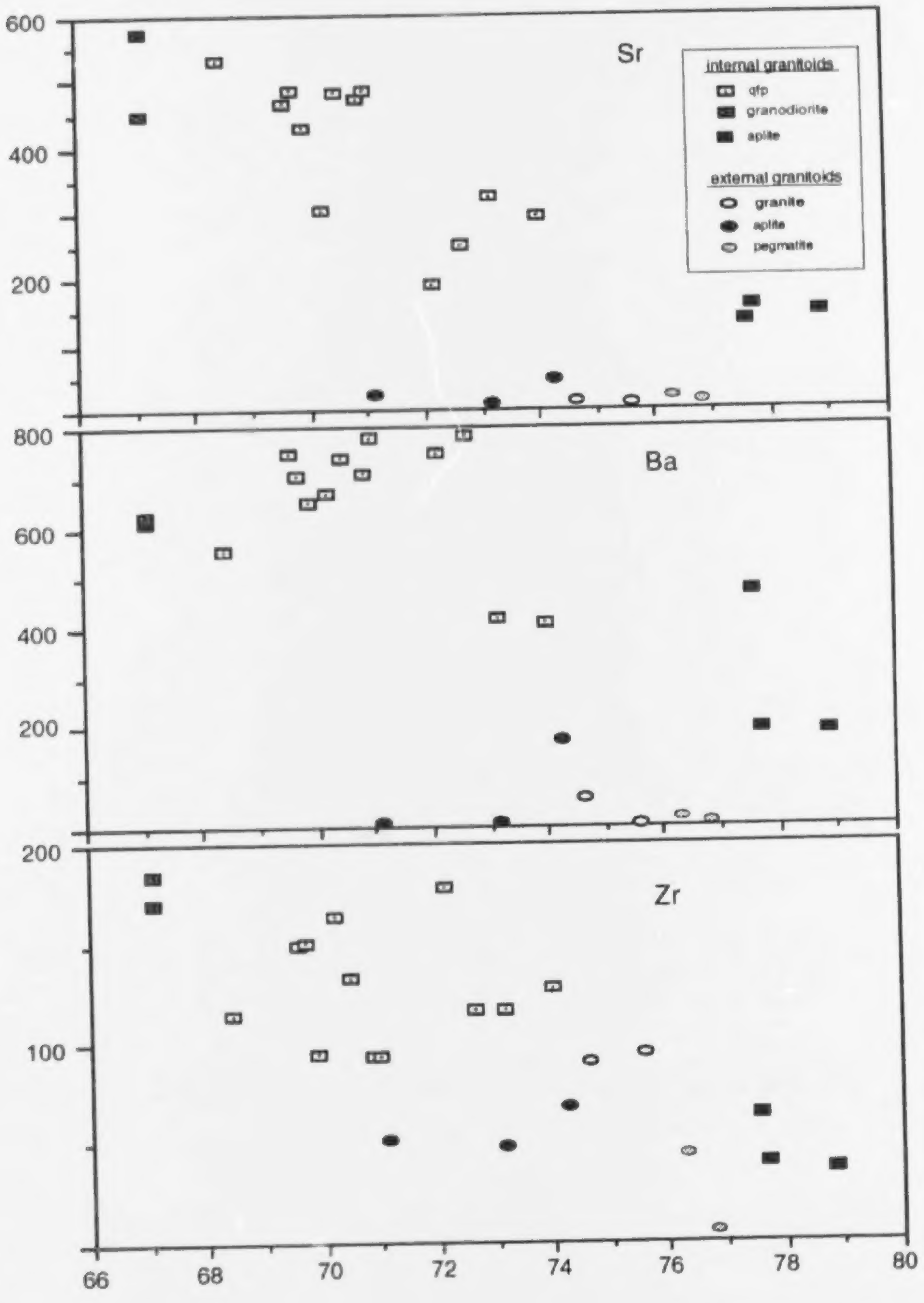

FIGURE 4-12. Trace element (Sr, Ba and Zr) Harker plots for felsic intrusives, Ulu Claims, N.W.T.. Trace elements in ppm by weight, SiO_2 in weight percent.

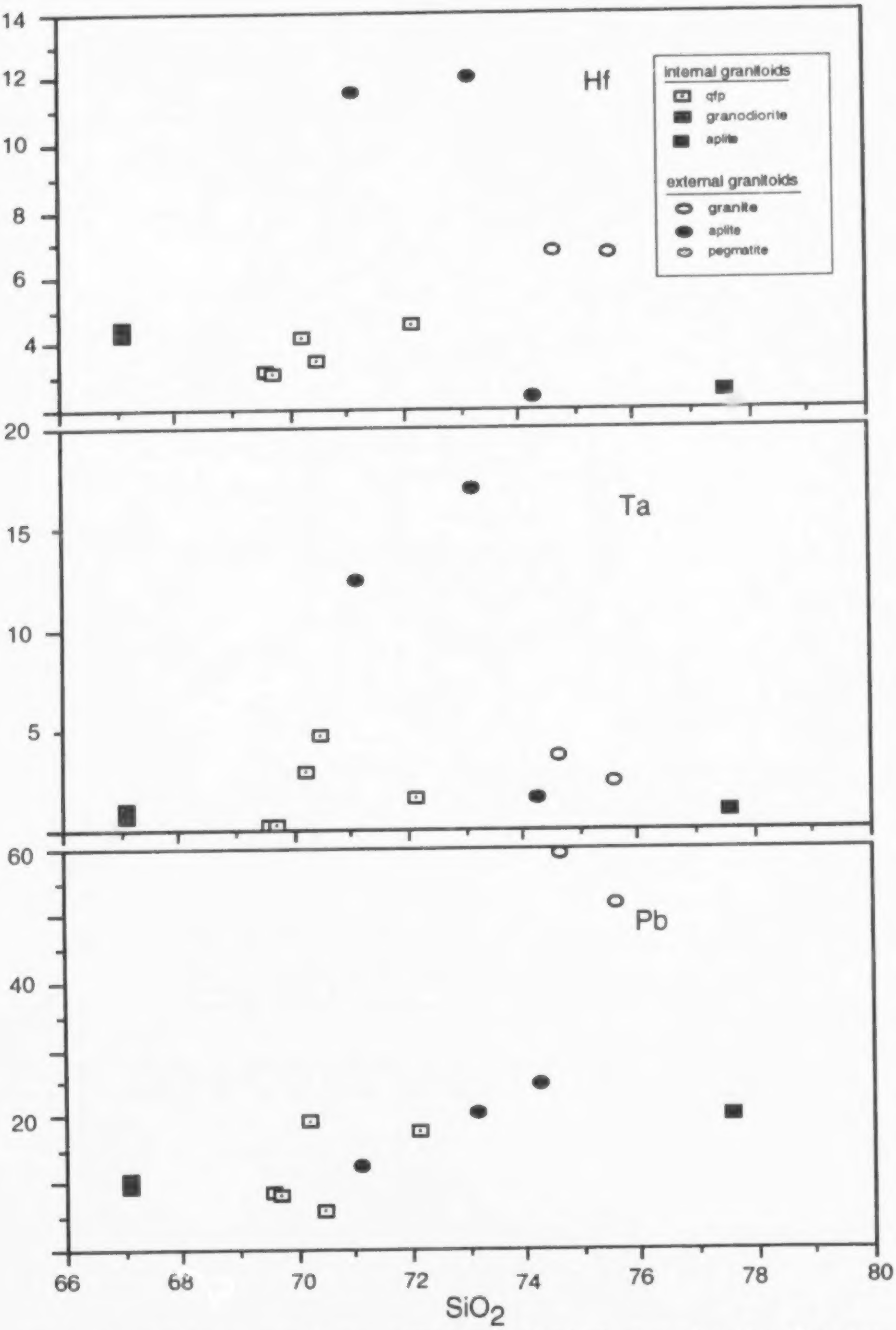

FIGURE 4-13. Trace element (Hf, Ta and Pb) Harker plots for felsic intrusives, Ulu Claims, N.W.T. Trace elements in ppm by weight, SiO_2 in weight percent.

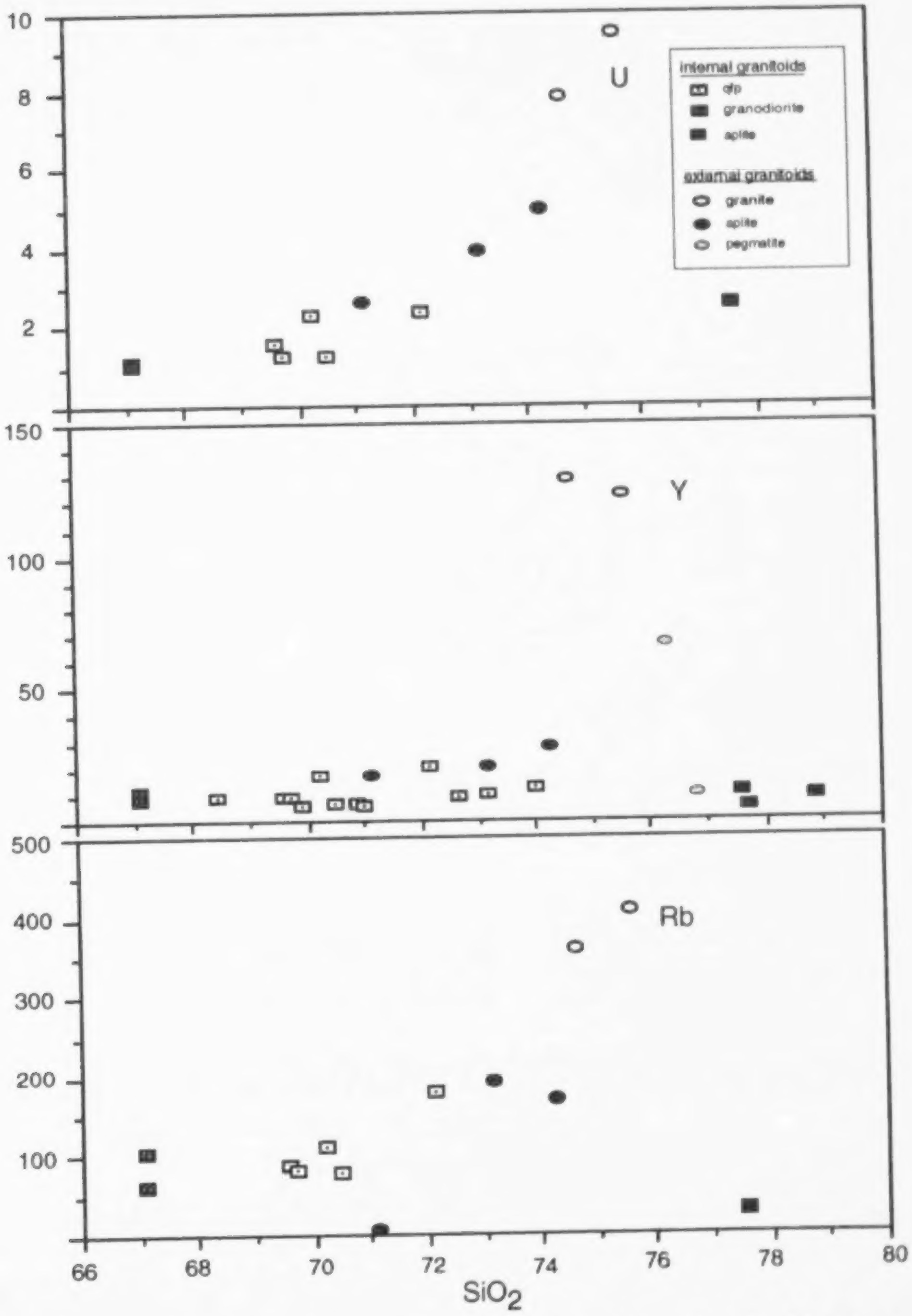

FIGURE 4-14. Trace element (U, Y and Rb) Harker plots for felsic intrusives, Ulu Claims, N.W.T. Trace elements in ppm by weight, SiO_2 in weight percent.

constituent lithologies of the internal and external granitoids as well as G-1 (standard granite, Mason and Moore, 1982) are given in Table 4-1.

	Internal Suite		External Suite			G-1
	QFP's and GD's	Grey aplites	Granite	Pink aplites	Pegmatite	Standard granite
n=	12	3	2	2	2	-
Ba	653	179	30	9	14	1220
Sr	409	146	11	17	16	250
Zr	135	47	92	50	25	210
Y	10	8	126	19	39	13
Nb	21	17	37	53	34	24
Rb	99	32	363	93	-	220
Th	8	6.4	25.4	9.1	-	50
Hf	3.9	2.5	6.7	11.8	-	5.2
Ta	1.6	1	3.0	14.7	-	1.5
U	1.6	2.5	8.7	3.3	-	3.4
La	23.8	6	10.6	2.4	9.5	101
Yb	0.9	0.8	13.5	6.7	-	1.1
Pb	11	20	55	16.5	-	48
Cs	5.7	0.3	10.4	4.8	-	1.5

TABLE 4.1. Average trace element contents (ppm) for internal and external suite granitoid rocks, Ulu Claims N.W.T. GD refer to granodiorites, QFP refer to quartz-feldspar porphyry dykes. Trace element contents of standard granite G-1 (Mason and Moore, 1982) shown for comparison.

The granodiorites and quartz-feldspar-porphyries of internal granitoid suite are characterized by high contents of Sr, Ba, Zr and La, and low concentrations of Hf, Ta, Pb, U, Y, Rb, Th and Cs, relative to the external granites. With the exception of Sr and Ta and Cs, the internal suite granodiorites and quartz-feldspar porphyries are depleted in the incompatible elements relative to the standard granite. The grey aplites are depleted in Ba, Sr, Rb, Zr, Hf, Ta, Y, Th, Cs and Nb relative to the less evolved members of the internal suite, and these elements display negative correlations with increasing silica content (Ba, Sr, Rb, Zr), or are at or near their detection limit (Hf, Ta, Y). U and Pb display positive correlation with increasing silica content, and are slightly enriched within the grey aplites.

The external granitoid suite exhibits a completely different pattern of trace element enrichment than the internal suite. The external granites are characterized by extreme depletion of Ba and Sr, and elevated Rb, Ta, Pb, U, Y, Th, Cs and Rb contents relative to the granodiorites and quartz-feldspar porphyries. Relative to the standard granite G-1, the external granites exhibit strong depletion in Ba, Sr, and Zr, strong enrichment in Y and Rb, and moderate enrichment of Nb, Hf, Ta, U, Pb and Cs.

Behavior of the trace elements in the external suite suite during differentiation of late stage distillates from the granites, also differs markedly from that observed within the internal suite. Elements such as Pb, U, Y, and Rb which are strongly enriched within the parental granites, exhibit significant depletion within the associated aplites. Conversely, Hf and Ta display strong enrichment within aplite dykes relative to the parental granites. The granite dyke collected in the Ulu West area, displays a unique trace element pattern, with decreased Ta, Hf, Pb, U, Y, Rb, but elevated Sr and Ba relative to the granite samples.

The differences in trace elements between the two suites may be expressed numerically using LIL element ratios (Rb/Sr and K/Rb) and these are given in Table 4-2 and are shown graphically in Figure 4-15.

	Internal Suite		**External Suite**	
	QFP/GD	Grey aplite	Granite	Pink aplite
n=	5	1	2	2
Rb/Sr (average)	0.35	0.24	34	8.95
Rb/Sr (range)	0.14-0.93	-	30-37	17.55-0.35
K/Rb (average)	296	635	113	334
K/Rb (range)	252-346	-	100-125	612-56

Table 4-2. Rb/Sr and K/Rb ratios for internal and external suite granitoids, Ulu Claims N.W.T.

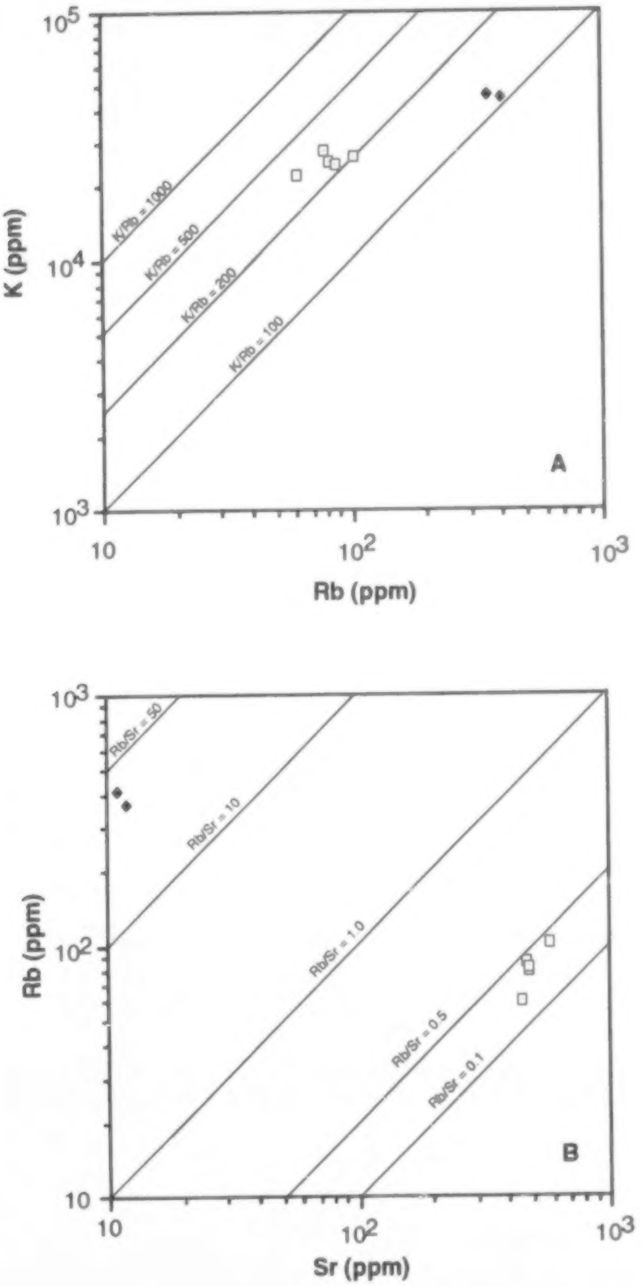

FIGURE 14-15. K/Rb (A) and Rb/Sr (B) variation diagrams for internal(open squares) and external granitoids (solid diamonds), Ulu Claims, N.W.T. Aplites, pegmatites and suspected contaminated dykes not plotted.

The high K/Rb and low Rb/Sr ratios of the internal intrusive suite at Ulu compare favorably with other synkinematic high Na/K Archean and younger trondhjemite-tonalite granitoid (TTG) suites world wide; Finland K/Rb = 150 - 500, Rb/Sr = 0.1-1.0, (Martin, 1987, 1983), Norway K/Rb = 246-470 (Size, 1975), Minnesota,. K/Rb = 332-408, Rb/Sr = 0.01 - 1.0, (Arth and Hanson, 1972), Nova Scotia, K/Rb = 210 (Albuquerue, 1977), Murchison Province, Western Australia, K/Rb = 305, Rb/Sr = 0.14 (Wang et al.,1993). The external suite granites display low Na/K and LIL element (high Rb/Sr ratios, low K/Rb ratios) characteristics common to late post-kinematic intrusives which commonly post-date TTG suites within Archean terranes (i.e, Yellowknife area, Slave Province (Drury, 1979), Australian Norseman-Wilna belt (Cassidy et al., 1991), Murchison Province, Western Australia (Wang et al., 1993) and Eastern Kaapvaal Shield, South Africa (Glikson and Jahn, 1985).

Rare earth element profiles are given for selected samples of the internal and external granitoid suites in Figure 4-16. The REE are normalized with chondritic values of Boynton (1985). Both the internal and external suites display distinctive and consistent REE patterns.

The internal granitoid suite is characterized by LREE enrichment and HREE depletion which results in a gently sloping, slightly concave downwards pattern. The high $(La/Yb)_N$ ratios of the internal suite rocks (11.28 to 37.32 for the dykes and plugs, 5.00 for the single grey aplite) and lack of significant negative Eu anomalies, reflect the fractionated nature of the REE and are typical of TTG granitoids (Barker and Arth, 1976; Albuquerque, 1977; Size, 1979; Martin, 1987; Martin et al., 1983; Arth and Hanson, 1972). Several samples display weak negative Eu anomalies, however these are restricted to the grey aplite, and several dykes from the Ulu West area which also display slightly elevated HREE contents. The weak negative Eu anomalies are likely due to removal of plagioclase from the melt during crystallization of the quartz-feldspar porphyries. The volume of this late stage differentiate was likely small, as no corresponding positive Eu anomalies are apparent within less differentiated members of this suite. The slightly elevated HREE from the Ulu west dykes may be attributed to contamination, possibly through assimilation of country rocks during emplacement. One sample of granodiorite exhibits minor LREE depletion, however, this is interpreted to be a post-crystallization disturbance, associated with the alteration and weathering observed in these rocks The overall REE pattern however, does not vary significantly from that of other rocks in the internal granitoid suite.

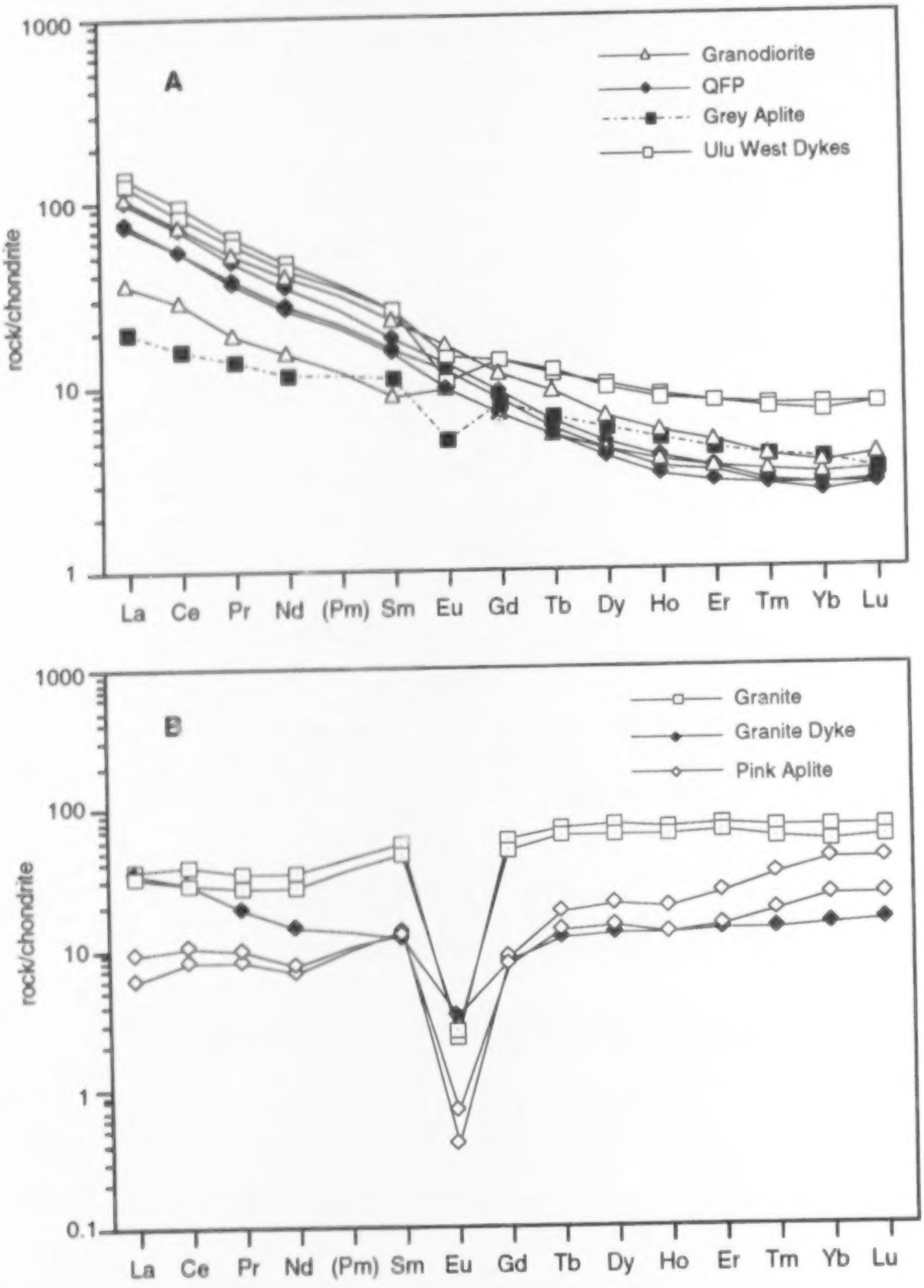

FIGURE 14-16. Chondrite normalized (Boynton, 1983) REE plots for internal (A) and external (B) granitoid suites,Ulu Claims, N.W.T.

The samples of the external granitoid suite are characterized by much flatter REE profiles with significant negative Eu anomalies. The granites display a convex upward pattern, while the pink aplites and dyke from the Ulu West area display a concave downward pattern. The $(La/Yb)_N$ ratios of the granites (0.50 and 0.56), pink aplites (0.15 and 0.41) and Ulu West dyke (2.43) reflect the higher HREE content of the rocks of this suite. The pink aplites contain an overall lower REE abundance than the parental granites, which is typical of anhydrous differentiates which generally contain lower REE contents than the parental magma (Hanson, 1980). This effect appears to be due to crystallization of mineral phases (most likely apatite and titanite) in the granite with high partition coefficients for the REE, resulting in the depletion of the REE within the distillates relative to the parent. The crystallization of apatite and titanite within the granite explains the discrepancy in the pattern of the REE between the granites and aplites (convex upwards versus concave downwards), as apatite and titanite have a slightly higher preference for the middle REE than for the LREE or HREE (Hanson, 1980).

The single granite dyke from the Ulu West area exhibits a unique profile, with some LREE depletion, which is thought to reflect contamination through assimilation of country rock.

The trace element and REE characteristics of igneous rocks are a function of several processes, including partial melting at the source of the melt, interaction of the magma with other lithologies or melts, crystallization, and finally post-crystallization processes. Behavior of a trace element during any stage of magma evolution is determined by its distribution between the melt coexisting mineral phases. The preference for a given trace element between a melt and a coexisting mineral phase may be described by a mineral/melt distribution coefficient (Kd) which is dependant both upon the temperature and the composition of the mineral and melt (Hanson, 1978). Large Kd's (>1) indicate that the trace element is preferentially incorporated into the mineral phase over the melt phase. Likewise small Kd's indicate that a trace element will not be incorporated into a mineral phase. Certain elements, such as zirconium which occur in low abundances, are present as integral structural elements of minor mineral phases (i.e. zircon), and do not exhibit true trace element behavior. The crystallization of trace mineral phases such as zircon or apatite however, may have a large effect on trace elements and REE patterns observed within a cogenetic suite. Elements variably termed large ion lithophile (LIL), incompatible, and hygromagmatic such as (Rb, Sr, Ba, Th, U, etc) generally have low Kds and are preferentially incorporated into the melt. These elements are particularly useful for qualitative source rock modelling, and for identifying residual phases and early crystal fractionates.

Examination of the trace element arrays of the igneous rock suites from the Ulu Claims indicates that each suite represents a unique source and differentiation history. The most obvious of these are the REE patterns of the two suites. The external granitoid suite displays strong negative Eu anomalies as well as extremely low Sr and Ba contents. This is best explained by removal of plagioclase from the melt which has large Kd's for Eu and Sr, and moderate Kd's for Ba (Hanson, 1980). The extremely low Ba contents of these granites also suggests that K-feldspar (high Kd for Ba) may have also been removed prior to crystallization.

The internal granitoids display HREE depletion which may be accounted for by a hornblende or garnet residuum during partial melting, as these minerals have high Kd's for the HREE (Hanson, 1980). In addition the internal granitoids have low Y contents relative to the external suite. Geochemically, Y behaves similarly to Yb (Cox et al., 1979), and would also be retained by hornblende and garnet. Alternately, Y has been shown to be incompatible during the melting of sediments (Pearce, 1989), suggesting that differences in Y content between the two suites may also reflect differing source lithologies.

The differences in the Rb content of the two suites cannot be explained by crystal fractionation, or by the presence of melt residua, but likely reflects the chemistry of the source region of the melts. Rb substitutes for K in K-feldspars and biotite (Hanson, 1978), and should therefore be readily incorporated into a partial melt at the eutectic minimum, and the K/Rb of the melt would be similar to K/Rb of the source rock. Examination of the Rb-poor internal suite on Figure 4-10 indicates that melting occurred above the eutectic minimum, which would result in all of the available K and Rb being incorporated into the melt, while the Rb rich external suite compositions are much nearer to the eutectic minimum. This implies a low K-Rb source for internal suite and a high K-Rb source for the external suite granites. Additionally the low Ba content of the external granites suggests some removal of K by crystal fractionation of K-feldspar, and therefore some Rb was also likely removed during this process, which suggests the original melt from which the granites crystallized contained even higher levels of Rb.

Petrogenesis

As demonstrated by the whole rock chemical relations, two distinct felsic intrusive episodes are present within the Ulu Claims. Geochemical data suggest that the melts from which these rocks crystallized originated from two distinct source regions, which can be largely constrained from major and trace element contents of these rocks. The internal suite of granitoids is analogous to trondhjemite-tonalite-granodiorites that are common within Archean terranes worldwide, while the external suite is chemically analogous to high K-post-kinematic granites.

The trondjemite-tonalites are low potassium, intrusive rocks which are further subdivided into two general categories: a high Al_2O_3 type (>15% wt %) and a low Al_2O_3 type (< 15 wt %) (Barker and Arth, 1976). With the exception of the most differentiated members of the suite, the internal granitoid rocks at Ulu fall into the high Al_20_3 designation. Characteristics of the high Al_2O_3 trondjhemites include low Rb but moderate to high Sr content, moderate LREE enrichment with HREE depletion, and no significant negative Eu anomalies (Barker and Arth, 1975), all of which are displayed by the internal granitoid suite at Ulu.

The genesis of trondhjemitic rocks has been widely investigated through empirical field studies (i.e. Barker and Arth, 1976; Barker, 1979; Martin, 1987;, Martin, et al., 1983; Size, 1979; Arth and Hanson, 1972; Albuquerque, 1976) and experimental studies (Johnston and Wyllie, 1988; Beard and Lofgren, 1991; Rapp et al., 1991), which has resulted in a plethora of hypotheses regarding the origins of these rocks including: 1) differentiation of wet basaltic magma, 2) partial melting of greywacke, 3) partial melting of eclogites, 4) partial melting of basalts or amphibolites, and 5) partial melting of pre-existing tonalitic basement. Differentiation of the wet basaltic magma may be discounted as a source for the Ulu trondjemites due to temporal and geological constraints. Partial melting of greywackes is not strongly favored for the formation of the Ulu trondjemites due to the high-K nature of the greywackes in the Ulu Claims area. Size (1979) also excludes greywackes as a source of Norwegian trondhjemitic rocks due to the HREE enrichment predicted in melts produced through the partial melting of greywackes.

Experimental studies have shown that partial melting of amphibolites and eclogites (Rapp et al., 1991; Beard and Lofgren, 1991) as well as tonalites (Johnston and Wyllie, 1988), leaving hornblende or garnet residua may produce melts consistent with the major, trace and rare earth element characteristics of trondhjemites. Quantitative trace element and REE modelling of Finnish trondhjemitic rocks (Martin, 1987; Martin et al., 1983) favor amphibolite or pre-existing tonalitic crust as a source of partial melting. Partial melting of an eclogitic source, is not favored (Martin, 1987), due to the high degree of partial melting (50%) of this lithology required to form a trondjhemitic magma (Martin, 1987; Rapp et al, 1991). The paucity of eclogitic rocks within presently preserved Archean terranes (Cunningham and Lambert, 1989), also does not support eclogites as a source of Archean trondhjemites.

Based upon available evidence, the internal intrusive suite within the Ulu Claims area likely originated through partial melting of amphibolites, or pre-existing tonalitic crust, however the former is currently favored due to a lack of evidence of pre-Yellowknife Supergroup basement in the Ulu Claims area.

The external granitoid suite within the Ulu Claims has a source of partial melting distinct from that of the internal suite. Based on the major and trace element characteristics of these rocks, a source of pre-existing sialic contentintal crust, most likely meta-sedimentary rocks with a strong pelitic component is suggested. The high degree of feldspar crystal fractionation evidenced by the low Eu, Sr and Ba contents of the external granites, suggests that these rocks may represent an evolved liquid composition. It is possible that these granites represent a highly evolved, late phase of the large batholiths surrounding the High Lake Belt. Regardless of whether the external granites represent an evolved fraction of a larger melt, or are representative of the extensive batholiths surrounding the High Lake Belt, major, trace and rare earth element data preclude any direct relationship through melting or differentiation with the internal granitoid suite present within the Ulu Claims.

5. U-Pb ZIRCON GEOCHRONOMETRY

INTRODUCTION

A U-Pb isotopic study of zircons from felsic and intermediate intrusive phases within the Ulu Claims was undertaken to constrain the temporal relationships between the ages of deformation, mineralization, and intrusion. Absolute ages determined for the internal granitoid suite (quartz-feldspar porphyries and granodiorites) and external granites would not only help elucidate the temporal relationships between these intrusive suites, but would also provide minimum ages for Type II mineralization (cross-cut by quartz-feldspar porphyries) and D_3 deformation (truncated by external granites).

Initially heavy minerals were extracted from small samples (5 kg) of the external granite and quartz-feldspar-porphyry, however these samples did not yield sufficient zircons of adequate quality for a reliable age. The following season three samples (10 kg) of internal granitoids and two samples of external granitoids were collected and again the zircon yield was poor. Despite the small sample size, analysis was attempted; the samples, however contained insufficient U and Pb for the mass spectrometric analysis.

Large (30-35 kg) samples were collected during the summer of 1993 which consisted of internal granitoids (quartz-feldspar porphyry [93HVRT-2] and granodiorite [93HVRT-3]), a dyke displaying geochemical characteristics of the internal granitoids from the Ulu West area (93HVRT-1) and an external granite (93HVRT-0). While these samples generally yielded sufficient quality zircons, only $^{207}Pb/^{206}Pb$ ages were obtained.

METHODS

In order to extract zircon for the age determinations, all samples were initially pulverized. The smaller samples (10 kg or less) were then sieved to -100 U.S. mesh size and the finest fractions were removed by repeated washing and pouring off of the suspended material. The larger samples were run on the Wilfley table in order to provide a heavy mineral concentrate.

Both the bulk samples and the heavy mineral concentrates were then purified by alternately settling in heavy liquids (tetrabromethane p=2.96 g/cm^3 and methylene iodide p=3.30 g/cm^3) and separating fractions of differing magnetic character using the Frantz isodynamic separator. The final zircon fraction was separated from material which sank in methylene iodide, and was nonmagnetic at

2 amperes with a tilt of 5° and a slope of 10° on the Frantz. During all stages of zircon extraction, steps were taken to avoid contamination, including rigorous cleaning of the crushers, disc mill and Wilfley table between samples, cleaning of all glassware with soap and water, and acetone and filtering of heavy liquids between each usage.

High quality zircons (those displaying a high degree of clarity and freedom from cracks, inclusions and cores) were then handpicked in ethanol from the zircon concentrates. The hand-picked zircons were air-abraded with pyrite and the final run fraction was re-picked. The U-Pb analytical procedure for the hand-picked, abraded zircons is described in Parrish et al., (1987).

Decay constants used were λ U_{238}=$1.55125*10^{-10}$ a^{-1} and λ U_{235}=$9.8485*10^{-10}$ a^{-1} and $^{238}U/^{235}U$ = 137.88 (Steiger and Jäger, 1977).

SAMPLE DESCRIPTIONS

Petrographic and geochemical characteristics of the intrusive units chosen for age determination are given in Chapter 3 and 4, respectively. Brief descriptions of the zircon morphologies for the four 1993 samples are given below.

93 HVTR-0

External suite granite collected adjacent to Flood Zone. Two distinct zircon morphologies were present in this sample and consisted of 1) a main population of white opaque to pale pink, clear stubby to elongate, euhedral prisms and rods (200-450 μm in length with 1:2 to 1:7 aspect ratios) with simple terminations; 2) a subordinate population of very clear to gemmy, pale pink-brown, euhedral, equant, multi-faceted trapezoids 150 to 200 μm in diameter. The zircon fraction run consisted primarily of the second morphology.

93 HVRT-1

Granitoid dyke (associated with internal suite) collected in Ulu West area. Zircon extracted from this sample consisted of brown-cloudy to pale pink-clear euhedral rods and stubby prisms both with complex terminations. A range of sizes from 720 to 100 μm with aspect ratios of 1:6 to 1:2.5 were present within the zircon population. The larger zircons were ubiquitously dark and cloudy, while the smaller stubby prisms tended to be pale pink and clear and made up the final run fraction for this sample.

93 HVRT-2

Quartz-feldspar-porphyry dyke (from internal suite) collected in East Limb area. Two main morphologies were present, a larger (650 to 400 μm) population of turbid, euhedral prisms (aspect ratios 1:4.5 to 1:2.5) with complex terminations which ranged in color from dark brown to white and a smaller (100 to 250 μm) population of pale pink-clear, rounded to complexly faceted, equant to football shaped (maximum aspect ratio 1:2.5) prisms. The larger zircons from this sample were commonly zoned and frequently contained cores. The final run fraction consisted primarily of clear, inclusion-free examples of the smaller morphology.

93 HVRT-3

Granodiorite plug (from internal suite) in Ulu West area. Zircons from this sample consisted of pale brown to pink 100 to 520 μm euhedral prisms (aspect ratios 1:2 to 1:4) with simple to complex double terminations. The majority of the zircons were turbid with zoning and cores. The run fraction consisted of clear, small, stubby prisms.

ANALYTICAL RESULTS

Analytical results are given in Table 5-1 and plotted on a concordia diagram in Figure 5-1.

Sample	wt (mg)	U (ppm)	Pb^1 (ppm)	Pb^2 (ppm)	$\frac{^{206}Pb}{^{238}U}$	$\frac{^{207}Pb}{^{235}U}$	$\frac{^{207}Pb}{^{206}Pb}$	$^{207}Pb/^{206}Pb$ age (Ma) ± 2σ
93HVRT 0	0.012	349	141.44	2.56	0.4710	11.0440	0.1701	2559 ± 3
					±0.094%	±0.131%	±0.051%	
93HVRT 1	0.014	109	54.12	0.03	0.5765	13.2814	0.1671	2529 ± 3
					±0.221%	±0.253%	±0.062%	
93HVRT 2	0.015	164	66.83	1.62	0.4730	10.7031	0.1642	2500 ± 22
					± 0.502%	±0.798%	±0.443%	
93HVRT 3	0.015	127	60.07	2.48	0.5465	12.9086	0.1713	2571 ± 8
					± 0.103%	± 0.249%	± 0.174%	

Pb^1- radiogenic lead, Pb^2-common lead, ^{204}Pb blank= 0.000143 ng. All errors one sigma., except as noted.

TABLE 5-1. Analytical data from Ulu Claims zircon samples.

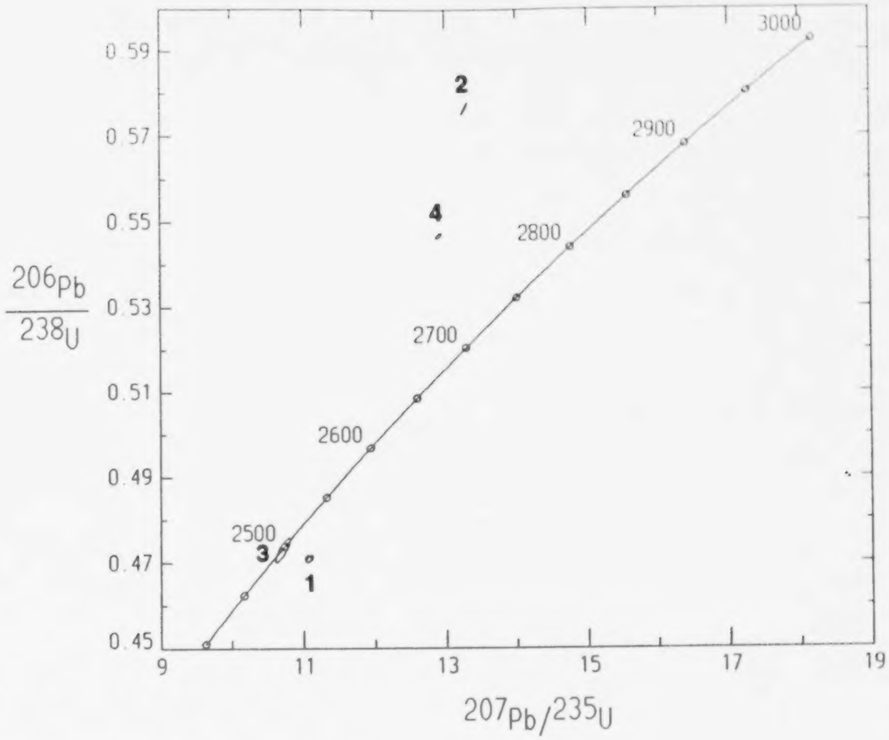

FIGURE 5-1. Concordia plot of U/Pb results for Ulu Claims zircons. 1) 93 HVRT-0, external suite granite, 2) 93 HVRT-1, internal suite dyke 3) 93 HVRT-2, internal suite quartz-feldspar porphyry dyke and 4) 93 HVRT-3, internal suite granodiorite.

DISCUSSION

The results of the U-Pb zircon systematics of the intrusives phases from the Ulu Claims are shown on a concordia plot in Figure 5-1. It can be seen that several of the samples plot above the concordia, a condition which does not normally occur within zircons, indicating that the uranium analysis for these samples has been compromised. Data points above the concordia indicate that either lead gain or uranium loss has occurred. The selection of high quality flaw free zircons should preclude significant U loss, as U occurs as an integral part of the zircon crystal structure. Although several samples plot below the concordia, all U analyses are suspect and are considered invalid.

The $^{207}Pb/^{206}Pb$ ages determined from the zircons of the intrusive units may be considered as a group to be valid, indicating a late Archean age for the intrusive activity. The range of ages (2500 - 2571 Ma) all clearly post-date U-Pb zircon ages (2690 Ma) for felsic volcanics (Henderson et al., 1993; Mortenson et al., 1988) within the High Lake Volcanic Belt. The temporal relationships given by the radiogenic ages agree with field relationships that the intrusive episodes are syn- to post-kinematic, and do not represent hypabyssal equivalents of the volcanic rocks found in the belt.

Although general ages of emplacement of the intrusive phases on the Ulu Claims are given by the $^{207}Pb/^{206}Pb$ ages, the mutual age relationships between the various units are ambiguous. The ages suggested by the Pb-Pb data for emplacement of the internal and external granitoid suites do not agree with geological relationships observed in the field. Since no valid U analyses are available for the zircons investigated, the degree of discordance, and hence the absolute error of the Pb-Pb ages is unknown. Due to the uncertainty of the U analysis, the Pb-Pb ages for both the internal and external granitoids should be regarded with caution with respect to both the absolute dates indicated for each intrusive body as well as the age relationships between the intrusive episodes.

6. GEOLOGY AND PETROGRAPHY OF MINERALIZATION

INTRODUCTION

Mineralization is found throughout the Ulu claims, and on the basis of occurrence, texture, mineralogy and temporal relationships, is divisible into three broad categories designated as Type I through III. Type I, stratiform base-metal mineralization is spatially limited to a contact between mafic volcanics and sediments in the western part of the claims. Type II mineralization consists dominantly of gold-arsenopyrite bearing replacement quartz veins, which are surrounded by an extensive hydrothermal alteration halo. Type II mineralization is the main exploration target on the claims and accounts for the bulk of the mineral inventory on the property. This mineralization type occurs in the central area of the claims predominantly within the core of the large north-south trending antiformal structure, and is hosted by mafic volcanics, and subordinate greywacke and gabbro. The third type of mineralization, Type III, consists of coarse, vuggy quartz veins, hosted by mafic volcanics, gabbros.and minor quartz feldspar porphyries. Mineralization within these veins occurs mainly as late fracture filling sulphides, including pyrite, pyrrhotite, chalcopyrite, native bismuth, gold, sphalerite, and rare arsenopyrite displaying a blocky habit. Type III veins show a strong relationship between bismuth and gold, although this relationship is not necessarily linear. Alteration is not significantly developed around these veins, however shearing is common in adjacent wallrock. Type III veins are found throughout the property, generally peripheral to Type II mineralization, and high densities of these veins are found in the western and northern portions of the claims.

TYPE I MINERALIZATION

Type I mineralization consists of stratiform base-metal occurrences and is very limited in areal distribution. Within the Ulu Claims Type I mineralization occurs only in one locality, proximal to a sediment-volcanic/gabbro contact in the western part of the property (Figure 6-1).

The Rhonda showing consists of sphalerite, galena, pyrite and pyrrhotite with gold and silver values hosted primarily within greywacke. Primary depositional textures of the sulfides have largely been eradicated by metamorphism, however recrystallized sphalerite occurs interstitially to clastic

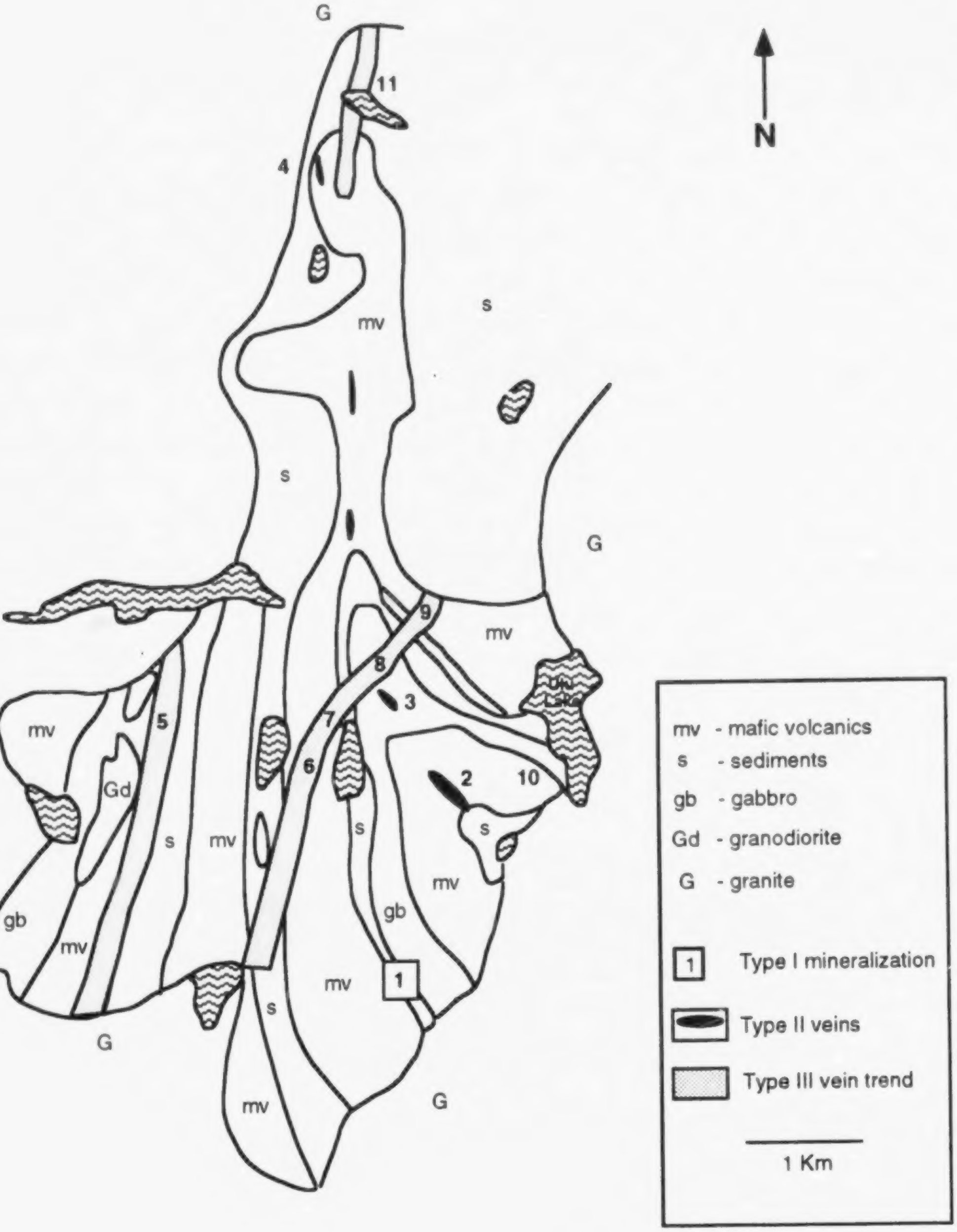
G
11
4
N
mv
s
s
G
9
mv
8
3
Ulu Lake
mv
5
7
G
6
2
10
Gd
s
mv
s
s
mv
gb
gb
mv
mv
1
s
G
mv
G
mv - mafic volcanics
s - sediments
gb - gabbro
Gd - granodiorite
G - granite
1 Type I mineralization
Type II veins
Type III vein trend
1 Km

FIGURE 6-1. Location of Type I, Type II and Type III mineralized zones Ulu Claims, N.W.T. Numbers refer to showings included in this study. Type I (1-Rhonda Lake). Type II (2-Flood Zone, 3-Gnu Zone, 4-NFN). Type III (5-Ulu west, 6-Emerald Lake, 7-GBZ, 8-Gnu, 9-Ravine, 10-East Limb, 11-NFN)

fragments within greywacke which is highly suggestive that mineralization was syn-depositional.

This type of mineralization is not considered a high priority target and therefore will not be examined in great detail. However, it is significant when considering the metallogenesis within the area. This mineralization type is considered to be of primary syngenetic exhalative origin, based on textural characteristics, and the occurrence of other syngenetic stratiform base metal mineralization in the Ulu Claims area (Ralph Claims) and within the High Lake Belt (High Lake deposit).

TYPE II MINERALIZATION

Introduction

Type II mineralization is the primary exploration target within the Ulu Claims, and consists of a main zone, the Flood Zone, and several peripheral zones displaying similar mineralogy, alteration and structural styles. Type II mineralization is hosted primarily by mafic volcanics, microgabbros and subordinate sediments. This mineralization type is characterized by grey quartz veins exhibiting a gold-arsenic geochemical signature surrounded by an extensive silicate mineral alteration halo. Type II mineralization is spatially restricted to the core of the the D_2 antiformal structure and is most abundant in the southern, open end of the fold. This study is focused on the Flood Zone, though several representative samples of peripheral zones, proximal to the Flood Zone, (the GNU zone and veins displaying similar geochemical signatures from the extreme north of the property, the NFN), are included for comparitive purposes (Figure 6-1).

Flood Zone Morphology and Structure

The Flood Zone is a tabular, steeply west dipping fracture system located within the west limb of the prominent D_2 antiformal structure. The zone consists of a series of quartz veins, 2-5 metres wide, which form a zone striking 300°. The Flood Zone is traceable on surface for 400 metres, and extends down dip for 600 metres with a steep westerly dip (Flood et al., 1991). Structural measurements taken of individual veins from an area of washed outcrop have a mean orientation of 155°/66° (Henderson et al., 1993). The veins strike more northerly than the zone itself indicating that the Flood Zone consists of a left stepping en echelon vein array (Henderson et al., 1993; Helmstaedt, 1992). Veins can be categorized as oblique extensional shear veins (Hodgson, 1989) and occupy a position equivalent to that of p-shears in a Riedel system (Helmstaedt, 1992).

Type II mineralization/alteration is almost totally confined to mafic volcanic/microgabbro units and terminates to the southwest and northeast against greywacke units. Volumetrically minor Type II mineralization occurs within sediments adjacent to the southeast volcanic/sediment contact. Mineralized zone development appears to be a function of mechanical anisotropies between the lithologies with mafic volcanics responding by brittle fracture compared to the ductile deforming greywackes. Maximum dilatancy within the Flood Zone occurs proximal to the southeast contact with sediments. This relationship suggests that rheological contrasts are also responsible for focussing of dilational zones, especially proximal to contacts.

The shear/fracture system hosting mineralization likely formed during D_2 deformation, and is consistent with the formation of a leg reef in a left lateral fault zone during early phases of folding (Helmstaedt, 1992). Assuming that the compressive stresses were oriented perpendicular to the axial surface of the fold, a left lateral fault zone could be expected to accommodate some of the shortening during folding (Helmstaedt, 1992).

Mineralized veins and associated alteration have been affected by a ductile deformation event which postdates most of the dominantly brittle deformation responsible for creation of the dilatant zones hosting mineralization (Helmstaedt, 1992). This ductile deformation resulted in a north-northwest striking, penetrative foliation which is restricted to the the alteration envelopes surrounding the mineralized veins, and does not extend into the surrounding unaltered host rock (Helmstaedt, 1992). Minor extension and boudinage of the quartz veins also occurred during this ductile deformation (Helmstaedt, 1992). The entire Flood Zone has also been affected by the regional D_3 deformation which has resulted in local undulation of the quartz veins, and crenulation of small veinlets and the north-northwest foliation associated with ductile shearing (Helmstaedt, 1992).

In summary, the structural characteristics of the Flood Zone indicate that initial dilatancies formed as fractures within the supracrustal package during the development of the regional D_2 fold structures. The fractures formed both as a result of shortening during folding, and contrasting rheological behavior between the mafic volcanics and the sediments. Type II mineralization appears to have been deposited initially under brittle deformation conditions, which progressed with time to a dominantly ductile phase of deformation. All phases of type II mineralization have been overprinted by regional D_3 deformation.

Vein Characteristics and Textures

Vein types associated with Type II mineralization within the Flood Zone are variable, although a distinct pattern in the progressive development of the veins is apparent. Type II mineralization appears to have a protracted depositional history under primarily brittle deformation conditions. Laminated and ribbon vein textures are common (Plates 6-1a,b), as are breccia veins (Plates 6-1c,d), and both types progressively grade into massive replacement veins. Replacement appears to have dominated during the termination of the mineralizing event, as re-brecciation of these veins is not apparent. Late ladder veinlet arrays and phantom veinlets are common within all vein types in Type II mineralization.

The ribbon veins contain septa of variably altered/mineralized wallrock which are oriented parallel to the walls of the veins. Veins of this type are generated by crack-seal mechanisms (Ramsay, 1989; Cox and Etheridge, 1983) at moderate to deep crustal levels, generally by open space filling during brittle deformation and high, oscillating P_{fluid} (Sibson, 1975; Barker, 1991). Breccia veins are common throughout the Flood Zone and are especially prevalent in large dilational zones near the southern sediment contact. These veins consist of angular, variably altered/mineralized wallrock fragments within a multiple generation quartz matrix. Alteration of wallrock fragments within the breccia veins appears to have occurred both prior to cataclasis and subsequent to breccia vein formation. Breccias also form in vein environments during brittle deformation and under extremely high P_{fluid} conditions (Colvine et al., 1988b).

Replacement veins within the Flood zone are essentially ribbon and breccia veins in which the wall rock has almost been entirely replaced by silica. The remnants of wallrock septa (or clasts) are manifested by the presence of refractory alteration phases such as Ti phases, tourmaline, and sulphide minerals (Plates 6-2c,d). Replacement veins generally form within ductile deformation zones under $P_{lithostatic}$ greater than $P_{hydrostatic}$ conditions, though ductile deformation may also be promoted by high fluid pressures (Colvine et al., 1988b).

Essentially all veins within Type II mineralization zones are cross-cut by late barren quartz veinlets which occur as ladder vein arrays (Hodgson, 1989) and phantom veinlets (Chace, 1949). Ladder veinlets occur as short extension gashes, and phantom veins are named after the difficulty in visually identifying their presence, due to the mineralogical similarity between host quartz and veinlet quartz. The timing of the ladder and phantom veinlets, though clearly later than the main vein filling stage, is uncertain.

A progressive sequence of vein formation, from ribbon and breccia veins to replacement veins is recorded during the main mineralizing stage within the Flood Zone. The complex developmental sequence displayed by the Type II veins is common to Archean Lode Gold Deposits (Hodgson, 1989; Colvine et al., 1988b). The presence of fluids during deformation may have a considerable effect on the deformation style observed within a shear system, and may affect the brittle-ductile transition point generally associated with the greenschist-amphibolite facies boundary. Brittle deformation may be induced or promoted by high P_{fluid}, and rocks altered by fluids (ie. silicified) may become resistant to shear and behave in a brittle fashion relative to unaltered rocks (Colvine et al., 1988b). This indicates that vein formation occurred initially under brittle deformation conditions with high P_{fluid} that at least periodically exceeded $P_{lithostatic}$ and progressed to ductile deformation conditions. This trend is mirrored by the gross external structural features of the shear/fracture system which also record a progressive shift from brittle to ductile conditions. Whether ductile conditions were induced by variations in crustal levels during zone formation, or by silicification and reduction of permeability with a corresponding increase in P_{fluid} is not clear. However, regardless of the mechanism responsible for this shift in deformation conditions, the veins and alteration halo were affected preferentially over surrounding unaltered host rocks. Ductility may have been enhanced by the presence of biotite within the alteration halo surrounding the veins.

Veins within the Gnu Zone are hosted within gabbroic rocks and display textural characteristics common to the Flood Zone, being comprised of both ribbon/laminated veins, and breccia veins. Replacement type veins derived from the former vein types have not been observed within the Gnu Zone.

In the NFN area the Type II veins are hosted within mafic volcanic rocks. Vein morphologies and textures differ slightly from those observed within Type II mineralization to the south. Veins here consists of more massive, discreet veins, and lack any appreciable halos of wallrock alteration. However, they contain altered wallrock clasts and show the same geochemical association of gold with arsenic as other Type II vein occurrences. Sphalerite is also relatively abundant within these veins, and arsenopyrite tends to be less abundant and occurs primarily as the coarser, blocky morphology. The differences observed may be due

Plate 6-1

Type II mineralized veins from the Flood Zone.

6-1a 90PAK-US-14
Ribboned quartz vein. The ribbons are the altered/sulphidated remnants of mafic volcanic wallrock septa incorporated into the vein during successive episodes of fracturing and silica flooding.

6-1b 90PAK-US-27
Crack and seal vein, with incorporation of planar mafic volcanic wallrock septa. Wallrock shows variable degree of alteration and up to 30% acicular arsenopyrite. Continued alteration of wallrock septa results in ribbons as seen in 90PAK-US-14 (Plate **6-1a**).

6-1c. 90PAK-US-25
Brecciated crack-seal vein containing fragments of mineralized mafic volcanics. Dark mass at left of photograph is massive tourmaline. Dark bands within wallrock are also due to the presence of tourmaline.

6-1d 90PAK-US-35
Breccia vein containing altered/mineralized mafic volcanic wallrock fragments.

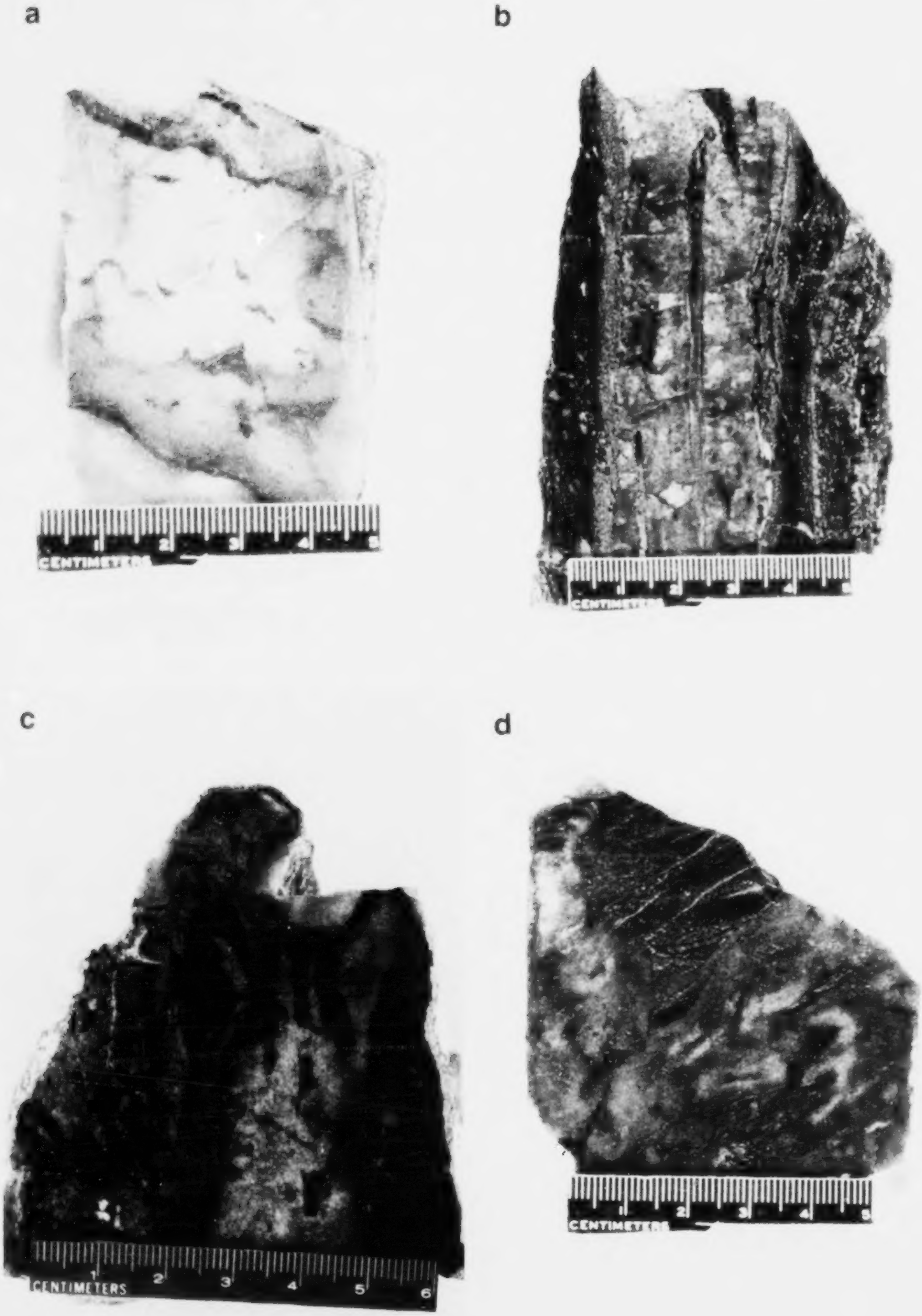
a
b
c
d
CENTIMETERS
CENTIMETERS
CENTIMETERS
CENTIMETERS

to slightly higher temperatures, and limited permeability within the northern, tight end of the fold.

Vein Mineralogy

As mentioned previously, vein morphology consists of ribbon and breccia veins, which in part have become replacement veins. Typical vein morphology consists of variably altered to almost totally replaced wallrock within a multistage quartz ± calcite matrix. Sulphide-gold mineralization is hosted primarily within altered wallrock incorporated as fragments within, and selvages adjacent to the veins. Minor amounts of sulphide and gold mineralization are present within quartz rich domains of the veins, and this in part may reflect skialithic wallrock in which only sulphide minerals remain.

Quartz

Quartz within Type II veins is the most abundant vein fill mineral, and occurs in two main forms. The most abundant is grey, fine-to medium-grained, and forms the bulk of the vein fill. The textures displayed by this main stage vein fill quartz vary from polygonal, with triple 120° grain boundary junctions and even extinction (Plates 6-2a,b), to highly embayed and sutured grains with subgrain development and undulose extinction. The microstructures displayed by this quartz type indicate that an episode of post depositional ductile deformation affected these veins (Robert and Kelly, 1987). Fluid inclusions within these quartz grains are largely at the rims of the crystals and very fine (< 100um) inclusions of tourmaline are common. The presence of refractory mineral phases as inclusions within quartz grains supports replacement as a significant mechanism in vein formation (e.g. Hodgson, 1989). Examination of Type II mineralized material by cathodoluminescence techniques reveals that two distinct varieties of main vein fill quartz exist. An earlier phase of quartz luminesces pale yellow, while later phases do not. Pale yellow luminescent quartz occurs as angular domains within the non-luminescent quartz, and along the vein-wallrock boundaries. Alteration and sulphide-gold mineralization appear to be associated with deposition of both the luminescent and non-luminescent phases of quartz.

The second type of quartz is coarser-grained, and occurs as relatively thin (1.0 - 0.25 cm) ladder and phantom veinlets cross-cutting earlier quartz. This quartz tends to be colorless to white and displays variable amounts of strain, manifested by undulatory extinction and deformation lamellae. Weakly embayed and sutured grain boundaries are common and incipient grains are rare. Negligible sulphide mineralization is associated with these late cross-cutting veinlets, which appear to have formed by brittle fracturing of previously formed veins. Microstructures displayed by the ladder and phantom veinlets suggest that the quartz within these veins has undergone considerably less deformation than the main stage quartz, and developed after the ductile deformational event which affected the bulk of the veins.

Wall rock Fragments / Vein Selvages

Vein selvages, wallrock fragments and septa host the vast majority of sulphides and gold found within Type II mineralization They will thus be considered as part of the vein assemblage, rather than associated silicate alteration, although the mineral assemblages are similar in both. Wallrock fragments and septa may make up a considerable percentage of the mineralized veins (Plates 6-1a-d). Alteration mineral assemblages observed within mafic volcanic wallrock fragments, septa and selvages immediately adjacent to veins are highly variable. This variability appears to be a function of water-rock ratio within individual veins during the mineralizing event, with very strongly altered or replaced wallrock representing major conduits.

Mafic volcanic wallrock fragments and septa incorporated within quartz veins, show an early silicate alteration assemblage of biotite + clinozoisite + titanite + sericite ± tourmaline ± epidote. This alteration assemblage generally occurs away from the immediate wallrock-vein boundaries or within the centers of moderately altered fragments and septa. Arsenopyrite and pyrrhotite may also form a significant portion of the early alteration assemblages,

Advanced alteration assemblages are found rimming clasts and are adjacent to vein-wallrock margins, often overprinting earlier alteration. The assemblage consists of hornblende/actinolite ± microcline ± quartz, and is transitional thru microcline ± quartz to complete quartz replacement.

Strongly altered mafic volcanic wallrock clasts and septa contain only quartz and microcline with sulphide minerals (arsenopyrite, pyrrhotite, pyrite), gold and refractory oxide and silicate alteration minerals such as titanite, and tourmaline (Plates 6-2c,d). The clasts and septa are commonly pink to black in color reflecting the presence of titanite and tourmaline respectively. In cases of extreme replacement, the presence of wallrock septa and fragments is not possible in hand specimen. They occur as sulphide rich domains within otherwise homogeneous quartz veins.

Within sedimentary host rocks, silicate alteration assemblages of vein selvages and wallrock clasts display less variability than within mafic volcanic hosts, reflecting the limited interaction of the mineralizing fluid due to limited permeability. Alteration assemblages consist primarily of sericite + biotite + clinozoisite. These phases may be overprinted by an advanced assemblage consisting of euhedral green hornblende and microcline.

Calcite

Calcite forms a very minor constituent of Type II mineralized veins, being more commonly associated with the outer alteration halos surrounding these veins. Within the veins, calcite occurs interstitial to quartz grains (Plate 6-2b) and occasionally as an alteration mineral associated with actinolite. The presence of calcite is easily detected with the aid of the cathodoluminescence microscope, because it luminesces bright orange. In general, calcite forms less than one percent of the veins.

Potassium Feldspar

Microcline is relatively common within the mineralized veins as masses of anhedral crystals associated with strong alteration. Microcline is the predominant silicate mineral within very strongly altered wallrock clasts (Plate 6-2d), and often forms thin selvages immediately adjacent to vein-wallrock contacts (Plate 6-6d). Tartan twinning within the microcline grains is not ubiquitous. The identification of potassium feldspar is aided by its blue luminescence under the cathodoluminescence microscope.

Amphibole

Amphibole, consisting primarily of pale green varieties (actinolite), is common within Type II veins. The amphiboles are usually found along the vein-wallrock contact, but individual amphibole crystals are common within the veins. Along vein-wallrock contacts, actinolite grains display poikiolitic textures, incorporating small anhedral quartz and microcline grains (Plate 6-6d).

Plate 6-2

Gangue mineralogy of Type II veins from the Flood Zone.

6-2a Photomicrograph, (xpl), 90PAK-US-14
Recrystallized vein quartz. Note equant morphology of individual crystals, predominance of triple 120° grain boundaries and lack of straining.

6-2b Photomicrograph, (xpl), 90PAK-US-25
Recrystallized vein quartz with carbonate. Note triple 120° and sutured grain boundaries between quartz grains, and the occurrence of carbonate (calcite) interstitial to and along quartz grain boundaries.

6-2c Photomicrograph, (ppl), 90PAK-US-14
Wallrock ribbon with mineral assemblage of arsenopyrite (opaque)+tourmaline+microcline+quartz. Tourmaline (brown mineral with pseudo-hexagonal cross-sections) makes up the majority of the photograph. In handspecimen (Plate **6-1a**) tourmaline bearing wallrock ribbons are black in color.

6-2d Photomicrograph, (ppl), 90PAK-US-8
Strongly altered/mineralized wallrock clast from breccia vein. Mineral assemblage consists of microcline+titanite (ti)+arsenopyrite (asp)+minor quartz and biotite.

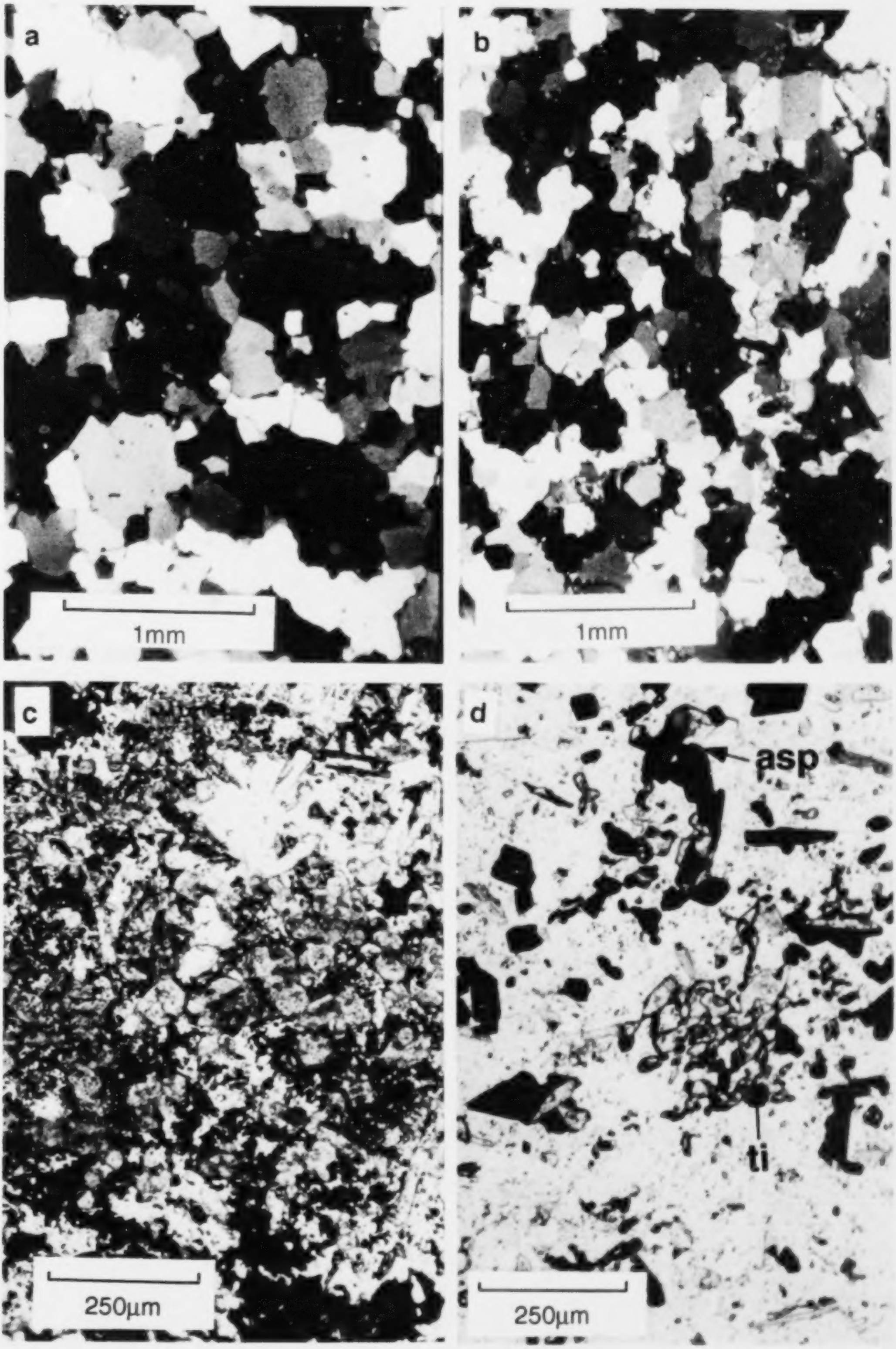
a
1mm
b
1mm
c
250μm
d
asp
ti
250μm

Apatite

Apatite, though uncommon, is distributed throughout the Type II veins. This mineral occurs as minute (<10um) anhedral crystals, and is found as single grains within the quartz rich portions of the veins, and as clusters of grains within altered wallrock fragments and septa. The identification of apatite is aided by its bright yellow luminescence under the cathodoluminescence microscope.

Titanite

Titanite is a relatively common mineral within altered mafic volcanic wallrock fragments and septa within Type II veins. Titanite forms euhedral diamond shaped crystals within moderately altered wallrock, and anhedral masses within strongly altered/replaced wallrock. The anhedral form of titanite within strongly altered wallrock often displays a distinct pink pleochroism. Titanite within Type II veins and alteration is clearly hydrothermal in origin, replacing ilmenite from the original mafic volcanics (Plates 6-2d, 6-4a, 6-5d). Titanite is commonly observed to form rims around corroded ilmenite grains within weak to moderately altered mafic wallrock (Plate 6-4a).

Tourmaline

Tourmaline is a brown to black, dravite-schorl variety (Plate 6-2c) and is a relatively common vein constituent. Tourmaline occurs with altered wallrock fragments and septa, as small (10um) euhedral crystals, often showing color zonation from brown to green in cross-section . This form of tourmaline appears to be an early alteration phase, which has remained stable during the alteration process due to its refractory nature. More rarely tourmaline occurs as 1-2 centimeter masses of black-blue blocky crystals (Plate 6-1c), or needle-like aggregates within quartz. The presence of very fine-grained (1µm), euhedral crystals of tourmaline as inclusions within quartz grains is a characteristic feature of the Type II veins.

Ore Petrology

Sulphide mineralogy within Type II veins consists of arsenopyrite, pyrrhotite, pyrite, and chalcopyrite, with trace amounts of sphalerite and galena. Sulphide mineralization occurs within altered wallrock, and domains of replaced wallrock. Broad halos of finely disseminated pyrrhotite and pyrite occur within the mafic volcanics peripheral to the mineralized veins.

Arsenopyrite

Arsenopyrite is the most abundant sulphide mineral within Type II mineralization, and occurs most commonly within wallrock clasts, and in altered wallrock adjacent to the veins (Plates 6-2 d,c, 6-3a-d, 6-4a,b,c). Various morphologies of arsenopyrite occur, with fine acicular crystals generally <25 µm being closely associated with high gold values. The abundance and occurrence of this morphology of arsenopyrite may be used as a visual guide to outline zones of economic mineralization. The acicular arsenopyrite occurs as individual, euhedral, needles, which are diamond shaped in cross-section, or as felted masses of these crystals. Rarely do individual crystals occur within the veins at quartz grain boundaries, however the majority of occurrences are within domains of altered or replaced wallrock. Anhedral inclusions of pyrrhotite and chalcopyrite are common within the acicular arsenopyrite. Atoll textures may be present (Plate 6-3a), with pyrrhotite forming the cores of arsenopyrite grains, suggesting that in part arsenopyrite may be replacing earlier pyrrhotite grains. A pale pink mineral forming rims on arsenopyrite grains was found by EDS-SEM analysis to be titanium enriched arsenopyrite (Flood et al., 1991).

A second morphology of arsenopyrite appears as blocky euhedral crystals, and anhedral masses and occurs within alteration zones surrounding the veins, and peripheral to zones containing the fine acicular crystals. Individual crystals of the blocky type of arsenopyrite, are generally > 50 µm. Although anomalous gold values are associated with veins and alteration assemblages containing blocky arsenopyrite, the values are generally subeconomic.

On the surface, zones rich in arsenopyrite may show significant alteration to scorodite, which forms a microcrystalline green-blue crust on the mineralized boulders. A second unknown form of arsenic rich weathering product is a pale orange film on arsenopyrite bearing rocks.

Association of fine acicular arsenopyrite with significant gold mineralization has been observed in several lode gold deposits (Kuryliw, 1988). Pressure, and more likely temperature gradients are responsible for the variation in arsenopyrite morphology observed within these gold deposits (Kuryliw, 1988). The acicular variety is associated with the higher temperature inner cores of mineralized zones, while the blocky variety occurs peripherally and presumably was deposited under slightly cooler conditions.

Pyrrhotite

Pyrrhotite is generally more abundant than pyrite within mineralized Type II veins. Within these mineralized veins, pyrrhotite occurs as euhedral grains or anhedral masses often encompassing arsenopyrite and gold grains. Intergrowths of pyrrhotite with chalcopyrite are common within the anhedral masses which commonly encompass acicular arsenopyrite grains. Pyrrhotite also occurs as small anhedral inclusions (10-20 μm) within arsenopyrite crystals.

Pyrrhotite is also common within alteration zones surrounding mineralized veins, occurring as fine disseminations, and as thin veinlets which parallel the foliation within the alteration zones. Fine disseminations of pyrrhotite also occur as broad halos surrounding mineralization and alteration within mafic volcanic host rocks.

Pyrrhotite from samples collected from surface showings and shallow drillholes ubiquitously display retrograde alteration (Plates 6-3b,c). A progression of alteration from pyrrhotite through to marcasite (displaying bird's eye textures), to Fe-oxides is observed.

Pyrite

Pyrite is relatively common within the Type II mineralized zones, and locally may be more abundant than pyrrhotite. Several morphologies of pyrite are present and deposition of this mineral occurs throughout the paragenetic sequence of vein fill. Pyrite associated with the main vein fill occurs as anhedral masses proximal to vein-wallrock margins, and is commonly intergrown with fine acicular arsenopyrite crystals, and pyrrhotite (Plates 6-3b,c).

A second occurrence of pyrite is as single, euhedral, cubic crystals, which vary in size from 250 μm to 2 mm, and are localized within quartz proximal to wallrock contacts. This occurrence of pyrite appears to be latest stage sulphide mineralization within Type II veins. These single pyrite crystals may show peculiar breccia textures, which appear to be a function of brittle behavior of the pyrite during recrystallization of the surrounding quartz (Plate 6-3d).

Retrograde alteration of the pyrite is not as common as that observed within pyrrhotite, although during petrographic observation, thin rims of an Fe-oxide rimming pyrite grains are visible.

Plate 6-3

Sulphide mineral relationships from Type II mineralization from the Flood Zone.

6-3a Photomicrograph, (ppl), 90PAK-US-25
Acicular arsenopyrite within altered wallrock fragments incorporated into quartz vein. Note diamond shaped cross-sections and atoll textures within large grains in center of photograph.

6-3b Photomicrograph, (ppl), 90PAK-US-25
Coexisting arsenopyrite (asp), pyrite (py) and pyrrhotite (po) within altered small wallrock fragment within a quartz vein. Pyrrhotite shows strong retrograde alteration to marcasite displaying 'birds eye' textures. Retrograde alteration of pyrrhotite is ubiquitous in Type II mineralization within surface and shallow drillcore samples.

6-3c Photomicrograph, (xpl), 90PAK-US-25
Close-up of coexisting arsenopyrite (asp), pyrite (py) and pyrrhotite (po), using a Normarski phase interference lense.

6-3d Photomicrograph, (ppl), 90PAK-US-16
Late pyrite (py) with brecciated textures occurring within vein quartz adjacent to arsenopyrite (asp) rich, altered mafic volcanic wallrock.

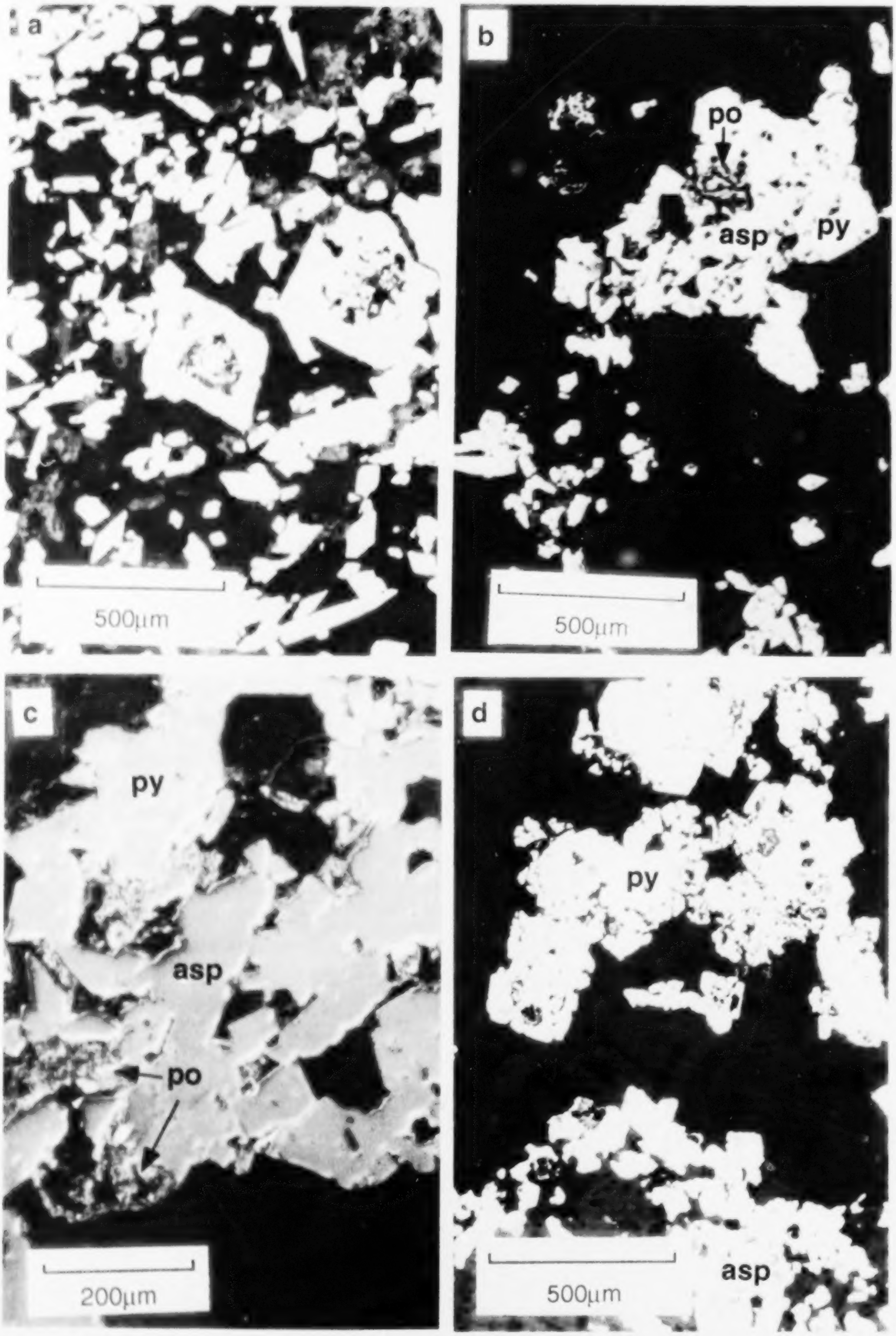
a
500µm
b
po
asp
py
500µm
c
py
asp
po
200µm
d
py
asp
500µm

Chalcopyrite

Chalcopyrite is a relatively rare sulfide mineral within Type II veins, occuring most commonly as anhedral inclusions to 10 μm within pyrrhotite grains. Chalcopyrite also occurs as similar sized inclusions within arsenopyrite and rarely as anhedral blebs within the quartz veins. No retrograde alteration of chalcopyrite is present, and it sometimes occurs as masses within Fe-oxides which presumably represent weathered pyrrhotite.

Sphalerite

Sphalerite is reported as a very minor constituent of Type II veins, occuring as small anhedral crystals (Peterson, 1991a). Sphalerite was not observed within Type II vein material in the current study.

Gold

Gold occurs in the native state and is found primarily within altered wallrock, within and adjacent to the veins. Individual grains of gold occur as anhedral masses and vary in size from 5 to 250 μm, with an average size of 100 μm. Gold occurs in several different settings within the mineralization, and there is a relatively strong correlation between gold and the presence of fine acicular arsenopyrite. In the polished thin-sections observed, gold occurs commonly as solid inclusions within arsenopyrite, as blebs adhering to its grains (Plates 6-3a,b,c), and within silicate minerals in close proximity to arsenopyrite (Plate 6-3b). In addition, gold rarely occurs at quartz grain boundaries within quartz veins themselves. A final episode of gold mineralization is as anhedral blebs associated with late euhedral pyrite crystals occuring proximal to vein-wallrock margins (Plate 6-3d). Preliminary S.E.M. analysis of gold grains associated with arsenopyrite (Smith, 1991) shows gold to be of a high fineness, with levels of arsenic and copper below detection. Gold to silver ratios are generally around 20:1, in agreement with geochemical assays.

Alteration

Within the Flood Zone, alteration envelopes consisting of silicification, potassium and boron metasomatism, as well as carbonation, extend for tens of metres into both hanging and footwall peripheral to the veins. Alteration typically consists of millimeter to centimetre scale quartz ± carbonate veinlets surrounded by a suite of alteration minerals. The intensity of alteration typically decreases

Plate 6-4

Gold in Type II mineralized veins from the Flood Zone.

6-4a Photomicrograph, (ppl) 90PAK-US-25
Native gold intergrown with acicular arsenopyrite within altered mafic volcanic wallrock fragment. Note titanite (ti) overgrowth on ilmenite (il) grains on left side of photograph.

6-4b Photomicrograph, (ppl), 90PAK-US-14
Native gold occuring with arsenopyrite, and within silicate gangue adjacent to the arsenopyrite grain.

6-4c Photomicrograph, (ppl), 90PAK-US-25
Native gold grain in contact with an arsenopyrite (asp) crystal, overgrown by pyrite (py), occurring within altered mafic wallrock fragment.

6-4d Photomicrograph, (ppl), 90PAK-US-10
Native gold grain in association with late pyrite, occurring within quartz adjacent to arsenopyrite rich altered mafic volcanic wallrock.

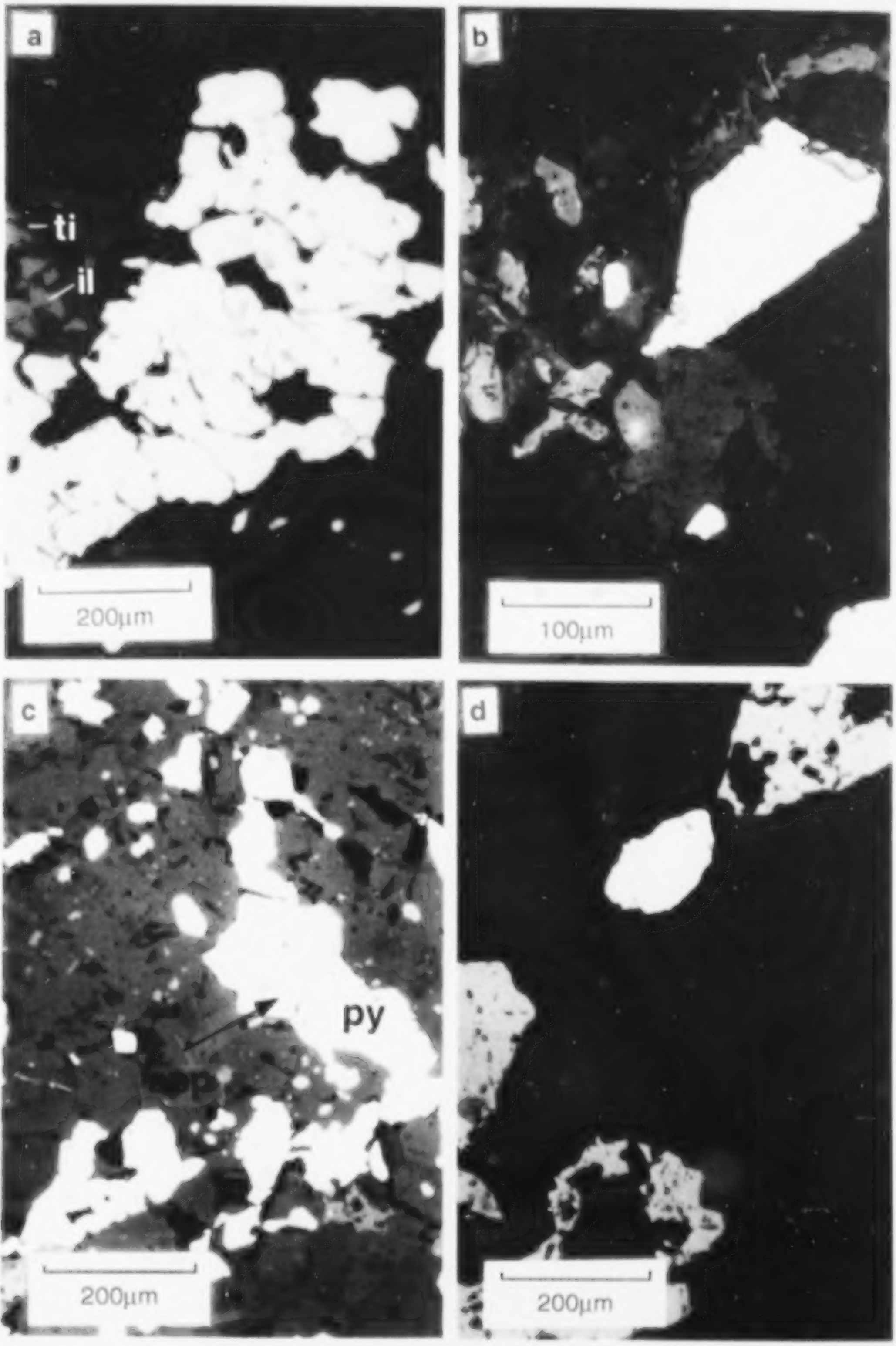
a
ti
il
200µm
b
100µm
c
py
200µm
d
200µm

away from the mineralized zones, and is generally governed by the density of the small veinlets, which in strong, pervasively altered rocks have overlapping alteration halos so as to obliterate completely the original host rock mineralogy. Veinlet style is variable, and is in part oriented and defines foliation within the altered rock, however stockwork veinlets are also relatively common. Regardless of veinlet type, it seems apparent that brittle fracturing is an important control on the development of the veinlets, and hence the alteration halos.

A distinct pattern of alteration assemblages occurs adjacent to the veins and in wallrock incorporated within the veins. Alteration appears to be progressive, with later assemblages overprinting earlier assemblages, as vein/veinlet formation occurs. A broad zonation is also apparent in macroscale, with alteration adjacent to mineralized veins consisting of actinolite/hornblende, microcline, quartz, clinozoisite and titanite, either as pervasive alteration or dense stockworking (Plates 6-6 a-d). Peripheral to this assemblage is an area of pervasive biotite alteration which is often centered about millimeter scale tourmaline rich veinlets (Plates 6-5 a-d). Clinozoisite, titanite, epidote, and sericite are also common within the area of pervasive biotite alteration. The outer most alteration assemblage is dominated by calcite/actinolite veins and veinlets. The dimensions of these outer calcite/actinolite veins are somewhat correlative to the overall size of the mineralized zones with which they are associated, with larger veins up to 0.50 metres wide being associated with extensive mineralization. No cryptic type alteration (Robert and Kelly, 1987) has been observed related to Type II mineralization, suggesting the dependance of alteration and mineralization on fracturing.

Alteration peripheral to mineralized sediments is very limited in extent, and is essentially identical to the alteration observed in wallrock clasts within the veins. Alteration assemblages within the sediment adjacent to mineralized veins consists of sericite + muscovite + biotite + clinozoisite, often with an overprint of euhedral green hornblende within strongly altered domains.

Vein Paragenesis

The overall paragenesis of Type II veins is shown diagrammatically in Figure 6-2. Main vein fill occurred under primarily brittle deformation conditions. A period of ductile deformation occurred near or slightly postdating the termination of the mineralizing event, followed by late brittle deformation and the

Plate 6-5

Examples of early alteration assemblages within mafic volcanics peripheral to Type II mineralization from the Flood Zone.

6-5a 90VD-25 (187.75m)
Drillcore sample of weak biotite alteration from mafic volcanics between several mineralized lenses. Biotite occurs as thin stringers and as a weak pervasive alteration mineral. Darker green domains occurring adjacent to biotite stringers are massive recrystallized (hydrothermal) hornblende.

6-5b Photomicrograph, (ppl), 90VD-25 (187.75m)
Relatively unaltered mafic volcanics with typical mineral assemblage of hornblende+plagioclase+ilmenite displaying an palimpsest texture of quickly chilled basalts (radiating aggregates of hornblende). Minor biotite alteration is visible in lower right of photograph.

6-5c Photomicrograph, (ppl), 90VD-25 (187.75m)
Details of biotite stringer. Note the biotite alteration is centered about a tiny tourmaline (tm) veinlet.

6-5d Photomicrograph, (ppl), 90VD-25 (187.75m)
Close-up of biotite replacing metamorphic hornblende. Note titanite (ti) grains after ilmenite within biotite alteration.

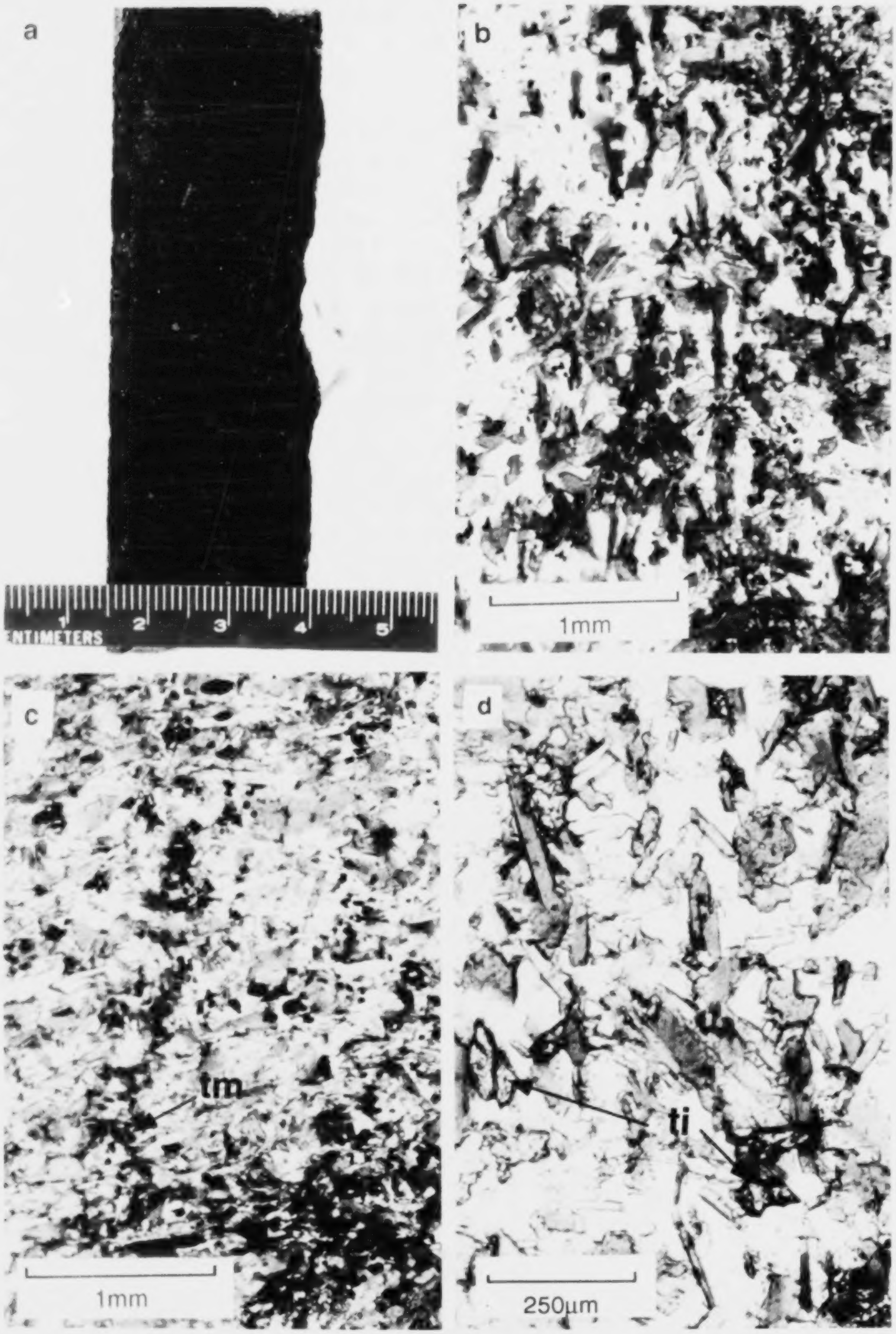
a
b
1 2 3 4 5
ENTIMETERS
1mm
c
tm
1mm
d
ti
250µm

Plate 6-6

Examples of advanced alteration assemblages within within mafic volcanics peripheral to Type II mineralization from the Flood Zone.

6-6a 90VD-47 (347.00m).
Drillcore sample of advanced alteration associated with Type II mineralized veins. Dark domains represent weakly or unaltered hornblende rich mafic volcanics. Degree of alteration appears to diminish away from sub-centimetre scale, irregular quartz veinlets. Sample contains 1/2% acicular arsenopyrite, occurring primarily at the boundary between weakly/unaltered mafic volcanics and clinozoisite rich alteration.

6-6b Photomicrograph, (ppl), 90VD-47 (349.90m)
Tourmaline (tm)+quartz+clinozoisite (cz) veinlet in unaltered hornblende rich mafic volcanics. Minor biotite is also present, associated with the veinlet.

6-6c Photomicrograph, (xpl), 90VD-47 (347.00m)
Alteration of mafic volcanics consisting of clinozoisite (displaying anomolous blue interference colors)+biotite+titanite with an overprint of late euhedral actinolite crystals (pale green) and minor euhedral acicular arsenopyrite (opaques). In handspecimen (Plate **6-6a**) the clinozoisite-rich alteration apppears as creamy white domains.

6-6d Photomicrograph, (xpl), 90VD-47 (347.00m)
Strong, advanced alteration of mafic volcanics consisting of actinolite+microcline+quartz adjacent to quartz veinlet.

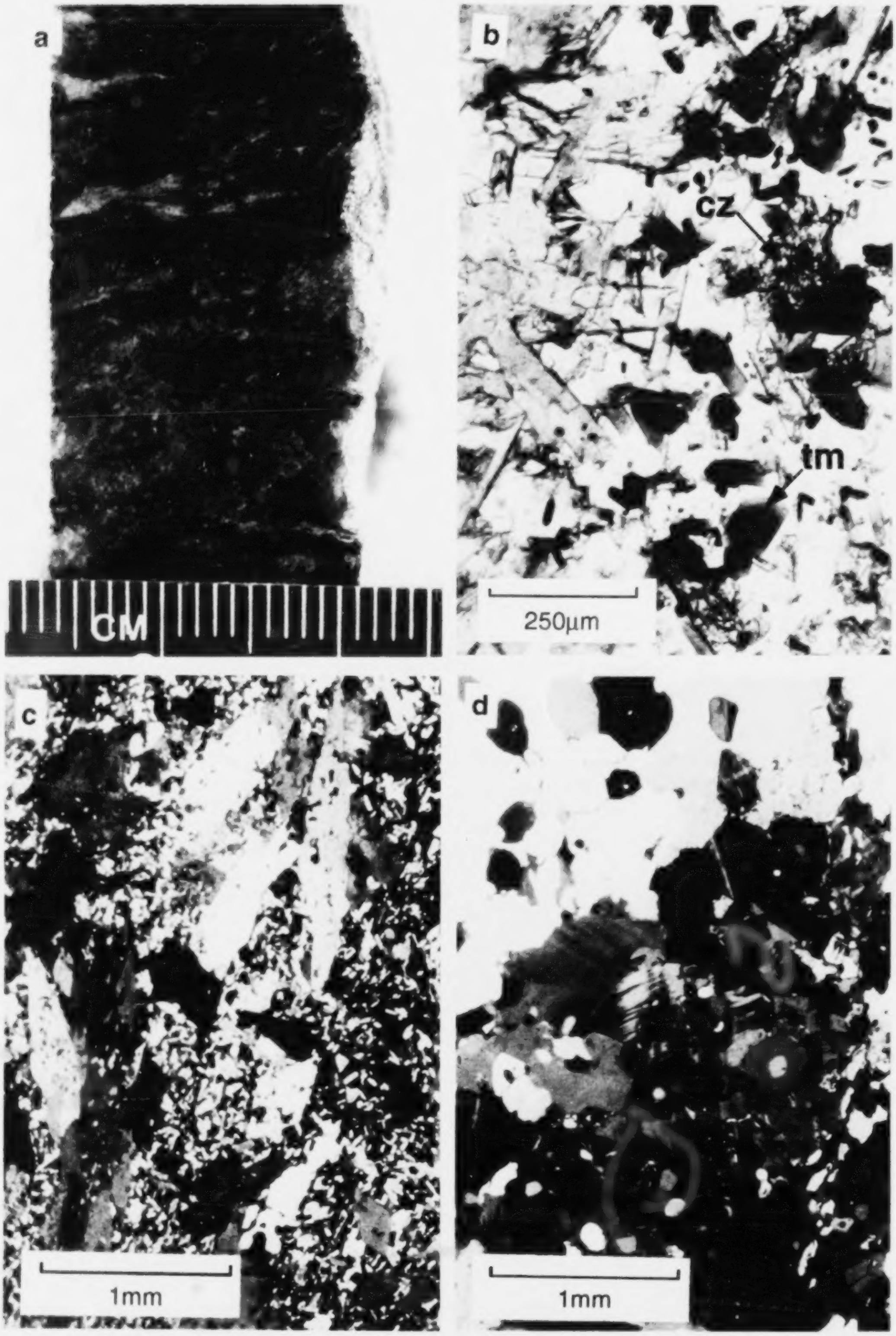
a
CM
b
cz
tm
250µm
c
1mm
d
1mm

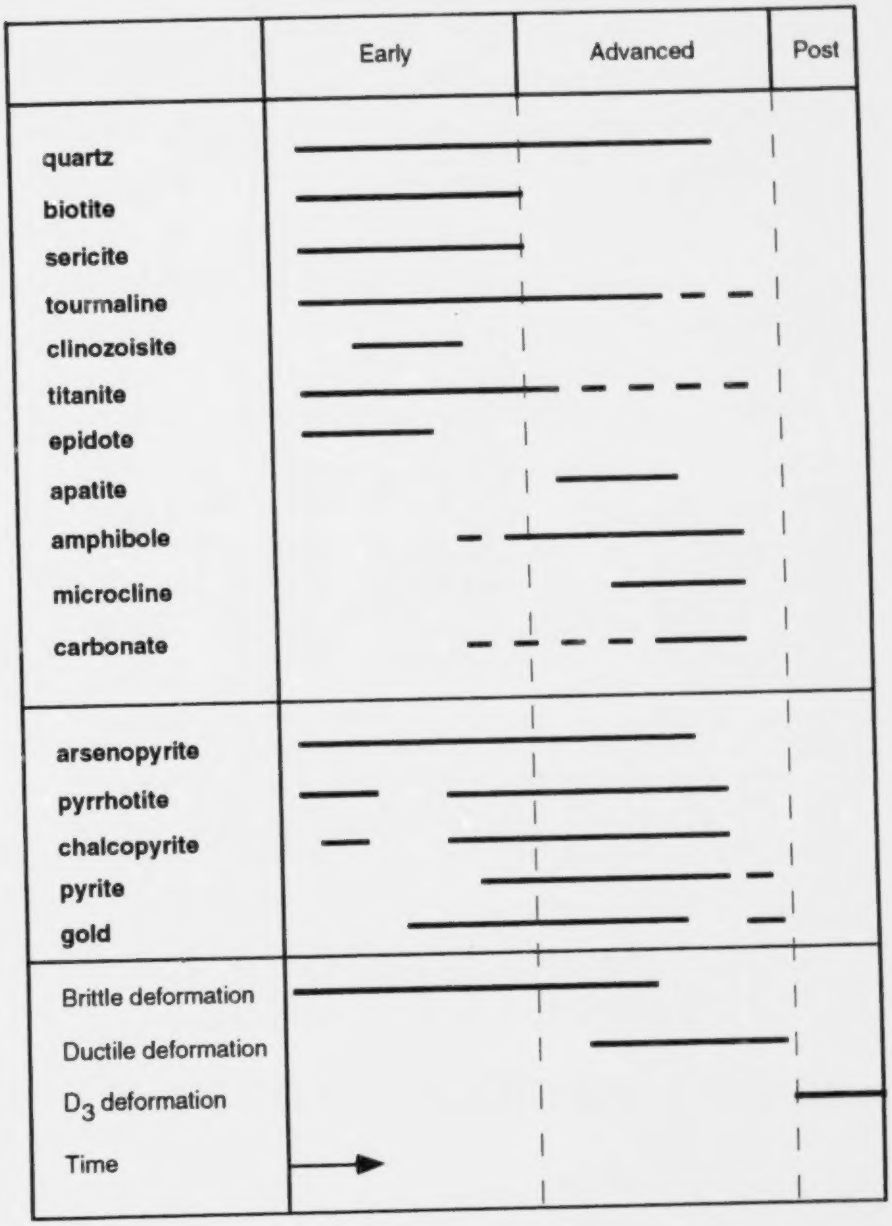

FIGURE 6-2. Mineralogy and paragenetic sequence for Type II mineralized veins, Ulu Claims, N.W.T. Early and advanced refer to stages of vein development. Alteration minerals are in terms of both intensity of alteration and time, with advanced alteration assembalges overprinting early mineral assemblages.

introduction of ladder and phantom veinlets. Alteration appears to have occurred throughout the formation of the mineralized veins.

The paragenetic sequence of deposition of the sulphide minerals appears to have been complex, however certain generalizations may be made. Deposition of sulphide minerals occurred during the initial, protracted brittle vein-forming event. Arsenopyrite was deposited throughout the formation of the veins, and was closely associated with alteration of the mafic volcanics. Pyrrhotite deposition was contemporaneous with arsenopyrite, as seen by the pyrrhotite inclusions and cores within arsenopyrite crystals, although the main pulse of pyrrhotite deposition appears to be slightly later than that of arsenopyrite due to the large amount of arsenopyrite enclosed within pyrrhotite grains. Chalcopyrite, being closely associated with pyrrhotite displays a similar paragenetic history. Petrographic studies suggest that pyrite deposition was initiated somewhat later than arsenopyrite and pyrrhotite, although these three minerals appear to have been deposited simultaneously towards the end of the mineralizing event. A discreet late phase of pyrite deposition is also observed. The main phase of gold deposition appears to have largely paralleled arsenopyrite deposition, with a possible late event associated with the late deposition of the euhedral pyrite crystals along the vein margins.

The proposed sequence of silicate mineral alteration for Type II mineralization (Figure 6-2) is in terms of both time and intensity of alteration, with each assemblage or mineral progressively overprinting earlier formed assemblages as alteration continues.

P-T Conditions of Mineralization Determined From Alteration Assemblages

Silicate alteration assemblages within and surrounding Type II mineralized veins may be used to assess the relative timing of alteration and therefore mineralization relative to peak metamorphic conditions. Systematic studies of alteration mineral assemblages associated with Archean Lode Gold deposits in the Archean Yilgarn Block have been conducted by Mueller (1992), Mueller and Groves (1991) and Witt (1991). These studies have categorized gold deposits into characteristic types based upon silicate alteration assemblages. General temperature conditions of formation have been established for each type.

The characteristic silicate alteration assemblage of quartz + biotite + amphibole (actinolite) + titanite + epidote (± clinozoisite), and the sulphide-oxide mineral assemblage of pyrrhotite + arsenopyrite ± pyrite ± ilmenite place Ulu Type II alteration within assemblage 3 of Witt (1991). Alteration assemblages of this type indicate that the temperature of formation was likely between 400°C and 500°C based on mineral equilibria reactions at 3 kbar pressure (Witt, 1991).

The alteration associated with Type II mineralization within the Ulu Claims fits the amphibole-biotite-calcite alteration type of Mueller (1992) and Mueller and Groves (1991). Many characteristics displayed by deposits of this type within the Yilgarn block of Australia are shared by Type II mineralization at Ulu including: 1) combination of structural and lithological controls are common, and appear to be a characteristic feature of this class of deposit, 2) inner prograde alteration is confined to the width of the shear, 3) the most prominent alteration minerals are calcic amphibole, biotite ± calcite, 4) laminated quartz reefs oriented subparallel to the principle foliation of shear zone are common, 5) pyrrhotite is predominant, although it may be accompanied by minor pyrite and locally significant amounts of arsenopyrite. Pyrrhotite is most commonly intergrown with small grains of chalcopyrite, 6) any deposits of this type are associated with swarms of porphyritic felsic dykes, which are commonly tonalitic, being K-poor and Na-rich.

Temperatures and pressures responsible for formation alteration assemblages of this type in Australia have been estimated at 3 kilobars and 450-480°C (Mueller and Groves, 1991) based on mineral stabilities and stratigraphic considerations. The temperature and pressure estimates for alteration assemblages of this type by Mueller and Groves (1991) are in general agreement with that predicted by the work of Witt (1991).

Timing of Mineralization and Alteration Relative to Regional Metamorphism

The timing of Archean Lode gold deposits within amphibolite grade rocks relative to peak metamorphism is currently a subject of ongoing research (e.g. Robert, 1992). The controversy principally revolves around whether or not these deposits have been metamorphosed along with their host rocks, and whether these deposits are deeper equivalents of far more common greenschist hosted deposits. Several lines of evidence strongly suggest that alteration associated with Type II mineralization occurred post peak metamorphism:

1) metamorphic overprinting of alteration assemblages is not observed within Type II mineralization, and alteration minerals are observed to replace peak metamorphic assemblages within mafic volcanics and sediments;

2) temperatures determined from mineral equilibria within alteration assemblages (Mueller and Groves, 1991 ; Witt, 1991) indicate temperatures of alteration (400-500°C) are less than temperatures recorded by peak metamorphic assemblage of hornblende + calcic plagioclase + ilmenite (525-625°C) within the mafic volcanic host rocks;

3) Type II alteration assemblages and mineralized veins contain abundant calcite. If alteration and mineralization have been metamorphosed at amphibolite grade would it is expected that the rocks would be decarbonated, with the formation of wollastonite by the following equation $CaCO_3+SiO_2 = CaSiO_3 + CO_2$ (Best, 1982). Lode gold deposit alteration assemblages which have been metamorphosed to amphibolite grade commonly contain andalusite, cordierite, staurolite, anthophyllite-cummingtonite and gedrite (Colvine et al., 1984), none of which are present within Type II alteration assemblages at Ulu.

TYPE III MINERALIZATION

Introduction

Type III veins consist of discreet quartz veins usually found in sheared mafic and gabbroic host rocks, although subordinate quantities of this mineralization type occur within quartz-feldspar porphyry and associated internal granitoids. Type III veins generally occur in swarms. Broad zones of veining and shearing which generally have a north-south to to northeast-southwest trend are discernable. These veins are variable in mineralogy and it is possible that more than one vein-forming event is represented by this category, however they are similar in morphology and texture. Type III veins occur throughout the property (Figure 6-1), but this study focuses on areas of high vein density (Ulu West and Emerald Lake) though veins of this type of mineralization were collected throughout the property (ie. East Limb, Ravine, NFN)

Occurrence and Vein Morphology

Type III veins occur within broad zones of shearing, although the shear fabric is not necessarily well developed. Individual veins may occur parallel to the shear fabrics, or in some case be oriented oblique to the fabric. Overall the fabric displayed by the rocks hosting these veins is generally conformable to the regional D_3 fabric. Veins display features which are suggestive that vein formation was synchronous with deformation such as rotation of extension veins into the plane of shear, and boudinage. Individual veins are less than one metre in width, and are variable in length, although the length of these veins is generally limited.

Within the NFN this vein type occupies dilatant zones occurring at the contact between the sediments and the volcanics. The veins are generally conformable with these contacts. As well, small veins occur adjacent to late granite-pegmatite dykes. In the Emerald Lake, Ravine, and East Limb areas, Type III veins are hosted exclusively within mafic volcanic and gabbroic lithologies.

In the Ulu West area, Type III mineralization trends are largely cospatial with internal intrusives, hosted in gabbros, and are both within and adjacent to dykes, and small plugs. Thin Type III veins also occur within quartz felspar porphyry dykes near the Flood Zone, and proximal to the Gnu Zone, and commonly occur as stockworks or at the contact between the dykes and wallrock. These veins may follow the dykes for some distance. The relationship between Type III mineralization and the internal granitoid suite indicate that Type III mineralization postdates these granitoid rocks, and that the dykes deformed in a preferential brittle fashion relative to the enclosing supracrustals, and in part acted as conduits for Type III mineralizing fluids.

External morphology of Type III veins suggest a multiple origin for the formation of these veins. Type III veins may be categorized as extension veins, as well as shear veins (Hodgson, 1989), and an overall, unifying structural theme for emplacement of these veins is lacking. The development of individual veins or sets of veins appear to be largely a function of local host rock rheology and geometry.

Vein Mineralogy

In comparison with Type II veins, the mineralogy of Type III veins is simple. The veins consist of coarse, granular quartz, and may contain pyrite filled vugs. Sulphide mineralogy is quite variable and follows a general zonation pattern throughout the Ulu Claims. The zonation appears to radiate from the external granitoids bounding the supracrustals, with barren veins found immediately adjacent to and perpendicular to the contact, followed by a chalcopyrite + molybdenite zone, followed by a pyrite ± pyrrhotite ± chalcopyrite ± bismuth ± gold zone. Local distribution of sulphide minerals within these veins is erratic regardless of mineralogy in all zones. Gold distribution appears to be a function of both total sulphide content, and the abundance of bismuth. Wallrock clasts are rare in this vein type, as is any appreciable wallrock alteration adjacent to the veins.

Quartz

Quartz within Type III veins is quite coarse-grained, generally greater than 2 millimetres, and varies from colorless-white, to smoky grey. Vugs with small crystals are fairly common and are often filled with pyrite. Quartz within these veins is variably strained (Plates 6-7b, 6-8c), but complete recrystallization is not observed. Individual quartz grains may have sutured to embayed grain boundaries and incipient grains and mortar textures may occur. Late cross-cutting quartz-filled fractures seen in Type II veins are not observed. No luminescence of quartz was observed during examination of Type III veins under the cathodoluminescence microscope. Fluid inclusions are very common in Type III vein quartz, occuring both as primary, but predominantly as multiple episodes of cross-cutting secondary trains.

Ore petrology

Sulphides

Common sulphides in Type III veins are pyrite, chalcopyrite and pyrrhotite, although molybdenite, and arsenopyrite may also occur. Occurrence of sulphides in these veins is invariably late, as fracture fill most commonly as coarse anhedral masses (Plate 6-8b), and secondarily as very fine-grained inclusion trails which cross quartz grain boundaries, and interstitial to quartz grains In several Type III vein occurrences, fracturing of quartz has been extreme, and quartz occurs as clasts within a pyrite/pyrrhotite matrix.

Abundances of sulphides in Type III veins is very variable, however pyrite is the most common, followed by pyrrhotite, and chalcopyrite. Molybdenite occurs as fine andehral masses associated with chalcopyrite, and its occurrence is generally restricted to the veins adjacent to the bounding granite in the Ulu West area. Arsenopyrite occurs as blocky crystals, associated with pyrite, pyrrhotite and chalcopyrite, but is not a common vein constituent.

Sulphide fracturing filling within Type III veins is often accompanied by clouding of quartz adjacent to the fractures, due to the presence of secondary fluid inclusions, likely from fluids associated with deposition of the sulphides.

Iron oxides are common within Type III veins as a replacement of pyrite and pyrrhotite, and pyrrhotite often displays retrogression to marcasite, with bird's eye textures (Plate 6-8b).

Native Elements

Native bismuth is common in Type III veins, and the presence of Au is strongly dependant on the presence of Bi. Bismuth occurs as small (generally less than 200 µm) inclusions within quartz, and commonly forms trains which cross quartz grain boundaries (Plate 6-8d) or may occur interstitial to quartz grains (Plate 6-7c). An unidentified grey opaque phase (Co-Ni-As sulphide?) occurring as rims on, and intergrown with bismuth was noted in several polished sections of Type III veins.

Gold occurs in the native state within Type III veins and ubiquitously occurs with bismuth in late inclusion trails, either as intergrowths or as solitary anhedral masses, which are rarely above 100 µm in size (Plates 6-7c,d).

Other Minerals

The only other mineral noted within Type III veins was an occurrence of a single crystal of scheelite along a late fracture within a vein in the Emerald Lake zone. This mineral was identified by its greenish fluoresence under the cathodoluminescence microscope.

Alteration

Alteration associated with Type III veining is not extensive, and broad alteration envelopes are not present. Within mafic lithologies, thin (1-2 cm) selvages of biotite-amphibole alteration may be present, but are not ubiquitous. Within the internal granitoid rocks, alteration associated with Type III veins is more wide spread, but subtle. Alteration is manifested as clouding of feldspars (sericitization) and chloritization of biotites. The degree of alteration in these rocks appears to be a function of their brittle rheology which has resulted in wide spread fracturing, and the development of stockwork veining. Similar alteration is also present within the external granitoids where barren veins occur at and proximal to the contact with supracrustals.

Paragenesis

Paragenesis of Type III veins is shown diagramatically in Figure 6-3. The development of these veins is simple in comparison to that of Type II veins. Petrographic textures indicate all sulphide/native element deposition was either at the termination of quartz deposition (vug filling and interstitial to quartz grains), or post-dated quartz deposition (fracture fill, and inclusion trails transcending quartz

Plate 6-7

Features of Type III mineralized veins.

6-7a 90PAK-US-47
Handspecimen of Type III mineralization from the Ulu West area. Coarsely crystalline grey quartz vein. Note massive pyrite occurring within vugs and between quartz grains.

6-7b Photomicrograph, (xpl), 90PAK-US-47
Quartz in thin section from 90PAK-US-47 (Plate **6-7a**). Note the sutured, embayed grain boundaries and strained nature of quartz grains.

6-7c Photomicrograph, (ppl), 90PAK-US-47
Grains of native bismuth occurring interstitial to quartz grains. Note small grain of native gold and native bismuth occuring within the quartz crystal to right of the large bismuth grain.

6-7d Photomicrograph, (ppl), 89VD-12 (24.9m)
Type III mineralized vein hosted within quartz-feldspar porphyry from the Flood Zone. Photograph shows native gold intergrown with native bismuth as inclusions within quartz crystals.

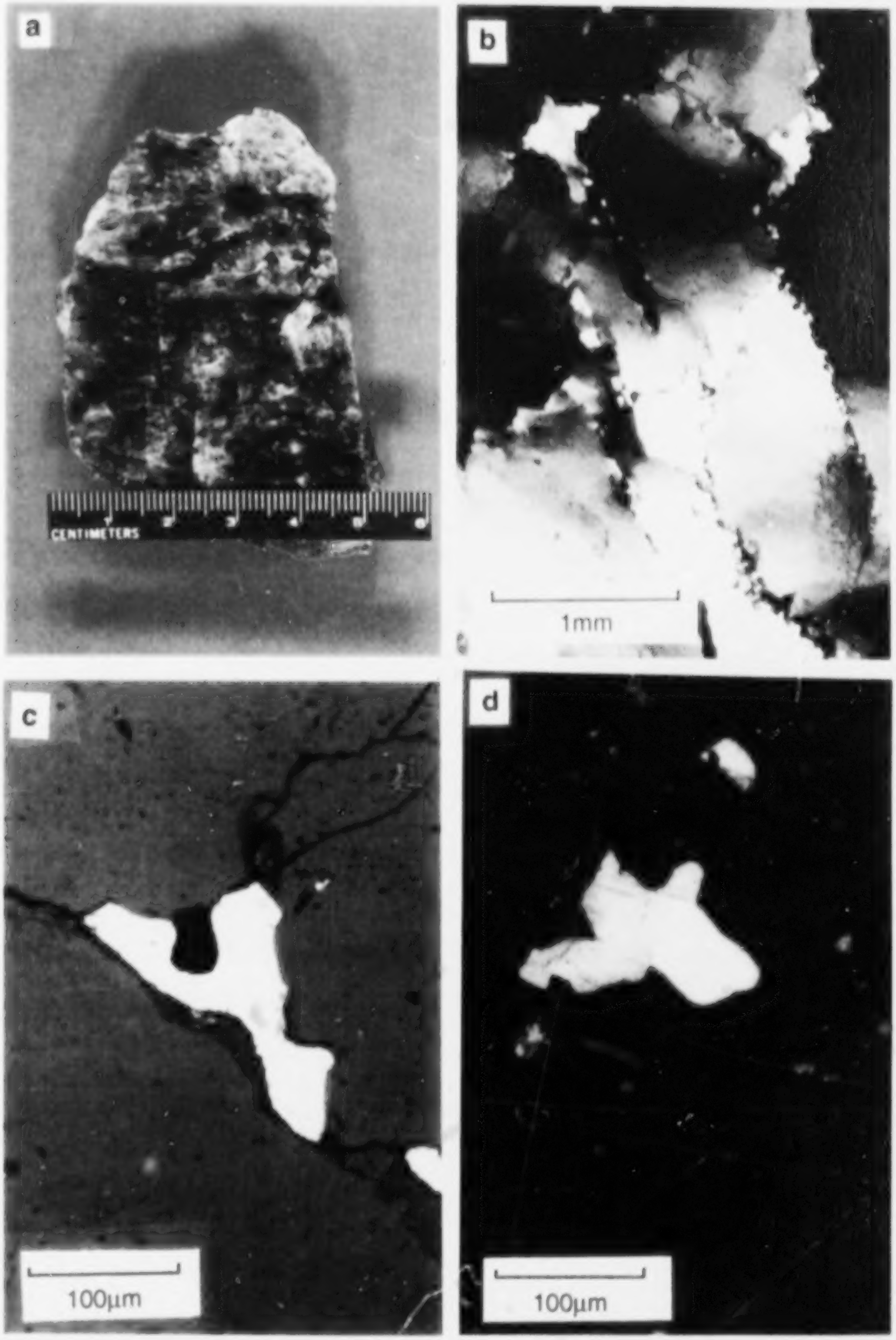
a
CENTIMETERS
b
1mm
c
100μm
d
100μm

Plate 6-8

Features of Type III mineralized veins.

6-8a 91VFT-3803
Handspecimen of Type III mineralized vein from the Emerald Lake area. Sample consists of coarsely crystalline white to clear quartz with chalcopyrite and pyrrhotite occurring as late fracture fill.

6-8b Photomicrograph, (ppl), 91VFT-3803
Pyrrhotite (displaying retrograde alteration to marcasite) occurring within late fractures.

6-8c Photomicrograph, (xpl), 91VFT-3803
Quartz in thin section from 91VFT-3803, displaying weakly embayed grain boundaries and weak straining. Note the abundant secondary solid and fluid inclusion trails transecting the quartz grain boundaries.

6-8d Photomicrograph, (ppl), 91VFT-3803
Close up of secondary inclusion trails from Plate **6-8c**, showing abundant native bismuth inclusions.

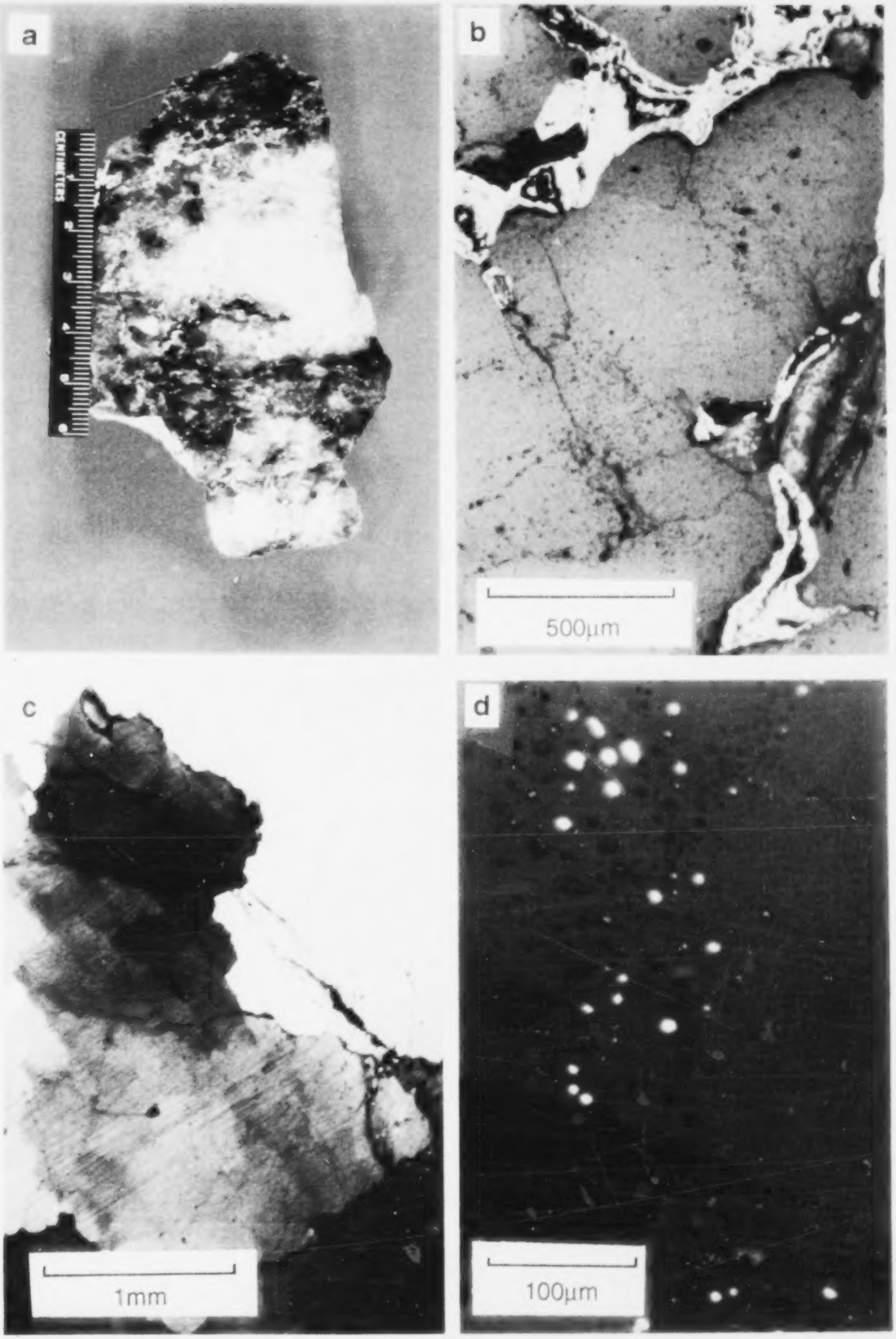
a
CENTIMETERS
b
500μm
c
1mm
d
100μm

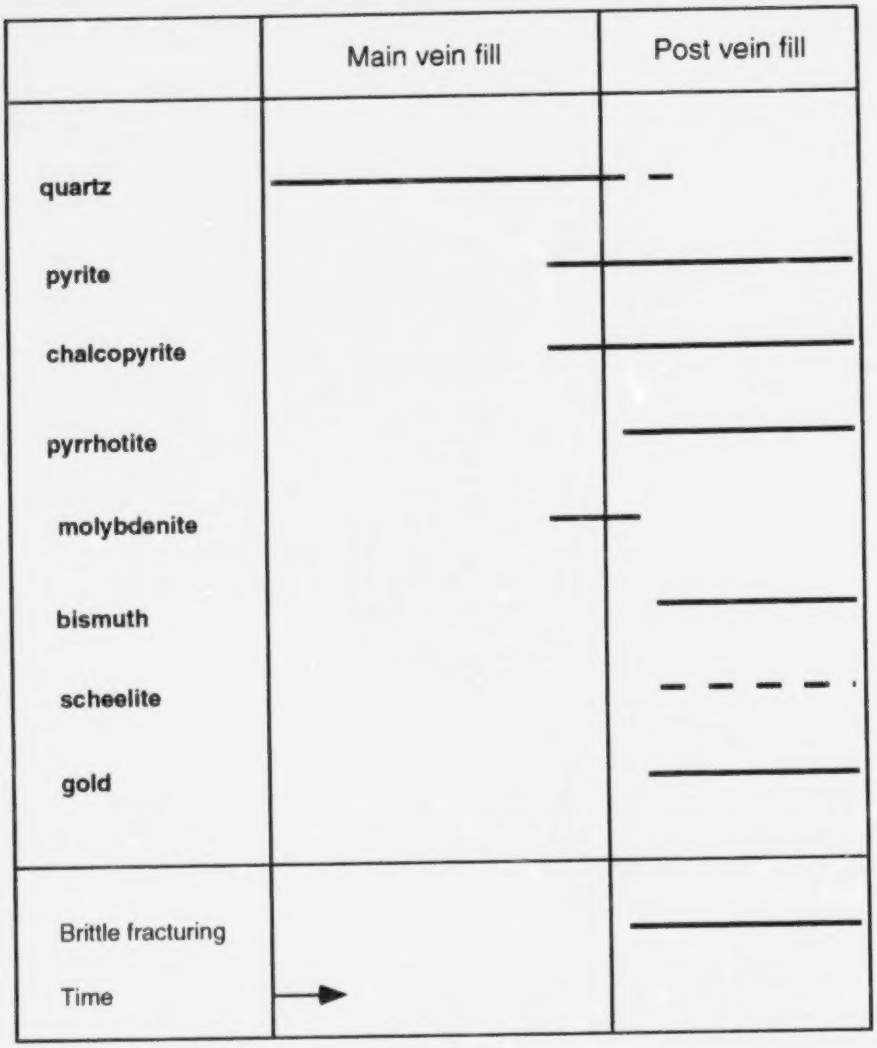

FIGURE 6-3. Mineralogy and paragenetic sequence for Type III veins, Ulu Claims, N.W.T.

grain boundaries). Type III vein styles (extension and shear) suggest emplacement occurred during an episode of shearing, and location and density of veining were largely controlled by rheological inhomogeneities within and between volcanic, sedimentary, and intrusive lithologies. Though the fabric within the rocks is in part conformable to regional D_3 cleavage, the emplacement of these veins is thought to be closely related to then intrusion of the external granitoid. The veins may have been localized within minor, post-D_3 shears associated with emplacement of the external granites.

7. GEOCHEMISTRY OF MINERALIZATION

ARSENOPYRITE GEOTHERMOMETRY

A study of the chemistry of Flood Zone arsenopyrite was undertaken to determine the temperature of formation via the arsenopyrite thermometer of Kretschmar and Scott (1976). Petrographic studies indicate that deposition of arsenopyrite occurred throughout the Type II mineralizing event and that gold is closely associated with the arsenopyrite. Gold is observed to form small inclusions within arsenopyrite grains, and occurs as larger grains interstitial to and adhering to arsenopyrite crystals. These relationships suggest that the temperature of crystallization of arsenopyrite within Type II mineralization would provide a reasonable temperature estimate of the gold mineralization. The use of the arsenopyrite geothermometer within Type II mineralization provides an alternative to microthermic measurements of fluid inclusions, which have largely been compromised in the Flood Zone due to recrystallization of quartz within this mineralization type.

Analytical Methods

Quantative analyses for Fe, As, S, and Cu were obtained for 213 points, 2 to 10 μm apart, along 19 traverses containing arsenopyrite, pyrite and pyrrhotite from three polished sections of mineralized material from the Flood zone. The data was collected by E. Peterson at the University of Utah using a Cameca SX-50 electron microprobe operating with an accelerating voltage of 20 kV, with a beam current of 20 nA. All elements were analyzed for 10 seconds with a spot size of 2 μm. Standards used for the analyses were marcasite for Fe and S, Cu_2O for Cu and GaAs for As (Peterson, 1991b). Absolute error (3 sigma) for microprobe analyses based upon 20,000 counts (corresponding to 10-20s count time) is approximately 2.75% (Smith, 1976).

A single automated electron microprobe run was used to collect the data. The traverse orientations likely include composite grains and in part may include grains which have been cut near growth zones (Peterson, 1991).

Introduction to The Arsenopyrite Thermometer

A T-X diagram based upon experimental work in the system Fe-As-S (Kretschmar and Scott, 1976) may used as an arsenopyrite geothermometer. Arsenopyrite is well suited for use as a thermometer, due to its refractive nature and its tendency to not readily re-equilibrate upon cooling. The arsenopryite thermometer may be used as long as the following conditions are met (Kretschmar and Scott, 1976):

1) The arsenopyrite must be from an equilibrium, a (S2) buffered assemblage. The arsenic content of arsenopyrite is very sensitive to sulphur activity, and when arsenopyrite is buffered with respect to sulphur activity, the As/S ratio is mainly a function of temperature (Koh et al., 1992). In order to fix arsenopyrite composition at any given temperature and pressure, at least two other phases in equilibrium with the arsenopyrite are required. The presence of only a single phase in equilibrium with arsenopyrite results in a range of temperatures for a given As content (i.e., Figure 7-1). While equilibrium is difficult to assess within ores, arsenopyrite may be assumed to be in equilibrium with other simultaneously deposited minerals with which it shares mutual grain boundaries (Kretschmar and Scott, 1976). The presence of pyrite and pyrrhotite coexisting with arsenopyrite in the Flood zone mineralization indicates that this criterion has been met as coexisting pyrite and pyrrhotite form a fixed point buffer with respect to sulphur (Barton and Skinner, 1979). The paragenetic sequence of sulphide mineral deposition within the Flood Zone indicates that for at least part of the time the deposition of arsenopyrite, pyrrhotite and pyrite were simultaneous;

2) Minor element content of the arsenopyrite must be less than one weight percent. Although the only minor element analyzed for within the Flood Zone arsenopyrite was Cu (generally less than 0.05 wt %), analytical totals of As, Fe, S and Cu indicate that vast majority of arsenopyrite must contain <1% combined minor element content;

3) A suitable standard must be used for microprobe evaluation of arsenopyrite.

The arsenopyrite thermometer has been used with reasonable success by several workers including Koh et al. (1992); Kay and Strong, (1983); Lowell and Gasparrini (1982). The arsenopyrite thermometer appears to be valid for ores metamorphosed to greenschist and lower amphibolite facies, however it provides low temperatures for ores within higher metamorphic grades and inconsistent temperatures for low-temperature hydrothermal ores (Sharp et al., 1985). Temperatures determined from the As content of arsenopyrite from Archean mesothermal gold deposits (i.e. Homestake and Contwoyto Lake, Sharp et al. (1985); Norseman, Australia, Golding (1982) from Mueller and Groves (1991)) which have not undergone significant post-mineralization metamorphism appear to be reasonable and in the case of the Norseman deposit are in general agreement

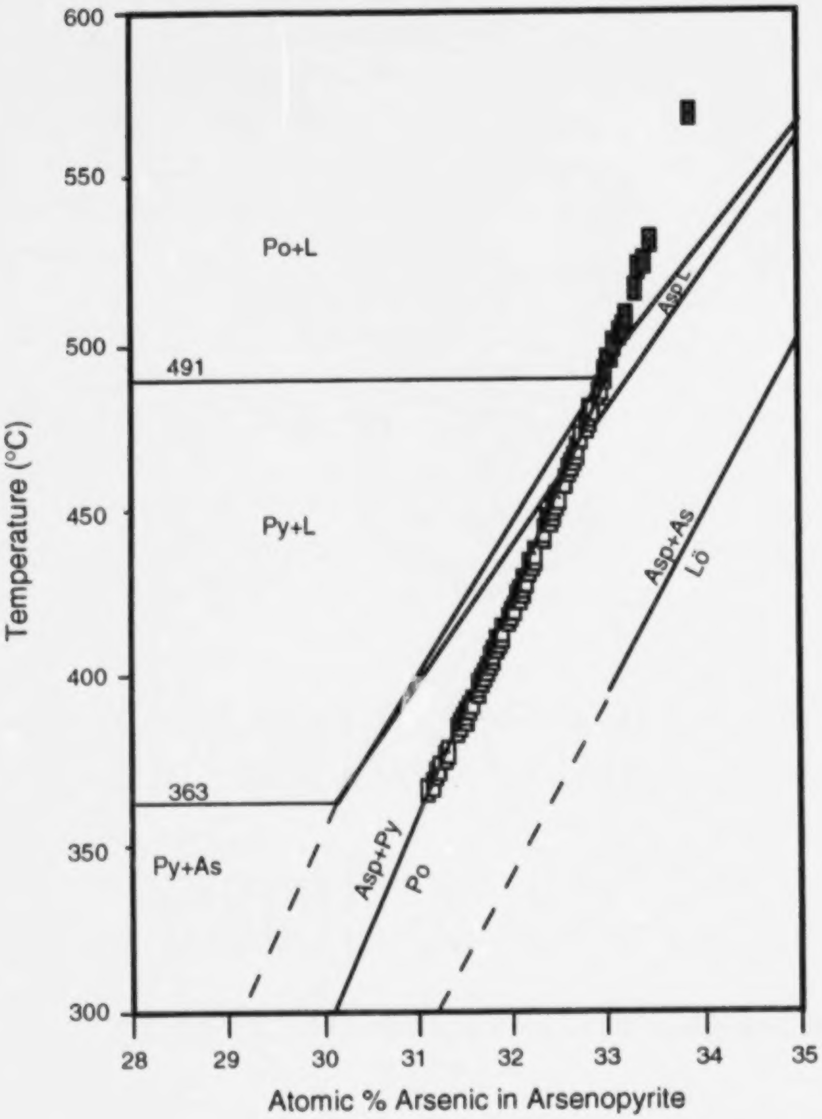

FIGURE 7-1. Pseudobinary T-X section along the pyrite-löllingite join showing arsenopyrite composition as a function of temperature, at.% As, and coexisting equilibrium phases. All assemblages include vapour. Ulu Type II mineralization arsenopyrite analyses are shown plotted as an equilibrium assemblage of asp+po +py. Shaded data points correspond to those analyses which plot outside the stability field for this assemblage (refer to text for further explaination). Asp-arsenopyrite, po-pyrrhotite, py-pyrite and lö-lollingite.
Modified after Kretschmar and Scott (1976).

with temperatures determined from mineral equilibria within alteration assemblages.

Flood Zone Sulphides

The Flood Zone arsenopyrite, pyrrhotite and pyrite composition data are presented in Appendix 3. The data are plotted on a S-Fe-As ternary composition diagram (Figure 7-2).

Pyrite

Flood Zone pyrites were analyzed as a secondary standard for the arsenopyrite (Peterson, 1991), and compositionally are very close to FeS_2. Of the 23 analyses of pyrite, Fe ranged from 32.83 to 33.96 at%, and have a mean value of 33.27 at%. These values are acceptable within analytical error.

Pyrrhotite

Thirty spot analyses of pyrrhotite were collected, and Fe contents ranged from 45.68 to 47.25 at%, and had a mean of 46.13 at%. The iron contents of the pyrrhotite display a distinct bimodal distribution (Figure 7-4) with the main population ranging from 45.68 to 46.25 at%, and a minor population at 46.88 to 47.25 at%. The pyrrhotite containing greater than 46.88 at% Fe were all from a single grain, while the main population is derived from 6 individual grains.

Temperatures determined from the Fe contents of Ulu pyrrhotite via the pyrrhotite-pyrite solvus of Arnold (1962) and Toulmin and Barton (1964) indicate that the main population of pyrrhotite formed at 575 to 625° C, while the pyrrhotite richer in Fe formed at 380 to 450°C. The latter temperatures are consistent with arsenopyrite temperatures while the main population is too high. Although suggestive of disequilibrium between arsenopyrite and pyrrhotite, this discrepancy in temperature may be due to several factors related to the tendency of pyrrhotite to undergo post-depositional change: 1). pyrrhotite from the solvus at high temperatures will continue to exsolve pyrite to near 300°C; 2). pyrrhotite may react with Fe and sulphur bearing solutions and change its composition whereas pyrite may not; 3) pyrrhotite reacts readily, and oxidation may cause pyrrhotite to become more sulphur rich (Craig and Scott, 1976; Barton and Skinner, 1979). The use of the pyrrhotite-pyrite solvus as a geothermometer has been largely disregarded due to these factors (Craig and Scott, 1976).

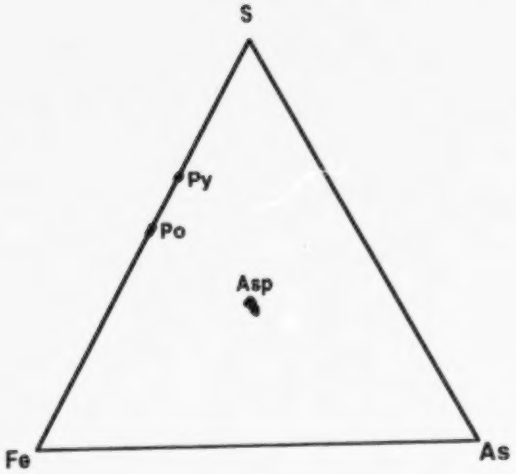

FIGURE 7-2. S-Fe-As ternary diagram showing the composition of arsenopyrites, pyrrhotites and pyrites from Type II Flood Zone mineralization.

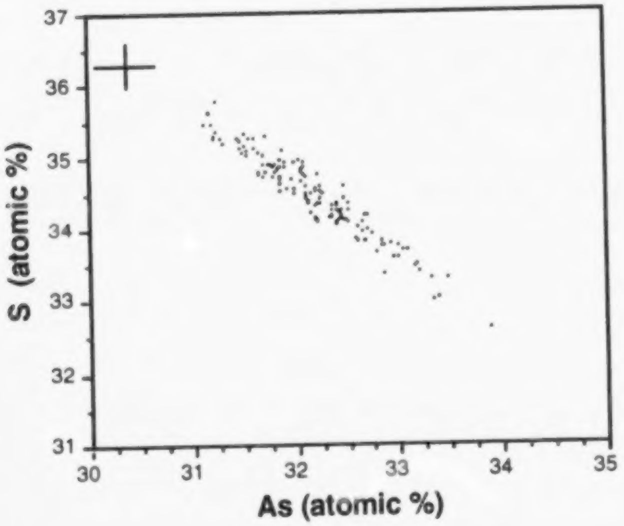

FIGURE 7-3. As/S variations in arsenopyrite from Type II Flood Zone mineralization. Cross in upper left shows error bars corresponding to analytical error for individual anlayses (~0.60 at%).

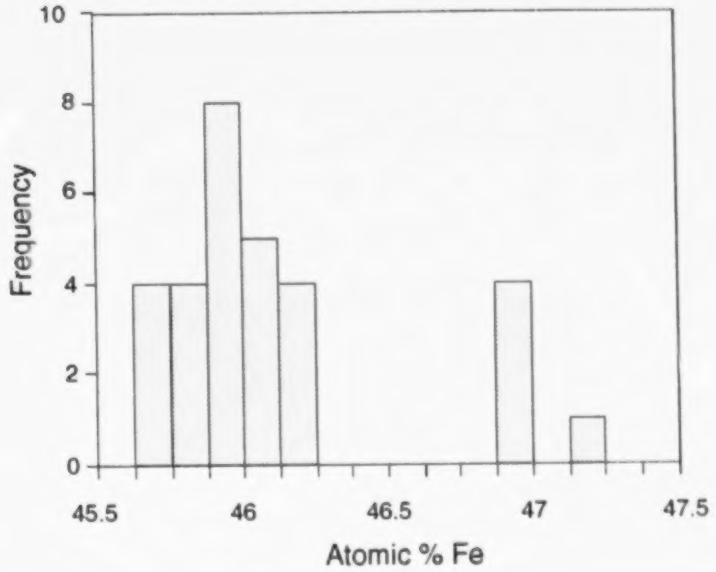

FIGURE 7-4. Atomic percent Fe in Type II Flood Zone pyrrhotite.

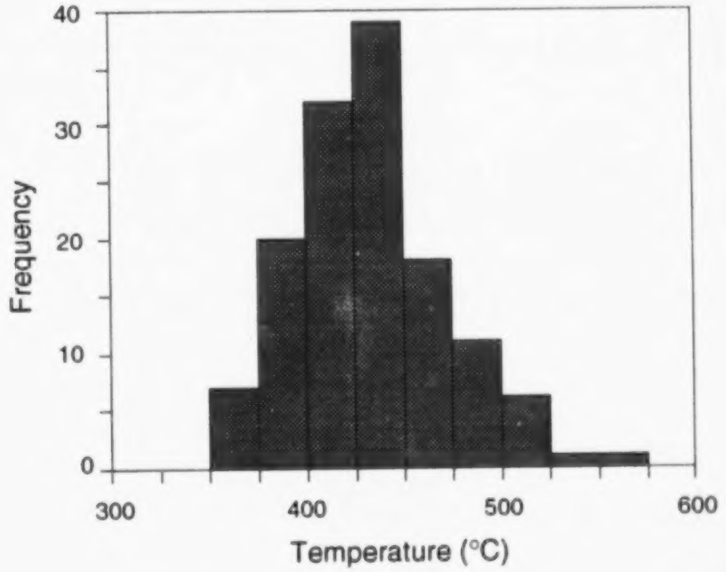

FIGURE 7-5. Distribution of temperatures determined by arsenopyrite geothermometry for Flood Zone Type II arsenopyrite.

Overall, temperatures derived by the pyrrhotite-pyrite solvus are for the most part inconsistent with arsenopyrite temperatures, likely due to the post-mineralization reactivity of pyrrhotite. For this reason, temperatures determined from Ulu pyrrhotite using the pyrrhotite-pyrite solvus are considered to be largely invalid, and are not indicative of disequilibrium between arsenopyrite, pyrite and pyrrhotite.

Arsenopyrite

One hundred and thirty nine analyses of arsenopyrite were collected. The arsenic content of the arsenopyrite varied from 31.11 to 33.88 at% (Figure 7-3), and averaged 32.18 at%. A two sigma error (absolute error 1.84 %) indicates that the mean analyses of 32.18 at% As corresponds to an analytical error of 0.60 at%, which translates to an uncertainty in derived temperatures of ± 46°C. Of the 139 arsenopyrite analyses only 6 contained above 33.3 at% As, the ideal stoichiometric amount, and all analyses were within the upper analytical limit of 33.3+0.60 at%. A significant number of the analyses contained less than 32.7 at% As (lower analytical limit). This is in good agreement with the arsenic content from arsenopyrite buffered by an equilibrium assemblage of pyrite and pyrrhotite analyzed by Kretschmar and Scott (1976), which rarely contain over 33.4 at% arsenic. Fe contents of the arsenopyrite range from 32.87 to 33.67 at%, and have a mean value of 33.34 at%, all within analytical uncertainty. Kretschmar and Scott (1976) noted natural arsenopyrite consistently displays a slight Fe deficiency, and this may account for Fe values less than 33.03 at % within the Flood Zone arsenopyrite.

Examination of the data within Appendix 3 indicates that considerable variation exists (outside of analytical error) within the arsenic content of individual grains. This variation may be due to several factors, the most important of which is compositional zoning within natural arsenopyrite. Kretschmar and Scott (1976) report that many natural arsenopyrite crystals are compositionally zoned. The zoning is concentric, composition change is stepped and irregular with no reversals, and within sulphur rich assemblages (ie., asp-py-po,) the centers of arsenopyrite crystals are sulphur rich relative to the rims. While this zonation pattern is observed within single grains from Flood Zone arsenopyrite, several traverses are in contradiction with oscillating arsenic contents. Unfortunately, detailed petrography is not available for the individual traverses, therefore the exact nature of these oscillations cannot be investigated. While these oscillations may actually be due to compositional variations within single grains representing complex zonation commonly observed within arsenopyrite (i.e. Cabri et al., 1989), the possibility that they represent oblique grain sections or very fine-grained crystal aggregates cannot be ruled out. The compositional variations observed in natural and synthetic arsenopyrite from sulphur-rich assemblages are due to changing conditions during crystallization of the arsenopyrite, and likely represent dis-equilibrium reflecting the kinetics of arsenopyrite growth and local $fS2$ fluctuations (Kretchsmar and Scott, 1976; Wu, et al., 1990). Kretchsmar and Scott (1976) however, point out that the compositional variation of zoned arsenopyrite lies within the equilibrium range for each assemblage, and that zoning reflects only minor and transitory conditions of dis-equilibrium during growth.

The As contents of the Flood Zone arsenopyrite have been plotted on the T-X section of Kretschmar and Scott (1976) (Figure 7-1). The data is interpreted to represent an equilibrium assemblage of coexisting asp-py-po, therefore the data has been plotted at the tie between the the pyrite and pyrrhotite fields. The temperatures derived from this plot, given by the formula $T= 1000/[-0.1365(100*\text{mole percent As}) + 5.8125] - 273.15$, indicate arsenopyrite deposition occured at temperatures varying from 366 to 569 °C. A frequency histogram of temperatures obtained from all arsenopyrite analyses is given in Figure 7-5 . Statistical analysis of the data indicate the mean temperature to be 433 ±46° C with a standard deviation of 38 °C. The distribution of temperatures is thought to reflect zonation within the arsenopyrite crystals, with the low temperature end correlating with As-poor zones (predominantly centers of crystals) and the high temperature end corresponding with high As zones (predominantly rims of crystals). Alternatively, the range in temperatures may also be partially attributable to variations in sulfur fugacity during arsenopyrite crystallization, as well as analytical error.

Only 7 of the 135 analyses give temperatures above 500°C and represent those analyses with greater than 33.3 at % As, which plot above the po-py-asp univariant point of 491°C. These analyses are possibly from very As rich rims, or may be represent spurious data points, although they are all generally within boundaries of analytical error (±46°C). Alternatively, arsenopyrite may have formed in equilibrium with only pyrrhotite, in which case all temperatures reported are maximums, and uncertainty associated with individual analyses are greater than 50°C (+46°C analytical uncertainty) due to the absence of a third equilibrium phase.

In summary, arsenopyrite deposition likely occured in equilibrium with pyrrhotite and pyrite, with a possible temperature interval of 145°C, between 360 and 515°C. This corresponds to sulphur fugacity range, between log -8 and log -5.5, assuming an equilibrium assemblage of arsenopyrite-pyrrhotite, pyrite. Since gold within Type II mineralization is strongly associated with arsenopyrite, deposition of gold occurred over a similar temperature range.

GEOTHERMOMETRY OF TYPE III VEINS

The temperature of the formation of auriferous Type III veins may be largely constrained by the presence of native bismuth. The intimate association of gold with the native bismuth suggests gold deposition occurred under near identical conditions. Native bismuth has a melting point of 271.5°C at 1 bar pressure, and this temperature decreases with increasing pressure at a rate of 7.6°C/kbar (Klement et al., 1962). Native bismuth has been used as a geothermometer for bismuth bearing veins (Kelly and Tourneaure, 1970; Brown, 1985) and the melting temperature of bismuth is in general agreement with other temperatures of vein formation (250-300°C) determined by independent geothermometers for the same vein systems.

The use of the melting temperature of native bismuth as a indication of the temperature of vein formation necessitates the assumption that the bismuth was precipitated in the solid form. Kelly and Tourneaure (1970) and Dagger (1972) suggest that the presence of spherical inclusions of native bismuth within other minerals indicate that bismuth was originally precipitated as a liquid. Additionally, Ramdohr (1969) reports the presence of radial fractures surrounding bismuth inclusions, a feature which is due to the expansion of bismuth during crystallization from an originally liquid inclusion.

Microscopic examination of the bismuth inclusion within the quartz of Type III veins reveals that the vast majority of these inclusions display a euhedral hexagonal habit, and that anhedral spherical forms are rare. This would suggest the bismuth inclusions within these veins were originally precipitated as solid phases. The possibility that the bismuth inclusions are occupying negative crystals within quartz cannot be ruled out, although the lack of expansion fractures adjacent to the inclusions may also preclude deposition of bismuth as a liquid phase.

Other sulphides (mainly chalcopyrite, pyrite, and pyhrrotite) within Type III veins also occur as late fracture fill and interstitial to quartz grains. Bismuth-gold inclusions and veinlets are not observed to occur within or cross-cut these other sulphides, which suggests that both sulphides and native elements were precipitated simultaneously, and at similar temperatures.

The late paragenetic position of bismuth with Type III veins suggests that deposition of bismuth-gold occurred as the result of decreasing temperature during the waning stage of vein formation, and indicates that the main stage of quartz deposition may have precipitated at slightly higher temperatures. A temperature range of 250-300° C is thus considered to be a reasonable estimate for Type III veins.

TRACE ELEMENT GEOCHEMISTRY OF MINERALIZATION

Chemical Analysis

In order to examine the trace element geochemistry, of both Type II and Type III mineralization, 53 representative analyses of auriferous Type II and Type III mineralized veins were selected from both surface and core samples. These samples were analyzed by inductively coupled plasma emission spectrometry (ICPES) at Acme Analytical Laboratories Ltd. of Vancouver for Mo, Cu, Pb, Zn, Ag, Ni, Co, Mn, Fe, As, U, Th, Sr, Cd, Sb, Bi, V, Ca, P, Cr, La, Ti, B, Al, Na, K, and W. In the analytical procedure, samples were pulverized and sieved to -80 mesh, a 0.50 gram sample digested with 3 ml of 3 parts HCl, 1 part HNO_3 and 2 parts H_2O at 95 °C for one hour, which was then diluted to 10 ml with water. This leach is partial for Mn, Fe, Sr, Ca, P, La, Cr, Mg, Ba, Ti, B, and W and limited for Na, K, and Al. Au analysis, for these samples is by atomic absorption from a 10 gram sample, ignited at 600°C, digested with hot aqua regia and extracted by MIBK, and analyzed by graphite furnace AA. Detection limits reported by Acme are as follows; Ag (0.10ppm), Cd (0.20ppm), Co, Cr, Cu, Mn, Mo, Ni, Sr, W, and Zn (1 ppm), As, B, Ba, Bi, La, Pb, Sb, Th, and V (2ppm), U (5ppm), P (0.001%,) and Al, Ca, Fe, K, Mg, Na, and Ti (0.01%).

Limited whole rock analysis by ICPES, by Acme Analytical Laboratories was also conducted on 4 select samples of Type II mineralized material (Tables 7-1, 7-2) in order to attempt mass balance calculations by comparison with equivalent non-mineralized host rock. Corresponding multi-element ICPES analysis as outlined above was also conducted on aliquots of these samples. Whole rock samples were analyzed for SiO_2, Al_2O_3, Fe_2O_3, MgO, CaO, Na_2O, K_2O, TiO_2, P_2O_5, MnO, Cr_2O_3, Ba, Cu, Zn, Ni, Co, Sr, La, Zr, Ce, Y, Nb, Ta, and loss on ignition (L.O.I.). Samples were prepared as follows; 0.20 gram sample are fused with 1.2 grams of $LiBO_2$ and dissolved in 100 ml of 5% HNO_3. Detection limits are 0.01% for oxides, 10 ppm for Sr and Y, 20 ppm for Zr and 5 ppm for Ba.

Element Variations in Type II and Type III Mineralization

While Type II and Type III veins are readily distinguishable on a hand sample scale both texturally and mineralogically, the ability to discriminate between these vein types geochemically using the ICPES multi-element data was also investigated. The Au plus 30 element ICPES analysis of material from auriferous Type II and Type III mineralization is considered to be of limited usefulness due to the limited and partial leach of many elements. However, by selection of an elemental suite of totally leached elements, (Au, As, Bi, Ag and Cu) systematic variations in the content of various metals within these vein types becomes apparent.

Other elements such as Mo, Pb, Zn, Ni, Co, U, Th, Cd and Sb which are totally leached, either are at or near their limit of detection (U and Th), display little variation between Type II and Type III, or are present only occasionally within one type, and hence are not particularly useful for discriminating between the mineralization types. As well, Type II mineralized material often contains a significant proportion of hostrock/silicate alteration minerals, while Type III veins are characterized by quartz and sulphide minerals. This may result in misleading geochemical signatures for certain elements in Type II veins due to their presence within refractory silicate/oxide minerals which are not completely digested. Of the elements not considered in detail, W, Sb and Zn occur sporadically throughout both mineralization types, and may be attributed to the presence of scheelite (W), stibnite (Sb), and sphalerite (Zn). Minor amounts of scheelite were identified within one Type III mineralized vein, and minute amounts of sphalerite were noted in Type II mineralization by Peterson (1991a). Significant amounts of sphalerite are present within Type II veins in the Northern Fold Nose area. Mo occurs with Cu within non-auriferous Type III veins, adjacent to the granitic batholith in the Ulu West area.

The elemental suite Au, As, Bi, Cu and Ag may be used to discriminate between auriferous Type II and Type III veins. Log-log, X-Y binary diagrams comparing the abundance of gold to the abundances of As, Bi, Cu, and Ag, and Bi to As, Ag and Cu are given in Figure 7-6. It can be clearly seen that distinct variations exist in the abundances of these elements between the two vein types. Type II

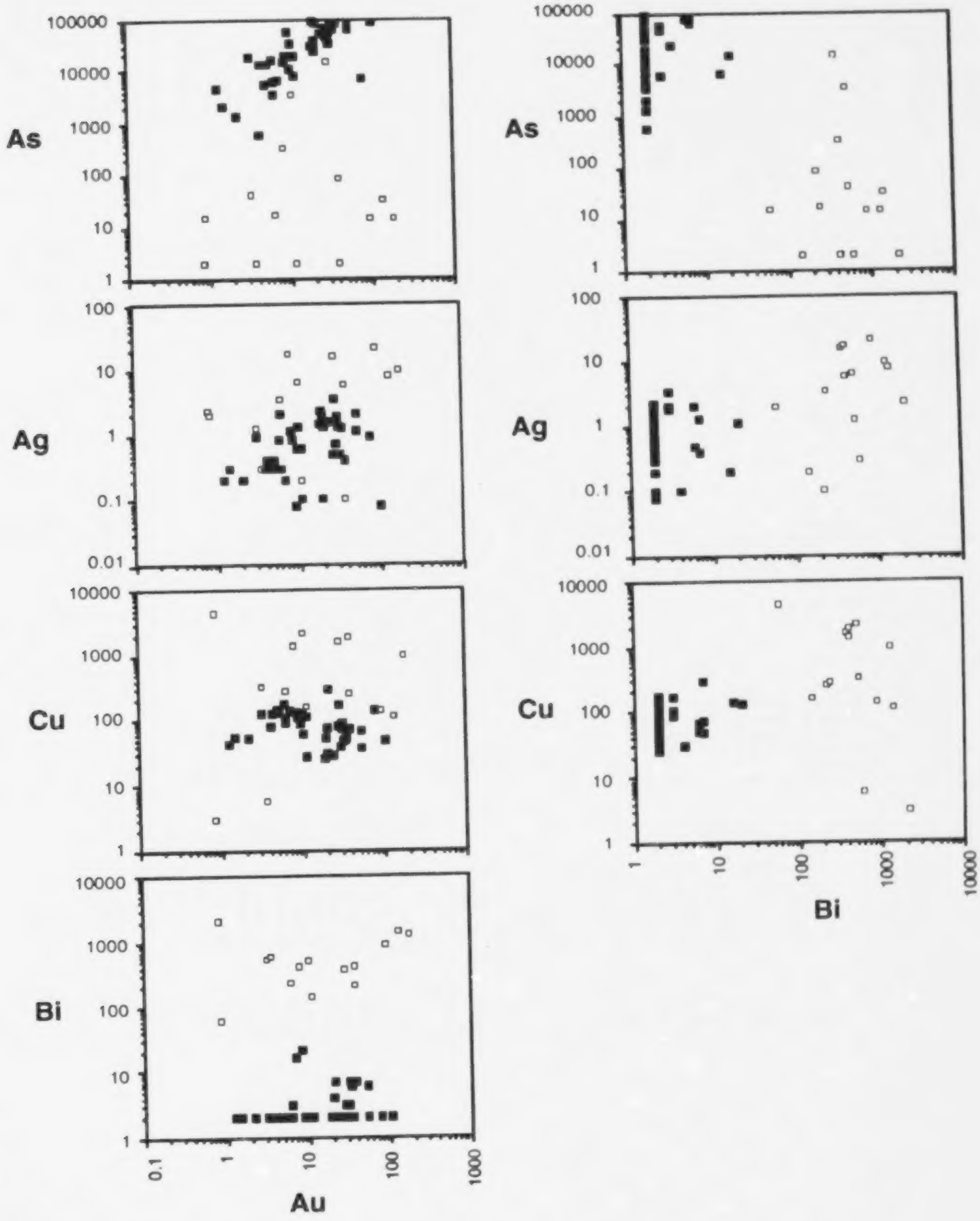

FIGURE 7-6. Log-log plots for Au vs. As, Ag, Cu, and Bi, and Bi vs. As, Ag and Cu. All elements in ppm. TYPE II veins as solid squares, TYPE III veins as open squares.

veins are generally characterized by high absolute abundances of As, and very low Bi (often at the detection limit) contents, while Type III veins contain variable but higher Bi contents, and variable but lower As contents. Type III veins also exhibit wide ranges in Cu, Ag, and As , while contents of these metals in Type II veins show limited concentration ranges.

Ag:Au ratios between the two vein types also vary considerably. Type II veins exhibit a very limited range in Ag:Au ratios, from 0.1 to 0.4 with the vast majority being below 0.3. Type III veins display a much wider range in Ag:Au ratios from 0 to 2.9. A main population occurs from 0 to 0.70, and an erratic secondary population from 2.2 to 2.9. No correlations between high Ag:Au ratios and other elements are apparent within Type III veins.

In summary, the element suite Au, Ag, As, Cu, and Bi may be used to geochemically discriminate between auriferous Type II and Type III veins. Type II veins are characterized by high As, low Bi, uniformly low Ag:Au (0.1 to 0.3) as well as a narrow range of Cu content. Auriferous Type III veins are characterized by wide variations in elemental abundances, lower As, higher Bi and a wide range in Ag:Au (0.1 to 2.9). The Bi content appears to be the best single element to differentiate between the two vein types, followed by As which shows only limited overlap. Ag and Cu are not as useful unless combined with other elements, as the populations of these elements within both veins overlap. Type III veins however, generally contain both a broader range in abundance, and greater maximums for these elements. The geochemical characteristics of the two vein types mirror the characteristics of these veins on a macro scale, with Type II veins being consistently uniform with respect to geochemistry and mineralogy, while Type III veins show large variations in content and concentration of the various elements, even on a relatively local scale.

GEOCHEMISTRY OF TYPE II MINERALIZATION

In order to investigate the geochemical changes that occurred during interaction of hydrothermal fluids with wallrocks, the chemistry of altered/mineralized versus unaltered equivalents of Type II mineralization will be examined. The isocon method of Grant (1986), based on a graphical solution to Gresens (1967) equation for metasomatic alteration, provides a method to determine volume (or mass) changes, as well as the changes in concentration in the various components. By comparing the concentration of immobile components within altered and non-altered rocks, an isocon line (straight line passing through the origin, and components showing no relative gains or losses) is established. The slope of the isocon defines the mass change within the altered rock and deviation of data points from this isocon defines the change in concentration for the corresponding elements, or oxides. Isocon slopes of less than one indicate an overall mass increase within the altered sample, which corresponds to a volume decrease of the original components. For complete background on the mathematical considerations, the reader is refered to Grant (1986) and Gresens (1967).

Although this method is applied mostly to the study of chemical changes within alteration assemblages associated with hydrothermal ore deposits, application of this technique to Type II replacement veins yields information on additions of elements from external sources during mineralization. By determining the presence of elements which have been immobile during the mineralization/alteration process, the mass change of precursor lithologies (i.e. the wallrock component of the veins) within Type II mineralization may be determined, and elemental additions and losses may be assessed. This technique is not applicable to Type III mineralization which consists of quartz-filled dilatancies, therefore all silicate (quartz) and sulphide components (Fe Au, Ag, Bi, Cu, As, W, Mo,S) may be considered to have been contributed from the mineralizing solution.

Evaluation of Immobile Elements.

Samples of mineralized veins within mafic volcanic and sedimentary hosts, and least altered equivalents adjacent to mineralization were collected from the Flood Zone. The samples collected within the mafic volcanic rocks were from a band of basaltic andesites (SiO_2 = 53-57%). In order to assess the presence of immobile elements, four whole rock analyses of basaltic andestites with SiO2 = 53-57% (Appendix 2) were compared to the mineralized equivalents. No mineralized examples of tholeiitic basalts or gabbros were collected, however, their geochemical behavior with respect to gains and losses of elements during mineralization/alteration is considered to be similar to that observed within the basaltic andesites (based upon petrographic evidence). Five analyses of unaltered greywacke and pelites were compared with mineralized equivalents.

The elements Ti, Zr and Y are largely considered immobile during metasomatic alteration processes (Winchester and Floyd, 1976, 1977; Pearce and Norry, 1979), although some mobility of these elements has been shown to occur during intense carbonatization (Hynes, 1980). These elements have been used widely to monitor gains and losses of chemical components during hydrothermal alteration associated with both base metal (MacLean and Kranidiotis, 1987; Finlow-Bates and Stumpfl, 1981,) and Archean lode gold deposits (Lhotka, 1988; Moritz and Crocket, 1991; Ludden, et al., 1984). As a test of immobility, the interelement ratios between immobile elements should remain constant between mineralized/altered samples and their least-altered equivalents. Binary plots of immobile elements from mineralized/altered and unaltered equivalents should result in an array of points lying on a common regression line, passing through the origin (MacLean and Kranidiotis, 1987; MacLean, 1990). In cases where elements were immobile during alteration/mineralization, the addition of other materials (i.e silica) dilutes their concentration and they will plot closer to the origin along the regression line.

Immobile Elements in Basaltic Andesites

Binary plots between Al, Ti, Zr and Y are given for Type II mineralized and least-altered equivalents of basaltic andesites (Figure 7-7) The contents of these elements within the unaltered population display little variation, suggesting that as a group, the basaltic andesites are geochemically homogeneous for this suite of elements. The plots indicate that the elements evaluated show dilution within the mineralized/altered samples and display limited mobility. Ti and Zr best fit the criteria for immobility, with the regression line closely approaching the origin. Both the Ti vs. Al and Zr vs. Al plots, have negative y intercepts, indicating that Al may exhibit slight mobility. Likewise the positive y intercept in the plot of Ti vs. Zr indicates that Ti may have been slightly mobile relative to Zr. However, all three plots have high correlation coefficients, and indicate very limited mobility for these three elements. Alternatively the small departures from ideality may reflect either the limited number of data points representing mineralized/altered samples, or analytical uncertainties. The plots of Y vs Ti, Zr and Al all indicate that Y was at least partially mobile during the interaction with hydrothermal fluids and was preferentially depleted relative to the other three elements, and hence is unsuitable as an immobile component for this study.

Immobile Elements in Sediments

Binary plots for Ti, Zr, Al and Y are given for sedimentary rocks representing greywackes, cordierite-bearing pelites and mineralized equivalents of greywackes in Figure 7-8. With the exception of Ti vs Al, all plots show a great deal

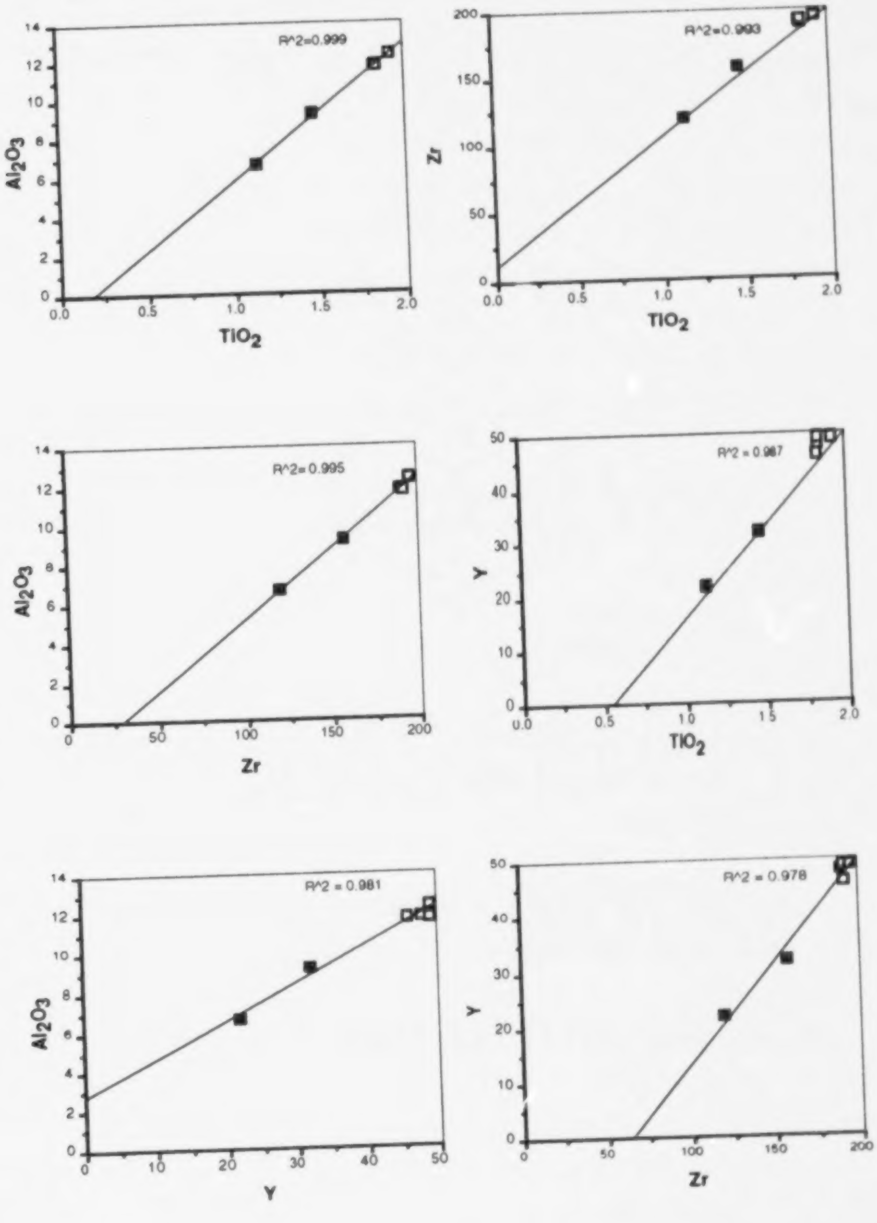

FIGURE 7-7. Immobile element X-Y plots for mineralized and non-mineralized basaltic andesites. Mineralized samples shown as solid squares, unmineralized samples as open squares. Al_2O_3 and TiO_2 in wt%, Zr and Y in ppm. Regression coefficients for each element pair is given in upper right of graph.

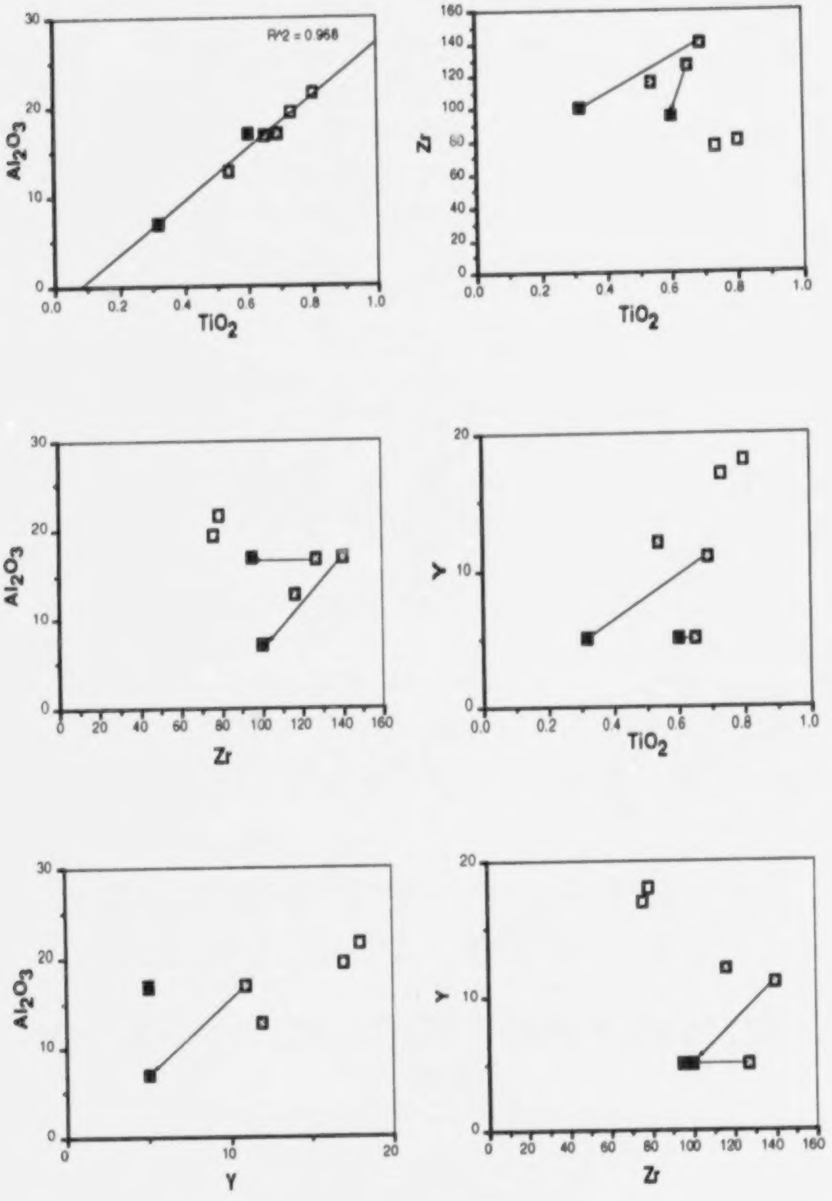

FIGURE 7-8. Immobile element X-Y plots from mineralized and nonmineralized sediments. Mineralized samples shown as solid squares, nonmineralized greywackes as grey squares and pelites as open squares. Tielines are between mineralized - nonmineralized pairs. Al_2O_3 and TiO_2 in wt %, Zr and Y in ppm.

of scatter, and data points do not lie on a common regression line. The scatter seen in the Al, Zr and Y plots is due to several factors. Primarily, it reflects the detrital nature of the sedimentary lithologies, and the inherent geochemical heterogeneities present within any one lithology and between lithologies from different facies. For example, the two analyses of cordierite-bearing pelite from the tops of the graded beds show consistently higher Y and Ti and lower Zr contents than the greywackes, while the three unaltered greywackes contain significant elemental variations amongst themselves. A possible exception to the observed lithological heterogeneities is the systematic variation of Ti with Al. Data points for this pair lie on a reasonable regression line for all samples. The nature of the relationship between the Al and Ti concentrations within pelitic and greywacke are likely detrital, not post-depositional chemical, in nature due to the immobile behavior of these elements.

The scatter between mineralized-unmineralized samples also represents differential mobility of these elements within the sediments. Tie lines between altered/mineralized sediments and their corresponding least/unaltered equivalents collected in close proximity are shown on the plots. Sample pairs in part display different relationships between the elements. In one sample pair, (91VLT 3048 - 3049) Ti, Y and Al all appear to exhibit immobile behavior, while Zr appears to become enriched relative to the other elements tested. Regression lines through these two samples all pass very close to the origin. In the other sample pair (91 VLT 3050 - 3051), with limited silica dilution, Ti and Al and Y display very little difference in concentration. The data points are extremely close together, making it difficult to get a good regression line. The Y concentrations are below detection limits reported. Zr shows significant depletion relative to the other immobile elements tested in this sample pair.

In summary, the test for immobility of Al, Ti, Zr, and Y between sediments and their mineralized equivalents, indicates that Ti, Al, and Y appear to have been relatively immobile during the Type II mineralization event. Zr shows preferential depletion in one sample, and preferential enrichment in another, indicating partial mobility of this element, or local and significant variations of Zr within these rocks prior to mineralization. For the purposes of constructing an isocon diagram, Ti and Al appear to be the least mobile elements. The low levels of Y (i.e. below detection) preclude its use in the construction of the isocon diagram. The geochemical heterogeneities of the sediments also necessitate the use of single mineralized-nonmineralized pairs collected in close proximity to each other in order to study the gains and losses of elements which occurred within these rocks during Type II alteration/mineralization, in order to arrive at meaningful interpretations.

Elemental Gains/Losses in Altered/Mineralized Basaltic Andesites

Gains and losses of 28 major and trace elements as well as L.O.I., for the altered/mineralized basaltic andesites are shown graphically in Figure 7-9 and are given in Table 7-1. Elements selected are those which displayed variations between mineralized and non-mineralized samples. Elements which were at or near the detection limit were not considered (ie. U, Th, Mo, La, Nb etc). The error associated with calculation of gains and losses within the basaltic andesites is considered to be approximately ± 20% based upon Ludden et al. (1984), considering the geochemical homogeneity of the unaltered protoliths and analytical errors of < 10%.

Examination of Figure 7-9 indicates that elemental gains and losses are similar for both weakly and strongly altered/mineralized basaltic andesite. Both samples show significant increases (i.e. > 20%) in Si, K, Au, Ag, As, Ba, Co, Cu, Pb, Ni, Sb, W, V, Cr, B, and volatiles (L.O.I.), and lesser, but consistent losses in Al, Fe, Mg, Ca, Na, Mn, Zn, and Y. The elemental additions and losses of major elements displayed by these samples are consistent with petrographic evidence displayed by Type II mineralization and alteration within this lithology, with increases in quartz (Si), microcline, and biotite (K), and progressive alteration accompanied by the destruction of amphibole, plagioclase and ilmenite, and the leaching of Fe, Mg, Ca and Na. The overall loss of iron from mineralized basaltic andesites, may be accounted for by the introduction of sulphur bearing fluids which stripped iron from silicate and oxide minerals to form sulphides. Au carried in sulphur complexes (HS^-) would be destabilized by these reactions leading to gold deposition associated with sulphides (Robert and Brown, 1986).

Significant enrichments occur in both samples for Au, Ag, Ag, Cu, Pb, Sb, W, and B. Au and Ag are ubiquitously contained within native Au, while As is present within arsenopyrite. Cu, Sb, and W enrichments are most likely due to the presence of chalcopyrite, stibnite and scheelite, although significant W may substitute for Ti in titanite (Kieth et al, 19??). Pb, while displaying increases of 1000% in both samples occurs in concentrations of less than 30 ppm in both samples. This element may be present as galena, although none has been noted in petrographic studies. Alternatively Pb may occur within potassium-bearing silicate

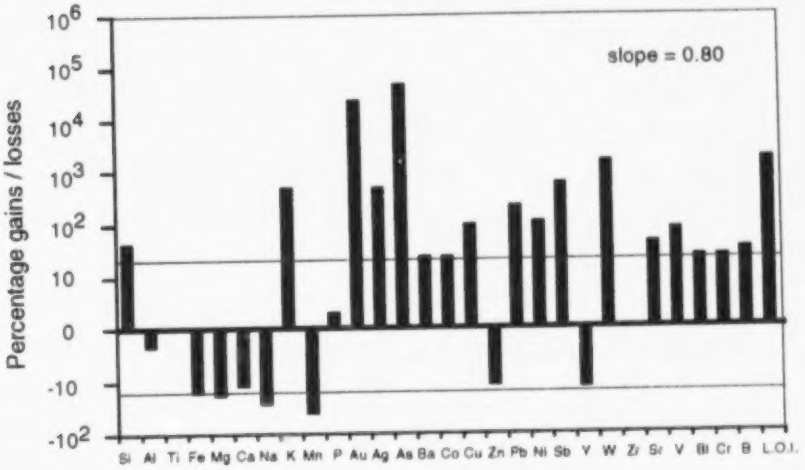

Weaky mineralized basaltic andesite
91 VLT 3052

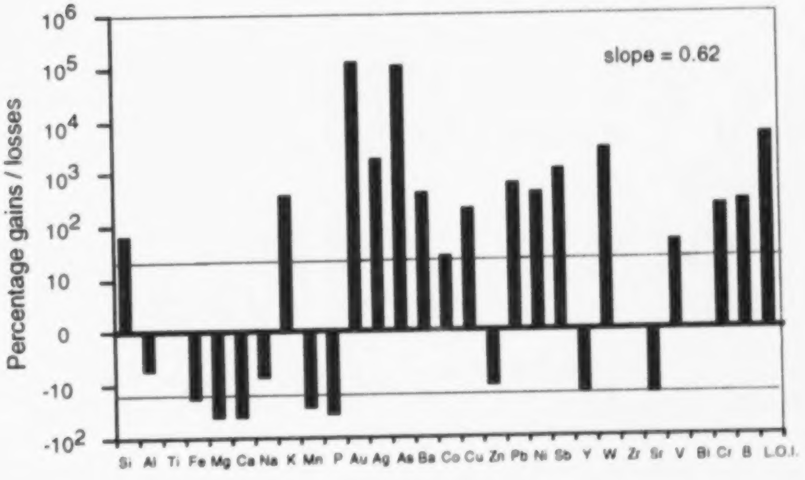

Mineralized basaltic andesite
90 VLT 3055

FIGURE 7-9. Percentage gains and losses for altered/mineralized basaltic andesites, Type II mineralization, Ulu Claims. Slope given in the right hand corner of diagram is the slope of the Ti-Zr isocon. Slopes less than one indicate mass increase. Error of ~20% is shown by horizontal line.

TABLE 7-1. Major and trace element chemistry of average basaltic andesite and mineralized basaltic andesites. Major oxides in weight %, Au in ppb, all other elements in ppm. Average gains/losses given in percentages for mineralized samples relative to average unaltered basaltic andesites, based upon immobile behavior of Ti and Zr. Isocon slope and mass change are also given. Mass change indicated for mineralized samples by assumption of constant Ti and Zr. Fe_2O_3 t = total iron.

	Basaltic andesite average n=4	91 VLT 3052 weakly mineralized	Gains/losses 91 VLT 3052 (percent)	91 VLT 3055 mineralized	Gains/losses 91 VLT 3055 (percent)
Isocon Slope	-	-	0.80	-	0.62
Mass Change%	-	-	25	-	61
SiO_2	56.34	66.20	38	66.81	57
Al_2O_3	11.90	9.25	-2	6.69	-6
TiO_2	1.86	1.46	-1	1.13	-1
Fe_2O_3 t	15.64	9.73	-18	6.69	-19
MgO	3.11	1.90	-19	0.64	-41
CaO	6.68	4.47	-13	1.45	-40
Na_2O	3.47	1.81	-28	1.89	-7
K_2O	0.35	1.83	443	1.36	327
MnO	0.21	0.08	-42	0.07	-29
P_2O_5	0.22	0.18	2	0.05	-39
Au	43	8360	19591	48600	114291
Ag	0.1	0.5	420	1.70	1638
As	78	32153	40237	77640	97292
Ba	145	146	21	594	347
Co	35	35	20	30	24
Cu	34	56	84	81	174
Zn	146	99	-12	74	-11
Pb	5	13	194	29	549
Ni	12	20	94	46	338
Sb	2	14	542	23	960
Y	48	32	-13	22	-16
W	1	14	1320	24	2338
Zr	192	157	2	120	0
Sr	162	191	38	72	-18
V	76	115	72	80	44
Bi	2	2	0	2	0
Cr	20	20	20	50	188
B	2.75	3	29	8	229
L.O.I.	0.2	3.1	1470	8.7	4288

alteration phases (biotite and microcline). B is present within tourmaline, which is common throughout the alteration and mineralization.

The elements Ba, Co, Ni, Cr, and V also display significant increases, however, they likely do not form individual mineral phases, but instead occur as substitutions within common silicate and sulphide mineral phases. Ba most likely occurs substitutes for K, V and Cr may occur within sericite or titanite, and Ni and Co may be present as as trace quantities within pyrrhotite or other sulphides

Although gains and losses of individual volatile phases (sulphur, CO_2 and H_2O) have not been determined, loss on ignition (L.O.I.), represents total volatiles, and for both samples displays significant increases. Petrographic examination suggests that this increase is mainly due to the addition of sulphur (in the form of sulphides) within the mineralized material, although CO_2 has also been added evidenced by the presence of carbonate minerals in mineralized Type II material.

Amongst the trace element suite selected, only Y and Zn display consistent losses for both samples. P and Sr display variable behavior between the two samples. The presence of presumably hydrothermal apatite within wallrock, and to a lesser degree vein quartz may explain the behavior of P which shows little change in 91VLT 3052, but depletion in 91VLT 3055 which shows much stronger silica dilution.

Elemental Gains/Losses in Altered/Mineralized Sediments.

Gains and losses of 29 major and trace elements as well as L.O.I., within altered/mineralized sediments are shown graphically in Figure 7-10 and given in Table 7-2. Criteria for elements selected are the same as for the basaltic andesites. Error associated with calculation of gains and losses within altered/mineralized sedimentary lithologies are considerably higher than those associated with the basaltic andesites. Lhotka (1988) suggests a confidence level of ±50% is more suitable for unaltered lithologies which display geochemically inhomogeneities. This error margin is considered reasonable for Ulu sediments where significant variation exists in the major and trace element contents of unaltered greywackes.

The gains and losses for the two mineralized sediment samples display a much higher degree of variability than the basaltic andesites. This difference is likely due to the heterogeneities within the non-mineralized precursors, and the degree of silicification. Sample 91VLT 3049 has a large proportion of vein quartz, while sample 91 VLT 3051 represents strong alteration and mineralization adjacent to quartz veining. Despite these limitations, certain trends are apparent. Both

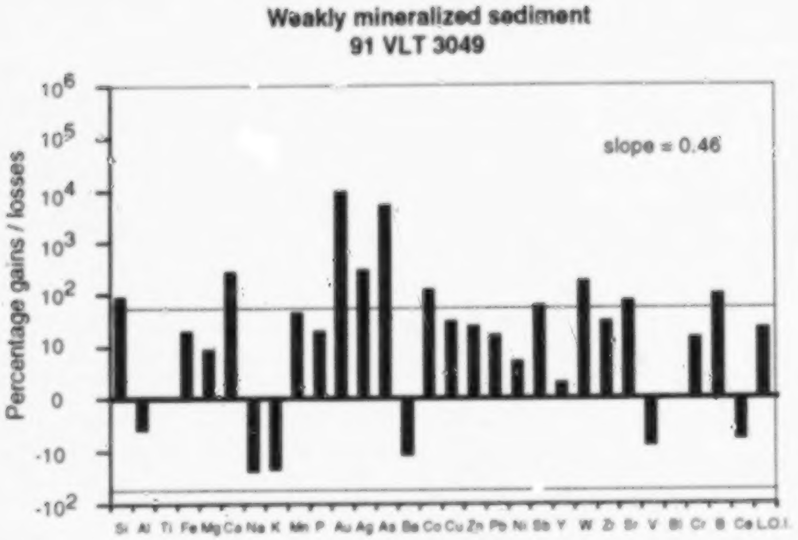

Weakly mineralized sediment
91 VLT 3049

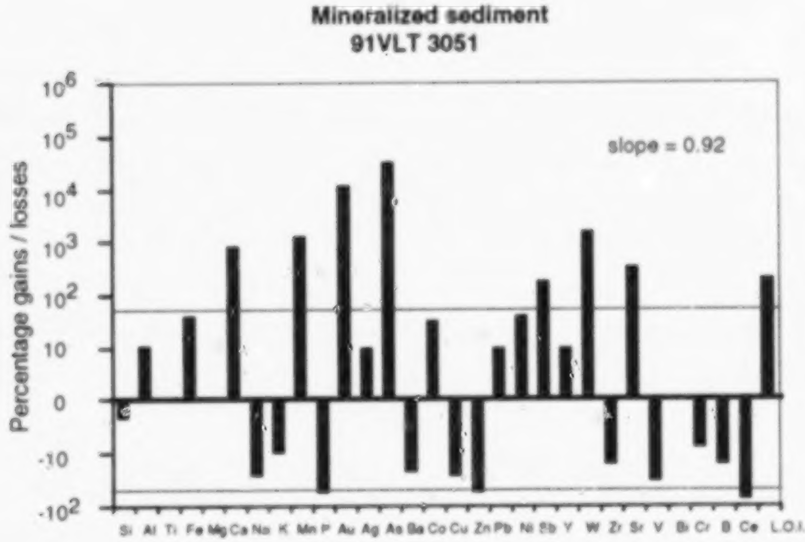

Mineralized sediment
91VLT 3051

FIGURE 7-10. Percentage gains and losses for mineralized/altered sediments, Type II mineralization, Ulu Claims. Slope given in upper right of diagrams is the slope of the Ti isocon. Slopes less than one indicate a mass increase. Error of ~50% is shown by horizontal line.

TABLE 7-2. Major and trace element chemistry of greywackes and mineralized equivalents. Major oxides in weight percent, Au in ppb, all other elements in ppm. Average gains and losses given in percentages for mineralized samples relative to unaltered equivalents (91VLT 3049 relative to 91 VLT 3048 and 91 VLT 3051 relative to 91 VLT 3050), based upon immobile behavior of Ti. Isocon slope (IS) and mass change (MC) are also given. Mass change (MC) indicated for mineralized samples by assumption of constant Ti. $Fe_2O_{3\,t}$ = total iron.

	91 VLT 3048 Greywacke	91 VLT 3049 Mineralized greywacke	Gain/losses 91 VLT 3049 (percent) IS=0.46 MC%=117	91 VLT 3050 Greywacke	91 VLT 3051 Mineralized greywacke	Gain/losses 91 VLT 3051 (percent) IS=0.92 MC%=9
SiO_2	64.13	80.89	80	66.51	59.65	-2
Al_2O_3	16.94	7.11	-4	16.60	16.89	10
TiO_2	0.69	0.32	0	0.65	0.60	0
Fe_2O_{3t}	5.93	3.75	17	5.49	6.91	34
MgO	3.04	1.64	8	2.44	2.22	-1
CaO	1.17	3.42	246	0.54	4.52	745
Na_2O	1.35	0.26	-27	0.61	0.39	-28
K_2O	5.11	1.18	-23	5.29	4.34	-10
MnO	0.06	0.05	37	0.05	0.60	1108
P_2O_5	0.11	0.07	18	0.12	0.04	-59
Au	17	1360	7954	123	12260	9875
Ag	0.1	0.3	254	0.1	0.1	8
As	147	6388	4300	126	35740	28273
Ba	795	266	-13	747	517	-23
Co	56	20	108	25	30	28
Cu	167	64	24	32	20	-30
Zn	124	55	21	128	46	-56
Pb	5	3	14	14	14	8
Ni	67	34	5	49	62	35
Sb	2	2	54	2	5	158
Y	11	5	-1	5	5	8
W	1	2	154	1	14	1308
Zr	140	100	25	127	95	-17
Sr	94	103	64	51	195	290
V	50	19	-8	41	24	-33
Bi	2	2	0	2	0	0
Cr	240	140	12	240	200	-9
B	3	4	87	4	3	-17
Ce	80	32	-6	113	20	-74
L.O.I.	1.4	0.9	18	1.6	4.3	176

samples display significant enrichments (i.e. >50%) of Ca, Au, Ag, As, Sb, W and Sr. The following elements also consistently exhibit increases within mineralized/altered samples, although the degree of enrichment may be below 50% ; Si, Fe, Mn, Pb, Ni, Y, and L.O.I. Losses, although less than the confidence limit (50%) are consistent for Na, K, Ba, V, and Ce. Inconsistent behavior during mineralization and alteration characterize P, Cu, Zn, Zr, Cr, and B.

Mineralogical basis for the geochemical changes observed within the sediments during mineralization/ alteration are essentially identical to those within the basaltic andesites, although variations in the pattern in gains/losses for the major elements reflects the differences in chemistry of the protoliths.

Mass Balance Consideration for Ulu Type II Mineralization

If the abundances of the different rock types involved in a mineralizing event are accurately known, the mass balance for an element may be quantified (Lhotka, 1988), and elements which have been added from mineralizing fluids may be identified. Unfortunately the volume of rock, both sedimentary and mafic volcanic, affected by Type II mineralizing fluids, cannot be accurately determined. However, it is likely that the mafic volcanics experienced greater water-rock ratios, due to the higher permeabilities of these rocks during the Type II mineralizing event.

Although quantitative mass balance calculations can not be made, several qualitative inferences may be drawn. The mineralized basaltic andesites exhibit losses of Fe, Mg, Ca, and Mn, the sediments exhibit gains of these elements. Likewise gains in K and Ba within mafic lithologies corresponds to losses of these elements in the sediments. It is likely that transfer of these elements occurred between these lithologies during mineralization and alteration, and that these elements were not entirely contributed by mineralizing fluids from external sources.

The element suite Au, Ag, As, Co, Pb, Ni, Sb, W, and L.O.I. show enrichment in all samples of mineralized material examined and may be considered to have been added from an external source during mineralization. Other elements which exhibit enrichment in the basaltic andesite, and variable behavior within the sediments, and are most likely added are, Cu, B, and Cr. Only Na displays consistent depletion in all samples studied and likely was mobilized and removed during the mineralization process. The remaining elements, Al, Ti, P, Zn, Y, and Zr, display limited enrichments and depletions and likely represent either analytical error, or local variations in mobility, possibly due to differential mineralogy.

In conclusion it appears that Au, Ag, As, Co, Pb, Ni, Sb, W, Cu, B, Cr, and L.O.I. were added from external sources during Type II mineralization. Major element gains and losses with the exception of Si, may be partially accounted for by mass transfer between the sediments and mafic volcanics, although significant K and Ba was likely added due to its strong enrichment within the mineralized mafic volcanics. Only Na was consistently depleted from both sediments and mafic volcanics.

8. LIGHT STABLE ISOTOPE STUDY

INTRODUCTION

A light stable isotope (O, H, C) study of gangue minerals from Type II and Type III veins was undertaken in order to elucidate the isotopic character of the fluids responsible for these mineral occurrences. The deposition of the gangue phases (mainly quartz with subordinate carbonate in Type II veins) is closely associated with sulphide and gold mineralization in both vein types and gangue. The ore minerals are considered to have been deposited from the same fluids. Whole rock oxygen isotope ratios have also been determined for the various host lithological units and intrusive phases in order to determine the extent of interaction between these hosts and the mineralizing fluids. While light stable isotopes provide few unambiguous constraints on the source of auriferous fluids within Archean lode gold deposits (Ho et al., 1992, Colvine et al., 1988b, Kerrich, 1987), systematic differences between the isotopic signature of Type II and Type III veins coupled with geological considerations allow inferences to be drawn about origins of the fluids that produced these two vein types.

ANALYTICAL PROCEDURES

Representative samples of alteration-free host rocks proximal to the Type II mineralized veins from the Flood Zone were selected primarily from drill core. Samples were pulverized.

Vein quartz samples from Type II and Type III veins were coarsely crushed, hand-picked and boiled in aqua-regia for one hour. Samples were then washed and hand-picked again to prevent contamination from other silicate phases. Samples for oxygen isotope analysis were pulverized. Samples for hydrogen isotope analysis consisted of -40 to -80 US mesh size fragments.

Quartz vein and whole rock samples were analyzed for oxygen by using the BrF_5 technique of Clayton and Mayeda (1963). Fluid inclusion waters were extracted directly from fluid inclusions by thermal decrepidation under vacuum at 1100°C. Production of hydrogen from the liberated aqueous phase was accomplished by reaction with zinc metal at 450°C (Coleman et al., 1982).

Carbonate samples consisted of calcite bearing Type II mineralization, and calcite veins. Whole rock samples were used because of the fine grained nature of the calcite which made mineral separation difficult. Carbonate samples were reacted with H_3PO_4 at 25°C following the method of McCrea (1950).

Mass spectrometric results are quoted in standard δ notation relative to standard mean ocean water (SMOW) for oxygen and hydrogen, and PeeDee Belemnite (PDB) for carbon. Analytical reproducibility of respective delta values was ± 0.4‰ for oxygen, ± 5‰ for hydrogen, and ± 0.10‰ for carbon.

SILICATE OXYGEN ISOTOPE STUDY

Results

Whole Rock

Whole rock oxygen isotope analyses of host rocks from the Flood Zone are given in Table 8-1 and are shown graphically in Figure 8-1. The $\delta^{18}O$ of altered mafic volcanics ranged between 7.5 and 8.2‰, while cogenetic gabbros yielded values of 6.1 and 5.9‰. A sample of quartz diorite thought to be related to the gabbros yielded a value of 6.7‰. A single analysis of greywacke yielded a $\delta^{18}O$ value of 9.2 ‰. Two analyses of quartz-feldspar-porphyries gave values of 9.0 and 8.8‰,and a grey aplite dyke had a $\delta^{18}O$ of 9.9‰. A single sample of external granite collected in the NFN area gave a $\delta^{18}O$ of 10.8‰.

Vein Quartz

Results of oxygen isotope analyses of vein quartz are given in Table 8-1 and shown graphically in Figure 8-1. Frequency histograms of $\delta^{18}O_{quartz}$ values from Type II and Type III veins are shown in Figure 8-2.

Type II Veins

A total of 10 vein quartz samples from auriferous veins from the Flood Zone were analyzed from both drill core and surface samples. Oxygen isotope values ranged from 12.4 to 14.4‰ and averaged 13.5‰. Two quartz samples of barren veins from the Flood Zone yielded $\delta^{18}O$ values of 10.9 and 11.1‰.

Three quartz samples from auriferous Type II veins from the Gnu Zone gave considerably lower $\delta^{18}O$ values between 10.5 to 10.8‰ averaging 10.7‰. Two analyses of Type II veins from the NFN yielded $\delta^{18}O$ values of 11.8 and 12.4‰.

Type III Veins

A total of 19 vein quartz samples from barren and auriferous Type III veins from locations throughout the Ulu Claims were analyzed. The oxygen isotope

TABLE 8-1. Ulu Claims stable isotope data.

Sample	Location	Sample Type	Mineral	$\delta^{18}O$ (‰SMOW)	δD (‰SMOW)	$\delta^{13}C$ (‰PDB)
90VD-44 (292.7m)	Flood Zone	QFP	whole rock	9.0		
90VD-39 (444.3m)	Flood Zone	QFP	whole rock	8.8		
92VD-141 513.6m)	Flood Zone	Grey Aplite	whole rock	9.9		
89VD-05 (19.5m)	Flood Zone	Mafic volcanic	whole rock	7.5		
90VD-42 (268.8m)	Flood Zone	Mafic volcanic	whole rock	8.2		
90VD-30	Flood Zone	Greywacke	whole rock	9.2		
90VD-88 (137.7m)	Flood Zone	Gabbro	whole rock	6.1		
90VD77 (174.6m)	Flood Zone	Gabbro	whole rock	5.9		
91 VKT 4205	Ulu West	Gabbro-diorite	whole rock	6.7		
GRAN NFN	NFN	External granite	whole rock	10.8		
90PAK-US-19	Flood Zone	Type II vein	quartz	14.3	-132	
90PAK-US-22	Flood Zone	Type II vein	quartz	13.8		
90PAK-US-44	Flood Zone	Type II vein	quartz	14.4		
90VD-19 (221.0m)	Flood Zone	Type II vein	quartz	14.3	-164	
90VD-25 (25-6)	Flood Zone	Type II vein	quartz	12.4		
90VD-27 (27-3)	Flood Zone	Type II vein	quartz	13.9	-125	
90VD-34 (223.4m)	Flood Zone	Type II vein	quartz	13.2	-108	
90VD-38 (222.3m)	Flood Zone	Type II vein	quartz	13.2	-108	
90VD-51 (388.5m)	Flood Zone	Type II vein	quartz	12.6	-162	
90VD-63 (403.5m)	Flood Zone	Type II vein	quartz	13.8	-67	
90PAK-US-32	Flood Zone	Type II min	calcite (wr)	11.4		-3.9
90PAK-US-34	Flood Zone	Type II min	calcite (wr)	11.5		-4.1
90VD-47 (349.0m)	Flood Zone	Type II min	calcite (wr)	12.3		-2.0
90 VD-30 (48.0m)	Flood Zone	Type II alteration	calcite (wr)	11.7		-4.6
92VD-140 129.5m)	Flood Zone	Type II alteration	calcite (vein)	10.3		+2.6
92VD-140 (160.0m)	Flood Zone	Type II alteration	calcite (vein)	10.3		+3.4
92VD-141 (229.5m)	Flood Zone	Type II alteration	calcite (vein)	9.0		+3.1
90PAK-US-46	Flood Zone	Barren quartz	quartz	10.9	-105	
90VD-32 (32-12)	Flood Zone	Barren quartz	quartz	11.1	-104	

TABLE 8-1. Ulu Claims stable isotope data.

Sample	Location	Sample Type	Mineral	$\delta^{18}O$ (‰SMOW)	δD (‰SMOW)	$\delta^{13}C$ (‰PDB)
91VKT-3550	Gnu Zone	Type II vein	quartz	10.8		
91VKT-3551	Gnu Zone	Type II vein	quartz	10.5		
91VKT-3422	NFN	Type II vein	quartz	11.8		
91VKT-3429	NFN	Type II vein	quartz	12.4		
89VD-12 (24.9 m)	Flood Zone	Type III vein	quartz	10.9	-59	
91VD-108 (535.0m)	Flood Zone	Type III vein	quartz	10.1		
89 VFT-622	East Limb	Type III vein	quartz	11.3		
90 VFT-3616	East Limb	Type III vein	quartz	11.4		
90PAK-47	Ulu West	Type III vein	quartz	9.5	-87	
90VBT-2470	Ulu West	Type III vein	quartz	9.7	-83	
91VKT-3446	Ulu West	Type III vein	quartz	9.4		
91VKT-3449	Ulu West	Type III vein	quartz	10.4	-121	
90VFT 2099	Emerald Lake	Type III vein	quartz	11.6		
91VFT 3630	Emerald Lake	Type III vein	quartz	9.9		
91VFT-3803	Emerald Lake	Type III vein	quartz	9.8	-60	
91VLT 3030	Emerald Lake	Type III vein	quartz	11.0		
GBZ	Emerald Lake	Type III vein	quartz	10.6		
91VKT-3562	Gnu Zone	Type III vein	quartz	10.3	-134	
91VMT 3708	Ravine	Type III vein	quartz	10.4	-115	
91VKT 3427	NFN	Type III vein	quartz	11.6		
NFNG	NFN	Type III vein	quartz	10.3	-73	
89VFT-64	NFN	Type III vein	quartz	11.4		
90 VD-30 (12.0m)	Flood Zone	Amyt-cc-ep-tm vn	quartz	13.0	-89	
90 VD-30 (12.0m)	Flood Zone	Amyt-cc-ep-tm vn	calcite	10.8		-5.7

TABLE 8-1. Ulu Claims stable isotope data.

Sample	**Location**	**Sample Type**	**Mineral**	**$\delta^{18}O$ (‰SMOW)**	**δD (‰SMOW)**	**$\delta^{13}C$ (‰PDB)**
92VD-141 (213.1m)	Flood Zone	Retrograde alt	calcite	15.5		-5.5

Abbreviations used.wr-whole rock, min-mineralization, vn-vein, amyt-amethyst, cc-calcite, ep-epidote, tm-tourmaline.

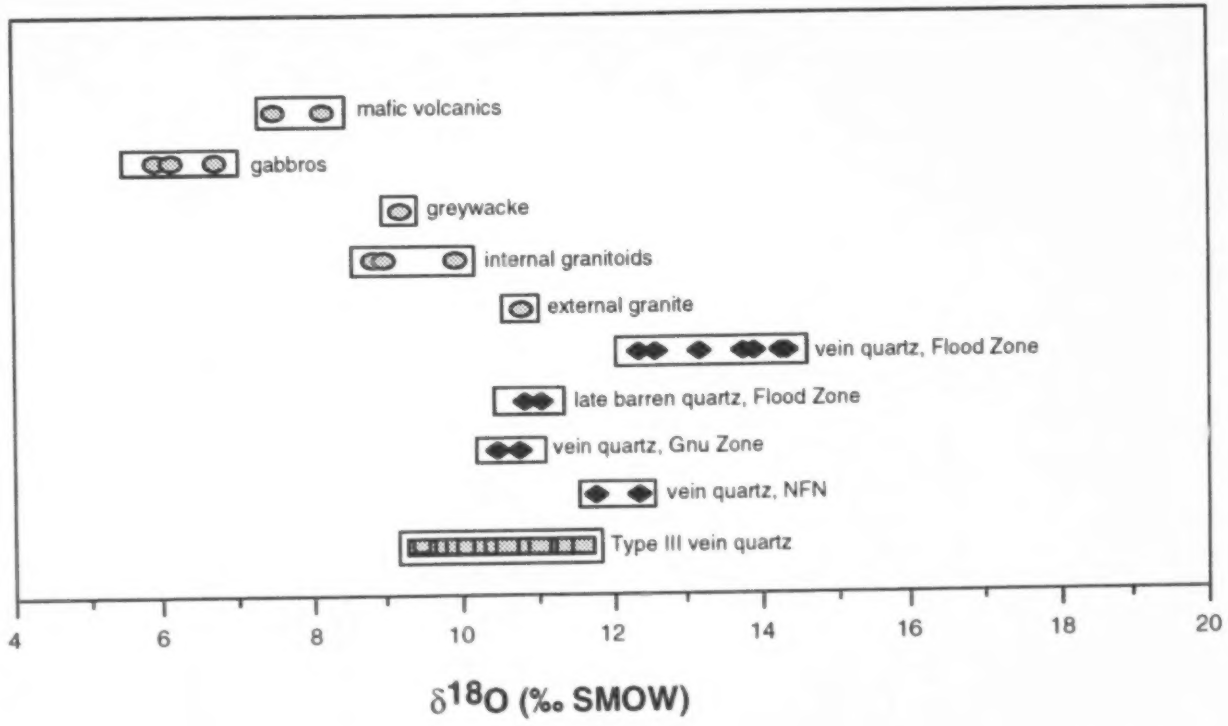

FIGURE 8-1. Oxygen isotope composition of whole rock and vein quartz samples from the Ulu Claims, N.W.T. Whole rock samples shown as shaded ellipses, Type II vein quartz as solid diamonds and Type III vein quartz as shaded rectangles.

values of these veins ranged from 9.4 to 11.6‰ and averaged 10.6‰. Some variation in the isotopic values exists between different Type III vein occurrences (Table 8-1) although this variation is generally less than 2‰.

Discussion of Results

Whole Rock Oxygen Isotope Data

Whole rock oxygen isotope analyses of host lithological units from the Flood Zone were conducted primarily to examine the isotopic relationships between these rocks and the auriferous quartz veins which they contain. The two samples of unaltered mafic volcanics average 8.9‰, considerably higher than the average of 5.7‰ for primary basic igneous rocks (Taylor, 1969). Gabbros which are interpreted to be hypabyssal equivalents of the basic volcanics have significantly lower $\delta^{18}O$ values (average 6.2‰), slightly higher than typical primary gabbros (5.7‰) (Taylor, 1969). The $\delta^{18}O$ enrichment within the mafic volcanics (relative to the cogenetic gabbros) may have been caused by several processes including synvolcanic spilitization of the extrusive units, or isotopic exchange of the fine-grained units with fluids during regional metamorphism.

The single analysis of greywacke gave a value of 9.2‰, and is in agreement with other Archean sedimentary rocks, which display significantly lower $\delta^{18}O$ values than most post-Archean metasedimentary rocks (Shieh and Schwarcz, 1977).

Three samples of the internal intrusive rocks averaged 9.2‰, which likely reflects the primary values of these rocks, and may be categorized as 'normal ^{18}O-granitic rocks' (Taylor, 1978) A single sample of external granite has a higher $\delta^{18}O$ value (10.8‰) and is classified as a 'high ^{18}O granitie' (Taylor, 1978). The isotopic composition of granitic rocks is indicative of the source from which the melts forming these rocks were derived from (Hoefs, 1980). The isotopic composition of the internal granitoid suite, place them within the high end of the 'normal 18O granites' (between 6 and 10‰) (Taylor, 1978). Such rocks may form through the the melting of a heterogeneous volcanic-sedimentary source (Hoefs, 1980). The high ^{18}O content external granite (i.e. $\delta^{18}O$ greater than 10‰) indicates derivation from a ^{18}O enriched sedimentary or metamorphic source (Hoefs, 1980). Although the isotopic compositions of the granitic rocks from the Ulu Claims cannot be used to definitively implicate source regions from which these rocks were derived, the isotopic values of the external and internal granitoids are in agreement with geochemical studies of these rocks (Chapter 4). Both studies indicate that the two suites were formed from different source rocks, with the internal suite having a mafic volcanic component, while a dominantly sedimentary source is implicated for the external suite.

Type II Veins

Results of oxygen isotope analyses of quartz from auriferous Type II veins from the Flood Zone, hosted primarily by mafic volcanic rocks, have an average $\delta^{18}O$ of 13.5‰, and vary from 12.4 to 14.4‰. No systematic variation of isotopic composition of quartz is apparent with increasing depth, although the highest values were obtained from surface samples. Observed variations in the $\delta^{18}O$ of the Flood Zone quartz may be attributable to several factors. Textural studies of these veins indicate a protracted multi-episodic origin for these veins. Variations may be due to slight differences in crystallization temperature of quartz, or changes in the $\delta^{18}O$ of local fluid reservoirs as a result of interaction and oxygen exchange with host rocks.

The ^{18}O enrichment of the vein quartz samples relative to the vein host rocks indicates that the host rocks were not in isotopic equilibrium with the mineralizing fluids (Kerrich, 1987). This disequilibrium is an invariable condition in Archean lode gold deposits (Kerrich, 1987; Colvine et al., 1988). Isotopic disequilibrium between host rocks and vein quartz is indicative of high water-rock ratios during the mineralizing event and implicates a high ^{18}O reservoir for the mineralizing fluids from a source external to the depositional site. These factors preclude lateral diffusion mechanisms (Boyle, 1961) for the formation of Type II veins.

Vein quartz samples from the Gnu Zone display consistently lower $\delta^{18}O$ values (average 10.7‰) than those from the Flood Zone. While these veins are mineralogically identical to those in the Flood Zone they are considerably narrower (50 cm), and are hosted within gabbroic rocks. The lower $\delta^{18}O$ values are interpreted as resulting from exchange with the host gabbros in response to much lower water-rock ratios during formation of these veins. A similar decrease in the $\delta^{18}O$ values of Type II veins (average 12.2‰) from the NFN, hosted within mafic volcanics, is again likely a result of decreased water-rock ratios.

The late barren quartz from the Flood Zone also have considerably lower $\delta^{18}O$ contents (average 11.0‰). One of the barren veins (90VD-32) occurs within the mineralized zone, and apparently post-dates the aurifreous veins. If these veins

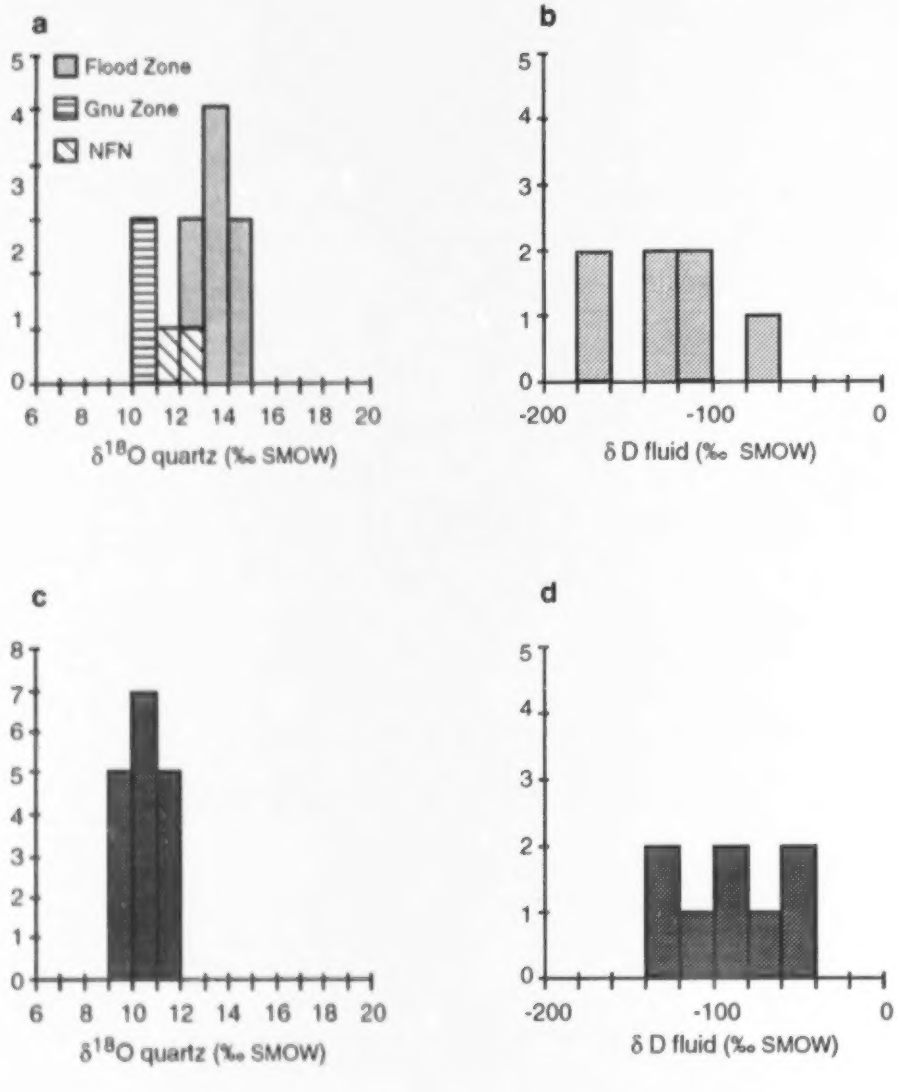

FIGURE 8-2. Oxygen isotopic composition of vein quartz and hydrogen isotopic composition from fluid inclusions from vein quartz: **a**. Oxygen, Type II mineralization, **b**. Hydrogen, Type II mineralization, **c**. Oxygen, Type III mineralization, **d**. Hydrogen, Type III mineralization.

were formed from the same fluid reservior as the auriferous portions of the veins then either higher temperatures prevailed, or the isotopic composition of the fluid had shifted, possibly through extensive exchange with wallrocks. The possibility that these veins were formed from an post-mineralization, independent fluid reservoir cannot be discounted.

Type III Veins

Type III veins occur as discreet dilatent fill structures with negligible wallrock alteration (Chapter 3). The oxygen isotope composition of quartz from these veins is therefore thought to directly reflect the fluids responsible for mineralization. Oxygen exchange with wallrocks is not considered to have been significant. Although ore minerals within this vein type occurs as late fracture fill and inclusion trails which cut quartz crystals, the quartz and ore minerals are interpreted to have been deposited from essentially the same fluids during a regime of decreasing temperature.

The variations in $\delta^{18}O$ of Type III vein quartz occur primarily between vein clusters (i.e. Ulu West-9.8‰ and East Limb-11.3‰), although local variations within single vein clusters also occur (i.e. Emerald Lake 9.8 to 11.6‰). This is interpreted as reflecting differing temperatures of quartz precipitation or localized variables, possibly induced by boiling, rather than changes in the primary isotopic composition of the fluid reservoir.

Other Veins

A single analysis of quartz, from a quartz-amethyst-calcite- epidote vein interpreted as an early metamorphic vein (Chapter 3) from mafic volcanics in drill core, gave a oxygen isotope value of 13.0‰

HYDROGEN ISOTOPE STUDY

A study of the hydrogen isotope systematics of fluid inclusion extracts from Type II and Type III auriferous quartz veins was undertaken to examine the nature of the fluids from which these veins precipitated. The use of hydrogen isotopes derived from fluid inclusion waters in the study of mineralizing fluids necessitates the assumption that the fluids present within the inclusions represent primary fluid compositions. Examination of doubly polished quartz chips from Type II and Type III mineralized quartz veins reveals complex populations of fluid inclusions within these veins, and this must be considered when interpreting the hydrogen isotope compositions derived from bulk fluid extraction.

Type II quartz consist of primary three phase (H_2O-CO_2-vapour) inclusions which have been swept to grain boundaries presumably during recrystallization, and several populations of dominantly aqueous secondary fluid inclusion trails which transect quartz grain boundaries. The abundance of these secondary inclusions is highly variable among the chips examined.

Type III quartz has not been recrystallized. Although primary inclusions were observed, secondary fluid inclusions intimately associated with solid bismuth±gold inclusions predominate. These inclusions are primarily two phase, aqueous, and commonly contain solid daughter salt crystals. Large, clearly secondary inclusions containing calcium chloride salts (antarcticite?) were observed in both mineralization types.

Results

Results of the hydrogen isotope study are given in Table 8-1 and frequency histograms of hydrogen isotope compositions of Type II and Type III veins are given in Figure 8-2. A total of seven deuterium analyses were obtained from bulk extraction of fluid inclusions in quartz from Flood Zone Type II veins. The values varied widely from -67 to -164‰ and averaged -115‰. Eight analyses of fluid inclusion waters from Type III veins from various locations yielded δD values between -59 and -134‰, averaging -87.5‰.

Interpretation of Hydrogen Isotopes

Large ranges in hydrogen isotopes are displayed by both vein types although the spread in values is larger within Type II veins. These ranges in values requires either a mixed fluid source or post deposition disturbance of the hydrogen isotope systematics within the inclusions. The possibility of the values being primary and representing a mixing of fluids from isotopically distinct reservoirs is not supported by the relatively narrow range of oxygen isotope values of vein quartz, as a corresponding shift in $\delta^{18}O$ values would be expected (Fyon et al., 1982).

The ranges in δD of the fluid inclusion waters from the Ulu Claims veins may be attributable to the presence of CH_4 or H_2 within the mineralizing fluids. Taylor (1979) indicates that the interaction of a CH_4 bearing hydrothermal fluid with an oxidizing environment would result in deuterium depletion within the H_2O

component of the fluid. Rye and Rye (1974) analyzed fluid inclusion waters from the Proterozoic Homestake mine and also recorded a large variation in δD values (-56 to -110‰) which they attributed to the presence of CH_4. The effects of methane on the δD systematics of fluid inclusion extracts from quartz of Archean lode gold deposits are also known. Fyon et al. (1982) and Wood et al. (1986) report ranges in δD for Archean fluids in the Timmins area (+5 to -50‰) and Hollinger Mine (-39 to -74‰) respectively. However these ranges differ in that they show an enrichment trend of deuterium relative to suspected primary values, attributable to the formation of CH_4 from CO_2 in a reducing environment (Taylor, 1979).

The δD depletion displayed by the fluid inclusion waters from the Ulu Claims may also be due to contamination by fluids that were trapped during late deformation, or any time during the last 2.6 billion years, which were unrelated to vein formation. The presence of calcium chloride-bearing brines that display low deuterium values as well as extreme depletion of oxygen has been documented from the Slave Province (Frape et al., 1984), . Although the oxygen isotope composition of the fluid inclusion waters was not analyzed, the extremely depleted δD values (especially within Type II veins) are consistent with the influence of high latitude meteoric waters.

While the cause of the depletion trends within these fluid inclusion extracts is unknown, it is apparent that the majority of the values are not indicative of the primary δD compositions of the mineralizing fluids. Comparison of the Ulu fluid inclusion extract δD with other Archean vein forming fluids (Fyon et al., 1982; Wood et al., 1986; Ho et al., 1993) suggests that the least depleted δD values from both the Ulu vein types are most representative of the isotopic signature of the primary mineralizing fluids. The processes which resulted in the depletion of deuterium from the Ulu veins apparently affected Type II veins to a greater extent than the Type III veins.

Using the least negative values, the δD signatures from Type II and Type III veins are -67‰ and -59 respectively. These deuterium values are consistent with a magmatic (-50 to -85‰) or metamorphic (+5 to -65 ‰) origin of the fluids (Taylor, 1979). The possibility of the involvement of meteoric waters cannot be ruled out based on the hydrogen isotopes alone, due to uncertainty of the geographic position of the High Lake Belt during the mineralization process, as well as uncertainty regarding the hydrogen isotope composition of ancient meteoric waters (Taylor, 1979).

CARBON ISOTOPE STUDY

Results

Results of the isotope study of carbonates from the Ulu Claims are given in Table 8-1 and shown in Figure 8-3. Four calcite-bearing whole rock samples of Type II mineralization-alteration were analyzed. These yielded $\delta^{18}O$ values between 10.3 and 11.4‰, and $\delta^{13}C$ value of -2 to -4.6‰. Three samples of calcite veins from the outer alteration zones surrounding the Flood Zone gave $\delta^{18}O$ value of 9 to 10.3‰ and $\delta^{13}C$ values of +2.6 to + 3.1‰.

Two calcite analyses of quartz-amethyst-calcite-tourmaline veins gave δ^{18} O values of 10.8 and 10.7‰ and $\delta^{13}C$ values of -5.7 and -6.1‰.

A single analysis of a calcite veinlet associated with late retrograde alteration within mafic volcanics from the Flood Zone yielded $\delta^{18}O$ of 15.5‰ and $\delta^{13}C$ of -5.5‰.

Discussion of Carbonate Isotope Results

The isotopic composition of carbon from vein carbonates depends not only on the δ^{13} C value of the total carbon in the ore forming fluid, but also upon the oxygen fugacity, pH, and temperature (Ohomoto and Rye, 1979). The ambient fluid oxidation potential must be constrained due to the redox potential dependence of $\delta^{13}C$ of hydrothermal carbonates (Kerrich, 1987). Insufficient data is available for the Type II mineralized veins in this regard, therefore conclusions on the carbon isotope composition of the mineralizing fluids are difficult to assess. In addition, the presence of methane within the mineralizing fluids (as discussed in the depletion observed in hydrogen isotopes of fluid inclusion waters) would affect the $\delta^{13}C$ values of coexisting carbonate species because of the strong enrichment of ^{12}C within reduced carbon (Hoefs, 1987).

In an empirical sense, the $\delta^{13}C$ compositions of hydrothermal calcite from Type II mineralization are generally comparable to carbon isotope values for other Archean Lode gold deposits (median value -3.5‰), in which magmatic or metamorphic carbon reservoirs are implicated (Colvine et al., 1988; Kerrich, 1987; Ho et al., 1993).

The analyses of calcite from alteration veins surrounding Type III mineralized veins yielded significantly enriched $\delta^{13}C$ values (+2.6 to +3.4‰) relative to calcite directly associated with mineralization (-2.0 to -4.6‰). The enrichment of ^{13}C within late stage carbonates within ore deposits has been

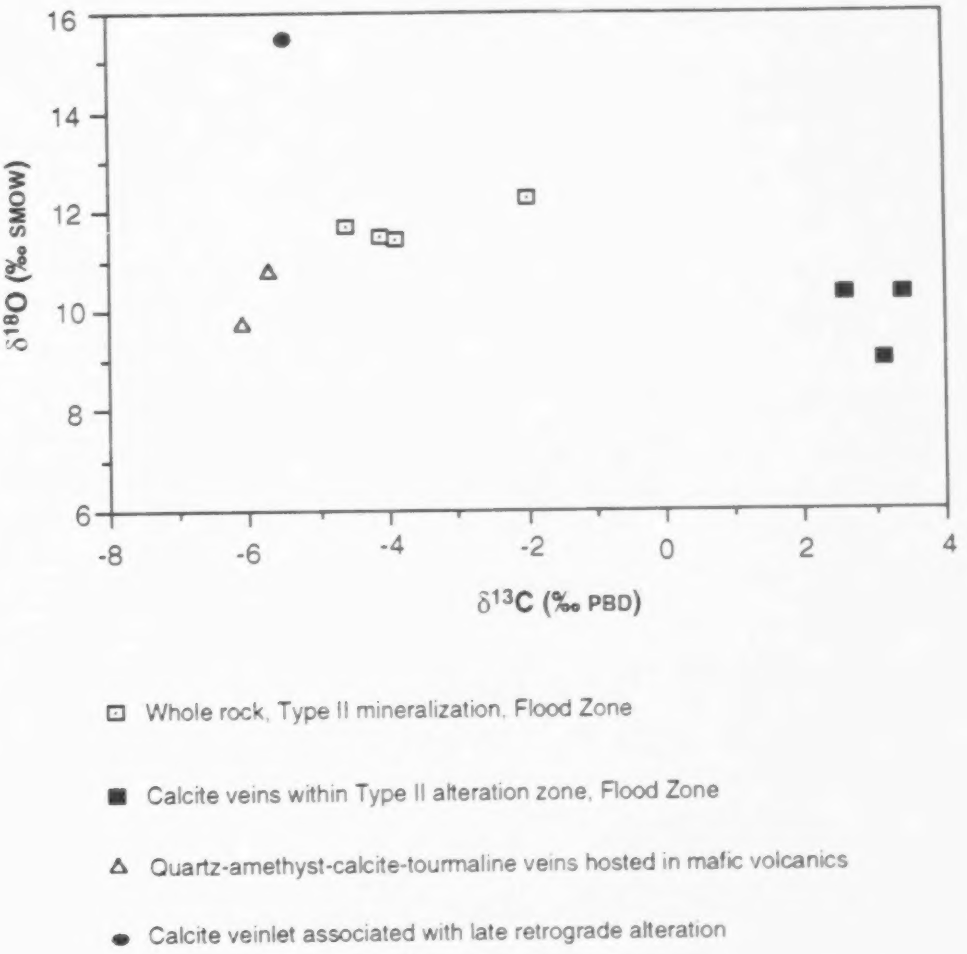

FIGURE 8-3. Carbon and oxygen isotope compositions of vein calcites from the Ulu Claims, N.W.T.

documented, and is likely attributable to cooling of the ore fluid, or decreasing CO_2/CH_4 ratios (Hoefs, 1987). Carbonate oxygen values record a corresponding decrease of up to 2‰ within calcite from the alteration veins. If this was a result solely because of temperature change, it would imply an increase in temperature in the alteration zones, an unlikely scenario. Therefore a decreasing CO_2/CH_4 ratio within the Type II mineralizing fluid best explains the differences in carbon isotope values of calcite directly associated with mineralization and those occurring within peripheral, late-stage alteration veins.

STABLE ISOTOPE COMPOSITIONS OF MINERALIZING FLUIDS

Calculated oxygen isotope compositions of Type II mineralizing fluids using the quartz-water fractionation equation of Matsuhisa et al. (1979) and a temperature range of 360 to 515°C from arsenopyrite geothermometry gives a range of $\delta^{18}O_{fluid}$ values of 8.2 to 12.3‰. The oxygen isotope composition of calcite directly associated with Type II mineralization range from 11.4 to 12.3‰. Calculation of co-existing hydrothermal fluids from which the calcite precipitated, using the calcite-water fractionation equation of O'Neil et al. (1969), and assuming a temperature range of 360 to 516°C (from arsenopyrite geothermometry) yields $\delta^{18}O_{fluid}$ values of 8.0 to 11.2 ‰, which are virtually identical to $\delta^{18}O_{fluid}$ values (8.2 to 12.3‰) calculated from the oxygen isotope composition of Type II quartz.

Calculated oxygen isotope compositions of Type III mineralizing fluids using the quartz-water fractionation equation of Matsuhisa et al. (1979), and a temperature range of 250 to 300°C based on the presence of native bismuth within these veins gives a range of $\delta^{18}O_{fluid}$ values of 0.6 to 4.7‰.

The range in values of calculated $\delta^{18}O_{fluid}$ and δD from fluid inclusion waters from Ulu Type II and Type III fluids are shown on a $\delta^{18}O$ vs. δD plot (Figure 8-4). Also shown are fields of calculated mineralizing fluid compositions for other Canadian and Australian Archean lode gold deposits (Kerrich and Watson, 1984; Kerrich, 1983; Fyon et al., 1982, 1983; Wood et al., 1986; Golding and Wilson, 1987; Golding, 1990), the isotopic composition of primary magmatic and metamorphic waters (Taylor, 1974, 1979) and the meteoric water line (Craig, 1961).

The complete range of fluid inclusion water extract δD values for the Ulu fluids are shown on the plot, however if the assumptions in the preceding section on deuterium are used, the primary fluid δD values likely are represented by the least negative δD portion of the fields. In this case the Ulu fluids are broadly comparable with other Archean mineralizing fluids.

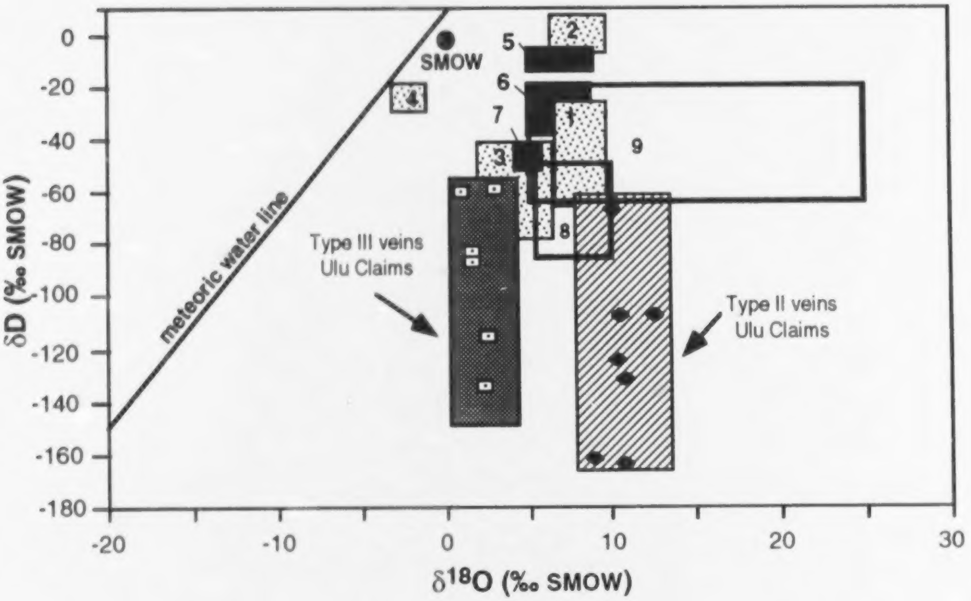

FIGURE 8-4. Plot of δD vs. $\delta^{18}O$ of hydrothermal fluids which generated Type II and Type III auriferous veins within Ulu Claims, N.W.T.. Also shown are fields of metamorphic (9) and magmatic (8) waters (Taylor, 1974, 1979), the meteoric water line (Craig, 1961) and calculated isotopic compositions of mineralizing fluids for other Canadian and Australian Archean auriferous veins; 1) Macassa (Kerrich and Watson, 1984; Kerrich, 1983), 2) Timmins (Fyon et al., 1982, 1983), 3) Hollinger (Wood et al., 1986), 4) Eldrich (Kennedy, 1985 from Kerrich, 1987), 5) Princess Royal, 6) Victory-Kambalda, and 7) Mount Charlotte (Golding and Wilson, 1987; Golding, 1990).

The $\delta^{18}O$ values of Type II fluids calculated from quartz-water and calcite-water fractionation equations vary from 8.0 to 12.3‰ which is within the range of $\delta^{18}O_{fluid}$ values of Canadian Archean gold deposits (Colvine et al., 1988). Using the least negative δD value obtained from Type II inclusions, the Type II fluids plot both within the magmatic and metamorphic fields (Figure 8-4). Although the influence of meteoric or ocean water can not be ruled out, extensive isotopic exchange with rocks must occur to make these fluids isotopically indistinguishable from magmatic and metamorphic fluids. As well, dominantly lithostatic fluid pressures recorded during the Type II mineralizing event (Chapter 6) may also preclude the involvement of meteoric water (Kerrich, 1987).

The isotopic composition of fluids involved in the formation of Type III veins have a distinctly different signature from Type II fluids. The Type III fluids display distinctly lower $\delta^{18}O_{fluid}$ values, ranging from 0.6 to 4.7 ‰. (Figure 8-4), which lie outside the fields for both metamorphic and magmatic waters. Similar $\delta^{18}O$ depleted fluids (relative to typical Archean lode gold fluids) have been implicated in the formation of Archean lode gold deposits which lie at high crustal levels, in which mixing of magmatic and/or metamorphic fluids with meteoric fluid reservoirs has been suggested (Kennedy and Kerrich, 1987; Ho et al., 1992; Groves, 1993)..

9. DISCUSSION AND SUMMARY

SUMMARY

The information presented within the preceding portions of this study are consistent with a complex history of deposition, tectonism, metamorphism and mineralization for the central portion of the High Lake Belt. The development of a genetic model to explain the presence of gold mineralization must account for many of these variables, especially the temporal relationships between different geologic events. The U-Pb study of the intrusive phases on the Ulu Claims (Chapter 5) was intended to resolve the temporal relationships both through absolute dating of the plutonic bodies, and relative ages of metamorphism and mineralization through cross-cutting relationships. Because of the ambiguous results obtained from the U-Pb study, the temporal relationships between geological events observed within the Ulu Claims must be constrained through field-based observations and textural considerations. The interpreted chronological order of significant geological events is presented in Figure 9-1.

The geological history began with the deposition of the mafic to felsic volcanics, emplacement of cogenetic hypabyssal equivalents of these rocks, and deposition of coeval sediments, followed by establishment of D_1 deformational features within these rocks. The tectonic setting in which the supracrustal rocks of the High Lake Belt were deposited is not clear, however this has significant ramifications for the later generation of granitic melts and generation of mineralizing fluids, and will be discussed in more detail. Following the deposition of the supracrustals a major tectonic event resulted in the establishment of D_2 structural elements, namely large isoclinal folds. Peak metamorphism within the supracrustal pile likely occurred post-D_2, but prior to Type II mineralization as suggested by the retrograde alteration assemblages associated with this mineralization. A D_2 to post-D_2 timing for peak metamorphism is in general agreement with Henderson et al. (1993) who state that the development of peak metamorphic minerals within the metasedimentary rocks predates the establishment of D_3 cleavages.

Type II mineralization post-dated the D_2 event through the focusing of Type II fluids into dilational sites formed during D_2 deformation. This mineralizing event was closely followed by, and terminated with, the emplacement of the internal granitoid suite, suggested by the cross-cutting relationships of Type II mineralization and quartz-feldspar porphyry dykes within the Flood Zone. The

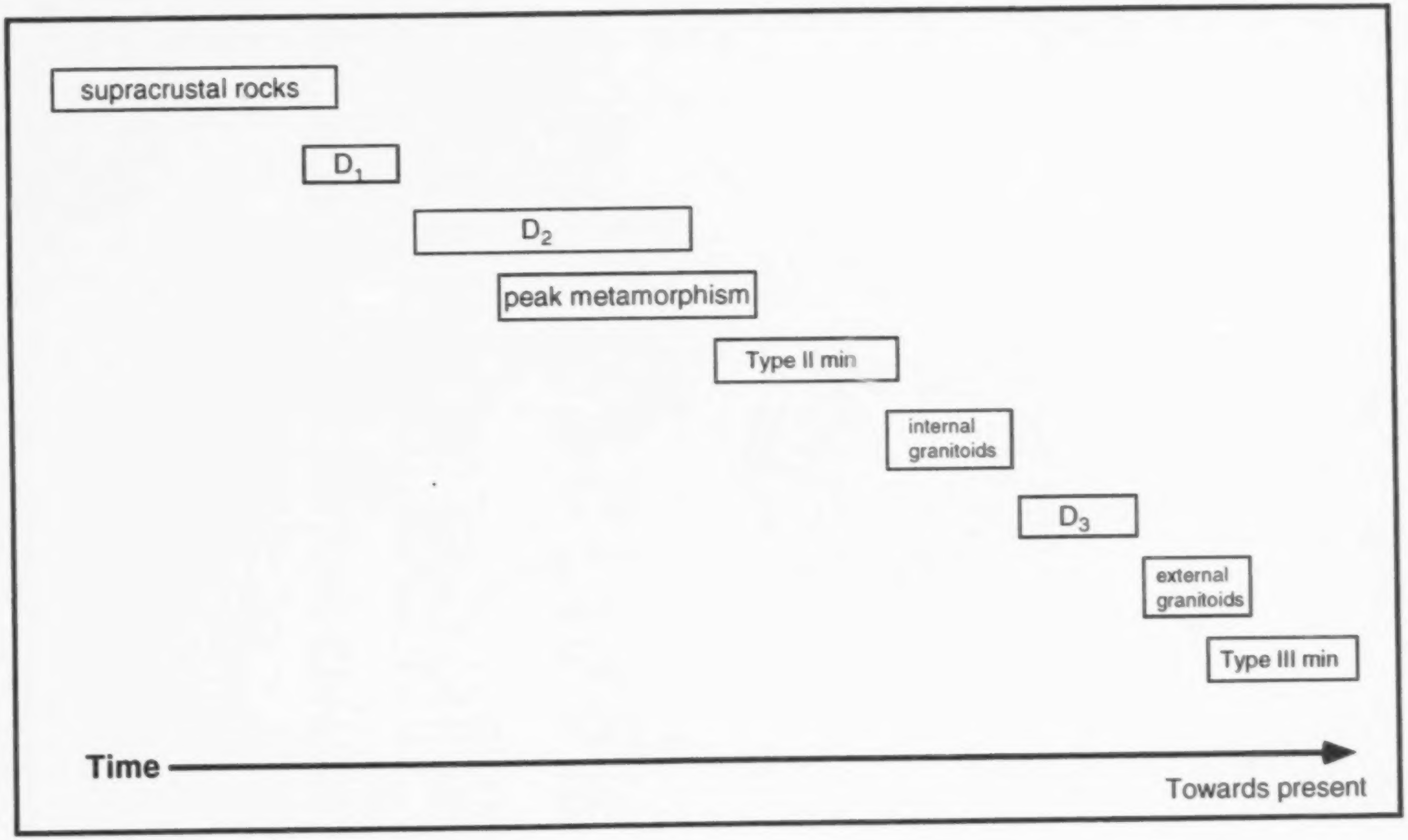
supracrustal rocks
D_1
D_2
peak metamorphism
Type II min
internal granitoids
D_3
external granitoids
Type III min
Time
Towards present

FIGURE 9-1. Order of Archean geological events for the Ulu Claims N.W.T. The temporal relationships between the geological events depicted in this diagram are based upon observations of field relationships and textural considerations.

entire package was then subjected to further tectonism and the establishment of the pervasive D_3 cleavage which affected all units except for the external granitoids. Emplacement of the external granitoids, and Type III mineralization within zones of deformation related to emplacement of these granites, marked the end of Archean activity in the area.

Post-Archean geological activity in the Ulu Claims area was restricted to the Proterozoic, during which the area was affected by faulting and the intrusion of several episodes of diabase dykes.

The characteristics of Type II and Type III veins are summarized within Table 9-1. The two vein types display distinctly different mineralogical, geochemical, structural and temporal characteristics. This suggests that Type II and Type III veins formed independently and do not represent members of a single hydrothermal system displaying regional scale geochemical zonation . The factors that controlled the localization of mineralization of Type II and Type III veins also differ significantly and are summarized below.

The formation of Type II veins appear to have been controlled by the presence of suitable D_2 structural elements, that within the Ulu Claims are largely restricted to the axial plane of the the large antiformal structure. Maximum dilatency occurred within the southern open end of the fold, and the rheological contrasts between sediments and mafic volcanics and gabbros appear to have played a major role in the development of dilatent structures. From the textural evidence (replacement of silicate wallrock) displayed by the ore and sulphide gangue minerals within the Type II veins, it is apparent that sulphidation reactions between the mineralizing fluids and mafic volcanics were responsible for the deposition of gold within these veins. This observation is supported by the conversion of hornblende to light-colored calcic amphiboles (actinolite) during alteration. This conversion would result in the lowering of the Fe/(Fe+Mg) ratios within the alteration amphiboles, indicating that iron was derived from hornblende and utilized in the formation of iron sulphide minerals. Similarly, the conversion of ilmenite ($FeTiO_3$) to titanite ($CaTiSiO_5$) within Type II mineralization and alteration supports the sulphidation mechanism. Gold was likely carried as $Au(HS)_2^-$ complexes which were destabilized during the sulphidation reactions with wallrock, and resulted in the deposition of gold along with iron sulphide minerals within the Type II veins

The geochemical studies of mineralized mafic volcanics and mineralized sediments (Chapter 7) raise the possibility that the interaction of mineralizing

	Type II auriferous veins	Type III auriferous veins
Host rocks	Mafic volcanics, gabbro, sediment	Mafic volcanics, gabbro, sediments, internal granitoids
Timing of veins	Post D2, pre D3	Post D3
Vein distribution	Extensive as individual veins or arrays	Limited lateral extent
Vein type	Ribbon and breccia veins grading into replacement veins	Extension and shear veins
Alteration	Extensive laterally alteration halo	Negligible
Vein gangue mineralogy	Quartz, calcite, microcline, titanite, tourmaline, biotite, actinolite	Quartz, coarse grained
Ore mineralogy	Arsenopyrite, pyrite, pyrrhotite, chalcopyrite, gold	Pyrite, pyrrhotite, chalcopyrite, molybdenite, bismuth, gold
Distribution of ore minerals	Consistent mineralogy and distribution within wallrock fragments and septa	Inconsistent mineralogy and distribution as late fracture fill and inclusions
Geochemical association of Au	As-Au	Bi-Au
Ag/Au in veins	Consistent (0.1-0.4)	Variable (0 to 2.9)
Au transport	HS^- complexes	Cl^- complexes
Au deposition	Sulphidation	Decreasing temperature
Temperatures of vein formation	360-515°C from arsenopyrite geothermometry	250-300°C from presence of bismuth (melting point = 271°C)
δ18O fluid[1]	8.2 to 12.3‰	0.6 to 4.7‰
δD fluid[2]	-67 to -164‰	-59 to -134‰

Notes 1. calculated from d^{18}Oquartz, 2. from direct analysis of fluid inclusions

Table 9-1. Characteristics of the Ulu Claims auriferous veins fluids with sediments may have played a role in the establishment of significant auriferous mineralization within the Flood Zone. This Type II vein occurrence appears to contain a significantly higher gold grade than other Type II vein occurrences within the axial plane of the D_2 antiform (Flood pers. com, 1993). The geochemical studies have shown that chemical exchange of major (K, Fe, Ca, Mg and Mn) and trace (Ba) elements likely occurred between the mafic volcanics and the sediments via the mineralizing fluids within the Flood Zone. Although the exact effect of this chemical transfer on the chemistry of the mineralizing fluids is unknown, it is conceivable that this may have played a role in the localization of auriferous mineralization within Type II veins.

Alteration assemblages associated with this vein type display vertical consistency, which suggests that the rocks relatively warm during the mineralization event. Alteration mainly occurred because of chemistry and not temperature difference between fluids and rocks. Pressures in excess of 3 kbar during Type II mineralization estimated from alteration mineral stabilities (Mueller, 1992), and a estimated Archean pressure gradient of 3.3 km/kbar (Grambling, 1981), indicate that Type II mineralization occurred at crustal depths of at least 10 km.

The stable isotopic composition of Type II mineralizing fluids ($\delta^{18}O$ fluid = 8.2 to 12.3‰, δD = -67‰, $\delta^{13}C$ = 3.5‰) do not allow unequivocal determination of the source of these fluids, however they are generally consistent with the oxygen isotope compositions of other Archean auriferous fluids (+5 to +12‰; Kerrich, 1987; Colvine et al., 1988b; Ho et al., 1992), and are suggestive of deep sourced metamorphic or magmatic fluid (Colvine et al., 1988, Ho et al., 1992, Groves, 1993). The lack of presently preserved plutonic rocks coeval with Type II mineralization favor a metamorphic derivation of the mineralizing fluids. However, the existence of an I-type granitoid at depth, or one totally removed during emplacement of the external granitoids, of which members of internal granitoid suite are late, high-level, manifestations cannot be ruled out.

Type III veins are interpreted to have been emplaced considerably later than the Type II veins. This interpretation is based largely upon the association of these veins with the external granites, as well as their presence within the internal granitoids which post-date Type II mineralization. The factors controlling the emplacement of Type III veins are somewhat ambiguous. However, they appear to occur within broad bands of weak shearing associated with the emplacement of the external granites, which in part follow the dykes of the internal granitoids. Local occurrence of Type III veins within these shear bands appears to have been influenced by local rheological contrasts. The internal granitoids reacted by both brittle fracture and as competent blocks, resulting in stockwork veins within these rocks, and as veins along dyke-wallrock contacts.

The differences in vein style and lack of alteration associated with the Type III veins also contrasts sharply with Type II veins, and suggests that the Type III veins were emplaced under different P-T conditions (lower P and T). Type III veins also lack the consistent mineralogy and geochemistry displayed by the Type II veins, and gradual change of sulphide minerals along specific vein trends suggests an overall zonation within these veins. The mechanisms responsible for deposition of gold also appear to differ from the sulphidation observed in Type II veins, and appears to have occurred independent of host rock composition. The occurrence of sulphide minerals, native bismuth and gold as late fracture fills, interstitial to quartz grains and as solid inclusions, indicate that deposition of these minerals occurred late, possibly as the result of declining temperatures. The fluid composition of inclusions within Type III veins was not examined in detail; however, the preliminary examination of doubly polished quartz wafers indicates the presence of abundant daughter salt crystals within fluid inclusions associated with sulphide and native elements within these veins. The presence of these daughter salts suggests that the fluids from which these veins were deposited were saline in nature, and that gold may have been transported as $AuCl_2^-$ complexes.

The isotopic compositions of the fluids responsible for the deposition of the Type III veins $\delta^{18}O$ = 0.6 to 4.7‰, δD = -59‰ display a significantly lower $\delta^{18}O$ content than Type II veins, although the δD values are similar. The calculated $\delta^{18}O$ fluid for Type III mineralization (0.6 to 4.7‰) is also lower than that of primary metamorphic and magmatic waters (Taylor, 1979). Fluids implicated in the formation of typical Archean lode gold deposits are typically richer in $\delta^{18}O$ (see above) and are of low salinity. (Kerrich, 1987, Ho et al., 1992, Groves, 1993). Type III fluids are not consistent with these typical Archean fluids but appear to be similar to lower $\delta^{18}O$, saline fluids generally associated with porphyry and skarn deposits in which the involvement of magmatic (± meteoric) waters has been demonstrated (Roedder, 1979; Beane and Titley, 1981; Einaudi et al., 1981). The temporal and spatial association of Type III veins with the external granitoids, and the presence of late pneumatolytic fluids and molybdenite within the external granitoids also suggest more than a casual link between the veins and external granitoids. The oxygen isotopes however, suggest contribution from a fluid reservoir that is not entirely compatible with a purely magmatic source. The apparent composition of Type III fluids may have been the result of incursion and the mixing of surface fluids (seawater or meteoric water) with magmatic fluids derived from the external granites. The influx of surface waters may have been possible because of shallower crustal levels during the emplacement of the external granitoids, and the absence of supra-lithostatic pressures present during Type II mineralization. The mixing of deep (magmatic or metamorphic) fluid sources with surface waters has also been suggested for other Canadian and Australian Archean Lode gold deposits (Kerrich, 1987, Groves, 1993) which display a similar negative $\delta^{18}O$ shift from typical Archean mineralizing fluids, as well as evidence of emplacement at high structural levels (occurrence within sub-greenschist facies rocks).

RELATIONSHIP OF MINERALIZATION TO TECTONIC SETTING

The origin of syn-to post-kinematic plutons and the generation of mineralizing fluids are related to broad thermal events which result from the tectonic setting of the High Lake Belt during the late Archean. A unifying tectonic model for the evolution of the Slave province remains elusive (see Chapter 2), with both ensialic rift and accretionary type models having been suggested. Aspects of the observed temporal relationships of geological events within the Ulu Claims will be examined in the context of both a rift and accretionary tectonic setting. This discussion is conceptual and highly speculative in nature. However, elements of a continental rift model are more consistent with the relationships observed at the Ulu Claims.

The association between Archean gold vein systems and syn-to post-kinematic tonalitic to trondhjemitic intrusive is recognized on a world wide basis; however, the temporal relationships between these rocks and gold mineralization are not consistent. In the majority of Archean gold producing areas, tonalites and trondhjemites are important host rocks for auriferous veins (i.e. Superior Province, Colvine et al., 1984, King and Kerrich, 1987; Callan and Spooner, 1988, Australia, Groves, 1993; Wang 1993) while in others, (i.e. Wang et al., 1993) including the Ulu Claims, gold mineralization pre-dates the emplacement of these rocks. These systematic in timing of plutonism and possible generation of metamorphically derived-auriferous fluids within the Archean may be related to tectonic setting. Generation of tonalitic to trondhjemitic magmas during the Archean has been related to both Archean continental rift (Thompson, 1989a,b) and accretionary

(Martin, 1986, 1987) related tectonic settings. Both models recognize the existence of significantly higher geothermal gradients during the Archean (25 to 40°C/km) than are present today (less than 10°C/km).

The metamorphic regimes displayed by the supracrustal package in the Ulu Claims area is one of high temperature-low pressure (Henderson et al., 1993). The formation of terranes displaying metamorphism of this type has been linked to continental rift environments (Thompson, 1989a,b: Wickham and Oxburgh, 1985). Petrogenetic models developed for these terranes (Thompson, 1989a,b) explain the relationships observed between the timing of the internal versus the external granitoid suites and the metamorphism observed within the Ulu Claims. In this model, tonalitic magmas are generated by the melting of basement or lower portions of a volcanic pile at deep crustal levels after previously thinned crust is affected by significant homogeneous shortening. It is plausible that within such a setting, generation of a metamorphic fluid would occur prior to partial melting, as a result of dehydration/devolatization at lower pressures and telescoping of the isotherms (Groves et al., 1987). In such a scenario any mineralization formed as a result of interaction these fluids (i.e, Type II fluids) with crust at higher structural levels could be cross-cut by trondhjemitic intrusions formed by subsequent melting at depth. Mineralization and sodic intrusives may display a strong spatial association because the fluid and magmas could potentially exploit the same zones of crustal weakness during their ascent through the crust. Following crustal thickening and generation of tonalite-trondhjemite melts as discussed above, crustal exhumation after thickening results in the rising of medium-T isotherms. This initiates partial melting of wet pelitic rocks deep within the supracrustal pile while at the same time maximum metamorphic grade is attained within pelitic rocks above the zone of melting. The S-type melts (i.e. external granitoids) then rise diapirically to higher crustal levels and transect metamorphic isograds. Type III mineralized veins are potentially formed at this time through the interaction of the cooling pluton and the incursion of surface waters. Formation of Type III veins occurs within the same rocks as the previously formed Type II veins, which are now at a higher structural level relative to the surface.

The one questionable aspect of the applicability of this model is the apparent overprinting of peak metamorphic minerals within mafic volcanics by Type II mineralization. This discrepancy must be considered in terms of both the initial metamorphic devolatization at the time of Type II mineralization, and the predicted timing of peak metamorphic minerals observed within pelitic rocks. The occurrence of post-peak metamorphic gold mineralization within Archean greenstones continues to be one of the major drawbacks of metamorphic devolatilization models, as the maximum generation of fluids would be expected to coincide with peak metamorphism (Groves et al., 1987, Mueller, 1987). Kerrich (1991) suggests that within regions of crustal thickening, peak metamorphism at depth will postdate metamorphism within the brittle-ductile zone by up to 40Ma, which would solve the apparent discrepancy of metamorphic fluids at depth overprinting peak metamorphic assemblages at higher crustal levels. This would necessitate that peak metamorphism within the Ulu mafic volcanics occurred during the initial crustal thickening event, and is not associated with the later rising of medium T isotherms during exhumation. The major ramification of such a scenario is that the cordierite and andalusite porphryroblastisis (Henderson et al., 1993) associated with the later high T event would have had to occurred only within aluminum-rich, pelitic units and have had negligible effect on Type II alteration mineral assemblages.

In the model of Martin (1986, 1987), subduction of oceanic crust in Archean thermal regimes resulted in the partial melting of mafic volcanic rocks within the subducted slab, and the generation of tonalitic and trondhjemitic magmas prior to dehydration of the slab. Within modern accretionary settings, the lower geothermal gradient results in dehydration of the subducted slab prior to partial melting, with the fluids rising to the overlying mantle wedge and inducing partial melting, generating the calc-alkaline magmatism observed at modern convergent plate boundaries (Martin, 1986, 1987). Such a model successfully explains the presence of voluminous tonalite-trondhjemite plutons within the Archean, and explains the systematic shift in REE between Archean and modern plutons associated with accretionary boundaries, as a result of differences in magma sources. If dehydration/devolatization of the subducted slab in the Archean occurred after the formation of tonalite-trondhjemitic melts, the fluids generated could then have mineralized the previously emplaced plutons. Such differences in tectonic setting may be used to explain the presence of voluminous tonalitic plutons hosting gold mineralization within Archean terranes in which accretionary processes have been identified, (i.e., Superior Province) and those possibly hosted in rift environments in which tonalites-trondhjemites are volumetrically insignificant and occur later than, but are intimately associated with auriferous mineralization (i.e. Ulu Claims).

Further support for a rift type tectonic setting for the Ulu area can be made by comparison of the Type II and Type III mineralization within the crustal continuum model (Groves, 1993; Colvine et al., 1988b) for Archean lode gold deposits. In this model, deeply sourced ore-forming fluids generated in Archean convergent plate margins ascend towards the surface along huge crustal scale hydrothermal systems, resulting in a vertical zonation of gold deposits hosted in deep granulites to shallow sub-greenschist rocks. The deposits at granulite to greenschist facies are characterized by consistent oxygen isotope systematics of vein quartz, indicative of a uniform fluid reservoir, while those hosted in sub-greenschist facies rocks often display $\delta^{18}O$ depletion, which implies the mixing of deeply sourced fluids with low $\delta^{18}O$ surface waters (Groves, 1993; Ho et al, 1992).

A similar depletion of $\delta^{18}O$ in the calculated isotopic composition of fluids associated with Type III mineralization on the Ulu Claims is observed. These veins however, are hosted within amphibolite grade rocks and occur at the same crustal level as the Type II veins whose geochemical and isotopic characteristics suggest emplacement at much higher P and T from a homogeneous deeply sourced fluid. These relationships are consistent with the interpretation that emplacement of Type III veins post-dated Type II mineralization, and occurred at significantly higher crustal levels. Thus the crustal continuum model (Groves, 1993) proposed for Archean convergent plate boundaries is not applicable to the Ulu Claims mineralization.

IMPLICATIONS AND RECOMMENDATIONS FOR EXPLORATION

Although the results of this study are ambiguous regarding the genesis of the gold mineralization within the Ulu Claims, they may be used to formulate strategies for gold exploration within the High Lake and analogous greenstone belts.

The application of the concepts to be presented here are contingent upon the identification of greenstone belts which display temporal and petrogenetic characteristics (principally the existence of a deformed volcanic pile intruded by syn-kinematic trondhjemitic rocks, followed by emplacement of extensive post-kinematic S-type plutons) consistent with those of the High Lake Belt in the Ulu Claims area. This which would suggest that these areas evolved in a similar tectonic setting. Henderson et al. (1993) state that relationships between granitic plutons and deformation within the High Lake Belt are similar to those seen in other belts (i.e. Hood River) in the north-central Slave province, which suggests that these areas would have the highest potential for hosting similar mineralization.

The potential occurrence of mineralized systems analogous to the Ulu Type II veins, may be investigated by identifying dilatencies associated with deformational events, which would be equivalent to the major D_2 compression in the High Lake Belt. Identification of these zones may be expedited by the occurrence of high Na, LREE depleted intermediate intrusive rocks (i.e. analogous to Ulu internal granitoids) which may have utilized similar zones of crustal weakness as Type II mineralizing fluids.

Favorable structures hosted within a heterogeneous package of supracrustal rocks should be the highest priority targets because of 1) the enhanced potential of dilatency due to rheological contrasts, 2) the apparent necessity of a high iron lithology (basic volcanic) as a geochemical trap, and 3) the possible dependance of mass transfer between volcanics and sediments, in the formation of economically interesting mineralized zones. Within extensive areas of sediments, the occurrence of iron formation within suitable structures may form an alternative exploration target. Broad zones of potassium and boron metasomatism and carbonatization within these areas may be indicative of mineralization which is not exposed on the surface.

Although Type III mineralization has been of little economic interest in the past due to the small size and erratic grades exhibited by these veins, further exploration is warranted, because of the potential extent of these vein systems implicated by this study. The association of the Type III veins with late granitic plutons raises several questions: 1) are these plutons representative of the bounding batholiths as a whole, or do they represent distinct, highly evolved portions of these plutons, and 2) if they are a discreet phase, what is their distribution. The boundaries of these plutons, whether adjacent to supracrustal rocks or older granitic rocks should be examined for evidence of hydrothermal activity, as the apparent independence of gold deposition upon host rock composition would not preclude the development of mineralized fracture zones within adjacent plutonic rocks

Finally, the geochemical associations of Au with As in Type II veins, and the association of Au with Bi in Type III veins may be used to discriminate between the two mineralization types. Such a discrimination may be useful in planning follow up investigations of auriferous samples obtained from reconnaissance scale sampling.

FURTHER STUDIES

It is apparent from the results of this study that the complexity and enigmas presented by the genesis of the Ulu auriferous deposits requires further investigation in order to fully understand the processes operating in the formation of Archean lode gold deposits.

The investigation of the composition and thermometric character of quartz hosted fluid inclusions of Type III mineralization would be of great benefit in understanding the conditions of vein formation. Such a study would yield information on the temperatures of entrapment, as well as fluid compositions and densities, which would be useful in determining pressures (i.e. depth of mineralization) as well as confirming or refuting speculations as to the salinity of these fluids. A fluid inclusion study would also aid in resolving the range in fluid inclusion δD compositions obtained in this study, as the presence of low temperature post-mineralization inclusions would be apparent, as would the presence of CH_4 within inclusions associated with mineralization. A fluid inclusion study of Type II mineralization would be of less use due to the recrystallization of quartz within these veins. Although changes in volume of the inclusions through recrystallization would prevent the collection of accurate P-T data, empirical information regarding fluid compositions could be obtained. In addition, the nature of the fluids present within the secondary inclusions could be investigated primarily regarding their possible effect upon the hydrogen isotope results obtained from these veins.

Mineral chemistry of alteration phases within Type II mineralization would be useful in demonstrating the sulphidation within these deposits, and would also provide information regarding the physiochemical conditions during mineralization. Similarly, a sulphur isotope study of sulphide minerals would allow the sources of sulphur to be investigated, and the oxygen and sulphur fugacities to be determined, which would be useful in the further interpretation of the carbon isotopes within Type II mineralization.

Further radiogenic isotope studies both in the form of U-Pb dating of intrusives and mineralization (titanite), and Pb-Pb, Rb-Sr and Sm-Nd systematics of host rocks, intrusives and mineralization, would prove useful in resolving temporal relationships, and providing further insight into the petrogenesis and the metamorphism of the host rocks and intrusive phases, and the sources of mineralizing fluids and solutes.

A field mapping and geochemical study of the external granitoids surrounding the High Lake Belt would be useful to investigate the chemical evolution of this extensive batholith, and the identification of possible late phases which may have played a significant role in the presence of Type III mineralized veins.

REFERENCES CITED

Albuquerque, C.A.R., 1977. Geochemistry of the tonalitic and granitic rocks of the Nova Scotia southern plutons. Geochimica et Cosmochimica Acta, v. 41, p.1-13.

Allison, I. and Kerrich, R., 1979. History of deformation and fluid transport in shear zones at Yellowknife: in Morton R.D., editor, Proceedings of the Gold Workshop, Yellowknife, Northwest Territories, p. 201-222.

Anderson, R. and Bryan D., 1980. Report on geological and geophysical surveys and diamond drilling, summer 1980, James River project 1955, District of Mackenzie, N.W.T. Internal company assessment report, Noranda Exploration Company Ltd., 40p.

Arnold, R.G., 1962. Equilibrium relations between pyrrhotite and pyrite from 325° to 743°C. Economic Geology, v. 57, p. 72-90.

Arth and Hanson, 1972. Quartz diorites derived by partial melting of eclogite or amphibolite at mantle depths. Contributions to Mineralogy and Petrology, v. 37, p. 161-174.

Barager, W.R.A., 1966. Geochemistry of the Yellowknife volcanic rocks. Canadian Journal of Earth Sciences, v. 3, p. 668-702.

Barager , W.R.A. and Goodwin, A.M., 1969. Andesites and Archean volcanism of the Canadian Shield: in McBirney, A.R., editor, Proceedings of the Andesite Conference, Oregon Department of Mines Bulletin, v. 65, p. 121-142.

Barker, A.J., 1990. Introduction to Metamorphic Textures and Microstructures. Blackie and Son Ltd, New York.

Barker, F., 1979. Trondhjemites: definition, environment and hypothesis of origin: In Barker, F., editor, Trondhjemites, Dacites and Related Rocks, Elsevier, Amsterdam, p.1-12.

Barker, F.,and Arth, J.G., 1976. Generation of trondjhemitic-tonalitic liquids and Archean bimodal trondjhemite-basalt suites. Geology, v. 4, p. 596-600.

Barley, M.E. and Groves, D.I., 1990. Deciphering the tectonic evolution of greenstone belts. The importance of contrasting histories to the distribution of mineralization in the Yilgarn Craton, Western Australia. Precambrian Research v. 46: p. 3-20.

Barton, P.B., Jr. and Skinner B.J., 1979. Sulphide mineral stabilities: in Barnes, H.B., editor, Geochemistry of Hydrothermal Ore Deposits, John Wiley and Sons, New York, p. 278-390.

Beane, R.E. and Titley, S.R., 1981. Porphyry copper deposits Part II. Hydrothermal alteration and mineralization: in Skinner, B.J., editor, Seventy-Fifth Anniversary Volume 1905-1980, Economic Geology, p. 235-269.

Beard, J.S. and Lofgren, G.E., 1991. Dehydration melting and water saturated melting of basaltic and andesitic greenstones and amphibolites at 1, 3 and 6.9 kb. Journal of Petrology, v. 32, part 2, p. 365-401.

Best, M.G., 1982. Igneous and Metamorphic Petrology. W.H. Freeman and Company, New York, 630p.

Blunt, J. and McConnell, G.W. 1968. Preliminary report and recommendations on the Hood River Project, Concessions 76-L-4, 76-L-10, 76-L-5. Internal company assessment report, Norman H. Ursel and Associates, 39p.

Bowring, S.A., Williams, I.S., and Compston, W., 1989. 3.96 Ga gneisses from the Slave Province, Northwest Territories, Canada. Geology, v. 17, p. 971-975.

Boyle, R.W., 1979. The geochemistry of gold and its deposits. Geological Survey of Canada Bulletin, v. 280, 584p.

Boyle, R.W., 1961. The geology, geochemistry and origin of the gold deposits of the Yellowknife district, Geological Survey of Canada Bulletin, v. 310, 193p.

Boynton, W.V., 1983. Cosmochemistry of the rare earth elements: meteorite studies: in Henderson, P., editor, Rare Earth Element Geochemistry, Elsevier, p. 63-114.

Brown, I.,J., 1985. Gold-bismuth-copper skarn mineralization in the Marn Skarn, Yukon. Unpublished MSc. Thesis, University of Alberta, 143p.

Burrows, D.R., Woods, P.C. and Spooner, E.T.C., 1986. Carbon isotope evidence for a magmatic origin for Archean gold-quartz vein ore deposits. Nature, v. 321, p. 851-854.

Burwash, R.A., Baadsgaard, H., Cambell, F.A., Cumming, G.L., and Folinsbee, R.E. 1968. Potassium-argon dates of diabase dyke systems, District of Mackenzie, N.W.T. Canadian Miming and Metallurgical Bulletin, vol LXVI, p. 303-307.

Byrne, N.J., 1971. Report on the 1970 mineral exploration program, Hood River area, District of MacKenzie, N.W.T. Internal company assessment report, Borealis Exploration Ltd. 38p.

Cabri, L.J., Chyrssoulis, S.L., Villiers, J.P.R., LaFlamme, J.,H.,G. and Boseck, P.R., 1989. The nature of 'invisible' gold in arsenopyrite. The Canadian Mineralogist. v. 27, p. 353-362.

Callan, N.J. and Spooner, E.T.C., 1989. Archean Au quartz vein mineralization hosted in a tonalite-trondhjemite terrane, Renabie Mine area, Wawa, Ontario, Canada: in Keays, R.R., Ramsay, W.R.H. and Groves, D.I., editors, The Geology of Gold deposits: The Perspective in 1988, Economic Geology Monograph 6, p. 9-18.

Cameron, E.M., 1988. Archean gold: relation to granulite formation and redox zoning in the crust, Geology, v. 16, p. 109-112.

Cameron, E.M. and Hattori, K., 1987. Archean gold mineralization and oxidized hydrothermal fluids. Economic Geology, v. 82, p. 1177-1191.

Cassidy, K.F., Barley, M.E., Groves, D.I., Perring, C.S. and Hallberg, J.A., 1991. An overview of the nature, distribution and inferred tectonic setting of granitoids in the late Archean Norseman-Wiluna Belt. Precambrian Research. v. 51, p. 51-83.

Chace, F.M., 1949. Origin of the Bendigo saddle reefs with comment on the formation of ribbon quartz. Economic Geology, v. 44, p. 561-597.

Clayton, R.N., and Mayeda, T.K., 1963. The use of bromine pentafluoride in the extraction of oxygen from oxides and silicates for isotope analysis. Geochimica et Cosmochimica Acta, v. 27, p. 43-52.

Coleman, M.L., Shepard, T.J., Durham, J.J., Rouse, J.E., and Moore, G.R., 1982. Reduction of water with zinc for isotopic analysis. Analytical Chemistry, v. 54, p. 993-995.

Colvine, A.C., 1988a. An empirical model for the formation of Archean gold deposits: products of final cratonization of the Superior province, Canada: in The Geology of Gold Deposits: The Perspective in 1988, Economic Geology Monograph 6, p. 37-54.

Colvine, A.C., Fyon, J.A., Heather, K.B. Marmont, S., Smith, P.M., and Troop, D.G. 1988b, Archean lode gold deposits in Ontario. Ontario Geological Survey Miscellaneous Paper 139, 210p.

Colvine, A.C., Andrews, A.J., Cherry, M.E., Dorocher, M.E., Fyon, A.J., Lavigne, M.J., Macdonald, A.J., Marmont, S., Poulsen, K.H., Springer, J.S. and Troop, D.G., 1984. An integrated model for the origin of Archean Lode Gold deposits. Ontario Geological Survey, Open File Report 5524, 98p..

Condie, K.C., 1976. Trace element geochemistry of Archean greenstone belts. Earth Science Reviews, v. 12, p. 393-417.

Condie, K.C., 1981. Archean greenstone belts. Elsevier, Amsterdam.

Cox, K.G., Bell, J.D. and Pankhurst, R.J., 1979. The Interpretation of Igneous Rocks, George Allen and Unwin, London, 450p.

Cox, S.F. and Etheridge, M.A., 1983. Crack-seal fibre growth mechanisms and their significance in the developement of oriented layer silicate microstructure. Tectonophysics, v. 92, p. 147-170.

Craig, H., 1961. Isotopic variations in meteroic waters. Science, v. 133, p. 1702-1703.

Craig, J. R. and Scott, S.D., 1976. Sulphide phase equilibria: in Ribbe, P.H., editor, Sulphide Mineralogy, Reviews in Mineralogy, Volume 1, Mineralogical Society of America, p. CS-1 - CS-104.

Cunningham, M.P. and Lambert, R.St.J., 1989. Petrochemistry of of the Yellowknife volcanic suite at Yellowknife, N.W.T. Canadian Journal of Earth Science, v. 26, p. 1630-1646.

Dagger, G.W., 1972. Genesis of the Mount Pleasant tungsten-molybdenum-bismuth deposit, New Brunswick, Canada. Transactions (Section B) of the Institute of Mining and Metallurgy, v. 81, p.73-102.

Davis, W.J., King, J., Fryer, B.J. and van Breemen, O., 1990. Petrogenesis and evolution of Late Archean granitoids in the central Slave Province: implications for tectonic developement of the Slave Province, Canada. Third International Archean Symposium, Exteneded Abstracts, p. 185-188.

Drury, S.A., 1977. Structures induced by granite diapirs in the Archean greenstone belt at Yellowknife, NWT: implications for Archean geotectonics. Journal of Geology, v. 85, p. 345-358.

Drury, S.A., 1979. Rare-earth and other trace element data bearing on the origin of Archean granitic rocks from Yellowknife N.W.T. Canadian Journal of Earth Science, v. 16, p. 809-815.

Easton, R.M., 1985. The nature and significance of pre-Yellowknife Supergroup rocks in the Point Lake area, Slave Structural Province, Canada. : in Ayres, L.D., Thurston P.C., Card K.D., and Weber W., editors, Evolution of Archean Supracrustal Sequences. Geological Society of Canada Special Paper 28, p. 153-167.

English, P.J., 1981. Gold quartz veins in metasediments of the Yellowknife supergroup, Northwest Territories: a fluid inclusion study. Unpublished M.Sc. Thesis, University of Alberta,109p.

Einaudi, M.T., Meinert, L.D., and Newberry, R.J., 1981. Skarn deposits: in Skinner, B.J., editor, Seventy-Fifth Anniversary Volume 1905-1980, Economic Geology, p. 317-391.

Finlow-Bates, T. and Stumpfl. E.F., 1981. The behavior of the so-called immobile elements in hydrothermally altered rocks associated with volcanogenic submarine-exhalative ore deposits. Mineralium Deposita, v. 16, p. 319-328.

Flood, E., Cowley, P., Muntanion, H. and Kleespies, P., 1991. Ulu Claims: 1990 Geological, Geochemical, Geophysical and Drilling Report. Internal Company Report, BHP Utah Mines Ltd., Vancouver B.C., 88p.

Folinsbee, R.E., 1955. Archean monazite in beach concentrates, Yellowknife Geologic Province, Northwest Territories, Canada. Transactions of the Royal Society of Canada, v. XLIX, Series III, p. 7-24.

Folinsbee, R.E., Baadsgaard, H., Cumming, G.L., and Grren, D.C., 1968. A very ancient island arc. Geophysical Monograph, No. 12, p. 441-448.

Frape, S.K., Fritz, P., and McNutt, R.H., 1984. Water-rock interaction and chemistry of groundwaters from the Canadian Shield. Geochim Cosmochimics Acta, v. 48, p. 1617-1627.

Fraser, J.A., 1964. Geological notes on the northeastern district of Mackenzie, Northwest Territories. Geological Survey of Canada Paper 63-40, 20p.

Frith, R.A., Loveridge, W.D. and Van Breemen, O., 1986. U-Pb ages on zircons from basement granitoids of the western Slave Structural Province, northwestern Canadian Shield. Current Research, Part A, Geological Survey of Canada, Paper 86-1A, p.113-119.

Fyon, J.A., Swarcz, H.P., Crocket, J.H., and Knyf, M., 1982. Gold exploration potential using oxygen, carbon, and hydrogen stable isotope systematics of carbonatized rock and quartz veins, Timmins area. Ontario Geological Survey, Miscellaneous Paper 103, p.59-64.

Fyon, J.A., Crocket, J.H. and Scwarcz, H.P., 1983. Application of stable isotope studies to gold metallogeny in the Timmins-Porcupine camp. Ontario Geological Survey, Open File Report 5464, 182p.

Fyon, J.A., Scwarcz, H.P. and Crocket, J.H., 1984, Carbonation and gold mineralization in the Timmins area Abitibi greenstone belt; genetic links with Archean mantle $C0_2$ degassing and lower crust granulitization. Geological Association of Canada Program with Abstracts, v. 9, p. 65.

Fyson, W.K., 1982. Complex evolution of folds and cleavages in Archean rocks, Yellowknife, N.W.T. Canadian Journal of Earth Sciences, v. 19, p. 878-893.

Fyson, W.K. and Helmstaedt, H., 1988. Structural patterns and tectonic evolution of supracrustal domains in the Archean Slave Province, Canada. Canadian Journal Of Earth Sciences, v. 25, p. 301-315.

Fyson, W.K., 1990. Structural developement of angular volcanic belts in the Archean Slave Province. Canadian Journal of Earth Science, v. 27, p. 403-413.

Glikson. A.Y., and Jahn, B.M., 1985. REE and LIL elements, Eastern Kaapvaal Shield, South Africa: evidence of crustal evolution by 3-stage melting: in Ayres, L.C., Thurston, P.C., Card, K.D. and Weber, W.,editors, Evolution of Archean Supracrustal Sequences. Geological Society of Canada Special Paper 28, p. 303-324.

Golding, S.D. and Wilson, A.F., 1987. Oxygen and hydrogen isotope relations in Archean gold deposits of the Eastern Goldfields Province, Western Australia: constraints on the source of Archean gold bearing fluids: in Ho, S.E., and Groves, D.I., editors, Recent Advances in Understanding Archean Gold Deposits. Geology Department and University Extension, The University of Western Australia Publication 11, p. 203-213.

Golding, S.D., McNaughton, N.J., Barley, M.E., Groves, D.I., Ho, S.E., Rock N.M.S. and Turner, J.V., 1989. Archean carbon and oxygen reservoirs: the significance for fluid sources and circulation paths for Archean mesothermal gold deposits of the Norseman-Wiluna Belt, Western Australia: in Keays, R.R., Ramsay, W.R.H., and Groves, D.I., editors, The Geology of Gold Deposits: the Perspective in 1988. Economic Geology Monograph 6. p. 376-388.

Grambling, J.A., 1981. Pressures and temperatures in Precambrian metamorphic rocks. Earth and Planetary Science Letters, v. 43, p. 63-68.

Grant, J.A., 1986. The Isocon diagram-a simple solution to Gresens' equation for metasomatic alteration. Economic Geology, v. 81, p. 1976-1982.

Gresens, R.L., 1967. Composition-volume relationships of metasomatism. Chemical Geology, v. 2, p. 47-55.

Groves, D.I., Phillips, N., Ho, S.E., Houstoun, S.M. and Standing, C.A., 1987. Craton-scale distribution of Archean greenstone gold deposits: Predictave capacity of the metamorphic model. Economic Geology, v. 82, p. 2045-2058.

Groves, D.I. and Phillips, G.N., 1987. The genesis and tectonic control on Archean gold deposits of the western Australian shield - a metamorphic replacement model. Ore Geology Reviews, v. 2, p. 287-322.

Groves, D.I., 1993. The crustal continuum model for late Archean lode gold deposits of the Yilgarn Block, Western Australia. Mineralium Deposita, v. 28, p. 366-374.

Hall, A., 1987. Igneous Petrology. Longman Scientific and Technical, England, 573p.

Hattori, K., 1987. Magnetic felsic intrusions associated with Canadian Archean gold deposits. Geology, v. 15, p. 1107-1111.

Hanson, G.N., 1980. Rare earth elements in petrogenetic studies of igneous systems. Annual Reviews of Earth Planet Science, v. 8, p. 371-406.

Hanson, G.N., 1978. The application of trace elements to the petrogenesis of igneous rocks of granitic compostion. Earth and Planetary Science Letters, v. 38., p. 26-43.

Helmstaedt, H., King, J., Goodwin, J.A. and Patterson, J.G., 1981. Geology of the southwest corner of the Yellowknife greenstone belt: in Morton R.D., editor, Proceedings of the Gold Workshop, Yellowknife, Northwest Territories, p. 223-239.

Helmstaedt, H., Padgham, W. A. and Brophy, J.A., 1986. Multiple dykes in the Lower Kam Group, Yellowknife greenstone belt-evidence for Archean seafloor spreading? Geology, v. 14, p.562-566.

Helmstaedt, H. 1992. Structural Observations on Flood and Flood South zones Ulu Project, High Lake Belt, N.W.T. Internal Report, BHP-Utah Mines Ltd. 9p.

Henderson, J.B., 1970. Stratigraphy of the Yellowknife Supergroup, Yellowknife Bay-Prosperous Lake area, District of Mackenzie. Geological Survey of Canada Paper 70-26: 12p.

Henderson, J.B., 1975a. Archean stromatolites in the Northern Slave Province, Northwest Territories, Canada. Canadian Journal of Earth Sciences, v.12, p. 1619-1630.

Henderson, J.B., 1975b. Sedimentology of the Yellowknife Supergroup at Yellowknife, District of Mackenzie. Geological Survey of Canada, Bulletin 246, 62p.

Henderson, J.B. 1981. Archean basin evolution in the Slave Province, Canada: in Kroner, A., editor, Precambrian Plate Tectonics. Elsevier, Amsterdam, p. 213-235.

Henderson, J.B., 1985. Geology of the Yellowknife - Hearne Lake area. District of Mackenzie: a segment across a Archean basin. Geological Survey of Canada, Memoir 414.

Henderson, J.B., Loveridge, W.D. and Sullivan, R.W., 1982. A U-Pb study of zircon from granitic basement beneath the Yellowknife Supergroup, Point Lake. District Research, Part C, Geological Survey of Canada, Paper 82-1C, p.173-178.

Henderson J.R., Henderson, M.N, Kerswill, J.A., Arias, Z., Lemkow, D., Wright, T.O. and Rice, R., 1993. Geology and mineral occurences of the southern part of High Lake greenstone belt, Slave Province, Northwest Territories. Current Research, part C, Geological Survey of Canada, Paper 93-1C, p. 125-136.

Ho, S.E., Groves, D.I., McNaughton, N.J. and Mikucki, E.J., 1992. The source of ore fluids and solutes in Archean lode gold deposits of Western Australia. Journal of Volcanology and Geothermal Research, v. 50, p. 173-196.

Hodgson, C.J., 1989. The structure of shear related ,vein type gold deposits: a review. Ore Geology Reviews, v. 4, p. 231-273.

Hoefs, J., 1987. Stable Isotope Geochemistry. Springer-Verlag, New York, 236 p.

Hoffman, P.F., 1986. Crustal Accretion in a 2.7-2.5 Ga "granite-greenstone" terrane, Slave Province, N.W.T.: a prograding trench-arc system? Geological Association of Canada, Program with Abstracts, v. 11, p. 82.

Hoffman, P.F., 1989. Precambrian geology and tectonic history of North America: in A.W. Bally and A.R. Palmer, editors, The Geology of North America-An overview. Geological Society of America, Boulder, Colorado, p. 497-512.

Hutchinson, R.W., 1976. Lode gold deposits: the case for volcanogenic derivation. Proceedings Volume, Pacific Northwest Mining and Metals Conference, Portland Oregon, 1975, Oregon Department Geology Minerals Industry, p. 64-105.

Hynes, A., 1980. Carbonitization and mobility of Ti, Y and Zr in Ascot Formation metabasalts, SE Quebec. Contributions to Mineralogy and Petrology, v. 75, p. 79-87.

Isachen, C.E., Bowring, S.A. and Padgham, W.A., 1991. Geology and U-Pb geochronology of The Dwyer Formation and underlying gneisses in the southern Slave Province: a basement-cover sequence beneath the Yellowknife Greenstone Belt? Geological Association of Canada, Program with Abstracts, v. 16, p. 59.

Jackson, V.A., Kerr, D., Bell, R., Howson, S. and Bailey,G., 1986. Preliminary geology of the Hood River Area, NTS L/10,15,16; EGS 1986-14, N.W.T. Geology Division, Department of Indian and Northern Affairs, Canada.

Jackson, V.A., 1991. Preliminary geological compilation of Kathawachaga Lake area NTS 76L. EGS 1991-3, N.W.T. Geology Division, Department of Indian and Northern Affairs, Canada.

Jenner, G.A., Fryer, B.J. and McLennan, S.M., 1981. Geochemistry of the Archean Yellowknife Supergroup. Geochemica et Cosmochimica Acta. v. 45, p. 1111-1129.

Johnston, A.D. and Wyllie, P.J., 1988. Constraints on the origin of Archean trondhjemites based on phase relationships of Nûk gneiss with H_20 at 15 kbar. Contributions to Mineralogy and Petrology, v. 100, p. 35-46.

Johnson, W. and Robinson, P., 1977. Geological and geophysical surveys Dean and Spot Groups, NTS-L-15, 110° 55'W, 66° 46'N, for Long Lac Mineral Exploration. Internal Company Assesssment report, 17p.

Kay, A. and Strong, D.F., 1983. Geologic and fluid controls on As-Sb-Au mineralization in the Moretons Harbour Area, Newfoundland. Economic Geology, v. 78, p. 1590-1604.

Kelly, W.C., and Tourneaure, F.S., 1970. Mineralogy, paragenesis and geothermometry of the tin and tungsten deposits of the Eastern Andes, Bolivia. Economic Geology, v. 65, p. 609.

Kerrich, R., 1983. Geochemistry of gold deposits in the Abitibi greenstone belt. Canadian Institute of Mining and Metallurgy, Special Volume 27, 75p.

Kerrich, R. and Watson, G.P., 1984. The Macassa Mine Archean lode gold deposit, Kirkland Lake, Ontario; geology, patterns of alteration and hydrothermal regimes. Economic Geology, v. 79, p. 1104-1130.

Kerrich, R., 1987. The stable isotope geochemistry of Au-Ag vein deposits in metamorphic rocks: in Kyser, T.K., editor, Short Course in Stable Isotope Geochemistry of Low Temperature Fluids, volume 13, Mineralogical Association of Canada, p. 287-336.

Kerrich, R. and Fyfe, W.S., 1988. The formation of gold deposits with particular reference to Archean greenstone belts and Yellowknife: II. Source of hydrothermal fluids, alteration patterns and genetic models. Contributions to the Geology of the Northwest Territories v. 3, p. 63-96.

Kerrich, R. 1989. Shear zone hosted mesothermal gold deposits; a review of geochemical evidence on the sources of fluids and solutes: in Bursnall, J.T. editor, Mineralization and Shear Zones; Geological Association of Canada Short Course Notes, v. 6.

Kerrich, R., 1991. Mesothermal gold deposits: in Robert F., Sheahan, P.A. and Green, S.B., editors, Greenstone Gold and Crustal Evolution, NUNA Conference Volume, Geological Association of Canada, 252p.

Keith, J.D., van Middelaar, W., Clark, A.H., and Hodgson, C. J., 19??. Granitoid textures, compositions, and volatile fugacities associated with the formation of tungsten dominated skarn deposits; in ?

King, R.W. and Kerrich, R., 1987. Fluorapatite fenitization and gold enrichment in sheeted trondhjemites within the Destor-Porcupine fault zone, Taylor Township. Ontario. Canadian Journal of Earth Science, V. 24, p. 479-502.

Klement, W., Jayarman, A. Jr. and Kennedy, G.C., 1962. Phase diagrams of arsenic, antimony, and bismuth at pressures up to 70 kbars. Physical Review, v. 131, p. 632-637.

Klein, J. 1976. Geophysical Survey, Indet claims, Hood River area, N.W.T. Internal company assessment report, Cominco Ltd. 12p.

Koh,Y., Choi, S. So, C., Choi, S., and Uchida, E., 1992. Application of arsenopyrite geothermometry and sphalerite geobarmetery to the Taebaek Pb-Zn (-Ag) deposit at Yeonhwa I mine, Republic of Korea. Mineralium Deposita, v. 27 p. 58-65.

Kretschmar, U., and Scott, S.D., 1976. Phase relations involving arsenopyrite in the system Fe-As-S and their application. Canadian Mineralogist, v. 14, p. 364-386.

Kuryliw, C.J., 1988. Some observations of gold zoning. The Northern Miner Magazine, September, 1988, p. 62-66.

Kusky, T.M., 1989. Accretion of the Archean Slave Province. Geology, v. 17, p. 63-67.

Lambert, M.B., 1976. The Back River Volcanic Complex, District of Mackenzie. Geological Survey of Canada Paper 76-1A, p. 363-367.

Lambert, M.B., 1978. The Back River Volcanic Complex - a cauldron subsidence structure of Archean age. Current Research, Part A, Geological Survey of Canada Paper 78-1A, p. 153-157.

Lambert, M.B., Burbidge, G., Jefferson, C.W., Beaumont-Smith, C. and Lustwerk, R., 1990. Stratigraphy, facies and structure in volcanic and sedimentary rocks of the Archean Back River volcanic complex, N.W.T. Current research, Part C, Geological Survey of Canada, Paper 90-1C, p. 151-165.

Le Bas, M.J., and Streckeisen, A.L., 1991. The IUGS systematics of igneous rocks. Journal of the Geological Society, London, v. 148, p. 825-833.

Lhotka, P.G., 1988. Geology and geochemistry of gold bearing iron formations in the Contwoyto Lake-Point Lake region, Northwest Territories, Canada. PhD. thesis. The University of Alberta.

Lhotka, P.G. and Nesbitt, B.E., 1989. Geology of unmineralized and gold bearing iron formation, Contwoyto Lake - Point Lake region, Northwest Territories, Canada, Canadian Journal of Earth Science v. 26, p. 46-64.

Lowell, G.R., and Gasparrini, C., 1982. Composition of arsenopyrite fron topaz-greisen veins in Southeastern Missouri. Mineralium Deposita, v. 17, p. 229-238.

Ludden, J.N., and Gelinas, L., 1984. Trace element mobility in alteration zones associated with Archean lode gold deposits. Economic Geology, v. 79, p. 1131-1141.

MacLean, W.H. and Kranidiotis, P., 1987. Immobile elements as monitors of mass transfer in hydrothermal Alteration: Phelps Dodge Massive Sulphide Deposit, Matagami Quebec. Economic Geology, v. 82, p. 951-962.

MacLean, W.H., 1990. Mass change calculations in altered rock series. Mineralium Deposita, v. 25, p. 44-49.

Martin, H., 1987. Petrogenesis of Archean Trondhjemites, tonalites, and granodiorites from Eastern Finland: major and trace element geochemistry. Journal of Petrology, v. 28, p. 921-953.

Martin, H., 1983. Major and trace element geochemistry and crustal evolution of Archean granodioritic rocks from eastern Finland. Precambrian Research, v. 21, p. 159-180.

Mason, B.H. and Moore, C.B., 1982. The Principles of Geochemistry. John Wiley and Sons, Toronto, 344p.

Matsuhisa, Y, Goldsmith, J.R. and Clayton, R.N., 1979. Oxygen isotope fractionation in thge system quartz-albite-anorthite-water. Geochimica et Cosmochimica Acta, v. 42, p. 173-182.

McCrea, J.M., 1950. On the isotopic chemistry of carbonates and a paleotemperature scale. Journal of Chemical Physics, v. 18, p. 849-857.

McGlynn, J.C. and Henderson, J.B., 1972. The Slave Province: in Price, R.A. and Douglas R.J.W., editors, Variations in Tectonic Styles in Canada: Geological Association of Canada, Special Paper 11, p. 506-526.

McKinstry, H.E. and Olhe, H.E. Jr., 1949. Ribbon structure in gold quartz veins. Economic Geology, v. 44, p. 87-109.

Meschede, M., 1986. A method of discriminating between different types of mid-ocean ridge basalts and continental tholeiites with the Nb-Zr-Y diagram. Chemical Geology, v. 56, p. 207-218.

Moritz, R.P., and Crocket, J.H., 1991. Hydrothermal wall-rock alteration and formation of the gold bearing quartz-fuchsite vein at the Dome Mine, Timmins Area, Ontario, Canada. Economic Geology, v. 86.

Mortenson, J.K., Thorpe, R.I., Padgham, W.A., King, J.E. and Davis, W.J., 1988. U-Pb zircon ages for felsic volcanism in the Slave Province, N.W.T. Radiogenic Age and Isotope Studies, Report 2, Geological Survey of Canada Paper 88-2, p. 85-95.

Mueller, A.G. and Groves, D.I., 1991. The classification of Western Australian greenstone hosted gold deposits according to wallrock alteration assemblages. Ore Geology Reviews, v. 6, p. 291-331.

Mueller, A. G., 1992. Petrogenesis of amphibole-biotite-calcite-plagioclase alteration and laminated gold-silver quartz veins in four Archean shear zones of the Norseman district, Western Australia. Canadian Journal of Earth Science, v. 29 p. 388-417.

Mullen, E.D., 1983. MnO/TiO2/P2O5: a minor element discriminant for basaltic rocks of oceanic environments and its implications for petrogenesis. Earth and Planetary Science Letters, v. 62, p. 53-62.

Myers, D., 1979. Geochemistry of the Con Mine, Yellowknife, N.W.T.; in Morton R.D., editor, Proceedings of the Gold Workshop, Yellowknife, Northwest Territories, p. 201-222.

O'Connor, J.T., 1965. A classification for quartz rich igneous rocks based on feldspar ratios. U.S. Geological Survey Professional Paper 525-B, p. 79-84.

Ojakangas, R.W., 1985. Review of Archean clastic sedimentation, Canadian Shield: major felsic volcanic contributions to turbidite and alluvial fan-fluvial facies association: in Ayres, L.D.,Thurston, P.C., Card, K.D. and Weber W., editors, Evolution of Archean Supracrustal Sequences. Geological Association of Canada Special Paper, 28, p. 23-47.

Ohmoto, H. and Rye, R.O., 1979. Isotopes of sulphur and carbon: in Barnes, H.B. editor, Geochemistry of Hydrothermal Ore Deposits, John Wiley and Sons, New York, p. 509-567.

O'Niel, J.R., Clayton, R.N. and Mayeda, T.K., 1969. Oxygen isotope fractionation in divalent metal carbonates, Journal of Chemistry and Physics, v. 51, p. 5547-5558.

Padgham, W.A. and Brophy, J.A., 1985. Gold deposits of the Northwest Territories; in Clark, L.A., editor, Gold in the Western Shield, CIMM Special Volume 38, p. 2-25.

Padgham, W.A., 1985. Observations and speculations on supracrustal successions in the Slave Structural Province. in Ayres L.D., Thurston, P.C., Card, K.D. and Weber, W., editors, Evolution of Archean Supracrustal Sequences. Geological Association of Canada Special Paper, 28, p. 133-151.

Padgham, W.A., 1992. Mineral deposits in the Slave Structural Province; lithological and tectonic setting. Precambrian Research, v. 58, p. 1-24.

Parrish, R.R., Roddick, J.C., Loveridge, W.D. and Sullivan, R.W., 1987. Uranium-lead techniques at the Geochronology Laboratory, Geological Survey of Canada. In Radiogenic age and isotope studies: report 1, Geological Survey of Canada, Paper 87-2, p. 3-7.

Pearce, J.A. and Cann, J.R., 1973. Tectonic setting of basic volcanic rocks determined using trace element analysis. Earth and Planetary Science Letters, v. 19, p. 290-300.

Pearce, J.A., 1975. Basalt geochemistry used to investigate post tectonic environment in Cypress, Tectonphysics, v. 25, p. 41-68.

Pearce, J.A. and Norry, M.J., 1979. Petrogenetic implications of Ti, Zr, Y and Nb variations in volcanic rocks. Contributions to Mineralogy and Petrology, v. 69, p. 33-47.

Pearce, J.A., 1989. Patterns of trace element behavior during crustal anatexis. Periodico Di Mineralogia, V. LVII, p.183.

Pearce, T.H., Gorman, B.E., and Birkett, T.C., 1977. The relationship between major element chemistry and tectonic environment of basic and intermediate volcanic rocks. Earth and Planetary Science Letters, v. 36, p. 121-132.

Peterson, E.U., 1991a. Mineralogy of Ulu samples. Internal Company Report, BHP Minerals Canada Ltd, 22p.

Peterson, E.U., 1991b. Reconnaissance arsenopyrite thermometry at Ulu. Internal Company Report, BHP Minerals Canada Ltd, 21p.

Ramdohr, P., 1969. The Ore Minerals and Their Intergrowths. Pergamon Press, New York, 1174p.

Ramsay, J.G., 1980. The crack-seal mechanism of rock deformation. Nature, v. 284, p. 135-139.

Ransom, A.H. and Robb, M.E., 1986. The Salmita gold deposit, Courageous Lake, Northwest Territories; in Clark, L.A., editor, Gold in the Western Shield, CIMM Special Volume 38, p. 307-321.

Rapp, R.P., Watson, E.B. and Miller, C.F., 1991. Partial melting of amphibolite/eclogite and the origin of Archean trondhjemites and tonalites. Precambrian Research,. v. 51, p. 1-25.

Rice, R.J., Long, D.G.F., Fyson, W.K. and Roscoe, S.M., 1990. Sedimentological evaluation of three Archean metaquartzite and conglomerate-bearing sequences in the Slave Province, N.W.T. Current Research, Part 1A, Geological Survey of Canada Paper., 90-1A, p. 305-322.

Ridler, R.H., 1976. Stratigraphic keys to the gold metallogeny of the Abitibi Belt. Canadian Mining Journal, v. 97, p. 81-88.

Robert, F. and Brown, A.C., 1986. Archean gold-bearing quartz veins at the Sigma mine, Abitibi Greenstone Belt, Quebec: part I. Vein paragenesis and hydrothermal alteration. Economic Geology, v. 81, p. 593-616.

Robert, F. and Kelly, W.C., 1987. Ore forming fluids in Archean gold bearing quartz veins at the Sigma mine, Abitibi greenstone belt, Quebec, Canada. Economic Geology, v. 82, p. 1464-1482.

Robert, F., 1992. GAC NUNA Research conference: greenstone gold and crustal evolution. Geoscience Canada, v. 18, no. 2, p. 83-86.

Robertson, D.K. and Cumming, G. L., 1968. Lead- and sulphur isotope ratios from the Great Slave Lake area, Canada. Canadian Journal of Earth Science, v. 5, p. 1269-1276.

Rock, N.M.S. and Groves, D.J. 1988. Can lamprophyres resolve the genetic controversy over mesothermal gold deposits? Geology, v. 16, p. 538-541.

Roedder, E., 1979. Fluid inclusions as samples of ore fluids: in Barnes, H.B., editor, Geochemistry of Hydrothermal Ore Deposits, John Wiley and Sons, New York, p. 684-737.

Rye, D.M. and Rye, R.O., 1974. Homestake Gold Mine, South Dakota: I. Stable Isotope Studies. Economic Geology, v. 69, p. 203-317.

Sharp, Z.D., Essene, E.J. and Kelly, W.C., 1985. A re-examination of the arsenopyrite geothermometer: preesure considerations and applications to natural assemblages. The Canadian Mineralogist, v. 23, p. 517-534.

Shieh, Y.N. and Schwarcz, H.P., 1977. An estimate of the oxygen isotope composition of a large segment of the Canadian Shield in northwestern Ontario. Canadian Journal of Earth Science, v. 14, p. 927-931.

Sibson R.H., Robert, F. and Poulsen, K.H., 1988. High angle reverse faults, fluid pressure cycling an mesothermal gold quartz deposits. Geology, v. 16, p. 551-555.

Size, W.B., 1979. Petrology, geochemistry and genesis of the type area trondhjemite in the Trondheim Region, Central Norwegian Caledonides. Norges geol. Unders, v. 351, p. 51-76.

Smith, D.W.G., 1976. Short Course in Microbeam Techniques: in Smith, D.W.G., editor, Mineralogical Association of Canada, Short Course, p. 182.

Smith, F., 1991. A mineralogical study of the gold bearing Archean Volcanics, Ulu property-BHP, N.W.T., Canada. Undergraduate Thesis, University of British Columbia, 29p.

Steiger, R.H.,and Jager, E., 1977. Subcommision on geochronology: Conventions on the use of decay constants in geo- and cosmo- chronology. Earth and Planetary Science Letters, v. 36, p. 359-362.

Swatton, S.P., 1987. Structure, mineralogy and stable isotopes - Bullmoose Lake gold deposit, N.W.T. Unpublished M.Sc. Thesis, University of Alberta, 137p..

Taylor, H.P. Jr., 1969. The oxygen isotope geochemistry of igneous rocks. Contributions to Mineralogy and Petrography, v. 19, p. 1-71.

Taylor, H.P., Jr, 1974. The application of oxygen and hydrogen isotope studies to problems of hyrothermal alteration and ore deposition. Economic Geology, v. 69, p. 843-883.

Taylor, H.P., 1978. Oxygen and hydrogen isotope studies of plutonic granitic rocks. Earth and Planetary Science Letters v. 38, p. 177-210.

Taylor, H.P., Jr, 1979. Oxygen and hydrogen isotope relationships in hydrothermal mineral deposits: in Barnes, H.B., editor, Geochemistry of Hydrothermal Ore Deposits, John Wiley and Sons, New York, p. 236-272.

Thompson, P.H., 1989a. A empirical model for metamorphic evolution of the Archean Slave Province and adjacent Thelon Tectonic Zone, north-western Canadain Shield, : in Daly J.S., Cliff, R.A. andYardley, B.W.D., editors, Evolution of Metamorphic Belts. Geol. Soc. Spec. Pub., 43, p. 245-263.

Thompson, P.H., 1989b. Moderate overthickening of thinned sialic crust and the origin of granitic magmatism and regional metamorphism in low-P-high-T terranes. Geology, v. 17, p. 520-523.

Thurston, P.C. and Chivers, K.M., 1990. Secular variation in greenstone developement emphasizing Superior Province, Canada. Precambrian Research, v. 46, p. 21-58.

Tirrul, R. and Bell, I., 1980. Geology of the Anialik River Greenstone Belt, Hepburn Island Map Area, District of Mackenzie. Geological Survey of Canada, Paper 80-1A, p. 157-164.

Toulmin, P. and Barton, P.B., 1964. A thermodynamic study of pyrite and pyrrhotite. Geochemica Cosmochemica Acta, v. 28, p. 641-671.

van Breeman, O., Davis, W.J. and King, J.E., 1991. Geochronology of granitoid rocks in the Archean Slave Province, N.W.T..Geological Association of Canada, Program with Abstracts, v. 16, p. 127.

Wang, L.G., McNaughton, N.J. and Groves, D.I., 1993. An overview of the relationship between granitoid intrusions and gold mineralization in the Archean Murchison Province, Western Australia. Mineralium Deposita, v. 28, p. 482-494.

Wickham, S.M, and Oxburgh, E.R., 1985. Continental rifts as a setting for regional metamorphism. Nature, v. 315, p. 330-333.

Winchester, J.A. and Floyd, P.A., 1976. Geochemical discrimination of different magma series and their differentiation products using immobile elements. Chemical Geology, v. 20, p. 325-343.

Winchester, J.A. and Floyd, P.A., 1977. Geochemical magma type discrimination: application to altered and metamorphosed basic igneous rocks. Earth and Planetary Science Letters, v. 28, p. 459-469.

Witt, W.K., 1991. Regional metamorphic controls on alteration associated with gold mineralization in the Eastern Goldfields province, Western Australia: implications for the timing and origin of Archean lode gold deposits. Geology, v. 19, p. 982-985.

Winkler, H.G.F., 1974. Petrogenesis of metamorphic rocks. 3rd edition, 320p. Springer-Verlag, New York.

Wiwchar, M.B., 1957. Consolidated Discovery Yellowknife Mine. Structural Geology of Canadian Ore Deposits v. 2, CIMM, Montreal, p.201-209.

Wood, P.C., Burrows, D.R. and Spooner, E.T.C., 1986. Au-quartz vein and intrusion-hosted Cu-Au-Ag-Mo mineralization, Hollinger-McIntyre Mines Timmins, Ontario: Geological characteristics, structural examination, igneous and hydrothermal alteration geochemistry, and light stable isotope (hydrogen and oxygen) geochemistry. Ontario Geological Survey Miscellaneous Paper 130, p. 115-137.

Wu, X., Delbove, F. and Touray, J.C., 1990. Conditions of formation of gold bearing arsenopyrite: a comparison of synthetic crystals with samples from Le Chatelet gold deposit, Creuse, France. Mineralium Deposita, v. 25, p. 8-12.

APPENDIX 1. Sample list

Abbreviations used:

acic - acicular
act - actinolite
alm - almandine
asp - arsenopyrite
bi - biotite
blky - blocky
bn - bornite
cb - carbonate
cm - centimetre
ep - epidote
gal - galena
GBZ - Gabbro breccia zone
hb - hornblende
kspar - potassium feldspar
mm - millimeter
mo - molybdenite
NFN - Northern fold nose
plag - plagioclase
po - pyrrhotite
P.S. - polished thin section
py - pyrite
QFP - quartz-feldspr porphyry
qtz - quartz
sph - sphalerite
T.S. - thin section
tm - tourmaline
tr - trace

APPENDIX 1. Sample list - Surface Samples

Sample I.D.	Location	Section	Description
89 VFT-64	NFN	P.S.	Type III mineralization. Grey, translucent, coarsely crystalline qtz vein with minor act. Contains coarse late fractures and vugs with py fill.
89 VRT-622	East Limb	-	Type III mineralization. Massive white/clear coarsely crystalline qtz vein. Selvage of massive po with 5% py blebs, and 20% rounded/milled qtz vein clasts.
90 PAK US-01	Flood Zone	-	Type II mineralization. Strongly silicified mafic volcanic with 25% acic asp.
90 PAK US-02	Flood Zone	2P.S	Type II mineralization Silicified mafic volcanic with acic asp bands.
90 PAK US -03	Flood Zone	P.S.	Type II mineralization. Act/kspar altered mafic volcanic breccia with siliceous matrix.
90 PAK US-04	Flood Zone	P.S.	Type II mineralization. Silicified act/hb altered mafic volcanics with 15% acic asp/py.
90 PAK US-05	Flood Zone	-	Type II mineralization. Semi-massive acic asp in contact with qtz vein. Vein with thin, wispy mineralized wallrock ribbons.
90 PAK US-06	Flood Zone	2P.S.	Type II mineralization. Semi-massive acic asp in act altered mafic volcanics, cross-cut by 1cm qtz, act, kspar asp veinlet.
90 PAK US-07	Flood Zone	P.S	Type II alteration. Altered mafic volcanic with 5% fine qtz stockworking, 5% po, tr blky asp.
90 PAK US-08	Flood Zone	P.S.	Type II mineralization. Acic asp mineralization in strongly altered mafic volcanic containing kspar, qtz and pink titanite, cross-cut by later qtz stockwork.
90 PAK US-09	Flood Zone	P.S.	Type II mineralization. Massive grey qtz vein with blebs and ribbons of acic asp, minor associated py, act and tm.
90 PAK US-10	Flood Zone	P.S.	Type II mineralization. Bands of acic aspy in qtz, k-spar, titanite matrix cross-cut by later qtz stockwork.
90 PAK US-11	Flood Zone	P.S.	Type II mineralization as 90 PAK US-10.
90 PAK US-12	Flood Zone	-	Type II mineralization. Massive grey qtz vein with finely disseminated and felted masses of acic asp, cross-cut by coarse grained qtz veinlet.
90 PAK US-13	Flood Zone	-	Type II mineralization. Qtz vein with crenulated ribbons of acic asp, minor associated act alteration, py.
90 PAK US-14	Flood Zone	P.S.	Type II mineralization. Grey qtz vein with ribbons and disseminations of fine acic asp, minor py.

APPENDIX 1. Sample list - Surface Samples

Sample I.D.	Location	Section	Description
90 PAK US-15	Flood Zone	-	Type II mineralization. White sucrosic (weathered?) qtz vein with acic asp ribbons.
90 PAK US-16	Flood Zone	-	Type II mineralization. Grey qtz vein in contact with mafic volcanics. Vein contains angular fragments of wallrock which are partially replaced by acic asp. Asp also occurs as a selvage along vein-wallrock contact.
90 PAK US-17	Flood Zone	P.S.	
90 PAK US-18	Flood Zone		
90 PAK US-19	Flood Zone	-	Type II mineralization. Massive qtz vein with 1cm cross-cutting qtz veinlet. Minor acic asp associated with secondary vein.
90 PAK US-20	Flood Zone	-	Type II mineralization. Altered mafic volcanic adjacent to qtz vein. Contains minor finely disseminated acic asp, and fine mm scale qtz stockworking.
90 PAK US-21	Flood Zone	-	Type II mineralization. Qtz veining/strong silicification containing altered mafic volcanic wallrock fragments, which are partially replaced by acic asp.
90 PAK US-22	Flood Zone	-	
90 PAK US-23	Flood Zone	-	Type II mineralization. Qtz vein with altered mafic partially replaced by acic asp. volcanic fragments. Vein contains massive cm scale blebs of black tm.
90 PAK US-24	Flood Zone	-	
90 PAK US-25	Flood Zone	P.S.	
90 PAK US-26	Flood Zone	-	Type II mineralization. As previous sample, but with abundant tm.
90 PAK US-27	Flood Zone	2 P.S.	Type II mineralization. Ribboned qtz veins in mafic volcanics. Massive acic asp selvages along vein wallrock contacts. Minor py in veins adjacent to asp selvages.
90 PAK US-28	Flood Zone	-	Type II mineralization. Silicified, act altered mafic volcanic, with minor acic asp and py.
90 PAK US-29	Flood Zone	-	Type II mineralization. Qtz rich mafic volcanics with acic asp stringers and blebs.
90 PAK US-30	Flood Zone	-	
90 PAK US-31	Flood Zone	P.S.	Type II alteration. Mafic volcanic with weak bi alteration and fine mm scale qtz stockworking.
90 PAK US-32	Flood Zone	T.S.	Type II alteration. Mafic volcanic with moderate act/bi alteration, with trace asp and py.
90 PAK US-33	Flood Zone	P.S.	Type II alteration. Strongly altered/silica flooded mafic volcanic.
90 PAK US-34	Flood Zone	P.S.	Type II mineralization. Altered mafic volcanics with cm scale qtz veins. Qtz veins with acic asp selvages.

APPENDIX 1. Sample list - Surface Samples

Sample I.D.	Location	Section	Description
90 PAK US-35 90 PAK US-36	Flood Zone Flood Zone	-	Type II mineralization. Grey qtz vein with angular mafic volcanic wallrock fragments, in part replaced with acic asp. Vein qtz contains finely disseminated acic asp.
90 PAK US-37	Flood Zone	2P.S.	Type II alteration. Act altered mafic volcanic with strong silica flooding and trace blky asp.
90 PAK US-38	Flood Zone	-	Type II mineralization. Strongly altered mafic volcanics with 30-40% qtz veining. Qtz veins with acic asp.
90 PAK US-39	Flood Zone	-	Type II mineralization. Grey qtz vein with massive acic asp selvages. Qtz contains finely disseminated acic asp.
90 PAK US-40	Flood Zone	-	Type II mineralization. Qtz vein in contact with mafic volcanics. Volcanics with act/kspar alteration and abundant acic asp.
90 PAK US-41 90 PAK US-42	Flood Zone Flood Zone	-	Type II mineralization. Qtz vein with acic asp. Asp occurs within skialithic wallrock fragments.
90 PAK US-44	Flood Zone	-	Type II mineralization. Qtz vein incorporating fragments of earlier mineralized qtz vein.
90 PAK US-45	Flood Zone	P.S.	Type II mineralization. Qtz vein with altered mineralized mafic volcanic wallrock fragments.
90 PAK US-46	Flood Zone	-	Qtz vein associated with Type II mineralization. Dark grey qtz vein with no alteration/mineralization.
90 PAK US-47	Ulu West	-	Type III mineralization. Coarsely crystalline white qtz vein containing 1% native bismuth.
90 PAK Gran	Flood Zone	T.S.	Bulk sample of pink granite for geochron collected near granite-sediment contact proximal to Flood Zone
90 PAK QFP	Flood Zone	T.S.	Bulk sample of qtz feldspar porphyry for geochron collected at exposure along sediment volcanic contact directly southeast of the Flood Zone
90 PAK Dyke	NFN	-	Pink alm bearing aplite/ pegmatite dyke associated with main granite dyke.
90 VBT-2470	Ulu West	-	Type III mineralization. Massive, grey to clear coarsely crystalline qtz vein with 5% py as late fracture fill.
90 VFT-2099	GBZ	-	Type III mineralization?. Massive white qtz vein with 5-10% py as late fracture fill. Trace cpy.

APPENDIX 1. Sample list - Surface Samples

Sample I.D.	Location	Section	Description
91 VFT-3616	East Limb	-	Type III? mineralization. White coarsely crystalline qtz vein with very finely disseminated sulphides along grain boundaries. Wallrock adjacent to vein (gabbro?) brecciated and altered (clinozoisite, act, bi). Blocky asp, py, po with wallrock fragments.
91 VFT-3630	Emerald Lake	-	Type III mineralization. Massive white to grey translucent qtz vein, with 5% vugs partially filled with py. Minor late sulphide py, asp occuring as late fill between qtz grains.
91 VFT-3631	Emerald Lake	-	Type III mineralization. Greyish vuggy qtz vein with py.
91 VFT-3666	Emerald/GBZ	-	Type III mineralization. Massive po selvage adjacent to qtz vein.
91 VFT-3697	Ulu 3	P.S.	Type I mineralization. Sample of syngenetic massive sulphide in sediment at sediment volcanic/gabbro contact. Contains abundant sph/gal±cpy. Sph occurs as 1-2 cm bands within sediments.
91 VFT-3803	Emerald Lake	P.S.	Type III mineralization. Coarsely crystalline qtz vein with cpy as late fracture fill.
91 VFT-3808	Emerald Lake	-	Type III mineralization. Massive po as selvage to qtz vein.
91 VFT-3822	Gnu Zone	P.S.	Type II mineralization. Silicified gabbro with banded grey qtz vein. Vein with acic asp selvages and acic asp bearing skialithic wallrock clasts. Minor late py.
91 VKT-3422	NFN	-	Type II mineralization. Qtz vein within shear at sediment/volcanic contact. Massive, clear, coarsely crystalline qtz with act/bi altered wallrock. Py is dominant sulphide as late fracture fill, as selvage along vein wall, and with blky asp within wallrock fragments
91 VKT-3427	NFN	-	Type II mineralization. Milky white barren qtz vein within sediments near sediment-granite contact.
91 VKT-3429	NFN	P.S.	Type III mineralization. Massive white coarsely crystalline qtz vein with 5% (sph, py, blky asp, po, and minor cpy). Sulphides along vuggy late fractures, with minor hornblende.
91 VKT-3430	NFN	P.S.	Type III mineralization. Qtz vein within sheared mafic volcanics. Massive white to clear coarsely crystalline qtz with blky asp, sph and py. Sulphides to 5% associated with hb are localized along late fractures

APPENDIX 1. Sample list - Surface Samples

Sample I.D.	Location	Section	Description
91 VKT-3446	Ulu 3	-	Type III vein. Massive white qtz vein in mafic volcanics. Late fractures with mo, cpy and py.
91 VKT-3447	Ulu 3	-	Type III vein. Veined/altered mafic volcanics at volcanic-granite contact.
91 VKT-3448	Ulu 3	-	Type III vein. Barren qtz vein in volcanics proximal to granite-volcanic contact.
91 VKT-3449	Ulu 3	-	Type III vein. Massive, barren white qtz vein in sediments adjacent to sediment volcanic contact.
91 VKT-3550	Gnu Zone	P.S.	Type II mineralization. Massive fine grained, sucrosic qtz vein with ribbons containing fine acic asp. Minor act altered gabbro wallrock fragments.
91 VKT-3551	Gnu Zone	-	Type II mineralization. Fine grained/sucrosic qtz with gabbro wallrock fragments. Wallrock with 2% fine acic asp.
91 VKT-3562	Gnu Zone	P.S.	Type III mineralization. Coarsely crystalline white qtz vein with 5-7% cpy, bn as late fracture fill.
91 VKT-3570	Ulu West	P.S.	Type III mineralization. Massive coarsely crystalline qtz vein, white to dark grey, with vuggy fracture. Trace po and native bismuth.
91 VLT 3030	Emerald Lake	P.S.	Type III mineralization. Massive white to clear, coarsely crystalline qtz, with 1% cpy occuring along late fractures.
91 VLT-3048	Flood Zone	-	Sediment. Greywacke collected adjacent to 91 VLT-3049 (Type II mineralization within sediments).
91 VLT-3049	Flood Zone	-	Type II mineralization within sediments at south end of Flood zone.
91 VLT-3050	Flood Zone	-	Sediment. Greywacke collected adjacent to 91 VLT-3051 (Type II mineralization within sediments).
91 VLT-3051	Flood Zone	-	Type II mineralization within sediments at south end of flood zone
91 VLT-3052	Flood Zone	-	Type II mineralization within mafic volcanics
91 VLT-3053	Flood Zone	-	Mafic volcanics adjacent to 91 VLT-3052.
91 VLT-3054	Flood Zone	T.S.	Mafic volcanics adjacent to 91 VLT-3055
91 VLT-3055	Flood Zone	-	Type II mineralization within mafic volcanics.
91 VLT-3056	Flood Zone	-	Gabbro with bi metacrysts collected from trench.

APPENDIX 1. Sample list - Surface Samples

Sample I.D.	Location	Section	Description
91 VLT-3057	Flood Zone	-	Altered gabbro collected from trench.
91 VMT-3708	Ravine	P.S.	Type III mineralization. Grey to white, coarsely crystalline qtz vein with 2-3% coarse py occuring along late fractures. Trace finely disseminated py, cpy and sph.
91 PAK-US-01	Flood Zone	-	Type II mineralization, hosted within laminated mafic volcanics proximal to volcanic/sediment contact.
91 PAK US-02	Flood Zone	2P.S	Type II mineralization hosted within greywacke at south end of Flood Zone. Sample of mineralization and typical unaltered wall rock.
91 PAK US-03	Flood Zone	P.S	Type II mineralization, hosted within greywacke as above.
91 PAK US-04	Flood Zone	-	Mafic volcanic. Dark, laminated mafic volcanics.
91 PAK US-05	Flood Zone	P.S.	Type II mineralization hosted within mafic volcanics.
91 PAK US-06	NFN	-	Type III qtz vein. Barren milky white qtz vein within granite, proximal to granite/sediment contact. Qtz veins generally normal to contact.
91 PAK US-08	NFN	P.S.	Type III mineralization. NFN main vein at sediment-volcanic contact. White to dark grey coarsely crystalline qtz vein with 20% sulphides (py>cpy>po>sph) occuring as late fracture fill and around grain boundaries.
GBZ	GBZ	-	Type III mineralization? Angular gabbro clasts in white qtz matrix.
GRAN NFN	NFN	T.S.	Bulk sample of granite. Collected north of NFN.
91 PAK QFP-2	East Limb	T.S.	Bulk sample of QFP . Collected in gabbro near sediment/gabbro contact. Coarse grained QFP with 5-10% grey qtz eyes. Minor cm scale qtz veins with thin bi selvages.
91 PAK QFP-3	East Limb	T.S.	Bulk sample of QFP for geochron. Collected from felsenmeer/ outcrop within east-west linear crosscutting gabbro. Medium grained, medium grained QFP, relatively pristine.
92 VKT-4204	Ulu West	T.S.	Granodiorite.
92 VKT-4205	Ulu West	T.S.	Gabbro/diorite.
92 VKT-4206	Ulu West	T.S.	Pink granitoid dyke.
92 VKT-4207	Ulu West	T.S.	Grey intermediate dyke.

APPENDIX 1. Sample list - Surface Samples

Sample I.D.	Location	Section	Description
92 VKT-4208	East Limb	T.S.	Pink aplite dyke collected proximal to eastern granite.
92 VKT-4209	East Limb	T.S.	Pink aplite dyke as above.
93 HVRT -0	Flood Zone	-	East granite.
93 HVRT-1	Ulu West	-	Granitoid dyke.
93 HVRT-2	East Limb	-	QFP.
93 HVRT-3	Ulu West		Granodiorite.

APPENDIX 1. Sample list - Core Samples

All mineralized/altered samples Type II unless noted otherwise.
Center of sample interval given for 5-20cm samples

DDH	interval (m)	P.S./T.S.	Description
89 VD-05	19.5-19.7	T.S.	Massive unaltered mafic volcanics.
89 VD-12	24.9	P.S.	Type III mineralized qtz vein in QFP. Abundant py.
89 VD-12	76.9-77.1	-	QFP.
89 VD-19	199.9-210.0	2 T.S.	Composite sample of hanging wall alteration in mafic volcanics, act, cb rich.
89 VD-19	221.0	-	Grey qtz vein in mineralized zone.
90 VD-22	191.0	-	Propylitic alteration associated with QFP?
90 VD-22	204.0	T.S	QFP with small phenocrysts.
90 VD-23	83.50	T.S.	Hanging wall alteration in mafic volcanics, act-bi rich.
90 VD-25	25-6	P.S.	Grey qtz vein in mineralized zone.
90 VD-25	152.0	T.S.	QFP with large (0.50 cm.) euhedral plag phenocrysts.
90 VD-25	187.5-187.88	T.S.	Weakly altered (bi) hanging wall mafic volcanics.
90 VD-25	195.7	P.S.	Banded mineralization.
90 VD-27	218.7	P.S.	Banded mineralization, with asp, bi, act.
90 VD-27	27-13	-	Grey qtz vein in mineralized zone.
90 VD-27	27-15	T.S.	Mafic volcanics with bi rich alteration.
90 VD-30a	litho	T.S.	Unaltered mafic volcanic (pillow basalt)
90 VD-30a	litho	2T.S	Sediment. Greywacke with cordierite porphyroblasts.
90 VD-30a	litho	T.S	Diabase.
90 VD-30a	12.00	2T.S.	Qtz, amethyst, cb, tm vein in mafic volcanics.
90 VD-30a	48.00	T.S.	Act-cb vein in mafic volcanics.
90 VD-31	367.50	T.S.	QFP.
90 VD-31	369.20	-	QFP.
90 VD-32	32-12	-	Qtz vein in mineralized zone.
90 VD-32	32-18	T.S.	Strong bi alteration in mafic volcanics adjacent to mineralization.
90 VD-32	32-26	P.S.	Grey qtz vein in mineralized zone.

APPENDIX 1. Sample list - Core Samples

All mineralized/altered samples Type II unless noted otherwise.
Center of sample interval given for 5-20cm samples

DDH	interval (m)	P.S./T.S.	Description
90 VD-32	324.00	-	QFP.
90 VD-34	222.80-224.60	-	Grey qtz vein in mineralized zone.
90 VD-36	109.71	-	Gabbro.
90 VD-36	137.36	-	Sediment.
90 VD-36	231.35	-	Mafic volcanic.
90 VD-38	221.70-223.50	-	Grey qtz vein in mineralized zone.
90 VD-39	444.30	-	QFP.
90 VD-41	9.00	T.S.	QFP.
90 VD-42	268.76	-	Unaltered mafic volcanic.
90 VD-42	61.27	-	Coarse grained massive gabbro.
90 VD-43	109.46-109.71	T.S.	QFP.
90 VD-43	322.00	P.S.	Grey qtz vein in mineralized zone.
90 VD-44	307.00	T.S.	Unaltered mafic volcanic.
90 VD-44	292.70	T.S.	QFP.
90 VD-44	565.50	-	Grey aplite dyke.
90 VD-45	387.87	-	Grey qtz vein in mineralized zone.
90 VD-47	347.00	P.S.	Banded mineralization.
90 VD-47	355.60	T.S.	Altered mafic volcanics (act, cb, ep) between mineralized zones.
90 VD-47	349.90	T.S.	Act rich altered mafic volcanics between mineralized zones.
90 VD-47	351.50	T.S.	Bi rich altered volcanics between mineralized zones.
90 VD-48	181.15	T.S.	Grey aplite.
90 VD-49	22.50	T.S.	QFP.
90 VD-51	388.50	-	Grey qtz vein in mineralized zone.
90 VD-54	80.65	-	QFP.
90 VD-55	66.24	-	Fine-medium grained "flow core gabbro".
90 VD-56	125.10	-	QFP.
90 VD-63	130.54-130.70	-	Gabbro.

APPENDIX 1. Sample list - Core Samples

All mineralized/altered samples Type II unless noted otherwise.
Center of sample interval given for 5-20cm samples

DDH	interval (m)	P.S./T.S.	Description
90 VD-63	289.87	-	Unaltered magic volcanic.
90 VD-63	403.25-404.00	-	Grey qtz vein in mineralized zone.
90 VD-64	46.25	T.S.	QFP with large phenocrysts.
90 VD 64	48.75	T.S.	QFP (chilled margin).
90 VD-68	240.80	-	Pillow basalt.
90 VD-68	353.050-353.22	-	Sediment.
90 VD-77	32.40	-	Sediment.
90 VD-77	174.52-174.73	-	Gabbro.
90 VD-77	184.63-184.81	-	Massive gabbro.
90 VD-77	314.64	-	Unaltered mafic volcanic.
90 VD-77	372.83	-	Pegmatite dyke.
90 VD-88	132.14-132.35	-	QFP.
90 VD-88	137.70	T.S.	Massive gabbro.
90 VD-89	406.15	-	Pegmatite dyke.
90 VD-90	512.11	-	Massive basalt.
90 VD-91	77.67	T.S.	"Flow core" gabbro.
91 VD-92	479.40	-	Gabbro with bi metacrysts.
91 VD-92	522.34	-	Unaltered mafic volcanics with amygdules.
91 VD-95	432.23	-	Massive fine grained unaltered mafic volcanic.
91 VD-96A	394.49	-	Unaltered mafic volcanic with amygdules.
91 VD-105	681.38	-	Unaltered mafic volcanics.
91 VD-108	535.18	-	Type III mineralized vein.
91 VD-108	551.45-553.24	T.S.	Pegmatite dyke.
91 VD-116	493.14	-	Type III mineralized vein.
91 VD-125	479.17	-	Unaltered mafic volcanics.
92 VD-140	129.50	-	Cb vein in hanging-wall of Type II mineralized zone.
92 VD-140	160.00	-	Cb vein in foot-wall of Type II mineralization.

APPENDIX 1. Sample list - Core Samples

All mineralized/altered samples Type II unless noted otherwise.
Center of sample interval given for 5-20cm samples

DDH	interval (m)	P.S./T.S.	Description
92 VD-141	120.90	-	Early qtz-cb -amethyst-ep vein.
92 VD-141	213.07	-	Late cb bearing retrograde alteration.
92 VD-141	229.50	-	Massive white cb vein.
92 VD-141	240.00	-	Qtz-cb-amethyst-ep vein.
92 VD-141	573.60	T.S.	Grey aplite Dyke.

APPENDIX 2. Whole Rock Chemistry

All major oxides reported in weight percent, trace elements reported in ppm.

C	Diamond drillcore samples
S	Surface samples

TYPE

MV	mafic volcanics
G	gabbro
GW	greywacke
CW	cordierite bearing sediment
QFP	quartz-feldspar porphyry dykes
GAP	grey aplite dykes
GD	granodiorite
QD	quartz diorite
GR	granite
AP	pink aplite dykes
GDY	granite dyke
PEG	pegmatite
D	diabase

ANALYSIS

A	Analysis performed by Acme Analytical Laboratories, Vancouver, British Columbia. Major oxide and trace element analysis by ICPES. Total iron reported as Fe_2O_3.
W	Analysis performed at Washington State University, Pullman, Washington. Major oxide and Cr, Sr, and Zr analysis by XRF. Total iron reported as FeO. All other trace and rare earth elements determined by ICP-MS analysis.

L.O.I - Loss on ignition.

APPENDIX 2. Whole Rock Chemistry

	C	C	C	C	C	C	C	C	C	C	C	C
DDH	89VD05	90VD36	90VD42	90VD44	90VD63	90VD68	90VD77	90VD90	90VD92	91VD95	91VD96A	91VD105
Depth	19.60	231.50	268.76	307.00	289.87	240.80	314.64	512.11	522.34	432.23	394.49	681.38
Type	MV	MV	MV	MV	MV	MV	MV	MV	MV	MV	MV	MV
Analysis	A	A	A	A	A	A	A	A	A	A	A	A
SiO2	52.56	52.72	51.23	51.11	50.81	57.16	53.80	55.15	51.09	53.54	51.11	51.20
TiO2	1.33	1.46	1.41	1.46	1.44	1.84	1.50	1.92	1.18	1.39	1.13	1.40
Al2O3	13.17	14.21	13.57	13.66	14.87	11.73	14.02	13.34	14.37	13.34	14.13	14.13
Fe2O3*	13.97	14.58	15.62	15.41	15.27	15.13	13.44	15.65	14.23	13.87	13.82	14.96
FeO												
MnO	0.20	0.23	0.22	0.25	0.24	0.23	0.23	0.22	0.22	0.25	0.22	0.25
MgO	5.62	5.14	5.31	5.65	5.35	3.00	3.94	3.15	6.26	4.74	6.01	4.78
CaO	10.19	8.42	8.90	7.45	8.61	6.39	9.72	7.52	8.06	8.00	9.45	10.47
Na2O	2.11	2.73	3.30	3.72	2.37	3.62	2.36	3.30	3.73	4.40	3.41	2.79
K2O	0.12	0.05	0.16	0.42	0.06	0.60	0.05	0.35	0.36	0.17	0.32	0.49
P2O5	0.16	0.18	0.14	0.17	0.19	0.23	0.16	0.22	0.12	0.15	0.10	0.14
Cr2O3	.009	.008	.008	.003	.003	.002	.007	.002	.012	.005	.014	.009
L.O.I.	0.40	0.10	0.10	0.60	0.50	0.10	0.50	0.10	0.30	0.20	0.30	0.20
Total	99.93	99.84	100.05	100.03	99.76	100.14	99.73	100.04	100.05	100.15	100.11	100.10
Ba	73	62	48	302	62	207	95	210	160	89	57	57
Sr	141	211	159	157	138	71	134	200	368	160	271	163
La	10	11	10	11	20	12	10	10	10	10	10	10
Zr	85	104	102	118	95	192	84	195	62	127	68	94
Y	17	34	27	31	36	49	34	49	17	32	17	26
Co	56		30	29		40		35	25	36	67	49
Ni	56		53	41		10		16	65	56	69	48
Nb	20	20	20	20	20	20	27	20	20	20	20	20

APPENDIX 2. Whole Rock Chemistry

	C	S	S	C	C	C	C	C	C	C	C	C
DDH	91VD125	91VLT3053	91VLT3054	90VD36	90VD42	90VD55	90VD63	90VD77	90VD77	90VD91	91VD92	90VD36
Depth	479.17			109.71	61.27	66.24	130.60	174.60	184.70	77.67	476.40	403.18
Type	MV	MV	MV	G	G	G	G	G	G	G	G	D
Analysis	A	A	A	A	A	A	A	A	A	A	A	A
SiO2	53.99	56.56	56.48	51.44	51.76	52.65	51.37	51.82	52.07	52.95	50.99	49.29
TiO2	1.34	1.84	1.83	1.07	1.07	1.39	1.00	1.27	1.29	1.40	0.98	3.20
Al2O3	12.53	11.80	11.71	14.22	12.00	13.55	15.41	13.04	13.73	13.62	13.88	12.41
Fe2O3*	14.39	16.01	15.77	13.46	17.79	15.03	12.23	14.45	14.98	13.77	13.46	14.93
FeO												
MnO	0.22	0.20	0.20	0.22	0.26	0.21	0.21	0.24	0.23	0.26	0.21	0.25
MgO	4.93	3.58	2.69	7.21	4.40	4.85	6.80	5.89	6.16	4.66	6.95	5.11
CaO	9.44	5.33	7.46	8.95	8.82	9.67	9.56	9.53	8.73	10.20	8.89	8.33
Na2O	2.53	3.73	3.21	2.41	2.45	2.24	2.22	2.58	2.49	2.49	3.28	2.75
K2O	0.42	0.39	0.06	0.10	0.37	0.27	0.46	0.40	0.14	0.37	0.64	1.03
P2O5	0.13	0.21	0.22	0.12	0.15	0.15	0.11	0.12	0.18	0.13	0.08	0.48
Cr2O3	.005	2.000	.002	.015	.002	.004	.025	.003	.006	.002	.017	.012
L.O.I.	0.10	0.20	0.40	0.10	0.30	0.10	0.40	0.30	0.20	0.20	0.60	1.80
Total	100.12	99.99	100.10	99.66	100.08	100.20	99.83	99.91	100.16	100.14	100.08	99.71
Ba	158	145	19	86	71	50	32	105	47	107	211	263
Sr	194	260	118	143	139	132	138	145	136	154	218	309
La	10	10	10	8	10	10	11	12	10	10	10	34
Zr	99	190	192	44	92	103	57	60	52	98	59	185
Y	25	48	46	19	29	28	20	16	24	25	10	36
Co	38	45	10		55	28			45	53	25	
Ni	35	10	20		10	40			16	38	65	
Nb	20	39	20	20	20	20	21	20	20	20	20	20

APPENDIX 2. Whole Rock Chemistry

	C	C	C	C	S	S	C	C	C	C	C	C
DDH	90VD68	90VD36	90VD68	90VD77	91VLT3048	91VLT3050	89VD12Q	90VD31Q	90VD39	90VD43	90VD44S	90VD48S
Depth	193.15	137.36	353.15	32.40			77.00	369.20	444.30	109.60	565.50	181.15
Type	D	GW	CW	CW	GW	GW	QFP	QFP	QFP	QFP	GAP	GAP
Analysis	A	A	A	A	A	A	A	A	A	A	A	A
SiO2	48.69	74.13	60.79	58.77	64.13	66.51	69.89	70.97	70.88	73.97	77.70	78.82
TiO2	2.94	0.54	0.73	0.80	0.69	0.65	0.36	0.34	0.36	0.31	0.07	0.06
Al2O3	13.05	12.84	19.44	21.55	16.94	16.60	15.51	15.51	15.11	14.20	12.58	13.00
Fe2O3*	14.24	4.32	6.50	6.56	5.93	5.49	2.96	2.53	3.03	2.48	0.93	0.85
FeO												
MnO	0.22	0.03	0.07	0.04	0.06	0.05	0.05	0.06	0.06	0.03	0.01	0.01
MgO	5.73	2.08	2.87	3.81	3.04	2.44	0.75	0.70	0.74	0.67	0.21	0.11
CaO	7.69	0.94	0.84	0.63	1.17	0.54	2.49	2.67	2.53	2.61	1.12	0.90
Na2O	2.42	2.92	1.15	1.59	1.35	0.61	4.89	5.07	4.66	4.22	6.56	6.07
K2O	1.58	1.36	4.67	3.35	5.11	5.29	1.69	1.48	1.28	0.99	0.37	0.04
P2O5	0.38	0.09	0.14	0.15	0.11	0.12	0.09	0.10	0.09	0.12	0.01	0.01
Cr2O3	.015	.021	.029	.029	.024	.024	.004	.004	.004	.005	.002	.002
L.O.I.	2.50	0.60	2.50	2.30	1.40	1.60	1.20	0.80	1.10	0.30	0.60	0.40
Total	99.77	99.96	99.87	99.91	100.17	100.12	100.06	100.06	100.04	100.04	100.21	100.68
Ba	4343	306	687	1772	795	747	649	780	709	408	193	188
Sr	396	150	86	104	94	51	430	485	472	294	157	147
La	20	34	23	31	29	15	17	3	9	49	10	2
Zr	154	116	76	79	140	127	94	93	93	128	40	36
Y	32	12	17	18	11	5	6	6	7	12	5	9
Co					13	25	28	20	27	20	20	21
Ni					67	49						
Nb	20	20	20	20	20	20						

APPENDIX 2. Whole Rock Chemistry

	C	C	C	C	C
DDH	90VD54	90VD56	90VD77	90VD88	90VD89
Depth	80.65	125.10	372.85	132.20	406.15
Type	QFP	QFP	PEG	QFP	PEG
Analysis	A	A	A	A	A
SiO2	68.42	73.15	76.28	72.68	76.80
TiO2	0.52	0.29	0.01	0.29	0.01
Al2O3	15.46	14.82	14.06	14.21	14.46
Fe2O3*	3.99	2.33	0.53	2.43	0.56
FeO*					
MnO	0.05	0.02	0.16	0.03	0.07
MgO	1.49	0.57	0.10	0.61	0.08
CaO	3.57	2.44	0.42	2.02	0.38
Na2O	4.20	4.68	5.00	5.51	6.01
K2O	1.33	0.79	2.50	1.03	0.95
P2O5	0.17	0.10	0.05	0.08	0.04
Cr2O3	.006	.004	.002	.007	.002
L.O.I.	0.70	0.80	0.70	0.70	0.40
Total	100.09	100.12	99.83	100.08	99.77
Ba	554	416	19	784	8
Sr	530	322	19	250	13
La	20	16	17	17	2
Zr	114	117	44	116	5
Y	9	10	67	9	10
Nb	49	20	47	20	20

APPENDIX 2. Whole Rock Chemistry

	C	C	S	S	S	S	S	S
DDH	90VD31BQ	90VD44	GRAN	92VKT4204	92VKT4205	92VKT4206	92VKT4207	92VKT4208
Depth	367.50	292.70						
Type	QFP	QFP	GR	GD	QD	GDY	QFP	AP
Analysis	W	W	W	W	W	W	W	W
SiO2	69.61	69.72	75.58	67.07	59.44	74.22	72.13	73.15
TiO2	0.34	0.33	0.03	0.39	0.79	0.08	0.31	0.00
Al2O3	15.54	15.41	13.25	17.84	16.90	13.69	14.19	16.06
FeO*	2.61	2.44	1.14	1.42	7.62	0.98	2.44	0.16
MnO	0.06	0.05	0.02	0.03	0.14	0.02	0.04	0.02
MgO	0.57	0.58	0.00	0.60	1.75	0.03	0.53	0.00
CaO	2.82	2.77	0.72	2.31	4.89	0.89	1.81	0.52
Na2O	4.80	4.87	4.44	5.79	4.50	4.27	3.18	8.29
K2O	2.43	2.50	4.44	2.65	1.84	4.30	4.46	1.08
P2O5	0.10	0.09	0.01	0.11	0.38	0.05	0.09	0.01
Total	99.18	98.76	99.63	98.21	98.24	98.53	99.19	99.28
Cr	3	8	0	7	1	11	10	14
Ba	747	704	3	612	519	170	749	9
Sr	466	483	11	573	347	46	191	11
Zr	149	151	95	170	147	68	178	48
Y	9	9	123	8	47	28	21	21
Nb	7.90	7.90	41.00	17.50	13.20	14.80	13.90	78.00
Rb	87.00	82.00	409.00	103.79	81.82	153.68	176.97	179.20
Th	5.75	3.95	24.41	8.67	3.74	8.16	14.99	9.58
Hf	3.15	3.06	6.72	4.53	3.89	2.43	4.57	12.05
Ta	0.32	0.31	2.39	0.62	0.56	1.51	1.58	16.95
U	1.57	1.25	9.49	1.11	0.68	5.00	2.36	3.89
Pb	8.76	8.31	51.93	10.63	4.57	24.86	17.49	20.3
Cs	6.51	3.97	13.78	2.42	10.82	8.01	16.81	9.42
La	30.66	22.83	11.35	11.19	31.31	10.38	43.35	1.90
Ce	55.54	42.10	30.58	22.54	59.91	22.74	76.88	6.43
Pr	5.58	4.42	4.22	2.28	7.11	2.23	7.81	0.98
Nd	20.10	16.32	20.36	8.92	30.59	8.45	27.74	3.94
Sm	3.54	3.07	10.75	1.72	7.38	2.33	5.01	2.60
Eu	0.98	0.87	0.17	0.71	2.23	0.24	0.79	0.03
Gd	2.40	2.14	14.92	1.81	7.17	2.15	3.50	2.19
Tb	0.30	0.27	3.40	0.25	1.33	0.54	0.54	0.83
Dy	1.55	1.45	23.49	1.41	8.64	3.86	3.17	6.33
Ho	0.29	0.26	5.11	0.28	1.83	0.87	0.62	1.37
Er	0.73	0.70	15.66	0.74	5.40	2.78	1.64	4.89
Tm	0.10	0.09	2.36	0.11	0.73	0.43	0.24	1.03
Yb	0.58	0.59	15.24	0.67	4.68	2.88	1.56	8.80
Lu	0.09	0.10	2.31	0.11	0.73	0.46	0.24	1.32

APPENDIX 2. Whole Rock Chemistry

	S	C	S	S	S	S
DDH	92VKT4209	92VD141	93HVRT0	93HVRT1	93HVRT2	93HVRT3
Depth		573.60				
Type	AP	GAP	GR	GDY	QFP	GD
Analysis	W	W	W	W	W	W
SiO2	71.10	77.58	74.62	70.20	67.09	70.48
TiO2	0.00	0.05	0.04	0.35	0.55	0.26
Al2O3	16.40	13.53	13.86	15.15	15.75	15.09
FeO	0.13	0.53	0.96	2.52	3.67	1.9
MnO	0.01	0.03	0.02	0.06	0.05	0.02
MgO	0.00	0.00	0.02	0.80	1.27	0.54
CaO	0.94	1.07	0.73	2.43	3.47	1.89
Na2O	9.46	3.51	4.80	4.28	4.86	5.31
K2O	0.49	1.97	4.53	3.26	2.17	2.78
P2O5	0.01	0.11	0.01	0.11	0.17	0.07
Total	98.53	98.28	99.59	99.16	99.05	98.34
Cr	10	11	9	12	19	5
Ba	9	470	56	668	624	740
Sr	23	134	12	304	449	481
Zr	52	64	90	164	185	133
Y	17	11	128	17	12	7
Nb	27.60	11.00	32.63	27.28	9.39	19.13
Rb	6.17	31.89	317.53	103.48	58.55	80.14
Th	8.55	6.37	26.44	9.40	5.57	5.23
Hf	11.6	2.53	6.77	4.18	4.25	3.52
Ta	12.38	0.95	3.62	2.84	1.05	4.69
U	2.63	2.54	7.86	2.32	1.03	1.24
Pb	12.63	20.04	59.26	19.16	9.33	5.88
Cs	0.15	0.28	6.98	3.91	4.85	1.26
La	2.80	6.00	9.89	38.03	32.06	23.72
Ce	8.27	12.76	23.86	67.65	58.75	42.33
Pr	1.19	1.64	3.23	6.96	6.20	4.39
Nd	4.70	6.96	15.78	25.12	23.77	15.73
Sm	2.48	2.14	9.01	4.98	4.34	2.87
Eu	0.05	0.37	0.19	1.05	1.24	0.72
Gd	1.98	2.06	12.98	3.50	2.90	1.82
Tb	0.63	0.32	2.99	0.57	0.42	0.25
Dy	4.40	1.88	20.3	3.08	2.16	1.30
Ho	0.88	0.36	4.63	0.60	0.40	0.23
Er	3.01	0.95	13.66	1.66	1.00	0.61
Tm	0.57	0.13	1.91	0.23	0.13	0.09
Yb	4.64	0.81	11.84	1.44	0.79	0.55
Lu	0.72	0.11	1.85	0.24	0.13	0.09

APPENDIX 3. CIPW Normative Mineralogy for Felsic Intrusive Rocks

All values in percent.
Rock type as in APPENDIX 2.

Mineral abbreviations used:

Q - quartz
C - corundum
Or - orthoclase
Ab - albite
An - anorthite
Di - diopside
Wo - wollastonite
Hy - hypersthene
Mt - magnetite
Il - ilmenite
Hm - hematite
Tn - titanite
Ru - rutile
Ap - apatite

APPENDIX 3. CIPW Normative Mineralogy for Felsic Intrusive Rocks

	89VD12Q	90VD31	90VD31Q	90VD39	90VD43	90VD44	90VD44S	90VD48S	90VD54	90VD56	90VD77	90VD88	90VD89	GRAN
Type	QFP	QFP	QFP	QFP	QFP	QFP	GAP	GAP	QFP	QFP	PEG	QFP	PEG	GR
Q	27.10	27.37	24.12	30.80	37.08	23.75	33.20	38.31	27.46	34.93	34.35	29.70	34.70	29.27
C	1.47	1.05	0.11	1.86	1.92	0.00	0.00	1.49	1.14	2.30	2.74	0.61	3.23	0.00
Or	10.15	8.81	14.52	7.71	5.95	14.94	2.19	0.24	8.00	4.74	14.91	6.16	5.62	26.45
Ab	44.63	45.86	43.58	42.68	38.52	44.23	58.88	54.59	38.37	42.71	45.34	50.09	54.07	40.20
An	11.96	12.69	13.55	12.20	12.37	12.95	3.79	4.41	16.89	11.64	1.77	9.62	1.63	3.14
Di	0.00	0.00	0.00	0.00	0.00	0.28	1.16	0.00	0.00	0.00	0.00	0.00	0.00	0.00
Wo	0.00	0.00	0.00	0.00	0.00	0.00	0.02	0.00	0.00	0.00	0.00	0.00	0.00	0.15
Hy	2.11	1.95	1.59	2.08	1.88	1.48	0.00	0.30	4.89	1.60	0.28	1.71	0.22	0.00
Mt	1.69	0.88	1.66	1.87	0.95	1.31	0.00	0.00	2.15	0.59	0.36	0.82	0.14	0.00
Il	0.51	0.48	0.48	0.51	0.44	0.46	0.02	0.02	0.74	0.41	0.01	0.41	0.01	0.03
Hm	0.19	0.71	0.19	0.08	0.65	0.41	0.65	0.59	0.00	0.88	0.13	0.71	0.29	0.72
Tn	0.00	0.00	0.00	0.00	0.00	0.00	0.12	0.00	0.00	0.00	0.00	0.00	0.00	0.02
Ru	0.00	0.00	0.00	0.00	0.00	0.00	0.00	0.03	0.00	0.00	0.00	0.00	0.00	0.00
Ap	0.19	0.21	0.19	0.19	0.26	0.19	0.02	0.02	0.36	0.21	0.11	0.17	0.08	0.02
Total	100.00	100.00	100.00	100.00	100.00	100.00	100.04	100.00	100.00	100.00	100.00	100.00	100.00	100.01

APPENDIX 3. CIPW Normative Mineralogy for Felsic Intrusive Rocks

	91VKT4204	**91VKT4205**	**91VKT4206**	**91VKT4207**	**91VKT4208**	**91VKT4209**	**91VD141**	**93HVRTO**	**93HVRT1**	**93HVRT2**	**93HVRT3**
	GD	**QD**	**GDY**	**QFP**	**AP**	**AP**	**GAP**	**GR**	**GDY**	**GD**	**QFP**
Q	16.46	10.57	29.33	30.39	17.87	11.78	45.32	25.95	25.04	20.14	22.56
C	1.65	0.00	0.56	1.18	0.34	0.00	4.18	0.00	0.48	0.00	0.09
Or	15.70	11.11	25.86	26.88	6.25	2.83	12.02	26.83	19.47	12.92	16.46
Ab	52.14	41.28	39.03	29.13	72.90	82.98	32.56	43.20	38.84	43.98	47.78
An	10.77	20.93	4.20	8.54	2.49	0.82	5.41	2.90	11.43	14.87	8.92
Di	0.00	1.08	0.00	0.00	0.00	0.00	0.00	0.11	0.00	1.08	0.00
Wo	0.00	0.00	0.00	0.00	0.00	1.48	0.00	0.19	0.00	0.00	0.00
Hy	1.66	10.67	0.08	1.49	0.00	0.00	0.00	0.00	2.23	3.73	1.49
Mt	0.00	2.45	0.00	1.36	0.03	0.01	0.00	0.00	1.42	2.16	0.00
Il	0.05	1.12	0.04	0.44	0.00	0.00	0.06	0.03	0.49	0.77	0.03
Hm	1.10	0.00	0.77	0.38	0.10	0.09	0.42	0.75	0.36	0.00	1.19
Tn	0.00	0.00	0.00	0.00	0.00	0.00	0.00	0.04	0.00	0.00	0.00
Ru	0.25	0.00	0.03	0.00	0.00	0.00	0.01	0.00	0.00	0.00	1.31
Ap	0.23	0.80	0.10	0.20	0.01	0.01	0.02	0.01	0.24	0.36	0.15
Total	100.00	100.00	100.00	100.00	100.00	100.00	100.00	100.01	100.00	100.00	100.00

APPENDIX 4. Sulphide Mineral Analyses

PO - pyhrrotite, ASP - arsenopyrite, PY - pyrite
Temp - temperature given by arsenopyrite geothermometer (Kretschmar and Scott, 1976)

Mineral	Analysis	Traverse	Element Weight Percent					Atoms				Temp °C
			As	Cu	Fe	S	Total	As	Cu	Fe	S	
SEC VD 10-19.4												
PO	2	1	0.00	0.00	58.68	39.68	98.36	0.00	0.00	45.92	54.08	
PO	3	1	0.00	0.01	58.92	39.92	98.84	0.00	0.01	45.87	54.13	
PO	4	1	0.07	0.03	59.10	40.28	99.47	0.04	0.02	45.69	54.25	
ASP	6	1	45.57	0.01	34.93	20.24	100.75	32.61	0.00	33.54	33.85	461
ASP	7	1	44.84	0.00	34.83	20.97	100.64	31.90	0.00	33.25	34.85	413
ASP	8	1	45.58	0.00	34.40	20.41	100.40	32.69	0.00	33.10	34.21	467
ASP	9	1	45.05	0.00	34.85	20.84	100.75	32.06	0.00	33.28	34.66	423
ASP	10	1	46.18	0.04	34.65	20.22	101.09	33.00	0.03	33.21	33.76	491
ASP	11	1	45.38	0.00	34.83	20.60	100.80	32.36	0.00	33.32	34.33	443
ASP	12	1	46.37	0.00	34.75	19.97	101.09	33.20	0.00	33.38	33.42	508
ASP	13	1	45.55	0.01	34.72	20.29	100.57	32.64	0.01	33.37	33.98	464
ASP	14	1	45.03	0.00	35.08	20.44	100.56	32.20	0.00	33.65	34.15	432
ASP	15	1	45.60	0.00	34.93	20.49	101.03	32.49	0.00	33.39	34.12	453
ASP	16	1	45.93	0.01	34.75	20.27	100.96	32.82	0.01	33.32	33.85	477
ASP	18	2	45.69	0.01	34.57	20.16	100.43	32.83	0.01	33.32	33.85	478
ASP	19	2	45.98	0.01	34.48	20.08	100.54	33.04	0.00	33.24	33.71	495
ASP	20	2	45.36	0.05	34.41	20.59	100.41	32.47	0.04	33.05	34.44	451
ASP	21	2	45.46	0.00	34.81	20.51	100.78	32.45	0.00	33.34	34.21	450
ASP	22	2	45.24	0.00	34.71	20.78	100.73	32.23	0.00	33.17	34.60	434
ASP	23	2	45.44	0.02	34.89	20.22	100.56	32.57	0.02	33.55	33.86	458
ASP	24	2	45.42	0.02	35.04	20.54	101.03	32.34	0.02	33.47	34.18	442
ASP	25	2	45.25	0.00	34.86	20.78	100.89	32.19	0.00	33.27	34.54	432
ASP	26	2	45.02	0.00	34.74	21.03	100.80	31.98	0.00	33.11	34.91	418
ASP	28	3	44.94	0.00	34.47	20.94	100.35	32.07	0.00	33.00	34.92	424
ASP	29	3	45.27	0.00	34.40	20.49	100.15	32.50	0.00	33.13	34.37	453
ASP	30	3	44.76	0.01	34.57	21.09	100.44	31.87	0.01	33.02	35.10	411
ASP	31	3	44.34	0.00	34.78	21.20	100.32	31.55	0.00	33.20	35.25	391
ASP	32	3	45.20	0.03	34.86	20.62	100.70	32.24	0.03	33.36	34.37	435
ASP	33	3	44.86	0.00	35.10	21.04	101.00	31.79	0.00	33.36	34.85	406
ASP	34	3	44.74	0.03	34.67	20.95	100.38	31.90	0.02	33.16	34.91	413
ASP	35	3	45.00	0.00	34.66	20.67	100.33	32.19	0.00	33.26	34.56	432
ASP	36	3	45.58	0.00	34.59	20.28	100.45	32.70	0.00	33.29	34.00	468
ASP	47	4	44.73	0.02	34.62	20.63	100.00	32.09	0.01	33.32	34.58	425
ASP	48	4	44.58	0.00	34.82	20.87	100.28	31.82	0.00	33.35	34.82	408

APPENDIX 4. Sulphide Mineral Analyses

Mineral	Analysis	Traverse	Element Weight Percent					Atoms				Temp °C
			As	Cu	Fe	S	Total	As	Cu	Fe	S	
ASP	49	4	45.00	0.02	34.67	20.58	100.27	32.23	0.02	33.31	34.44	434
ASP	50	4	45.39	0.04	34.70	20.52	100.64	32.44	0.03	33.27	34.27	449
ASP	51	4	54.40	0.00	34.40	19.98	99.79	32.84	0.00	33.38	33.78	479
ASP	52	4	45.23	0.03	34.80	20.37	100.42	32.41	0.02	33.45	34.12	447
ASP	54	4	44.12	0.00	34.52	21.07	99.71	31.59	0.00	33.15	35.26	393
ASP	55	4	45.92	0.00	34.41	19.84	100.71	33.17	0.00	33.35	33.49	505
ASP	56	4	45.14	0.02	34.55	20.27	99.98	32.50	0.02	33.37	34.11	453
PO	57	4	0.07	0.00	58.10	39.52	97.69	0.04	0.00	45.75	54.21	
PO	58	4	0.00	0.01	58.59	39.42	98.02	0.00	0.01	46.04	53.95	
PO	59	4	0.00	0.00	58.55	39.58	98.13	0.00	0.00	45.92	54.08	
PO	60	4	0.07	0.00	58.25	39.71	98.03	0.04	0.00	45.70	54.26	
PO	61	4	0.09	0.00	58.23	39.72	98.04	0.05	0.00	45.68	54.27	
PO	62	4	0.05	0.00	58.50	39.50	98.05	0.03	0.00	45.94	54.04	
PO	63	4	0.00	0.02	58.39	39.57	97.98	0.00	0.02	45.85	54.13	
ASP	64	5	44.16	0.00	34.25	21.03	99.44	31.71	0.00	32.99	35.30	401
ASP	65	5	44.83	0.00	34.93	20.73	100.48	31.99	0.00	33.44	34.56	419
ASP	66	5	45.25	0.00	34.62	20.05	99.92	32.66	0.00	33.52	33.82	465
PO	68	5	0.05	0.02	59.50	38.60	98.15	0.03	0.00	46.93	53.04	
PO	69	5	0.01	0.00	59.41	38.64	98.08	0.01	0.01	46.88	53.11	
PO	70	5	0.06	0.00	60.02	38.44	98.52	0.04	0.00	47.25	52.71	
PO	71	5	0.04	0.00	59.83	38.76	98.63	0.02	0.00	46.97	53.00	
PO	72	5	0.09	0.00	59.39	38.55	98.03	0.05	0.00	46.91	53.04	
ASP	75	5	46.73	0.02	34.42	19.25	100.42	33.88	0.02	33.49	32.61	569
ASP	76	5	45.11	0.02	34.67	20.43	100.23	32.36	0.02	33.37	34.25	444
ASP	77	5	44.68	0.00	34.55	20.61	99.85	32.10	0.00	33.30	34.60	426
ASP	78	5	44.69	0.00	34.33	20.87	99.90	32.03	0.00	33.01	34.96	421
SEC VD-17-36.6												
ASP	79	6	43.96	0.02	34.60	21.55	100.13	31.23	0.02	32.98	35.77	372
ASP	80	6	44.42	0.01	35.07	21.28	100.78	31.46	0.01	33.32	35.22	385
ASP	81	6	44.73	0.01	34.81	20.95	100.50	31.86	0.00	33.26	34.87	410
ASP	82	6	44.61	0.01	34.76	20.91	100.28	31.84	0.01	33.28	34.87	409
ASP	83	6	45.03	0.00	34.93	20.69	100.65	32.11	0.00	33.41	34.48	426
ASP	84	6	44.99	0.00	34.40	20.77	100.17	32.21	0.00	33.04	34.75	433
ASP	85	6	46.03	0.00	34.77	20.07	100.87	32.98	0.00	33.41	33.61	490
ASP	86	6	44.68	0.00	34.95	20.85	100.48	31.85	0.00	33.42	34.74	409
ASP	87	6	45.05	0.00	34.69	20.89	100.64	32.08	0.00	33.15	34.77	425
ASP	88	6	45.10	0.00	35.26	20.80	101.16	31.98	0.00	33.54	34.48	418

APPENDIX 4. Sulphide Mineral Analyses

Mineral	Analysis	Traverse	Element Weight Percent					Atoms				Temp °C
			As	Cu	Fe	S	Total	As	Cu	Fe	S	
ASP	89	7	44.75	0.00	34.46	20.71	99.92	32.11	0.00	33.16	34.73	426
ASP	90	7	46.08	0.00	34.45	19.72	100.24	33.30	0.00	33.40	33.30	516
ASP	91	7	45.83	0.00	34.52	20.14	100.49	32.92	0.00	33.27	33.81	485
ASP	92	7	45.20	0.00	34.56	20.51	100.27	32.40	0.00	33.24	34.37	446
ASP	93	7	44.63	0.00	34.96	20.68	100.27	31.91	0.00	33.54	34.56	413
ASP	94	7	45.19	0.00	34.67	20.42	100.28	32.41	0.00	33.36	34.22	447
ASP	95	7	44.84	0.05	34.50	20.29	99.68	32.35	0.04	33.39	34.21	443
ASP	96	7	44.75	0.00	34.74	20.55	100.04	32.10	0.00	33.44	34.46	426
ASP	97	7	46.09	0.00	34.61	19.51	100.20	33.34	0.00	33.62	33.01	522
ASP	98	7	46.18	0.00	34.59	19.56	100.33	33.39	0.00	33.55	33.05	524
ASP	100	7	45.55	0.03	34.73	20.34	100.65	32.61	0.02	33.35	34.02	461
ASP	101	7	44.39	0.01	34.59	20.14	99.13	32.20	0.01	33.65	34.14	432
ASP	102	7	46.01	0.00	34.83	20.08	100.92	32.94	0.00	33.45	33.60	487
ASP	103	7	43.84	0.00	35.15	21.19	100.18	31.20	0.00	33.55	35.24	371
ASP	104	7	44.78	0.00	34.89	20.29	99.95	32.22	0.00	33.67	34.11	434
ASP	105	7	44.49	0.00	34.95	20.96	100.39	31.70	0.00	33.41	34.90	400
ASP	108	7	44.97	0.03	34.94	20.63	100.57	32.10	0.03	33.46	34.42	426
ASP	109	8	45.26	0.01	34.90	20.36	100.53	32.40	0.00	33.52	34.07	446
ASP	110	8	44.32	0.01	34.34	21.31	100.99	31.31	0.01	33.49	35.19	377
ASP	111	8	44.90	0.01	35.53	21.12	101.55	31.64	0.00	33.58	34.78	396
ASP	112	8	44.81	0.00	35.08	20.97	100.85	31.81	0.00	33.41	34.78	407
ASP	113	8	44.49	0.01	35.04	20.88	100.42	31.71	0.01	33.51	34.78	400
ASP	114	8	44.50	0.00	34.92	20.70	100.11	31.85	0.00	33.53	34.62	410
ASP	115	8	44.45	0.00	35.08	21.23	100.75	31.50	0.00	33.35	35.16	388
ASP	116	8	44.88	0.01	34.89	20.84	100.61	31.97	0.01	33.34	34.69	417
ASP	118	8	45.08	0.03	35.11	20.54	100.75	32.15	0.02	33.60	34.23	429
PY	119	9	0.05	0.00	46.41	54.01	100.47	0.03	0.00	33.03	66.95	
PY	120	9	0.07	0.03	46.47	53.58	100.15	0.04	0.02	33.22	66.72	
PY	121	9	0.04	0.02	46.19	54.11	100.37	0.02	0.01	32.87	67.09	
PY	122	9	0.00	0.05	46.76	53.99	100.80	0.00	0.03	33.20	66.77	
PY	123	9	0.01	0.00	46.60	54.13	100.74	0.01	0.00	33.07	66.92	
ASP	124	10	45.30	0.05	34.72	20.40	100.47	32.45	0.04	33.36	34.15	450
ASP	125	10	44.69	0.01	34.72	20.99	100.42	31.85	0.01	33.19	34.95	409
ASP	126	10	45.35	0.02	34.97	20.50	100.84	32.35	0.02	33.46	34.17	443
ASP	127	10	45.80	0.00	34.56	20.23	100.58	32.85	0.00	33.25	33.39	479
ASP	128	10	44.70	0.00	35.18	20.74	100.61	31.85	0.00	33.62	34.53	409
ASP	129	10	45.51	0.00	35.07	20.49	101.08	32.40	0.00	33.50	34.10	447
ASP	130	10	45.51	0.00	34.54	20.35	100.40	32.65	0.00	33.24	34.11	464

APPENDIX 4. Sulphide Mineral Analyses

Mineral	Analysis	Traverse	Element Weight Percent					Atoms				Temp °C
			As	Cu	Fe	S	Total	As	Cu	Fe	S	
ASP	131	10	45.21	0.05	34.73	20.37	100.37	32.41	0.05	33.41	34.13	447
ASP	132	10	45.55	0.02	34.53	20.20	100.31	32.74	0.02	33.30	33.94	471
ASP	133	10	45.35	0.01	34.75	20.39	100.50	32.47	0.01	33.39	34.13	452
ASP	135	11	44.26	0.02	35.16	21.64	101.07	31.16	0.01	33.21	35.61	368
ASP	136	11	43.69	0.02	34.98	21.30	99.98	31.11	0.02	33.42	35.45	366
ASP	137	11	44.26	0.03	35.02	21.15	100.45	31.46	0.02	33.39	35.13	385
ASP	138	11	44.29	0.01	34.76	21.08	100.14	31.59	0.01	33.27	35.13	393
ASP	139	11	44.34	0.00	35.08	20.84	100.26	31.65	0.00	33.59	34.76	397
ASP	140	11	44.61	0.00	35.27	20.93	100.81	31.68	0.00	33.59	34.73	399
ASP	141	11	44.31	0.00	34.99	21.10	100.40	31.52	0.00	33.40	35.08	389
ASP	142	11	44.68	0.00	34.67	20.93	100.27	31.89	0.00	33.20	34.91	412
ASP	143	11	44.02	0.02	35.20	21.30	100.54	31.21	0.02	33.49	35.29	371
ASP	144	11	45.15	0.00	35.16	20.48	100.79	32.21	0.00	33.65	34.13	433
ASP	145	12	44.74	0.00	35.00	21.04	100.78	31.76	0.00	33.33	34.90	404
ASP	146	12	44.60	0.03	34.93	20.99	100.54	31.73	0.02	33.34	34.90	402
ASP	147	12	46.27	0.01	34.74	20.00	101.01	33.14	0.00	33.38	33.48	503
ASP	148	12	45.25	0.00	35.04	20.65	100.95	32.20	0.00	33.45	34.34	433
ASP	149	12	44.66	0.00	35.09	20.89	100.64	31.77	0.00	33.50	34.73	405
SEC VD 11-42.6												
PY	150	13	0.01	0.03	47.38	53.70	101.12	0.01	0.02	33.61	66.36	
PY	151	13	0.03	0.01	46.49	53.89	100.42	0.02	0.01	33.11	66.87	
PY	152	13	0.00	4.00	47.64	53.16	100.84	0.00	0.03	33.96	66.02	
PY	153	13	0.00	0.03	46.57	53.31	99.90	0.00	0.02	33.39	66.59	
PY	154	13	0.00	0.00	45.85	53.71	99.56	0.00	0.00	32.89	67.11	
ASP	155	13	45.02	0.00	34.60	20.63	100.25	32.24	0.00	33.24	34.53	435
ASP	156	13	44.08	0.00	34.59	20.88	99.55	31.65	0.00	33.31	35.04	397
ASP	157	13	43.96	0.00	34.51	21.10	99.57	31.50	0.00	33.17	35.33	388
ASP	158	13	44.33	0.00	35.04	21.07	100.44	31.54	0.00	33.44	35.02	390
ASP	159	13	43.89	0.00	35.00	21.16	100.04	31.28	0.00	33.47	35.25	375
ASP	160	13	44.13	0.01	35.17	21.36	100.67	31.24	0.01	33.40	35.35	373
ASP	161	13	44.44	0.00	34.80	21.02	100.26	31.69	0.00	33.29	35.02	399
ASP	162	13	44.97	0.00	34.81	21.64	100.42	32.14	0.00	33.38	34.48	429
ASP	163	13	44.55	0.01	34.23	20.71	99.50	32.08	0.01	33.06	34.85	424
ASP	164	13	43.84	0.01	34.52	21.20	99.56	31.18	0.01	34.52	35.46	381
PY	165	14	0.07	0.01	46.70	54.08	100.85	0.03	0.01	33.13	66.83	
PY	166	14	0.14	0.00	46.44	54.20	100.77	0.07	0.00	32.95	66.98	

APPENDIX 4. Sulphide Mineral Analyses

Mineral	Analysis	Traverse	Element Weight Percent					Atoms				Temp °C
			As	Cu	Fe	S	Total	As	Cu	Fe	S	
PY	167	14	0.14	0.00	46.09	54.08	100.31	0.07	0.00	32.83	67.10	
PY	168	14	0.12	0.00	46.25	53.93	100.31	0.06	0.00	32.97	66.97	
ASP	170	14	45.44	0.00	34.80	20.60	100.83	32.39	0.00	33.28	34.32	446
ASP	171	14	45.24	0.00	34.79	20.70	100.73	32.25	0.00	33.27	34.48	436
ASP	172	14	44.66	0.00	34.40	20.75	99.81	32.06	0.00	33.13	34.81	423
ASP	173	14	45.58	0.02	34.51	20.05	100.15	32.85	0.02	33.37	33.76	480
ASP	174	14	45.20	0.00	34.47	20.38	100.05	32.5	0.00	33.25	34.25	453
PO	175	15	0.04	0.00	58.58	39.93	98.25	0.02	0.00	45.90	54.08	
PO	176	15	0.03	0.02	58.87	39.58	98.51	0.02	0.02	46.04	53.92	
PO	177	15	0.00	0.00	58.83	39.55	98.38	0.00	0.00	46.06	53.94	
PO	178	15	0.02	0.00	58.98	39.95	98.96	0.01	0.00	45.87	54.12	
PO	179	15	0.00	0.01	59.13	39.52	98.66	0.00	0.01	46.20	53.79	
PY	181	15	0.00	0.03	46.91	53.12	100.06	0.00	0.02	33.64	66.35	
PY	182	15	0.00	0.00	46.99	52.88	99.87	0.00	0.00	33.78	66.22	
PY	183	15	0.00	0.00	46.66	53.22	99.88	0.00	0.00	33.48	66.52	
PY	184	15	0.01	0.02	46.64	53.43	100.10	0.01	0.01	33.38	66.60	
PO	185	16	0.02	0.00	58.92	39.56	98.50	0.01	0.00	46.09	53.90	
PO	186	16	0.02	0.02	59.05	39.77	98.87	0.01	0.01	46.00	53.97	
PO	187	16	0.00	0.02	59.32	39.63	98.97	0.00	0.02	46.21	53.78	
PO	188	16	0.11	0.02	59.30	39.74	99.18	0.07	0.02	46.10	53.82	
PO	189	16	0.00	0.00	59.31	39.59	98.90	0.00	0.00	46.24	53.76	
PY	190	17	0.03	0.00	46.91	53.65	100.58	0.01	0.00	33.42	66.57	
PY	191	17	0.04	0.00	46.58	53.86	100.48	0.02	0.00	33.17	66.81	
PY	192	17	0.00	0.00	46.38	54.07	100.45	0.00	0.00	32.99	67.01	
PY	193	17	0.00	0.01	46.71	54.09	100.81	0.00	0.01	33.14	66.85	
PY	194	17	3.00	0.05	45.99	53.62	99.69	0.02	0.03	32.98	66.98	
ASP	195	17	45.72	0.01	34.87	20.09	100.69	32.79	0.01	33.54	33.66	475
ASP	196	17	45.07	0.02	34.84	20.57	100.50	32.22	0.02	33.41	34.36	434
ASP	197	17	45.34	0.05	34.74	20.52	100.65	32.40	0.04	33.30	34.26	446
ASP	198	17	44.17	0.01	34.89	21.20	100.28	31.43	0.10	33.31	35.26	384
ASP	199	17	44.17	0.01	34.98	21.03	100.18	31.49	0.00	33.46	35.04	387
ASP	200	17	44.79	0.00	34.79	20.51	100.09	32.13	0.00	33.48	34.38	428
ASP	201	17	45.49	0.00	34.41	20.38	100.27	32.66	0.00	33.14	34.20	465
ASP	202	17	44.68	0.04	34.41	20.76	99.89	32.05	0.03	33.12	34.80	423
ASP	203	17	44.79	0.01	34.83	20.50	100.13	32.12	0.01	33.52	34.35	427
ASP	204	17	44.31	0.02	34.56	20.80	99.69	31.81	0.02	33.29	34.89	407
PO	205	18	0.02	0.01	58.44	39.46	97.93	0.01	0.01	45.94	54.04	

APPENDIX 4. Sulphide Mineral Analyses

Mineral	Analysis	Traverse	Element Weight Percent					Atoms				Temp °C
			As	Cu	Fe	S	Total	As	Cu	Fe	S	
PO	206	18	0.02	0.00	58.69	39.57	98.28	0.01	0.00	45.98	54.01	
PO	207	18	0.02	0.00	58.54	39.65	98.21	0.01	0.00	45.87	54.12	
PO	208	18	0.09	0.00	58.79	39.64	98.51	0.05	0.00	45.96	53.99	
PO	209	18	0.03	0.01	58.94	39.50	98.47	0.02	0.00	46.13	53.85	
ASP	210	19	44.71	0.00	35.03	20.85	100.60	31.84	0.00	33.47	34.70	409
ASP	211	19	46.17	0.03	34.15	19.67	100.00	33.46	2.00	33.20	33.31	530
ASP	212	19	44.98	0.00	34.01	20.50	99.50	32.47	0.00	32.94	34.59	451
ASP	213	19	45.61	0.00	34.12	19.87	99.59	33.09	0.00	33.22	33.69	499

APPENDIX 5. Formulae Used for Stable Isotope Calculations

Calculation of fluid-mineral oxygen isotope fractionation:

Quartz-H_2O

$\delta^{18}O$ (quartz) - $\delta^{18}O$ (H_2O) = $3.34(10^6/T^2) - 3.31$ (Matsuhisa et al., 1979).

Calcite - H_2O

$\delta^{13}C$ (calcite) - $\delta^{13}C$ (H_2O) = $2.78(10^6/T^2) - 3.39$ (O'Neil et al., 1969).

Where;
T = temperature in K